

https://dspace.org/

Can one develop a biomarker to detect movement disorder types?

Kim, Kimoon

2017
https://hdl.handle.net/10539/24187
Kim, Kimoon (2017) Can one develop a biomarker to detect movement disorder types?, University of the Witwatersrand, <https://hdl.handle.net/10539/24187>

Downloaded from a DSpace repository. https://dspace.org/

CAN ONE DEVELOP A BIOMARKER TO DETECT MOVEMENT DISORDER TYPES?

Kimoon Kim

A dissertation submitted to the Faculty of Engineering and the Built Environment, University of the Witwatersrand, Johannesburg, in fulfilment of the requirements for the degree of Master of Science in Engineering.

Johannesburg, 2017

DECLARATION

I declare that this dissertation is my own, unaided work. It is being submitted to the Degree of Master of Science to the University of the Witwatersrand, Johannesburg. It has not been submitted before for any degree or examination to any other University.



……

……**05**…….. day of ……**October**…….. year ……**2017**……..

ABSTRACT

This study presents the development of a potentially new biomarker for three different movement disorders: Huntington's Disease (HD), Parkinson's Disease (PD) and Essential Tremors (ET). A Leap Motion® gaming device was used to record the trajectories of subjects' forefinger as they trace simple patterns in the air. The patterns used were step-function, triangle and circle. The recorded signals were analysed using transform functions and Fourier analysis. Both analysis types yielded features from which differences between the four categories studied: PD, HD, ET and control subjects, were sought and displayed in both graphical and numerical forms. The X-axis and Y-axis of the signals were separately analysed and yielded different results. For the step-function pattern, no distinct differences between the four categories were found from the transfer function analysis whereas the Y-axis of the signal could distinguish between the categories. For the triangle pattern, the X-axis features provided a discrimination between the categories while the Y-axis feature did not. For the circle pattern, neither X-axis nor Y-axis features were able to distinguish between the categories. A Fourier analysis showed a better discrimination ability for both X- and Y- axis. This study is a preliminary one and all results indicate that more subjects of all categories are needed to develop a bio-marker for the diseases studied and that a higher order transfer function analysis is required. However, the methodology outlined in this work, comprising of both the experimental system and the analysis showed a potential to produce a biomarker for movement disorders.

ACKNOWLEDGEMENTS

I would like to thank my supervisors, Professor Vered Aharonson and Professor David Rubin for their supervision and assistance. I would like to thank Dr Dave Anderson, a Neurologist at the Wits Donald Gordon Medical Centre (WDGMC), for recruiting the required patients for this study. I would also like to thank my family and friends as well as all the study participants without whom this research would not have been possible.

CONTENTS **Page**

DECLARATION **2**

ABSTRACT **3**

ACKNOWLEDGEMENTS **4**

1 INTRODUCTION **27**

1.1 Literature Review **28**

1.1.1 Parkinson's Disease 28

1.1.2 Essential Tremor 31

1.1.3 Huntington's Disease 32

1.1.4 Biomarkers 35

2 METHODOLOGY **39**

2.1 Leap Motion **39**

2.2 Leap Motion Location Setup **39**

2.3 Leap Motion Software Setup **41**

2.4 Patients Recruitment **43**

3 CONTROL SYSTEMS MODELLING APPROACHES **44**

3.1 PID Model **45**

3.2 Black Box Model Method **49**

4 RESULTS **54**

4.1 Black Box Model: Step Function Pattern **57**

4.2 Black Box Model: Triangle Pattern **69**

4.3 Black Box Model: Circle Pattern **81**

4.4 Fourier Analysis **85**

4.5 Concluding Discussions and Future Recommendations **93**

5 CONCLUSION **97**

REFERENCES **99**

APPENDIX A – ETHIC CLEARANCE DOCUMENTS **106**

APPENDIX B – SOFTWARE SETUP **112**

APPENDIX C – X & Y DATA PLOTS FROM STEP-FUNCTION PATTERN **115**

APPENDIX D - X & Y DATA PLOTS FROM TRIANGLE PATTERN **161**

APPENDIX E – X & Y DATA PLOTS FROM CIRCLE PATTERN **199**

APPENDIX F – FFT ANALYSIS OF R^2 DATA FROM CIRCLE PATTERN **218**

LIST OF FIGURES

Figure 2.2.1: Top view configuration of the Leap Motion with the laptop. 40

Figure 2.2.2: Front view configuration of the Leap Motion with the laptop. 40

Figure 2.2.3: Side view configuration of the Leap Motion with the laptop.....41

Figure 2.3.1: The Leap Motion Diagnostic Visualizer [41].....43

Figure 3.1.1: A diagram of a unity feedback system. 45

Figure 3.1.2: Simulink model of a PID. 46

Figure 3.1.3: Spring-damper human arm/hand model [46]. 46

Figure 3.2.1: MATLAB's system identification toolbox.....49

Figure 3.2.2: An example of an X, Y and Z axis plot from control subject 1. 50

Figure 3.2.3: Importing data using the system identification toolbox. 51

Figure 3.2.4: Transfer Functions estimation 51

Figure 4.1: Measured (black) and simulated model (blue) output of control subject 10 with 95.0% best fit. 55

Figure 4.2: Measured (black) and simulated model (blue) output of control subject 3 with -34.3% best fit. 55

Figure 4.3: Pole-zero plot of the estimated transfer function for control subject 1. 56

Figure 4.1.1: Combined X-axis data pole-zero plot for control subjects (blue) - conjugate counterparts are mirror image. 57

Figure 4.1.2: Combined X-axis data pole-zero plot for ET patients (green) - conjugate counterparts are mirror image. 58

Figure 4.1.3: Combined X-axis data pole-zero plot for PD patients before medication (red) - conjugate counterparts are mirror image. 58

Figure 4.1.4: Combined X-axis data pole-zero plot for PD patients after medication (red) - conjugate counterparts are mirror image. 59

Figure 4.1.5: Pole-zero plot between the control subjects (blue) and ET patients (green) using X-axis data - conjugate counterparts are mirror image. 60

Figure 4.1.6: Pole-zero plot between control subjects (blue) and PD patients before medication (red) using X-axis data - conjugate counterparts are mirror image. 60

Figure 4.1.7: Pole-zero plot between control subjects (blue) and PD patients after medication (red) using X-axis data - conjugate counterparts are mirror image. 61

Figure 4.1.8: Pole-zero plot between PD patients before medication (black) and PD patients after medication (red) using X-axis data - conjugate counterparts are mirror image. 61

Figure 4.1.9: An example of a Y-axis measured data plotted against simulated output data from the step-function pattern with 90.2% best fit. 62

Figure 4.1.10: Combined Y-axis data pole-zero plot for control subjects (blue) - conjugate counterparts are mirror image. 63

Figure 4.1.11: Combined Y-axis data pole-zero plot for ET patients (green) - conjugate counterparts are mirror image. 63

Figure 4.1.12: Combined Y-axis data pole-zero plot for PD patients before medication (red) - conjugate counterparts are mirror image. 64

Figure 4.1.13: Combined Y-axis data pole-zero plot for PD patients after medication (red) - conjugate counterparts are mirror image. 64

Figure 4.1.14: Pole-zero plot between control subjects (blue) and ET patients (green) using Y-axis data - conjugate counterparts are mirror image. 65

Figure 4.1.15: Pole-zero plot between control subjects (blue) and PD patients before medication (red) using Y-axis data - conjugate counterparts are mirror image. 66

Figure 4.1.16: Pole-zero plot between control subjects (blue) and PD patients after medication (red) using Y-axis data - conjugate counterparts are mirror image. 66

Figure 4.1.17: Pole-zero plot between PD patients before medication (black) and PD patients after medication (red) using Y-axis data - conjugate counterparts are mirror image. 67

Figure 4.2.1: An example of an X-axis measured data plotted against simulated output data from the triangle pattern with 98% best fit. 69

Figure 4.2.2: Combined X-axis data pole-zero plot for control subjects (blue) - conjugate counterparts are mirror image. 70

Figure 4.2.3: Combined X-axis data pole-zero plot for ET patients (green) - conjugate counterparts are mirror image. 70

Figure 4.2.4: Combined X-axis data pole-zero plot for PD patients before medication (red) - conjugate counterparts are mirror image. 71

Figure 4.2.5: Combined X-axis data pole-zero plot for PD patients after medication (red) - conjugate counterparts are mirror image. 71

Figure 4.2.6: Pole-zero plot between the control subjects (blue) and ET patients (green) using X-axis data - conjugate counterparts are mirror image. 72

Figure 4.2.7: Pole-zero plot between control subjects (blue) and PD patients before medication (red) using X-axis data - conjugate counterparts are mirror image. 73

Figure 4.2.8: Pole-zero plot between control subjects (blue) and PD patients after medication (red) using X-axis data - conjugate counterparts are mirror image. 73

Figure 4.2.9: Pole-zero plot between PD patients before medication (black) and PD patients after medication (red) using X-axis data - conjugate counterparts are mirror image. 74

Figure 4.2.10: An example of a Y-axis measured data plotted against simulated output data from the triangle pattern with 88.6% best fit. 75

Figure 4.2.11: Combined Y-axis data pole-zero plot for control subjects (blue) - conjugate counterparts are mirror image. 76

Figure 4.2.12: Combined Y-axis data pole-zero plot for ET patients (green) - conjugate counterparts are mirror image. 76

Figure 4.2.13: Combined Y-axis data pole-zero plot for PD patients before medication (red) - conjugate counterparts are mirror image. 77

Figure 4.2.14: Combined Y-axis data pole-zero plot for PD patients after medication (red) - conjugate counterparts are mirror image. 77

Figure 4.2.15: Pole-zero plot between control subjects (blue) and ET patients (green) using Y-axis data - conjugate counterparts are mirror image. 78

Figure 4.2.16: Pole-zero plot between control subjects (blue) and PD patients before medication (red) using Y-axis data - conjugate counterparts are mirror image. 79

Figure 4.2.17: Pole-zero plot between control subjects (blue) and PD patients after medication (red) using Y-axis data - conjugate counterparts are mirror image. 79

Figure 4.2.18: Pole-zero plot between PD patients before medication (black) and PD patients after medication (red) using Y-axis data - conjugate counterparts are mirror image. 80

Figure 4.3.1: An example of a R^2 measured data plotted against simulated output data from the circle pattern with 63% best fit. 82

Figure 4.3.2: Combined R^2 data pole-zero plot for control subjects (blue) - conjugate counterparts are mirror image. 83

Figure 4.3.3: Combined R^2 data pole-zero plot for ET patients (green) - conjugate counterparts are mirror image. 83

Figure 4.3.4: Combined R^2 data pole-zero plot for PD patients after medication (red) - conjugate counterparts are mirror image. 84

Figure 4.4.1: An example of a FFT plot of a 'good' control subject. 85

Figure 4.4.2: An example of a FFT plot of ET patient 1. 87

Figure 4.4.3: An example of a FFT plot of PD patient 1 (before and after medication) using R^2 data. 88

Figure 4.4.4: Average feature values shown graphically from tables 4.4.1, 4.4.2, 4.4.3 and 4.4.4. 90

Figure 4.4.5: Scatter plot of the number of peaks versus the first peak magnitude of all subjects. 90

Figure A2.1: Human Research Ethics Committee (Medical) Certificate. 108

Figure A3.1: Page 1 of 3 of information document shown to study subjects. 109

Figure A3.2: Page 2 of 3 of information document shown to study subjects. 110

Figure A3.3: Page 3 of 3 of information document shown to study subjects. 111

Figure B1: Leap Motion system architecture [41]. 112

Figure B2: Sample code to respond to events and inputs [41]. 113

Figure B3: Sample code for Quickstart object [41]. 113

Figure B4: Code sample in detecting finger coordinates [41]. 114

Figure C1: Pole-zero plot of control subject 1 using X-axis data. 115

Figure C2: Measured (black) and simulated model (blue) output of control subject 1 with 82.0% best fit. 115

Figure C3: Pole-zero plot of control subject 2 using X-axis data. 116

Figure C4: Measured (black) and simulated model (blue) output of control subject 2 with 86.5% best fit. 116

Figure C5: Pole-zero plot of control subject 3 using X-axis data. 117

Figure C6: Measured (black) and simulated model (blue) output of control subject 3 with -34.3% best fit - omitted from the analysis. 117

Figure C7: Pole-zero plot of control subject 4 using X-axis data. 118

Figure C8: Measured (black) and simulated model (blue) output of control subject 4 with 84.4% best fit. 118

Figure C9: Pole-zero plot of control subject 5 using X-axis data. 119

Figure C10: Measured (black) and simulated model (blue) output of control subject 5 with 89.3% best fit. 119

Figure C11: Pole-zero plot of control subject 6 using X-axis data. 120

Figure C12: Measured (black) and simulated model (blue) output of control subject 6 with 33.9% best fit - omitted from the analysis. 120

Figure C13: Pole-zero plot of control subject 7 using X-axis data. 121

Figure C14: Measured (black) and simulated model (blue) output of control subject 7 with 88.8% best fit. 121

Figure C15: Pole-zero plot of control subject 8 using X-axis data. 122

Figure C16: Measured (black) and simulated model (blue) output of control subject 8 with -25.5% best fit - omitted from the analysis. 122

Figure C17: Pole-zero plot of control subject 9 using X-axis data. 123

Figure C18: Measured (black) and simulated model (blue) output of control subject 9 with 94.7% best fit. 123

Figure C19: Pole-zero plot of control subject 10 using X-axis data. 124

Figure C20: Measured (black) and simulated model (blue) output of control subject 10 with 95.0% best fit. 124

Figure C21: Pole-zero plot of ET patient 1 using X-axis data. 125

Figure C22: Measured (black) and simulated model (blue) output of ET patient 1 with -134.8% best fit - omitted from the analysis. 125

Figure C23: Pole-zero plot of ET patient 2 using X-axis data. 126

Figure C24: Measured (black) and simulated model (blue) output of control ET patient 2 with 92.1% best fit. 126

Figure C25: Pole-zero plot of ET patient 3 using X-axis data. 127

Figure C26: Measured (black) and simulated model (blue) output of ET patient 3 with 89.5% best fit. 127

Figure C27: Pole-zero plot of ET patient 4 using X-axis data. 128

Figure C28: Measured (black) and simulated model (blue) output of ET patient 4 with 92.3% best fit. 128

Figure C29: Pole-zero plot of ET patient 5 using X-axis data. 129

Figure C30: Measured (black) and simulated model (blue) output of ET patient 5 with 24.9% best fit - omitted from the analysis. 129

Figure C31: Pole-zero plot for PD patient 1 before and after medication using X-axis data. 130

Figure C32: Measured (black) and simulated model (blue) output of PD patient 1 before and after medication with 85.1% and 93.3% best fit respectively. 130

Figure C33: Pole-zero plot for PD patient 3 before and after medication using X-axis data. 131

Figure C34: Measured (black) and simulated model (blue) output of PD patient 3 before and after medication with 89.7% and -89.6% (omitted from the analysis) best fit respectively. 131

Figure C35: Pole-zero plot for PD patient 4 before and after medication using X-axis data. 132

Figure C36: Measured (black) and simulated model (blue) output of PD patient 4 before and after medication with 82.6% and -39.2% (omitted from the analysis) best fit respectively. 132

Figure C37: Pole-zero plot for PD patient 5 before and after medication using X-axis data. 133

Figure C38: Measured (black) and simulated model (blue) output of PD patient 5 before and after medication with 87.7% and 90.9% best fit respectively. 133

Figure C39: Pole-zero plot for PD patient 6 before and after medication using X-axis data. 134

Figure C40: Measured (black) and simulated model (blue) output of PD patient 6 before and after medication with 82.0% and 92.8% best fit respectively. 134

Figure C41: Pole-zero plot for PD patient 7 before and after medication using X-axis data. 135

Figure C42: Measured (black) and simulated model (blue) output of PD patient 7 before and after medication with 90.2% and 89.3% best fit respectively. 135

Figure C43: Pole-zero plot for PD patient 8 before and after medication using X-axis data. 136

Figure C44: Measured (black) and simulated model (blue) output of PD patient 8 before and after medication with 78.2% and 86.8% best fit respectively. 136

Figure C45: Pole-zero plot for PD patient 9 before and after medication using X-axis data. 137

Figure C46: Measured (black) and simulated model (blue) output of PD patient 9 before and after medication with 89.9% and 93.5% best fit respectively. 137

Figure C47: Pole-zero plot of control subject 1 using Y-axis data. 138

Figure C48: Measured (black) and simulated model (blue) output of control subject 1 with 90.2% best fit. 138

Figure C49: Pole-zero plot of control subject 2 using Y-axis data. 139

Figure C50: Measured (black) and simulated model (blue) output of control subject 2 with 86.9% best fit. 139

Figure C51: Pole-zero plot of control subject 3 using Y-axis data. 140

Figure C52: Measured (black) and simulated model (blue) output of control subject 3 with 85.4% best fit. 140

Figure C53: Pole-zero plot of control subject 4 using Y-axis data. 141

Figure C54: Measured (black) and simulated model (blue) output of control subject 4 with 86.2% best fit. 141

Figure C55: Pole-zero plot of control subject 5 using Y-axis data. 142

Figure C56: Measured (black) and simulated model (blue) output of control subject 5 with 91.9% best fit. 142

Figure C57: Pole-zero plot of control subject 6 using Y-axis data. 143

Figure C58: Measured (black) and simulated model (blue) output of control subject 6 with 69.2% best fit. 143

Figure C59: Pole-zero plot of control subject 7 using Y-axis data. 144

Figure C60: Measured (black) and simulated model (blue) output of control subject 7 with 84.1% best fit. 144

Figure C61: Pole-zero plot of control subject 8 using Y-axis data. 145

Figure C62: Measured (black) and simulated model (blue) output of control subject 8 with 64.5% best fit. 145

Figure C63: Pole-zero plot of control subject 9 using Y-axis data. 146

Figure C64: Measured (black) and simulated model (blue) output of control subject 9 with 84.2% best fit. 146

Figure C65: Pole-zero plot of control subject 10 using Y-axis data. 147

Figure C66: Measured (black) and simulated model (blue) output of control subject 10 with 49.4% best fit. 147

Figure C67: Pole-zero plot of ET patient 1 using Y-axis data. 148

Figure C68: Measured (black) and simulated model (blue) output of ET patient 1 with 90.5% best fit. 148

Figure C69: Pole-zero plot of ET patient 2 using Y-axis data. 149

Figure C70: Measured (black) and simulated model (blue) output of ET patient 2 with -3.7% best fit - omitted from the analysis. 149

Figure C71: Pole-zero plot of ET patient 3 using Y-axis data. 150

Figure C72: Measured (black) and simulated model (blue) output of ET patient 3 with 83.6% best fit. 150

Figure C73: Pole-zero plot of ET patient 4 using Y-axis data. 151

Figure C74: Measured (black) and simulated model (blue) output of ET patient 4 with 74.4% best fit. 151

Figure C75: Pole-zero plot of ET patient 5 using Y-axis data. 152

Figure C76: Measured (black) and simulated model (blue) output of ET patient 5 with 92.1% best fit. 152

Figure C77: Pole-zero plot for PD patient 1 before and after medication using Y-axis data. 153

Figure C78: Measured (black) and simulated model (blue) output of PD patient 1 before and after medication with 87.6% and 81.0% best fit respectively. 153

Figure C79: Pole-zero plot for PD patient 3 before and after medication using Y-axis data. 154

Figure C80: Measured (black) and simulated model (blue) output of PD patient 3 before and after medication with 77.5% and 55.7% best fit respectively. 154

Figure C81: Pole-zero plot for PD patient 4 before and after medication using Y-axis data. 155

Figure C82: Measured (black) and simulated model (blue) output of PD patient 4 before and after medication with 85.4% and 82.3% best fit respectively. 155

Figure C83: Pole-zero plot for PD patient 5 before and after medication using Y-axis data. 156

Figure C84: Measured (black) and simulated model (blue) output of PD patient 5 before and after medication with 82.1% and 84.6% best fit respectively. 156

Figure C85: Pole-zero plot for PD patient 6 before and after medication using Y-axis data. 157

Figure C86: Measured (black) and simulated model (blue) output of PD patient 6 before and after medication with 84.0% and 83.6% best fit respectively. 157

Figure C87: Pole-zero plot for PD patient 7 before and after medication using Y-axis data. 158

Figure C88: Measured (black) and simulated model (blue) output of PD patient 7 before and after medication with 64.7% and 82.4% best fit respectively. 158

Figure C89: Pole-zero plot for PD patient 8 before and after medication using Y-axis data. 159

Figure C90: Measured (black) and simulated model (blue) output of PD patient 8 before and after medication with 44.1% (omitted from the analysis) and 72.1% best fit respectively. 159

Figure C91: Pole-zero plot for PD patient 9 before and after medication using Y-axis data. 160

Figure C92: Measured (black) and simulated model (blue) output of PD patient 9 before and after medication with 80.0% and 89.3% best fit respectively. 160

Figure D1: Pole-zero plot of control subject 1 using X-axis data. 161

Figure D2: Measured (black) and simulated model (blue) output of control subject 1 with 89.2% best fit. 161

Figure D3: Pole-zero plot of control subject 2 using X-axis data. 162

Figure D4: Measured (black) and simulated model (blue) output of control subject 2 with 76.5% best fit. 162

Figure D5: Pole-zero plot of control subject 3 using X-axis data. 163

Figure D6: Measured (black) and simulated model (blue) output of control subject 3 with 94.2% best fit. 163

Figure D7: Pole-zero plot of control subject 4 using X-axis data. 164

Figure D8: Measured (black) and simulated model (blue) output of control subject 4 with 98.0% best fit. 164

Figure D9: Pole-zero plot of control subject 5 using X-axis data. 165

Figure D10: Measured (black) and simulated model (blue) output of control subject 5 with 86.3% best fit. 165

Figure D11: Pole-zero plot of control subject 6 using X-axis data. 166

Figure D12: Measured (black) and simulated model (blue) output of control subject 6 with 89.7% best fit. 166

Figure D13: Pole-zero plot of control subject 7 using X-axis data. 167

Figure D14: Measured (black) and simulated model (blue) output of control subject 7 with 94.7% best fit. 167

Figure D15: Pole-zero plot of control subject 8 using X-axis data.....168

Figure D16: Measured (black) and simulated model (blue) output of control subject 8 with 96.1% best fit. 168

Figure D17: Pole-zero plot of control subject 9 using X-axis data.....169

Figure D18: Measured (black) and simulated model (blue) output of control subject 9 with 96% best fit. 169

Figure D19: Pole-zero plot of control subject 10 using X-axis data.....170

Figure D20: Measured (black) and simulated model (blue) output of control subject 10 with 94.3% best fit. 170

Figure D21: Pole-zero plot of ET patient 1 using X-axis data. 171

Figure D22: Measured (black) and simulated model (blue) output of ET patient 1 with 97.2% best fit. 171

Figure D23: Pole-zero plot of ET patient 2 using X-axis data. 172

Figure D24: Measured (black) and simulated model (blue) output of control ET patient 2 with 91.1% best fit. 172

Figure D25: Pole-zero plot of ET patient 3 using X-axis data. 173

Figure D26: Measured (black) and simulated model (blue) output of ET patient 3 with 69.7% best fit. 173

Figure D27: Pole-zero plot of ET patient 4 using X-axis data. 174

Figure D28: Measured (black) and simulated model (blue) output of ET patient 4 with 84.2% best fit. 174

Figure D29: Pole-zero plot of ET patient 5 using X-axis data. 175

Figure D30: Measured (black) and simulated model (blue) output of ET patient 5 with 90.2% best fit. 175

Figure D31: Pole-zero plot for PD patient 3 before and after medication using X-axis data. 176

Figure D32: Measured (black) and simulated model (blue) output of PD patient 3 before and after medication with 82.1% and 90.6% best fit respectively. 176

Figure D33: Pole-zero plot for PD patient 4 before and after medication using X-axis data. 177

Figure D34: Measured (black) and simulated model (blue) output of PD patient 4 before and after medication with 91.0% and 87.16% best fit respectively. 177

Figure D35: Pole-zero plot for PD patient 5 before and after medication using X-axis data. 178

Figure D36: Measured (black) and simulated model (blue) output of PD patient 5 before and after medication with 86.2% and 93.6% best fit respectively. 178

Figure D37: Pole-zero plot for PD patient 6 before and after medication using X-axis data. 179

Figure D38: Measured (black) and simulated model (blue) output of PD patient 6 before and after medication with 93.0% and 93.8% best fit respectively. 179

Figure D39: Pole-zero plot of control subject 1 using Y-axis data 180

Figure D40: Measured (black) and simulated model (blue) output of control subject 1 with 81.4% best fit. 180

Figure D41: Pole-zero plot of control subject 2 using Y-axis data 181

Figure D42: Measured (black) and simulated model (blue) output of control subject 2 with -105.4% best fit - omitted from the analysis 181

Figure D43: Pole-zero plot of control subject 3 using Y-axis data 182

Figure D44: Measured (black) and simulated model (blue) output of control subject 3 with 51.9% best fit. 182

Figure D45: Pole-zero plot of control subject 4 using Y-axis data 183

Figure D46: Measured (black) and simulated model (blue) output of control subject 4 with 80.6% best fit. 183

Figure D47: Pole-zero plot of control subject 5 using Y-axis data....184

Figure D48: Measured (black) and simulated model (blue) output of control subject 5 with -83.3% best fit - omitted from the analysis....184

Figure D49: Pole-zero plot of control subject 6 using Y-axis data....185

Figure D50: Measured (black) and simulated model (blue) output of control subject 6 with 62.7% best fit. 185

Figure D51: Pole-zero plot of control subject 7 using Y-axis data....186

Figure D52: Measured (black) and simulated model (blue) output of control subject 7 with 62.5% best fit. 186

Figure D53: Pole-zero plot of control subject 8 using Y-axis data....187

Figure D54: Measured (black) and simulated model (blue) output of control subject 8 with 63.9% best fit. 187

Figure D55: Pole-zero plot of control subject 9 using Y-axis data....188

Figure D56: Measured (black) and simulated model (blue) output of control subject 9 with 88.6% best fit. 188

Figure D57: Pole-zero plot of control subject 10 using Y-axis data....189

Figure D58: Measured (black) and simulated model (blue) output of control subject 10 with 85.5% best fit. 189

Figure D59: Pole-zero plot of ET patient 1 using Y-axis data. 190

Figure D60: Measured (black) and simulated model (blue) output of ET patient 1 with -54.4% best fit - omitted from the analysis. 190

Figure D61: Pole-zero plot of ET patient 2 using Y-axis data. 191

Figure D62: Measured (black) and simulated model (blue) output of ET patient 2 with -110.0% best fit - omitted from the analysis. 191

Figure D63: Pole-zero plot of ET patient 3 using Y-axis data. 192

Figure D64: Measured (black) and simulated model (blue) output of ET patient 3 with 70.7% best fit. 192

Figure D65: Pole-zero plot of ET patient 4 using Y-axis data. 193

Figure D66: Measured (black) and simulated model (blue) output of ET patient 4 with 83.3% best fit. 193

Figure D67: Pole-zero plot of ET patient 5 using Y-axis data. 194

Figure D68: Measured (black) and simulated model (blue) output of ET patient 5 with 53.0% best fit. 194

Figure D69: Pole-zero plot for PD patient 1 before and after medication using Y-axis data. 195

Figure D70: Measured (black) and simulated model (blue) output of PD patient 1 before and after medication with 81.5% and 76.3% best fit respectively. 195

Figure D71: Pole-zero plot for PD patient 3 before and after medication using Y-axis data. 196

Figure D72: Measured (black) and simulated model (blue) output of PD patient 3 before and after medication with 60.6% and 79.8% best fit respectively. 196

Figure D73: Pole-zero plot for PD patient 4 before and after medication using Y-axis data. 197

Figure D74: Measured (black) and simulated model (blue) output of PD patient 4 before and after medication with 71.3% and 82.5% best fit respectively. 197

Figure D75: Pole-zero plot for PD patient 5 before and after medication using Y-axis data. 198

Figure D76: Measured (black) and simulated model (blue) output of PD patient 5 before and after medication with 71.3% and 73.1% best fit respectively. 198

Figure E1: Pole-zero plot for control subject 1 using R^2 data. 199

Figure E2: Measured (black) and simulated model (blue) output of control subject 1 with 27.6% best fit - omitted from the analysis. 199

Figure E3: Pole-zero plot for control subject 2 using R^2 data. 200

Figure E4: Measured (black) and simulated model (blue) output of control subject 2 with 32.4% best fit - omitted from the analysis. 200

Figure E5: Pole-zero plot for control subject 3 using R^2 data. 201

Figure E6: Measured (black) and simulated model (blue) output of control subject 3 with 31.0% best fit - omitted from the analysis. 201

Figure E7: Pole-zero plot for control subject 4 using R^2 data. 202

Figure E8: Measured (black) and simulated model (blue) output of control subject 4 with 59.3% best fit. 202

Figure E9: Pole-zero plot for control subject 5 using R^2 data. 203

Figure E10: Measured (black) and simulated model (blue) output of control subject 5 with 15.5% best fit - omitted from the analysis. 203

Figure E11: Pole-zero plot for control subject 6 using R^2 data. 204

Figure E12: Measured (black) and simulated model (blue) output of control subject 6 with -1.3% best fit - omitted from the analysis.....204

Figure E13: Pole-zero plot for control subject 7 using R^2 data. 205

Figure E14: Measured (black) and simulated model (blue) output of control subject 7 with -1.7% best fit - omitted from the analysis.....205

Figure E15: Pole-zero plot for control subject 8 using R^2 data. 206

Figure E26: Measured (black) and simulated model (blue) output of control subject 8 with 58.3% best fit. 206

Figure E17: Pole-zero plot for control subject 9 using R^2 data. 207

Figure E18: Measured (black) and simulated model (blue) output of control subject 9 with 7.1% best fit - omitted from the analysis. 207

Figure E19: Pole-zero plot for control subject 10 using R^2 data. 208

Figure E20: Measured (black) and simulated model (blue) output of control subject 10 with 55.1% best fit. 208

Figure E21: Pole-zero plot of ET patient 1 using R^2 data.....209

Figure E22: Measured (black) and simulated model (blue) output of ET patient 1 with 16.4% best fit - omitted from the analysis. 209

Figure E23: Pole-zero plot of ET patient 2 using R^2 data.....210

Figure E24: Measured (black) and simulated model (blue) output of ET patient 2 with 63.0% best fit. 210

Figure E25: Pole-zero plot of ET patient 3 using R^2 data.....211

Figure E26: Measured (black) and simulated model (blue) output of ET patient 3 with 44.6% best fit - omitted from the analysis. 211

Figure E27: Pole-zero plot of ET patient 4 using R^2 data.....212

Figure E28: Measured (black) and simulated model (blue) output of ET patient 4 with 17.4% best fit - omitted from the analysis. 212

Figure E29: Pole-zero plot of ET patient 5 using R^2 data.....213

Figure E30: Measured (black) and simulated model (blue) output of ET patient 5 with 2.0% best fit - omitted from the analysis. 213

Figure E31: Pole-zero plot for PD patient 1 before and after medication using R^2 data. 214

Figure E32: Measured (black) and simulated model (blue) output of PD patient 1 before and after medication with -9.9% (omitted from the analysis) and 50.8% best fit respectively. 214

Figure E33: Pole-zero plot for PD patient 3 before and after medication using R^2 data. 215

Figure E34: Measured (black) and simulated model (blue) output of PD patient 3 before and after medication with 21.3% and 16.7% best fit respectively - omitted from the analysis.....215

Figure E35: Pole-zero plot for PD patient 4 before and after medication using R^2 data. 216

Figure E36: Measured (black) and simulated model (blue) output of PD patient 4 before and after medication with 28.2% (omitted from the analysis) and 71.49% best fit respectively. 216

Figure E37: Pole-zero plot for PD patient 5 before and after medication using R^2 data. 217

Figure E38: Measured (black) and simulated model (blue) output of PD patient 5 before and after medication with 18.87% and -90.1% best fit respectively - omitted from the analysis. 217

Figure F1: A FFT plot of control subject 1 using R^2 data. 218

Figure F2: A FFT plot of control subject 2 using R^2 data. 218

Figure F3: A FFT plot of control subject 3 using R^2 data. 219

Figure F4: A FFT plot of control subject 4 using R^2 data. 219

Figure F5: A FFT plot of control subject 5 using R^2 data. 220

Figure F6: A FFT plot of control subject 6 using R^2 data. 220

Figure F7: A FFT plot of control subject 7 using R^2 data. 221

Figure F8: A FFT plot of control subject 8 using R^2 data. 221

Figure F9: A FFT plot of control subject 9 using R^2 data. 222

Figure F10: A FFT plot of control subject 10 using R^2 data. 222

Figure F11: A FFT plot of ET patient 1 using R^2 data. 223

Figure F12: A comparison FFT plots between ET patient 1 and control subject 10 using R^2 data. 223

Figure F13: A FFT plot of ET patient 1 using R^2 data. 224

Figure F14: A comparison FFT plots between ET patient 2 and control subject 10 using R^2 data. 224

Figure F15: A FFT plot of ET patient 1 using R^2 data. 225

Figure F16: A comparison FFT plots between ET patient 3 and control subject 10 using R^2 data. 225

Figure F17: A FFT plot of ET patient 1 using R^2 data. 226

Figure F18: A comparison FFT plots between ET patient 4 and control subject 10 using R^2 data. 226

Figure F19: A FFT plot of ET patient 1 using R^2 data. 227

Figure F20: A comparison FFT plots between ET patient 5 and control subject 10 using R^2 data. 227

Figure F21: A FFT plot of PD patient 1 (before and after medication) using R^2 data. ...228

Figure F22: A comparison FFT plots between PD patient 1 (before and after medication) and control subject 10 using R^2 data. 228

Figure F23: A FFT plot of PD patient 3 (before and after medication) using R^2 data. ...229

Figure F24: A comparison FFT plots between PD patient 3 (before and after medication) and control subject 10 using R^2 data. 229

Figure F25: A FFT plot of PD patient 4 (before and after medication) using R^2 data. ...230

Figure F26: A comparison FFT plots between PD patient 4 (before and after medication) and control subject 10 using R^2 data. 230

Figure F27: A FFT plot of PD patient 5 (before and after medication) using R^2 data. ...231

Figure F28: A comparison FFT plots between PD patient 5 (before and after medication) and control subject 10 using R^2 data. 231

Figure F29: A FFT plot of PD patient 6 (before and after medication) using R^2 data. ...232

Figure F30: A comparison FFT plots between PD patient 6 (before and after medication) and control subject 10 using R^2 data. 232

LIST OF TABLES

Table 1.1.3: Risk of developing HD by the count of trinucleotide repeat [20]. 33

Table 4.4.1: Control subject's features from the FFT of R^2 data.....86

Table 4.4.2: ET patient's features from the FFT of R^2 data. 87

Table 4.4.3: PD patient's features (before medication) from the FFT of R^2 data.....89

Table 4.4.4: PD patient's features (after medication) from the FFT of R^2 data. 89

1 INTRODUCTION

Extensive research has been done on characterising the different types of neurological movement disorders e.g. Huntington's Disease (HD) and Parkinson's Disease (PD). Most of these diseases can only be diagnosed through clinical observations performed by healthcare professionals (e.g., through symptoms and progression of the disease) and by using a rating scale to assess the severity of the disease, which often takes a lot of time and resources. Therefore, this work attempts to develop some new biomarkers (tests which can characterise a disease) which could differentiate between the types of movement disorders and their severity. These new biomarkers will be based on computational analysis of a patient's hand movements when performing specific tasks to determine whether the biomarker can detect various movement disorder. The research objective is thus to identify features in the graphical and numerical representations of the hand movements, which may have clinical value to neurologists in terms of identifying and classifying some movement disorders and assessing their severity.

Chapter 1 will review relevant literature on neurological movement disorders and the various biomarkers that have attempted to diagnose them. The current research methodology, using the Leap Motion, is presented in Chapter 2. Chapter 3 describes various attempts of using control theory's graphical and numerical outputs to identify and classify various movement disorders in the data acquired. Chapter 4 extends Chapter 3's attempt by using a different signal processing technique to identify and classify various movement disorders. Summary and conclusions are discussed in Chapter 5.

1.1 Literature Review

1.1.1 Parkinson's Disease

The cause of PD is not yet fully understood, but doctors are often able to diagnose patients with PD from the symptoms they exhibit [1]. Patients with PD often exhibit common motor impairment symptoms e.g. tremor, muscle rigidity and bradykinesia, and are usually joined by additional primary symptoms e.g. balance, posture, and difficulty in walking [1]. These symptoms are expressed because the nerve cells that are responsible for their correct functioning have deteriorated (e.g., PD is primarily caused by the degeneration of certain nerve cells called substantia nigra in the basal ganglia) [1]. The deterioration of the substantia nigra causes many signs and symptoms that define PD [1]. Although symptoms differ from patient to patient, the most common symptoms are generally grouped into categories which are: initial, primary and secondary symptoms [1].

According to Golbe *et al.*, the first symptom that is often experienced in the initial stage of PD is "weakness" [2]. Yet, this is a misleading statement as "weakness" does not refer to the weakening of the muscles (most patients with PD have strong muscles) [2]. In PD context, "weakness" refers to the inability to initiate movements at the previous level of accuracy and speed, which is one of the main reasons patients seek medical attention [2]. Together with "weakness", shaking or trembling is usually present and starts on one side of the body (unilateral) and slowly progresses to the opposite side [2]. This can take many years as symptoms differ from patient to patient [2]. It is important to note that PD symptoms (e.g., tremors) are often intensified under stressful situations, therefore doctors can diagnose patients with PD by doing physical tests which puts the body under stress (e.g., rapidly alternating movement evaluation) [2].

The primary motor symptoms of PD are usually an indicator of PD [3]. The three most common symptoms are: tremor, muscle rigidity, and bradykinesia, while gait, balance problems and impairment of posture may or may not develop later in a patient with PD [2]. Tremor at rest, called shaking palsy due to a slow rhythmic tremor motion, is the main distinguishing symptoms of PD from other diseases [3]. The tremor usually starts in one side of the body and later advances to the other side [2]. According to Jankovic, the tremor should not be confused with essential tremor in which the shaking stops once your body is still [4]. The tremors usually reduce or disappear when an individual with PD performs a purposeful movement, however tremors may still be present when performing various movements (called postural or sustention tremors) [4]. Rigidity occurs when there is tightness or increase in muscle tone and can sometimes be mistaken for arthritis, although arthritis maybe present [4]. Bradykinesia is a Greek word for "slow movement" and an individual with bradykinesia has decreased fine motor coordination (e.g., inability to perform everyday tasks such as using cutlery and buttoning up a shirt). Thus, the individuals may need help with everyday tasks [2].

The most disabling primary motor symptoms of PD, which usually occurs in the late stage of PD, is balance and posture problems [2] [3]. The patient is unable to keep a steady, upright posture due to their balance or equilibrium being off. Therefore, the patients cannot take corrective action when they are pushed and this results in the patient falling [3]. Doctors, when testing for PD, often push a patient lightly to see whether they continue taking steps backward to prevent them from falling [2].

PD diagnoses are dependent on clinical observation, i.e. diagnosing a disease by looking at the diseases' characteristic traits [5] [6]. This is done by matching symptoms to a list pre-provided for each diseased. However, this is difficult as symptoms differ from patient to patient. Therefore, some standardized approved biomarkers are used by doctor to diagnose PD. Hoehn and Yahr scale, and Unified Parkinson's Disease Rating Scales

(UPDRS) are the most common biomarker tests that are used [7] [8]. These tests are often used to rate an individual on the severity of the disease and to what extent the treatments are helping [7] [8].

According to Davie, there are no cures or medications for PD that slows or stops progression (at the time of the writing of this dissertation) [9]. However, there are treatments which are designed at supressing or reducing the symptoms associated with PD [9]. In the initial stage of PD, patients are advised against taking medication until they experience some sort of "functional disability" from the decrease in dopamine in the substantia nigra and striatum [5]. Doctors may prescribe levodopa to bring dopamine levels to normal levels, which may reduce the signs and symptoms associated with PD [10]. Medications that contains dopamine agonists (e.g., Mirapex™) can also lessen the signs and symptoms associated with PD by mimicking the actions of dopamine [11]. However, long-term usage of these medications may build tolerances and may require a change in drug [2]. An intrusive method known as Deep Brain Stimulation (DBS) or subthalamic stimulation can also be used to supress the symptoms associated with PD by electrically stimulating the basal ganglia [12]. This is done surgically by implanting electrodes into the brain so that small currents can be passed through the brain, blocking the abnormal nerve signal that causes tremors [12]. However, deep brain stimulation is only considered an option if the medical treatment is non-effective [2].

1.1.2 Essential Tremor

Essential tremor (ET) is the most common type of movement disorder that causes involuntary and rhythmic shaking of the body (e.g., most commonly the hands, head, and voice) [13]. However, it is also the least understood movement disorder as there is no known cause for this disorder [14]. There is evidence which suggests that ET is genetic; however this is not widely accepted as people with no family history of tremor sometimes develop ET [13].

According to Elble, ET is characterized by a postural and/or kinetic tremor which involves the hands and/or forearms [15]. The tremors are often stronger on one side of the body (usually dominant side) and intensifies with voluntary movements [15]. The tremors are generally within the 4-12 Hz frequency range and symptoms range from mild (e.g., difficulty in undertaking precise tasks such as threading a needle) to a severe or disabling case (e.g., require assistance to help with their daily activities such as: feeding, dressing and taking care of their personal hygiene) [16]. Individuals usually do not know they have ET and only usually find out when they seek medical attention [17].

According to Elble, the diagnosis of ET is only done through clinical observations as there are no lab tests or scans to successfully diagnose ET [15]. The neurologist will assess the individual and look for symptoms such as bilateral action tremor (postural or kinetic) of the hands and forearms and/or an isolated head tremor [15]. The neurologist will also look for symptoms such as unilateral rest tremor, rigidity and bradykinesia to rule out other possible movement disorders (e.g., PD) [15]. Once the neurologist determines that there is an absence of other neurologic signs, the doctor will use secondary diagnostic criteria to assist in the diagnosis [15]. The secondary diagnostic criteria consist of looking at family history to establish if any blood related family member ever had or has ET [17].

There is no cure for ET, but there are medications (e.g., propranolol) that could possibly be used to improve the tremors [18]. Unfortunately, it is estimated that nearly half of ET patients will not respond to the given medications. If the tremors are severe, the doctor might suggest surgical treatment such as DBS [18].

1.1.3 Huntington's Disease

HD was first discovered by George Huntington in 1872 and was originally called Huntington's chorea (where "chorea" is the Greek word for dancing) because the uncontrolled muscle movement looked like a jerky dance movement [19]. Today, HD is known as a hereditary neurodegenerative disorder, which gradually results in an uncontrolled muscle movement and coordination, psychiatric disorders, and the loss of thinking ability (cognition) [20]. These symptoms occur from the progressive breakdown of nerve cells in parts of the brain (e.g., the caudate, the putamen and, eventually, the cerebral cortex) [20].

According to Myers, the breakdown of nerve cells is caused by a specific gene called Huntingtin gene (HTT) in the alleles [21]. If one of the alleles is dominant, then HTT will be dominantly expressed [21]. A child will have a 50% chance of inheriting the disease if one the parents have HTT [21]. If the HTT gene is inherited, the individual is also at risk to develop HD in his/her lifetime [21]. The HTT's trinucleotide repeat is used to identify an individual's risk [21]. The count of the trinucleotide repeat determines the likelihood of developing HD as seen in Table 1.1.3 [20].

Table 1.1.3: Risk of developing HD by the count of trinucleotide repeat [20].

Repeat count of trinucleotide repeat	**Risk**
< 28	None – Individuals will not develop HD
29 – 34	Individuals will not develop HD; however, next generation is at risk
35 – 39	50 % - Individual may or may not develop HD, although next generation is at risk
≥ 40	Individuals will develop HD

If an individual has HD, the symptoms usually begin between 30 and 50 years of age, however symptoms can start at any age (e.g., about 8% of cases start before the age of 20 years) [22]. The progression of the disease can be tracked and is divided into three stages: early, middle and late stage [22]. Although there are only three stages, some physicians tend to add an additional stage called the prodromol stage which occurs before diagnosis [23].

In the prodromol stage, the individual shows minor signs of motor symptoms and cognitive changes. During this stage, minor motor symptoms may develop such as: difficulty with coordination of hands and abnormal eye movements. Some patients in the prodromal stage also show signs of depression, anxiety and occasionally psychosis [23]. These symptoms slowly increase over time and usually individuals seek medical attention just before the early stage of HD.

According to Ho and Nance *et al.*, an individual in the early stages of HD may show some involuntary movements (e.g., chorea occurs where unpredictable involuntary movements occur), non-coordination or difficulty in walking, changes in facial expressions and difficulty in solving problems [24] [25]. The individual also shows changes in mood and shows signs of anxiety, depression, irritability, and apathy [24] [25]. There are cognitive changes where individuals show memory loss and executive dysfunction (e.g., slow processing speed and problem solving) [24] [25]. The individual will find it more difficult to work at the level they used to work at (e.g., jobs and activities at home) [24] [25].

According to Ho and Nance *et al.*, in the middle (moderate) stage of HD, the involuntary movements increase and the individual will find it more difficult to maintain control of voluntary movements because of the fast decline in their motor functions [24] [25]. They will also have difficulties in speaking and swallowing, and their thinking and reasoning abilities will diminish progressively [24] [25]. When patients reach this stage, there is an increase in suicide rate, and this may be as a result of their loss of independence [24] [25].

According to Ho and Nance *et al*, the late (advanced) stage occurs when an individual is fully dependent on others for their care [24] [25]. There are changes in motor symptoms where they can no longer voluntarily control their muscles thus being unable to walk, speak and swallow [24] [25]. They are, however, able to recognise their families and friends and comprehend language as cognition can remain the same during this stage [24] [25]. HD usually takes between 10-25 years from early to late stage, before the person eventually succumbs to the disease [24] [25].

According to Roos, HD diagnosis, like PD, is dependent on clinical observations using neurological and psychological tests [26]. The neurologist will initially interview the individual and ask for a detailed family medical history to rule out other medical conditions [26]. The doctor will then assess the individual's physical deterioration (e.g., involuntary movement, difficulty in swallowing, talking and walking), cognitive loss (e.g., loss of focus, inability to plan, decision making, forgetfulness) and psychiatric turmoil (e.g., anxiety, depression, irritability, mood swings) [26]. If the doctor suspects that the individual has HD, then the individual may be asked to undergo further examinations for a conclusive diagnosis [26]. A brain imaging scan (e.g., computed tomography (CT) and magnetic resonance imaging (MRI)) may be used as a diagnostic tool to look at parts of the brain, specifically the caudate nucleus and putamen, to determine whether there is nerve deterioration [27]. A genetic test can also be used to analyse the deoxyribonucleic acid (DNA) in the blood for the HD mutation [28]. Once an individual has been confirmed to have HD, a Unified Huntington's Disease Rating Scale (UHDRS) is used to assess the progression of HD [29]. This scale tests for motor and cognitive functions, and not limited to behavioural abnormalities [29].

1.1.4 Biomarkers

Biomarkers are clinical and diagnostic tools that should correctly identify and observe any medical signs (e.g., health and illness related issues) accurately and reproducibly, using science [30]. Extensive research has been done in creating a biomarker to characterize different types of neurological movement disorders (e.g., PD, HD, ET, etc.); however, none has been successfully validated as an objective assessment tool [31]. Movement disorder experts, such as neurologists and doctors, rely on experience and clinical examinations to identify different types of movement disorders (e.g., the diagnosis of PD is done clinically and therefore prone to misdiagnosis as a result of human error) [32]. Studies have shown that movement disorder experts misdiagnose early

PD 10% of the time [32]. This means that among the six million people affected worldwide with PD, at least six hundred thousand will be misdiagnosed [32]. Therefore, movement disorder experts often use additional diagnostic tools or methods to prevent misdiagnosis of different diseases (e.g., genetic biomarkers, blood, cerebrospinal-fluid (CSF), tissue based biomarkers, neuroimaging).

Genetic biomarkers are used to identify certain neurological movement disorders; however, this path is often expensive and time consuming and only used as a method of elimination for HD. HD can be identified long before the first symptoms appear as the disease is caused by the trinucleotide repeat in the HTT genes. Unfortunately, there are no verified genetic biomarkers for PD and ET. However, according to Lesage, there are evidences which suggest that genetic factors may play a role in the development of PD [33]. 75% of Juvenile-onset PD (age of onset <20 years) is caused by an autosomal recessive disorder of the PARK2 or parkin gene [33]. There are test kits available commercially to quantitatively test for the PARK2, but this method is not applicable to patients who are older than 20 years, as most patients with PD (≥85%) are sporadic and not inherited [33]. Although ET is one of the most common neurological disorders, it remains poorly understood [34]. There are studies which have identified three gene loci for familial ET but more research is needed [35].

Numerous potential blood, CSF and Tissue based biomarkers have been studied, but thus far there are no blood, CSF and Tissue based biomarkers for PD, HD and ET that have been proven and validated [36]. In the case of PD, detecting the ∝-synuclein in the patient's plasma has been the most promising as it is one of the main components in Lewy bodies which develop inside nerve cells in PD. A study has shown that it detected up to 85% of PD among patients. In the case of HD, a recent study has identified a potential biomarker (mitochondrial DNA within the plasma) that can be used to track the progression of the disease in the future [37]. The study (using mice) showed that

mitochondrial DNA within the blood plasma elevated just before the first symptoms of HD appeared and decreased at later stages of the disease [37].

Neuroimaging technique such as MRI has been used to track progression and diagnosis of PD and HD, however, most neurologists and doctors avoid using this technique, as it is expensive and technically demanding [32]. A paper by Vaillancourt *et al.* has suggested that using a different MRI technique known as Diffusion Tensor Imaging (DTI) can be used to diagnose PD [38]. This technique takes images of the caudal portion substantia nigra of PD patients and compares it to age-matched healthy controls. It has successfully separated PD patients from control patients, 100% of the time [38]. However, more research is needed.

All these afore-mentioned techniques are technically challenging and time consuming, therefore many individuals and companies have sought to create "technological biomarkers" or devices to pick out unique characteristics from various movement disorders (e.g. devices which pick out freezing symptoms in PD patients throughout the day). These biomarkers are often used in conjunction with clinical observations to detect the small, but significant, changes in movement which are usually an indicator of early neurological movement disorder. Some neurologists use these devices to track the progression of the disease of an individual and some use it to check whether the medications prescribed are effective. Some of these "biomarkers" are discussed below.

APDM is a company that creates wearable technologies. The wearable sensor measures gait and balance using the gyroscope and accelerometer sensors [39]. These wearables are used to estimate the severity of movement disorders like PD [39]. The subject is required to take a predefined test to measure the subject's gait, balance and postural sway [39]. The information is then pipelined to the Mobility Lab software to analyse the subject's

result against normative values from control subjects [39]. The deviation from the normative values may suggest a neurological movement disorder [39].

MovAlyzeR by NeuroScript is a movement analysis software that measures and interprets handwriting and pattern drawings using a pen, tablet or a mouse [40]. The software automatically evaluates any possible neurological movement disorder from handwriting and pattern drawing tests (e.g., an Archimedes spiral tests is done to get movement sequence and drawing a continuous circle over a designated point on a tablet to measure both active and at-rest tremors) [40].

Despite the attempts described above, the diagnosis of neurological movement disorders today is performed clinically by movement disorder experts, using relative scales, and there are no verified biomarkers that have been successfully validated as an objective assessment tool [31]. There have been many potential biomarkers that have been brought out commercially as seen in [39] and [40], but they are either too expensive or not effective at all. However, through years of research and using existing biomarkers, clinicians agree that measuring the movement profiles that exhibit symptoms (e.g., rest tremors, weakening of their muscles, etc.) from their fingers, hands and arms could potentially be the key to creating a successful biomarker. A device can be programmed and trained to pick out these subtle differences from the patient's neurological movement disorder symptoms. Hopefully this will enable a new biomarker device to be created, so that it may be able to successfully categorise the different movement disorders with minimal misdiagnosis.

2 METHODOLOGY

2.1 Leap Motion

A gaming device called a Leap Motion has been used in this study. A Leap Motion camera is a commercially available peripheral device that is designed to be placed on any desktop environment. It plugs into a computer via an USB cable and works on any Windows, Mac or Linux platforms. It senses the movement of the hands, using infrared lights in a hemispherical area. Through clever filtering, processing and complex mathematics, the movement is mimicked and displayed onto the computer screen.

The Leap Motion has dimensions of 12.7mm x 30.48mm x 76.2mm. It has two infrared cameras which process images at a rate of 200 frames per second (fps). It has an interaction area of 150˚ (angle) long side and 120˚ (angle) short side with interaction distance of 600mm above and each side of the controller.

2.2 Leap Motion Location Setup

The Leap Motion controller is a mobile device; therefore, a location to place the Leap Motion was required. The best location to place the device (in terms of manoeuvrability and ergonomics) was found to be between the keyboard and the subject. This enabled the hand to move freely while keeping the elbow down and bent. Therefore, the Leap Motion controller was placed in front of the keyboard. The location of the Leap Motion controller relative to the laptop is in figure 2.2.1, figure 2.2.2 and figure 2.2.3. This ensured the measurements were repeatable and reproducible under the same conditions.



Figure 2.2.1: Top view configuration of the Leap Motion with the laptop.

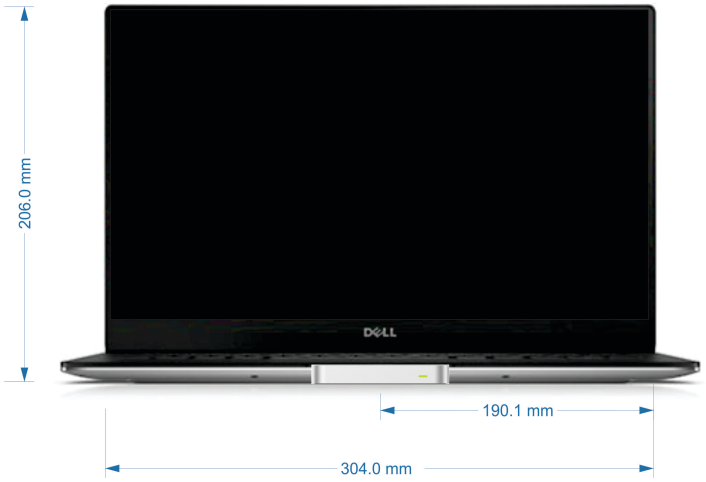

Figure 2.2.2: Front view configuration of the Leap Motion with the laptop.



Figure 2.2.3: Side view configuration of the Leap Motion with the laptop.

The Leap Motion controller uses a right-hand coordinate system in millimetre. Its frame of reference is the device itself where a coordinate of [50, 50, -50] means x=+5cm, y=+5cm and z=-5cm from the origin which is located at the top and the centre of the device. The Leap Motion controller will be used to track the tip of patient's dominant index fingertip position which will be recorded onto a text file.

2.3 Leap Motion Software Setup

A software was created to replicate the hand and finger movements on the computer screen using the C++ programming language with OpenCV and Leap Motion native libraries. The development of this software application is shown in Appendix B. However, there were three problems associated with using this methodology.

The first problem that was noted was that there was a distinct lag between the movement of the hands and the tracking points on the screen. This created an illusion of the finger dragging the tracking points. The second major problem was that the Leap Motion device's recording time interval would jump between 80 and 200 fps. A constant fps was required to match the time interval between the movement of the finger and the collection of the data to minimize aliasing. The third and final problem was that the 3-dimensional

movement (X, Y and Z components) of the hand and fingers projected as a 2-dimensional movement (X and Y components) on the computer screen. This created an unwanted distortion in data capture because the people participating in the experiment would forget that there are Z components and only focus on the X and Y axis movement. It was then decided to take a different approach after much debate.

The author then decided to use the Leap Motion Diagnostic Visualizer tool provided by Leap Motion to view motion tracking data generated by the Leap Motion Controller. This solved all the problems noted in the previous attempted application. The Leap Motion Diagnostic Visualizer tool eliminated the lag between the movement of the hands and the tracking points on the screen. The data collection time interval could also be set at a constant 200 fps. The Leap Motion Diagnostic Visualizer tool also replicated the hand and fingers movement visually. The only problem that was noted was that the tool was not an open source platform, therefore the step-up, triangular and circular patterns could not be drawn and integrated with the Leap Motion Diagnostic Visualizer tool. This problem was easily fixed by tracing out the required pattern on a transparent plastic sheet and placing it on top of the screen. This solved the ‘lag’ problem that was experienced by the previous application.

The grid provided by the Leap Motion Diagnostic Visualizer tool as seen in figure 2.3.1 has the following borders: top-left corner (-250; 350), top-right corner (250; 350), bottom-left corner (-250; 0) and bottom-right corner (250; 0). Therefore, it was easy to further optimize the application to only record data when the patient’s finger crosses the X-axis at -250.

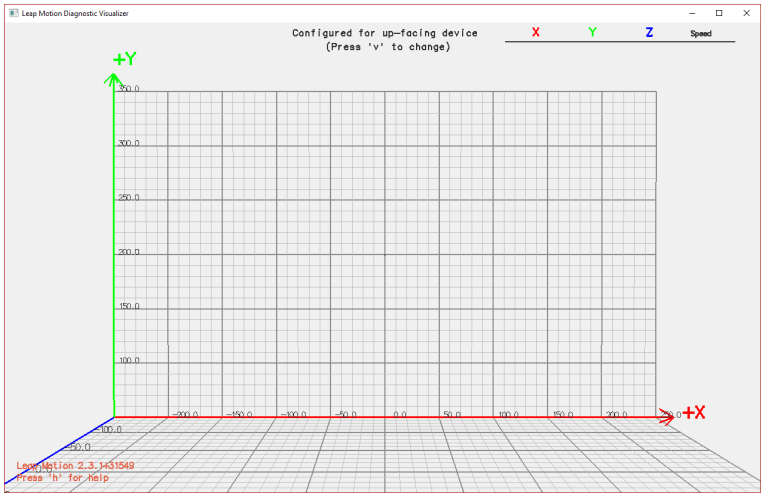

Figure 2.3.1: The Leap Motion Diagnostic Visualizer [41].

2.4 Patients Recruitment

The patients were recruited at the Wits Donald Gordon Medical Centre (WDGMC) and Charlotte Maxeke Johannesburg Academic Hospital in terms of the ethics application (Appendix A). All 3 patients' types: PD (8 patients), HD (4 patients) and ET patients (5 patients), as well as control subjects (10 subjects) from the staff at the School of Electrical and Information Engineering at the University of the Witwatersrand, Johannesburg participated. All patients and control subjects had the procedure explained and signed an informed consent form. No deviation from the patients' treatment regimens were performed for this study. However, some patients with PD were required to be on medication and others were off medication for their routine clinical assessment, and this information was noted so that these differences could be compared.

3 CONTROL SYSTEMS MODELLING APPROACHES

Extensive research has been done throughout the years by researchers in the field of biology and robotics to understand and develop control theory models (e.g., feedback system), that describes the automatic control systems of the human body. Examples of a control system model of the human body includes but is not limited to: the temperature regulatory system, the action potential of nerve cells and the mechanical movements of the human arm and hands. These control systems are often modelled successfully using appropriate mathematical models (e.g., mechanical, electrical, and thermal systems) that are derived from physical laws and experimental data. Once derived, these models are tested and validated to the system from which it was modelled (e.g., the temperature regulatory system model should behave similarly to the human regulatory system with the same given input). However, most individuals will have a different control system model, therefore the modelled system is adjusted to have certain parameter ranges which it must lie in, to accommodate most people. Any model that deviates from the "validated" model will indicate that something is inherently wrong. Therefore, it was only logical to use similar control modelling techniques to see whether the different neurological movement disorders (e.g., PD, HD and ET) have different control system models.

Movement disorder experts, such as neurologists, rely on experience and clinical observation to differentiate various neurological movement disorders. They observe muscle movements which are normally the characteristic traits of movement disorders (e.g., tremors, muscle rigidity, walking, etc.). Therefore, in this research, the patient's hand and arm mechanical movements were studied as a control system because it was assumed that the control system of the patient without movement disorders would be different to that of patients who have some sort of movement disorders.

3.1 PID Model

The signals captured from the patients were modelled as the output of following unity feedback system in figure 3.1.1. This model was chosen because many studies have been done to show that a human body consists of many control systems that can be modelled as a unity feedback system, e.g. the simple act of pointing a finger at an object or a temperature regulatory system (homeostasis) [42]. Wiener, proposed that the best technique for modelling both living and mechanical systems are information theory and feedback control theory [43].

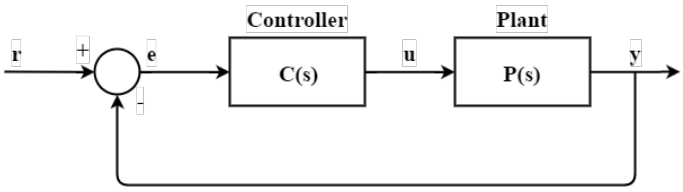

Figure 3.1.1: A diagram of a unity feedback system.

A simple Proportional, Integral and Derivative (PID) controller (C(s)) was chosen to be used as a controller for the plant (P(s)) which is the human hand/arm model. A PID controller was chosen as a controller, as there are many articles which describe them as having a greater tracking capability than other controllers when using it to control a robotic hand. A Simulink model is shown in figure 3.1.2.

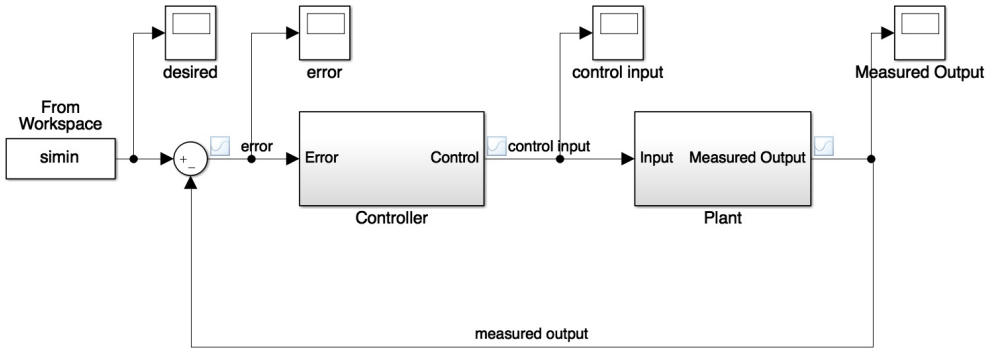

Figure 3.1.2: Simulink model of a PID.

The plant model chosen was a simple spring-mass-damper system because a lot of research has been done in modelling human organs as a three-parameter mass–spring–damper system [44] [45]. Speich *et al*, describes the development of a linear lumped-parameter hand and arm model for the tele-manipulation system [46]. They modelled the dynamics of the human arm and hand as a spring and damper model shown in figure 3.1.3 [46].

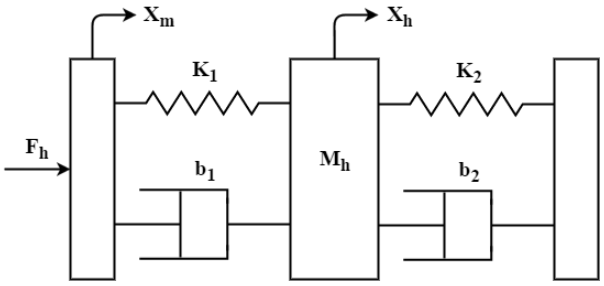

Figure 3.1.3: Spring-damper human arm/hand model [46].

Speich *et al.* labelled the motion of the human arm as x_h, the mass as m_h, the contact force between the manipulator (machine that measures hand movements) and the human as F_h, and the motion of the manipulator as x_m. In addition, Speich *et al.* has given the stiffness coefficient of the human as K_1 and K_2, and the damping coefficient of the human

as b_1 and b_2. They then converted the equation of motion for the mass of the human, m_h, as a Laplace notation shown in equation 1 [46].

$$\frac{x_m}{F_h} = \frac{(m_h s^2+(b_2+b_1)s+(K_2+K_1))s}{m_h b_1 s^3+(m_h K_1+b_1 b_2)s^2+(K_1 b_2+b_1 K_2)s+K_2 K_1} \quad (1)$$

The best parameters for the human hand/arm model are when: b_1=4.5 Ns/m, b_2=7.9 Ns/m, K_1=48.8 N/m, K_2=375 N/m and m_h=1.46 kg [46].

The proposed idea was to tune the PID controller parameter for each of the patient's dataset that best describes the captured data (y) for a given simulated data (r). The simulated data (r) was the actual path the patient traced that was on the computer screen (e.g., step function, triangular function and circle) and the captured data (y) would be the measured data from the Leap Motion. It was aimed that the optimal controller's transfer function for each of the different neurological movement disorders be found and plotted on a pole-zero plot to compare stability.

However, some problems were encountered when going this route. One of the problems was that the human hand/arm plant parameters from Speich *et al.* were from data acquired from subjects who did not have any neurological movement disorders. An incorrect PID tuning would result from using the same human hand/arm plant parameters plant models for PD, HD and ET patients, who may be different due to factors such as a decrease in muscle strength. This may result in an incorrect conclusion from biased parameters. However, a confirmation on this conclusion is required.

This model may also be used as a selection tool to see whether an individual may or may not have any movement disorder. This can be done by creating a model from subjects who did not have any neurological movement disorders and plugging in various PD, HD and ET patient's data to see if the model behaves correctly. If the model behaved correctly, one can assume that the subject does not have any neurological movement

disorders and vice versa. However, this approach may not work because the plant model from subjects who did not have any neurological movement disorders may be able to replicate patient's, who have neurological movement disorders, control model. There are many factors that influences the result and therefore more research is needed.

The same experiment using the tele-manipulation system needs to be done on PD, HD and ET patients to determine their best parameters respectively to objectively compare their PID pole-zero plots to compare stability. Therefore, a new unbiased model needed to be developed and the next logical step would be to model the control process as a black box model.

3.2 Black Box Model Method

It was determined that the best approach was to treat the control process as a black box model that has just an input (the patterns the patient sees on the computer screen) and an output (patient's hand and arm movement data that were collected from Leap Motion controller). All the required information would be contained within the black box model (e.g., PID controller, plant and feedback mechanism) which eliminates the need to "guess" the patient's model. This resulted in a more accurate model of movement of patients with various neurological movement disorders.

MATLAB's system identification tool (shown in figure 3.2.1 below) was used to find the transfer function using data obtained from the PD, ET and control subjects for each of the patterns. HD patient's data were collected but was not used, as most of them struggled to complete the given tasks as they were in the late stages of HD.

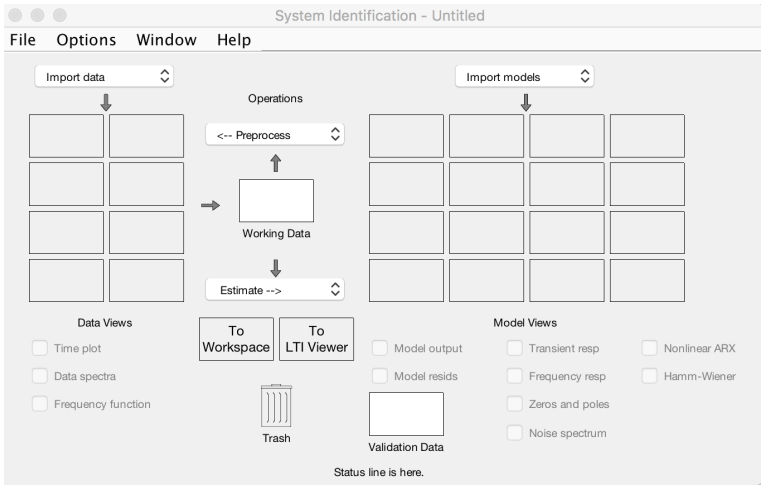

Figure 3.2.1: MATLAB's system identification toolbox.

Before the system identification tool was used, each of the patient's measured data was separated into its X, Y and Z components. An example of PD patient's X, Y and Z-axis data from the step-function pattern is shown in figure 3.2.2.

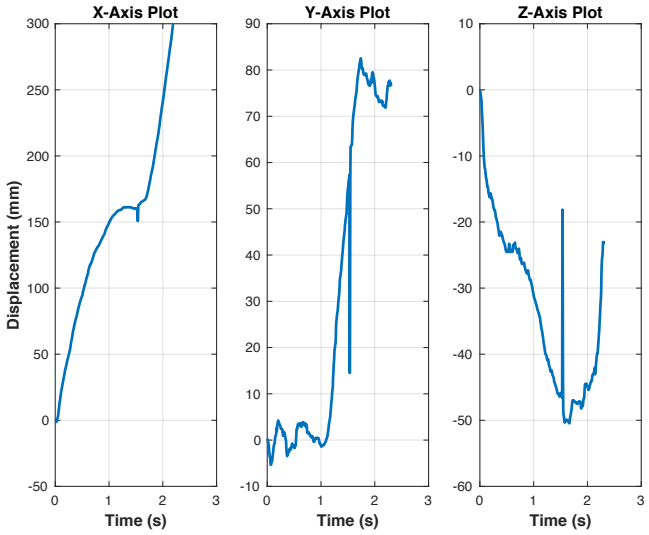

Figure 3.2.2: An example of an X, Y and Z axis plot from control subject 1.

The modelling and analysis was carried out for each of the three types of inputs separately: step-function, triangular and circular patterns and for the X and Y signals separately. The Z axis signals were not analysed due to time constraints. The signal was broken down into its their respective vectors and analysed independently. This allowed the data to be plotted on a Cartesian coordinate system that could be easily analysed without complexity.

The process of finding the transfer functions using the toolbox was as follows: The input signals were the data the patients had to follow on the screen (e.g., X-axis trajectories and it's time component) and the output signals were the patient's tracking data taken from the Leap Motion device. The signals were imported and the sample time with respect to $200Hz$ (0.005s) and starting time (set to 0 as the data was captured initially) were inserted in the toolbox fields as shown in figure 3.2.3.

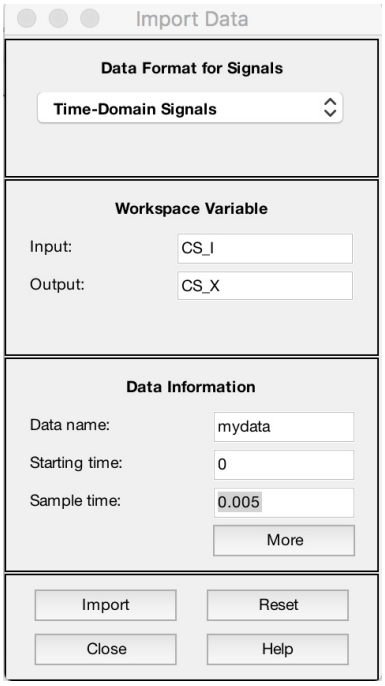

Figure 3.2.3: Importing data using the system identification toolbox.

A transfer function model was then estimated by the toolbox as shown in figure 3.2.4.

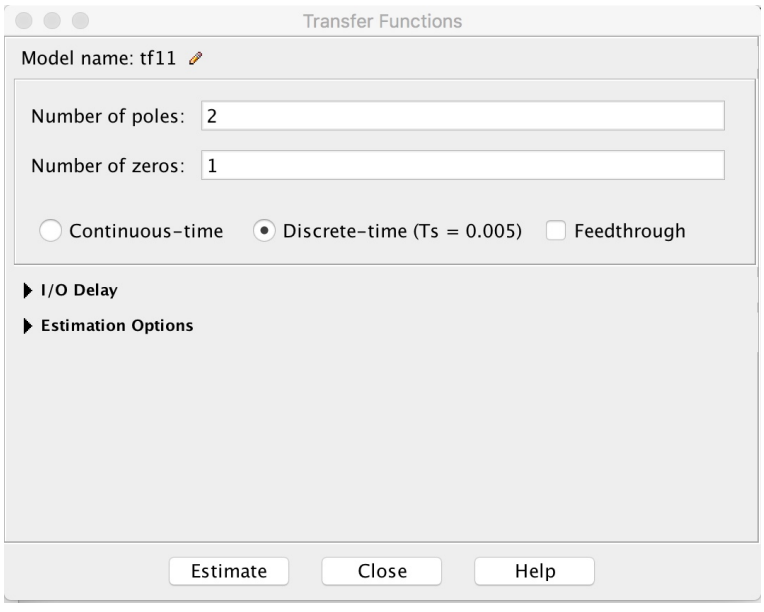

Figure 3.2.4: Transfer Functions estimation

The system identification tool requires an input of the number of poles and zeros chosen for the transfer function. This choice was performed iteratively, using the MATLAB's

Normalized Root Mean Square (NRMSE) criterion to determine goodness of fit, and searching for the best match among the following choices. The MATLAB's NRMSE criterion is given mathematically in equation 2 [48].

$$fit = 100(1 - \frac{\|y-\hat{y}\|}{\|y-mean(y)\|}) \quad (2)$$

where y is the validation data output and $\hat{y}$ is the system generated output and is calculated in percentage [48].

Initially, a second order transfer function with two poles and no zeros were estimated as a reference. Thereafter a second order transfer function with one zero and two poles were estimated and compared to the transfer functions with two poles and no zeros to see which estimation best described the patients. A second order transfer function was chosen as a starting point as it was the simplest model and the minimum order at which oscillation and damping could be captured. It was also the minimum model that could generate the results.

The NRMSE criterion was used as a threshold to exclude from the analysis cases where the model does not fit the actual trajectory and therefore no features can be derived from it. The threshold was chosen as 50% NRMSE using MATLAB's "goodnessOfFit" function. This 50% NRMSE criterion was heuristically selected by the author and is trade-off to include as much data as possible while maintaining an adequate fit between measured and simulated data. A higher NRMSE threshold selection would have resulted in insufficient data to analyse.

Only trajectories that exceeded this threshold were included in the pole-zero analysis. Separate analysis on X and Y coordinates of the signal was adequate for trajectories of angular shapes (step and triangles). For the circular trajectories, a polar analysis was performed and an R^2 signal was calculated from the circle pattern's X and Y signals. An

additional spectral analysis for the R^2 signal was performed using MATLAB's Fast Fourier Transform (FFT).

4 RESULTS

The data was collected from 10 control subjects, 5 ET patients and 8 PD patients (before and after medication). Fortunately, all 10 control subjects and 5 ET patients could complete all the trajectories in the experiment's protocol. Unfortunately, there were some inconsistencies with PD patients. All 8 PD patients (before and after medication) could complete the step-function pattern test, however out of the 8 PD patients, only 4 PD patients could complete the triangle and circle pattern test. This was mainly due to the PD patients wanting to take their medications as soon as possible after the consultation. In some cases, the PD patients could complete only one of the four repeated triangle shapes that was shown on the screen. Therefore, computational analysis was performed only on one triangle pattern to ensure consistency of data analysis. Some data are omitted as some patients were not able to complete the task given. Only data that consisted of full tasks was analysed.

Two examples of a transfer function match are presented in figures 4.1 and 4.2, where the subject's data is shown as a black line and a simulated output from the same subject's estimated transfer function is shown as a blue line. Both cases are control subject's X-axis data for a step-function trajectory. The graph on figure 4.1 demonstrates a best fit of 95.0% using MATLAB's NRMSE criterion, whereas the second case is an example of a transfer function match of less than 50% as shown in figure 4.2.

Although the measured data for both cases (figures 4.1 and 4.2) may seem superficially similar, MATLAB produced two very different transfer functions because they are, in fact, different. For example, when comparing the time axes one can observe that one motion is much slower than the other.

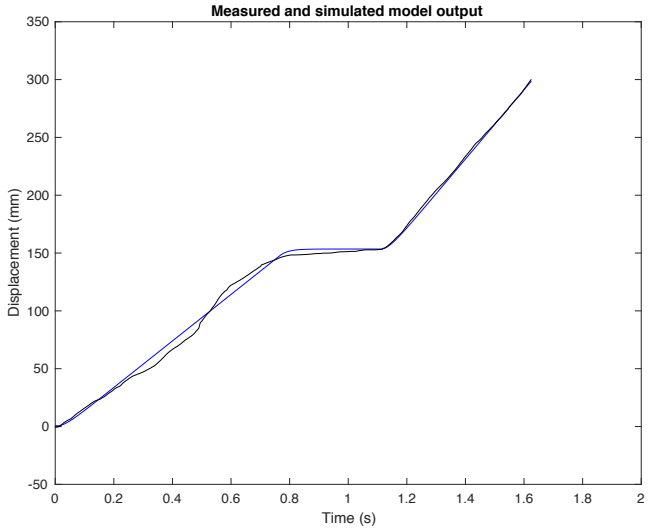

Figure 4.1: Measured (black) and simulated model (blue) output of control subject 10 with 95.0% best fit.

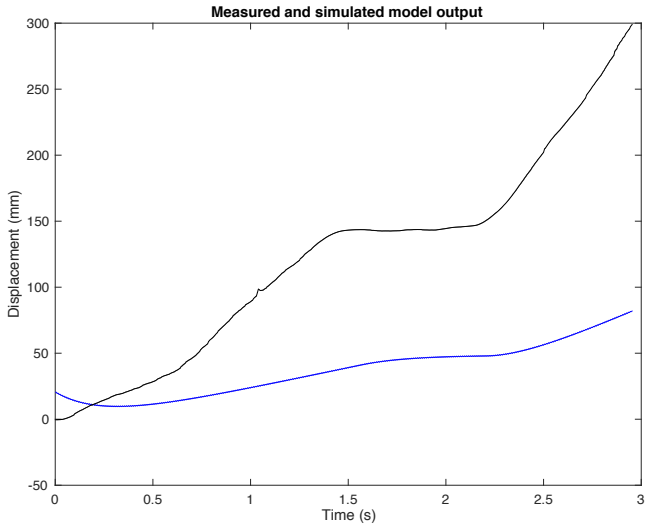

Figure 4.2: Measured (black) and simulated model (blue) output of control subject 3 with -34.3% best fit.

Obviously, any further analysis of the transfer function in figure 4.2 cannot yield reliable results. All cases where the estimated transfer function match was lower than 50% using MATLAB's NRMSE criterion were thus rejected and not included in the analysis from

the step-function, triangular wave and circle pattern. The exclusion of inaccurate models could result in skewing the results. However, this dissertation concentrates on developing the methodology for finding a biomarker and the validity of modelling. Thus, the removal of inaccurate models was necessary to perform the analysis involved. The analysis for the first case, of subject 1, where matching was good is presented in figure 4.3.

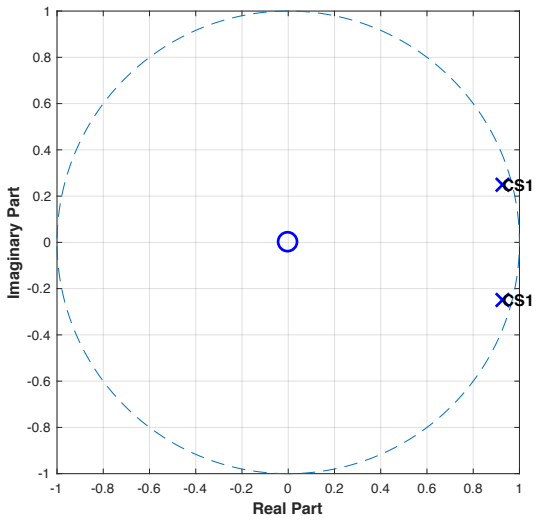

Figure 4.3: Pole-zero plot of the estimated transfer function for control subject 1.

The zero of the estimated transfer function, with two poles and one zero, has a very small magnitude (close to 0) and therefore looked like a transfer functions with no zeros. It was concluded that the number of zeros did not influence the model and therefore all transfer functions were modelled with two poles and one zero.

The black box model analysis for the three trajectories performed in the protocol: step-function, triangular wave and circle are described in the following sections: 4.1, 4.2 and 4.3. Conjugate counterparts do exist and are a mirror image. However, only one quadrant of the complete z-plane was shown to see the pole-zero plots clearly.

4.1 Black Box Model: Step Function Pattern

The process shown above was applied with all the PD, ET and control subject's X and Y-axis data and each of the subject's pole-zero plots and trajectories are given in Appendix C. The pole-zero plots from each subgroup: control subjects, ET patients, PD patients before medication and PD patients after medication are then combined and plotted in figures 4.1.1, 4.1.2, 4.1.3 and 4.1.4 respectively. However, control subjects (3, 6 and 8), ET patients (1 and 5) and PD patients after medication (8 and 4) have been excluded from the pole-zero plots as their best fit lines (shown Appendix C) did not meet the threshold criteria. These pole-zero plots have been excluded from the figures as the transfer functions involved do not pass the fit criterion. This also can be seen visually from the large differences between the measured and simulated best fit lines.

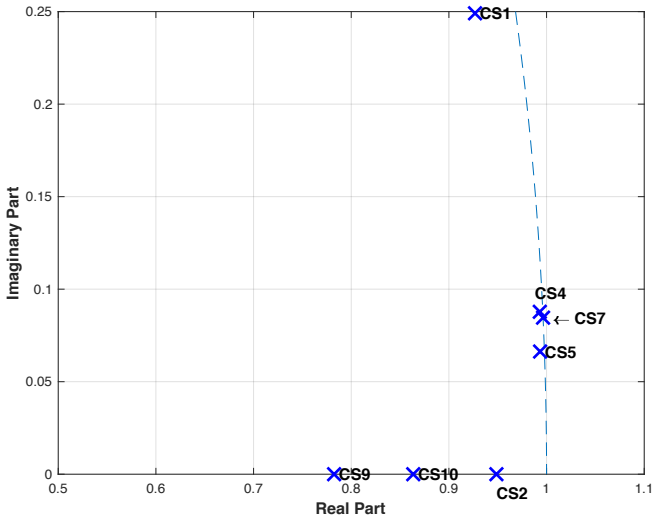

Figure 4.1.1: Combined X-axis data pole-zero plot for control subjects (blue) - conjugate counterparts are mirror image.

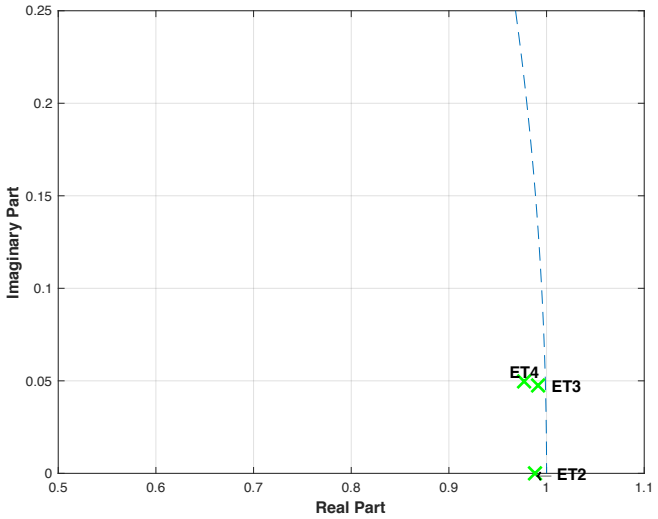

Figure 4.1.2: Combined X-axis data pole-zero plot for ET patients (green) - conjugate counterparts are mirror image.

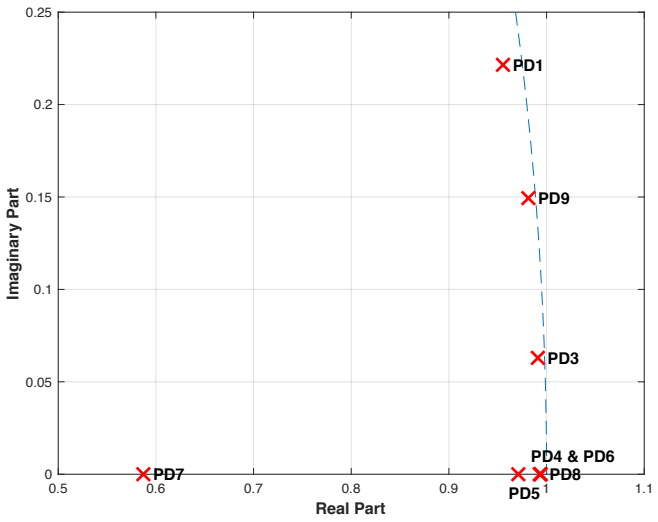

Figure 4.1.3: Combined X-axis data pole-zero plot for PD patients before medication (red) - conjugate counterparts are mirror image.

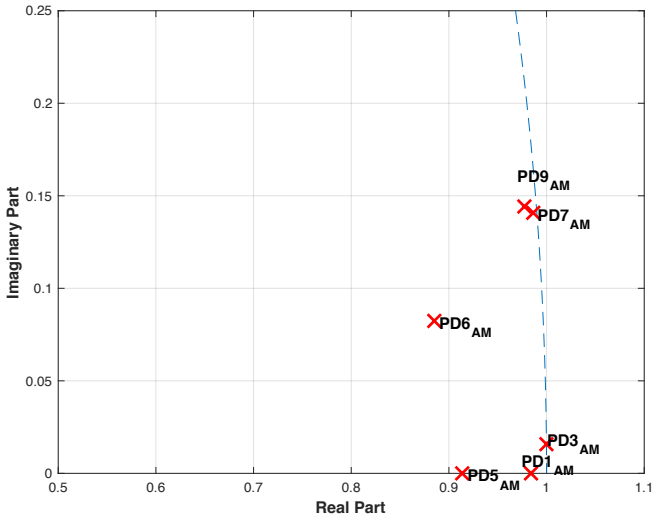

Figure 4.1.4: Combined X-axis data pole-zero plot for PD patients after medication (red) - conjugate counterparts are mirror image.

The pole-zero plots shown in figures 4.1.1, 4.1.2, 4.1.3 and 4.1.4 show that all the estimated transfer functions are stable because the poles are within the unit circle. The poles on the real-axis with no imaginary components, may indicate that their transfer function have an exponentially decaying property. The transfer functions that have poles with imaginary component may indicate that the system have a damped oscillatory property. The results above indicate that using a 2nd order transfer function to describe the subject's X-axis step-function pattern data is not good enough to distinguish between different diseases and controls. A higher order poles may be required to effectively describe the test subject's X-axis data.

Although not entirely useful, a comparison between each of the movement disorders was plotted to see if there were any clear distinctions (e.g., areas, patterns) between them. This was done to give more insight into the sizes of the parameters involved i.e. the inaccuracies within a class can be much smaller than the differences between classes. The pole-zero plots between control subjects and ET patients, control subjects and PD patients

(before medication), control subjects and PD patients (after medication), and PD patients (before medication) and PD patients (after medication) are shown in figures 4.1.5, 4.1.6, 4.1.7 and 4.1.8 respectively.

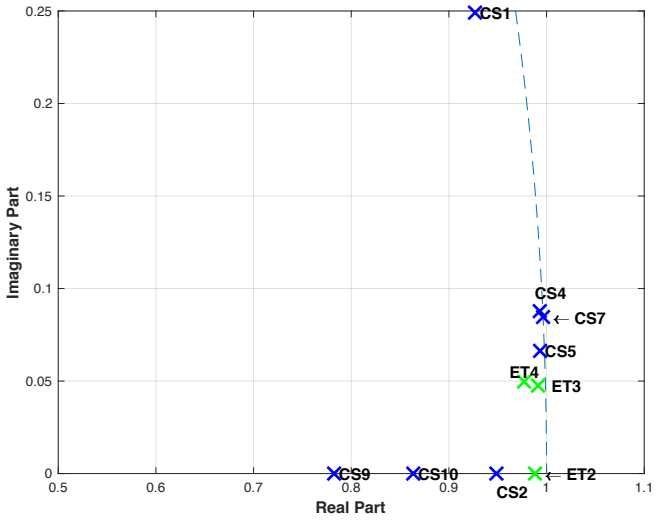

Figure 4.1.5: Pole-zero plot between the control subjects (blue) and ET patients (green) using X-axis data - conjugate counterparts are mirror image.

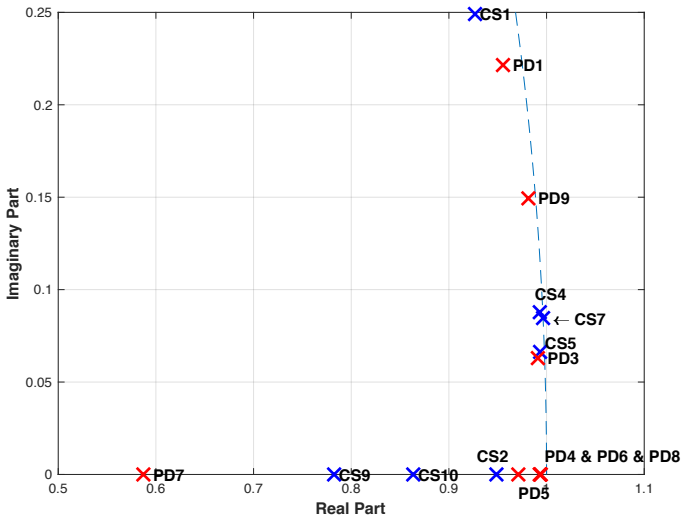

Figure 4.1.6: Pole-zero plot between control subjects (blue) and PD patients before medication (red) using X-axis data - conjugate counterparts are mirror image.

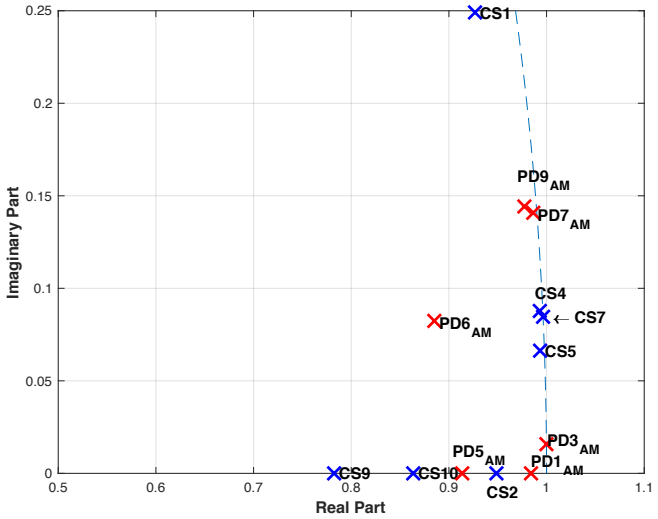

Figure 4.1.7: Pole-zero plot between control subjects (blue) and PD patients after medication (red) using X-axis data - conjugate counterparts are mirror image.

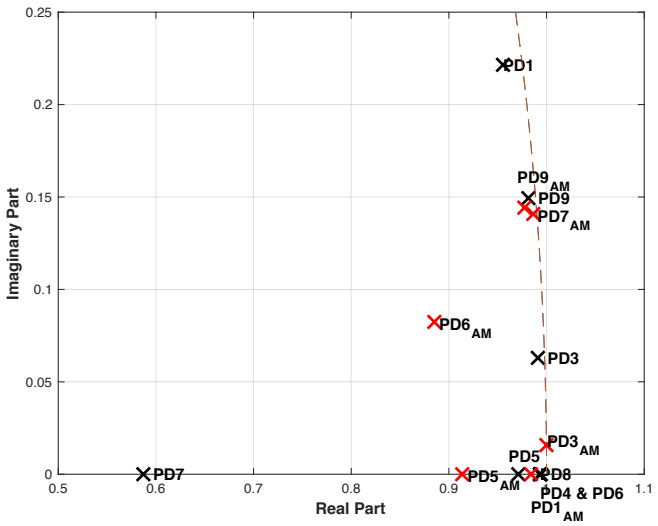

Figure 4.1.8: Pole-zero plot between PD patients before medication (black) and PD patients after medication (red) using X-axis data - conjugate counterparts are mirror image.

The pole-zero plots between control subjects and PD patients before medication in figure 4.1.6, control subjects and PD patients after medication in figure 4.1.7, and PD patients

before medication and PD patients after medication in figure 4.1.8 shows that no definite distinct areas or patterns can be made within the plots. However, the control subjects and ET patients in figure 4.1.5 shows areas of separation between them. This needs to be verified by obtaining more data.

The pole-zero plots and trajectories of the Y-axis data for all subjects are shown in Appendix C. An example of a "good" Y-axis plot is shown below in figure 4.1.9. The combined pole-zero plots from control subjects, ET patients and PD patients before medication and PD patients after medication are shown in figures 4.1.10, 4.1.11, 4.1.12 and 4.1.13 respectively.

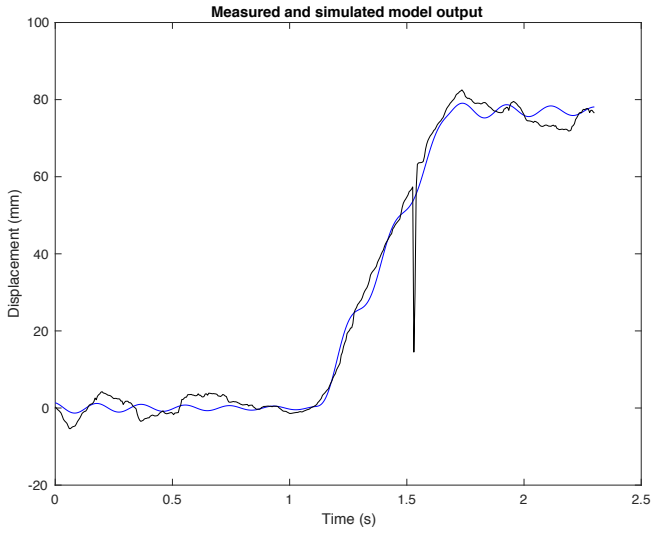

Figure 4.1.9: An example of a Y-axis measured data plotted against simulated output data from the step-function pattern with 90.2% best fit.

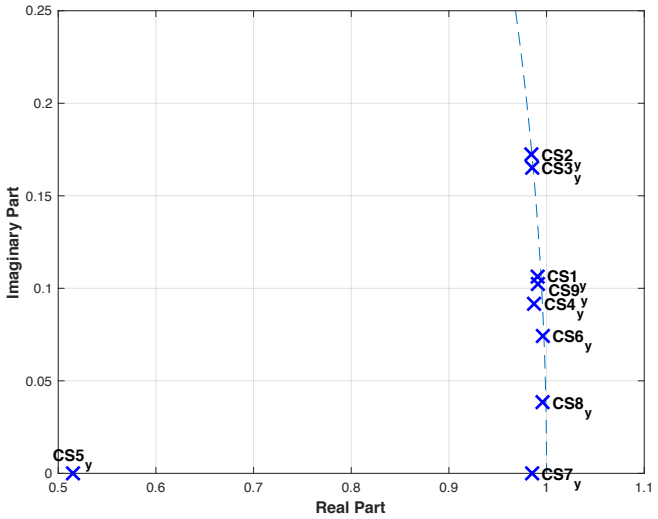

Figure 4.1.10: Combined Y-axis data pole-zero plot for control subjects (blue) - conjugate counterparts are mirror image.

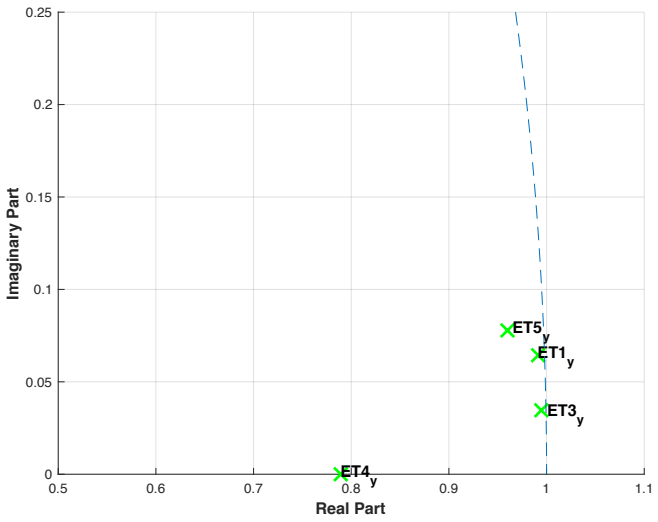

Figure 4.1.11: Combined Y-axis data pole-zero plot for ET patients (green) - conjugate counterparts are mirror image.

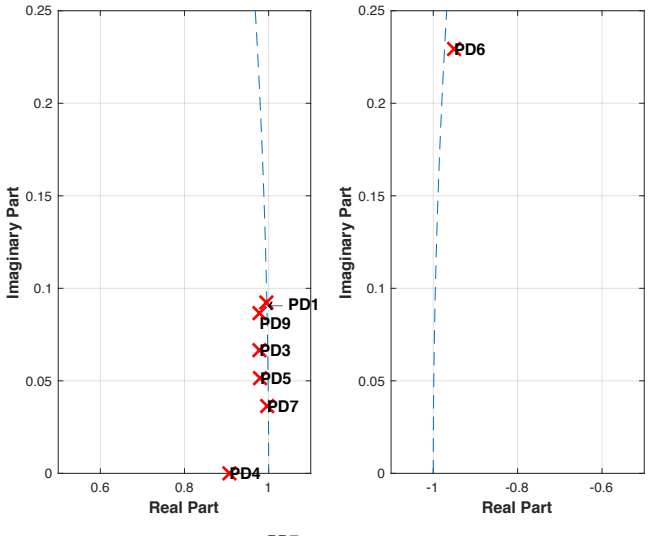

Figure 4.1.12: Combined Y-axis data pole-zero plot for PD patients before medication (red) - conjugate counterparts are mirror image.

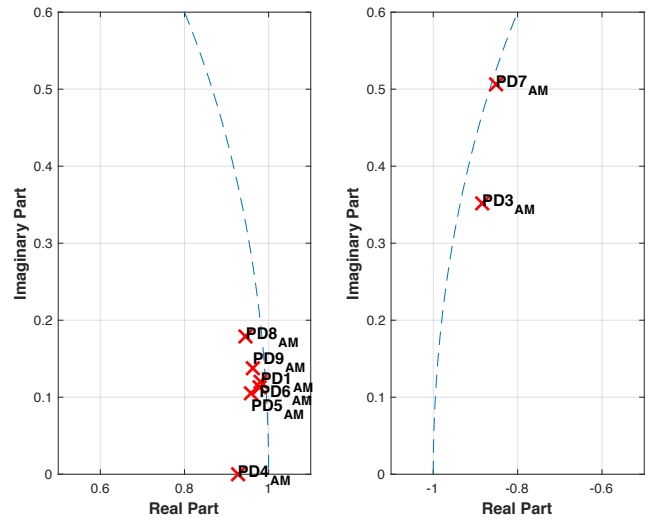

Figure 4.1.13: Combined Y-axis data pole-zero plot for PD patients after medication (red) - conjugate counterparts are mirror image.

The pole-zero plots shown in figure 4.1.10, 4.1.11, 4.1.12 and 4.1.13 show that a 2nd order transfer function can be used to describe the subject's Y-axis data from the step-function

pattern as different diseases and controls could be distinguished. A higher order pole's transfer function is not required to effectively describe the test subject's Y-axis data.

A comparison between each of the movement disorders were then plotted to see if there were any clear distinctions (e.g., areas, patterns) between them. The pole-zero plots between control subjects and ET patients, control subjects and PD patients (before medication), control subjects and PD patients (after medication), and PD patients (before medication) and PD patients (after medication) are shown in figures 4.1.14, 4.1.15, 4.1.16 and 4.1.17 respectively.

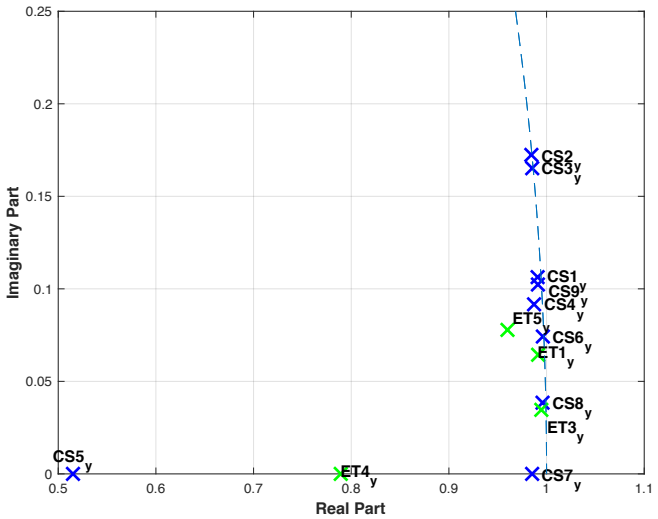

Figure 4.1.14: Pole-zero plot between control subjects (blue) and ET patients (green) using Y-axis data - conjugate counterparts are mirror image.

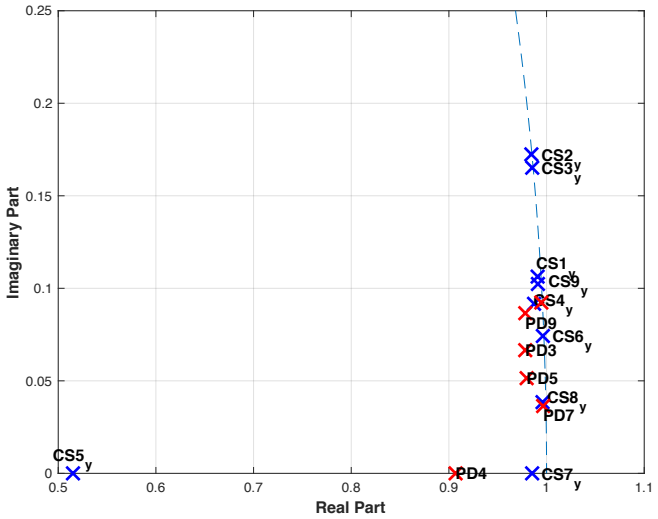

Figure 4.1.15: Pole-zero plot between control subjects (blue) and PD patients before medication (red) using Y-axis data - conjugate counterparts are mirror image.

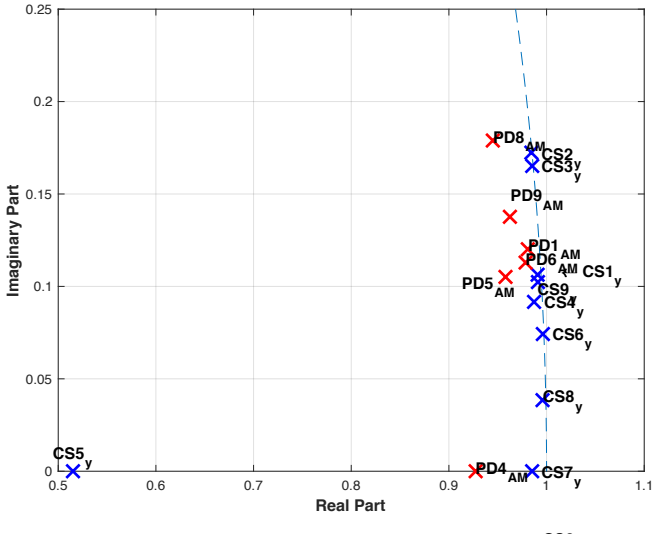

Figure 4.1.16: Pole-zero plot between control subjects (blue) and PD patients after medication (red) using Y-axis data - conjugate counterparts are mirror image.

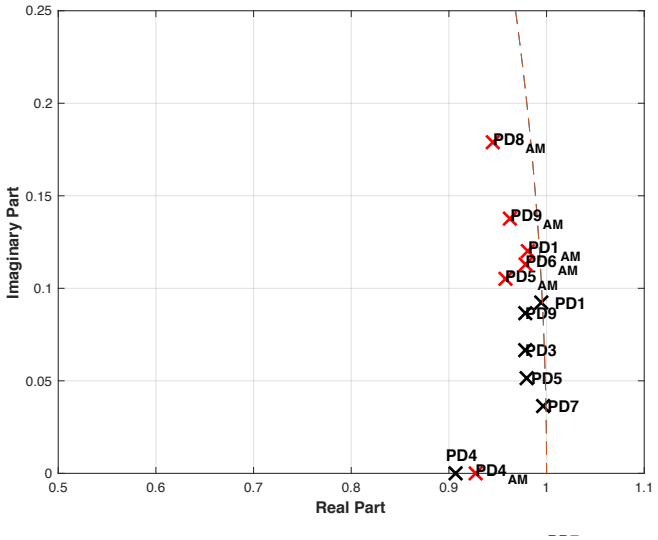

Figure 4.1.17: Pole-zero plot between PD patients before medication (black) and PD patients after medication (red) using Y-axis data - conjugate counterparts are mirror image.

The pole-zero plots between the control subjects and ET patients in figure 4.1.14 and control subjects and PD patients before medication in figure 4.1.15 shows that the poles are within similar areas and therefore no patterns or areas could be determined.

However, the pole-zero plot between the control subjects and PD patients after medication in figure 4.1.16 shows that there is a trend differentiating between PD patients after medication and controls. The poles of the transfer functions associated with these patients (after medication) have separate areas from the control subjects' transfer functions poles area. This can be visually observed in the figure's red crosses and blue crosses distinct areas. This is seen by the red crosses having distinct areas to that of the blue crosses even though they are close to each other. However, more PD patient's Y-axis data (after medication) from the step-function patterns are needed to verify the trends. The trends are reliable because the estimated transfer functions of the control subjects and PD patients (after medication) closely resembles the measured Y-axis data from the step-

function pattern (e.g., the average best fit for control subject's Y-axis data was 79.2% while the average best fit for PD patient's Y-axis data (before medications) was 77.0%).

Similarly, the pole-zero plot between PD patients before medication and PD patients after medication in figure 4.1.17 also shows distinct areas of separation within the pole-zero plot. The PD patient's poles (before medication) and PD patient's poles (after medication) are each clumped into their respective areas where PD patient's poles (before medication) poles are shown to have a larger imaginary part. However, more PD patient's Y-axis (before and after medication) data from the step function pattern are needed to verify the trends. The trends are reliable because the outputs of the estimated transfer functions of the PD patients (before and after medication) closely resembles the measured Y-axis data from the step-function pattern (e.g., the average best fit for PD patient's X-axis data (before medication) was 77.0% while the average best fit for PD patient's X-axis data (after medications) was 78.9%).

A conclusion was drawn that more step-function patterns for Y-axis data from PD patients (before and after medication) are required to distinguish between the categories. The step-function's analysis using Y-axis data and using a 2nd order transfer function showed promising results. Whereas using a 2nd order transfer function for the X-axis data from the step-function signal was not accurate enough. But why the differences?

An a priori assumption could be that the two degrees of movement would require the same control system, however the data shows otherwise, and implies that the body uses a different control system for the X and Y motion. Further research is required to verify this hypothesis.

4.2 Black Box Model: Triangle Pattern

The control subjects, ET and PD patients had to follow a repeated triangle pattern after they completed the step-function pattern test. Similarly, to the step-function test, the repeated triangle pattern was shown on the computer screen and the subjects had to trace the pattern using their dominant fingers using the Leap Motion. During data cleaning, the X and Y-trajectories were separated for all the test subjects. Only one triangle from the repeated triangle data was chosen because most of the test subjects drew one to two successful triangle patterns only. An example of a "good" X-axis plot for the triangle pattern is shown below in figure 4.2.1.

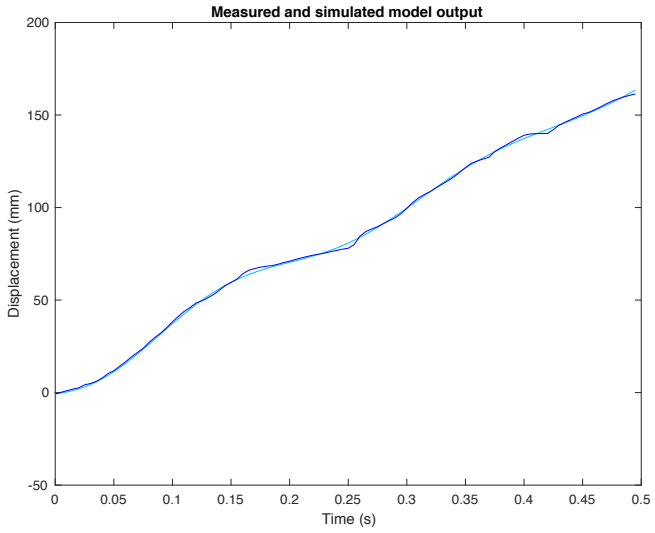

Figure 4.2.1: An example of an X-axis measured data plotted against simulated output data from the triangle pattern with 98% best fit.

This chapter explores the subject's X and Y-axis data from one triangle pattern. Each of the control subjects, ET and PD patient's X and Y-axis pole-zero plots and trajectories are given in Appendix D.

The X-axis pole-zero plots from the control subjects, ET and PD patients (before and after medication) are then combined into their respective groups and plotted in figure 4.2.2, 4.2.3, 4.2.4 and 4.2.5 respectively.

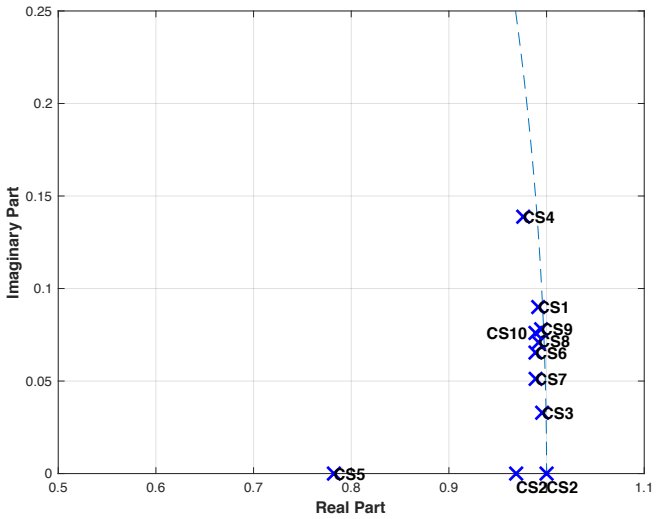

Figure 4.2.2: Combined X-axis data pole-zero plot for control subjects (blue) - conjugate counterparts are mirror image.

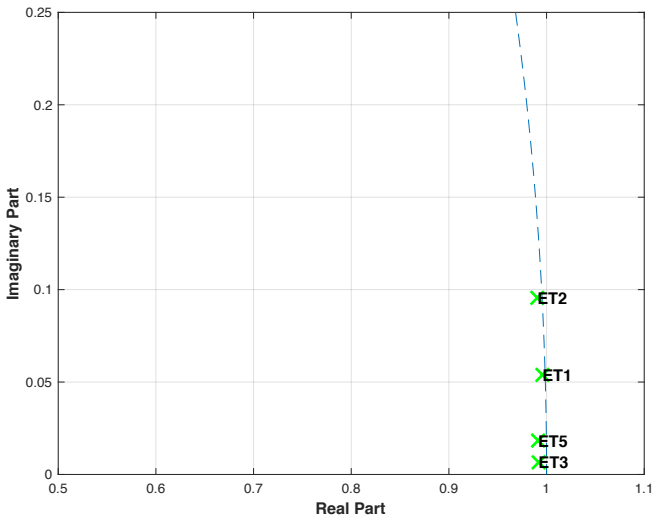

Figure 4.2.3: Combined X-axis data pole-zero plot for ET patients (green) - conjugate counterparts are mirror image.

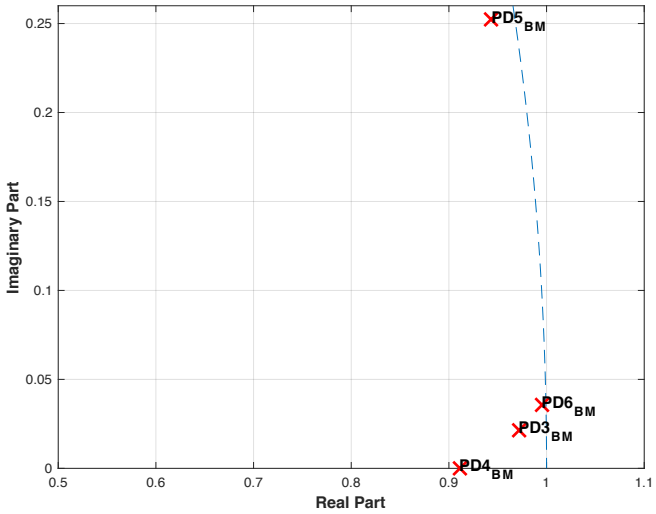

Figure 4.2.4: Combined X-axis data pole-zero plot for PD patients before medication (red) - conjugate counterparts are mirror image.

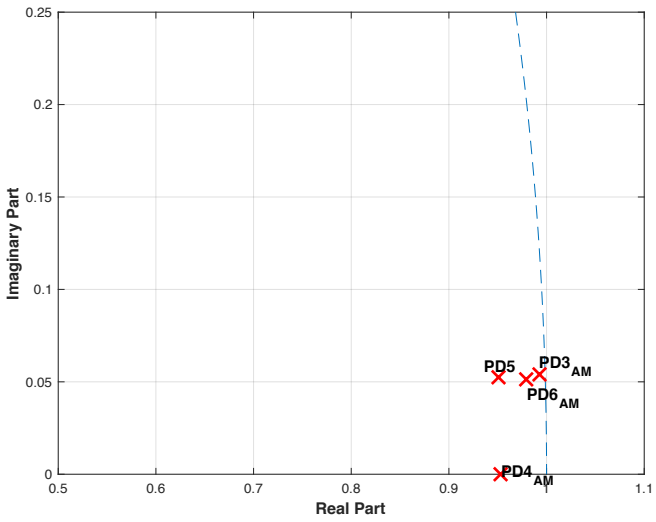

Figure 4.2.5: Combined X-axis data pole-zero plot for PD patients after medication (red) - conjugate counterparts are mirror image.

The pole-zero plots shown in figures 4.2.2, 4.2.3, 4.2.4 and 4.2.5 show that using a 2nd order transfer function can be used to describe the subject's X-axis data from the triangle pattern as different diseases and controls could be distinguished. This is due to the high

accuracy seen in the fit between the simulated and measured output seen in Appendix D. A higher order pole's transfer function is not required to effectively describe the test subject's X-axis data for the triangle pattern.

The combined X-axis data pole-zero plots are compared with each other to see whether there were any clear distinctions (e.g., areas, patterns) between them. The pole-zero plot between control subjects and ET patients, control subjects and PD patients (before medication), control subjects and PD patients (after medication), and PD patients (before medication) and PD patients (after medication) are shown in figures 4.2.6, 4.2.7, 4.2.8 and 4.2.9 respectively.

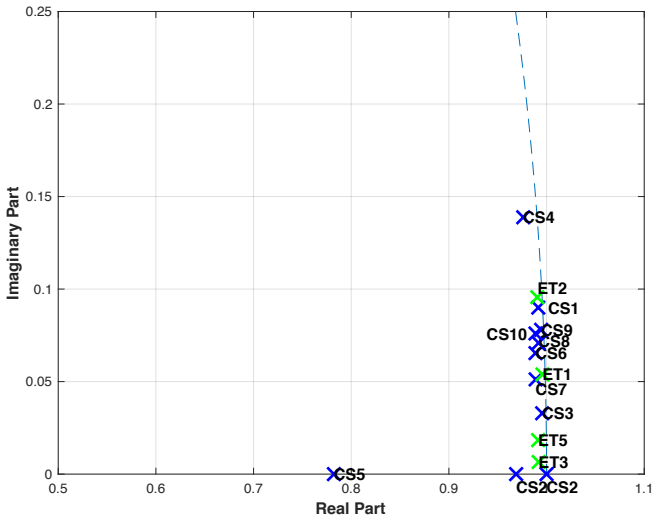

Figure 4.2.6: Pole-zero plot between the control subjects (blue) and ET patients (green) using X-axis data - conjugate counterparts are mirror image.

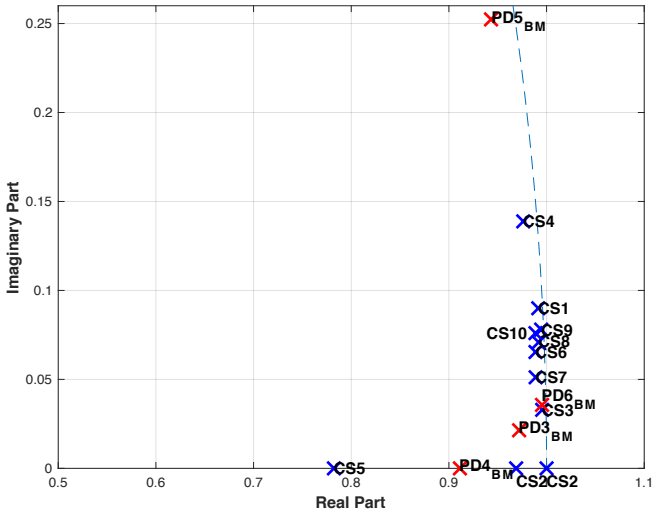

Figure 4.2.7: Pole-zero plot between control subjects (blue) and PD patients before medication (red) using X-axis data - conjugate counterparts are mirror image.

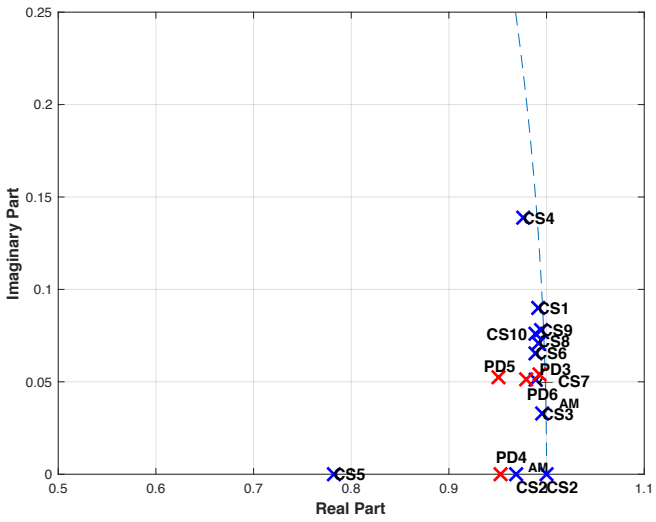

Figure 4.2.8: Pole-zero plot between control subjects (blue) and PD patients after medication (red) using X-axis data - conjugate counterparts are mirror image.

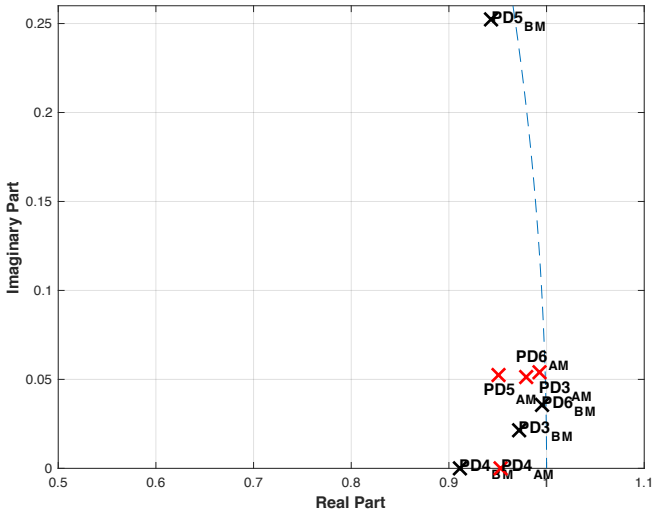

Figure 4.2.9: Pole-zero plot between PD patients before medication (black) and PD patients after medication (red) using X-axis data - conjugate counterparts are mirror image.

The pole-zero plots between the control subjects and ET patients in figure 4.2.6 show that the poles are within similar areas and therefore no patterns or areas could be determined.

The pole-zero plot between the control subjects and PD patients before medication in figure 4.2.7, the pole-zero plots between the control subjects and PD patients after medication in figure 4.2.8 and the pole-zero plot between PD patients before medication and PD patients after medication in figure 4.2.9 shows some trends. Each of the plots show that each test subjects' group have their own distinct clusters. However, more PD patient's X-axis data (before and after medication) from the triangle pattern are needed to verify the trends. Yet, the trends are reliable because the estimated transfer functions of the control subjects and PD patients (before and after medication) closely resembles the measured X-axis data from the triangle pattern (e.g., the average best fit for control subject's X-axis data was 98.0% while the average best fit for PD patient's X-axis data

(before medications) was 93.0%. Similarly, the average best fit for PD patient's X-axis data (after medications) was 93.8%).

A conclusion was made that more repeated triangle pattern's X-axis data from PD patients (before and after medication) are required to verify the trends seen above. The analysis of the X-axis data of the repeated triangle, using the black box methodology showed promising results as clusters could be identified in the pole-zero plots for the different diseases and for the control subjects.

The above-mentioned was repeated with the Y-axis data also from the same one triangle pattern. Similarly, each of the subject's pole-zero plots and trajectories are shown Appendix D. An example of a "good" Y-axis plot for the triangle pattern is shown below in figure 4.2.10.

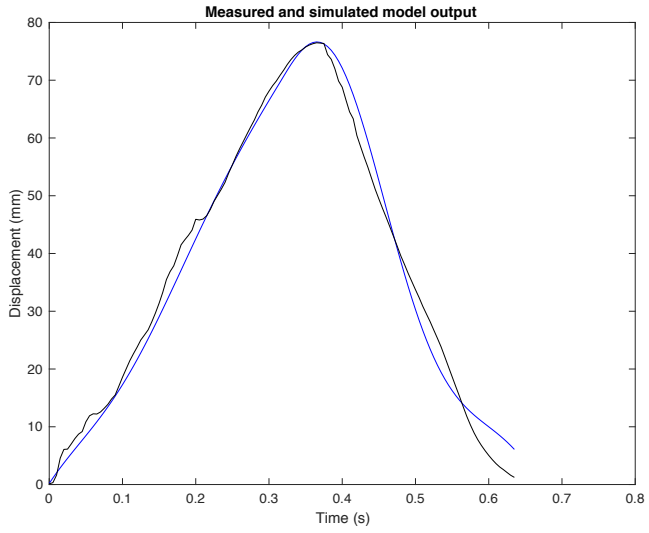

Figure 4.2.10: An example of a Y-axis measured data plotted against simulated output data from the triangle pattern with 88.6% best fit.

The combined Y-axis pole-zero plots from control subjects, ET patients and PD patients before and after medication are shown in figures 4.2.11, 4.2.12, 4.2.13 and 4.2.14 respectively.

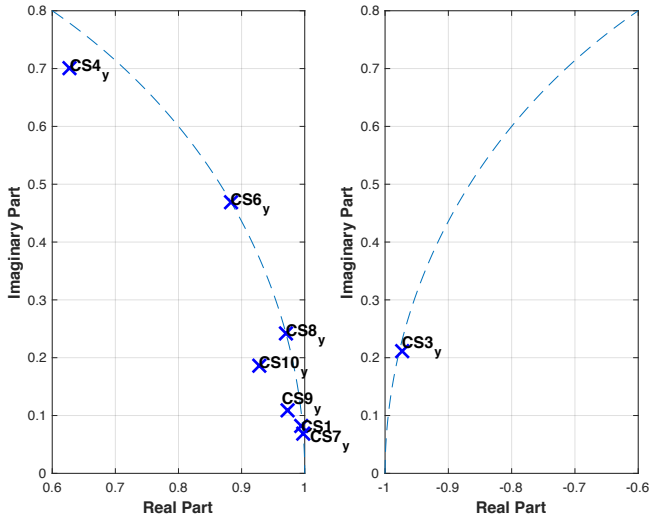

Figure 4.2.11: Combined Y-axis data pole-zero plot for control subjects (blue) - conjugate counterparts are mirror image.

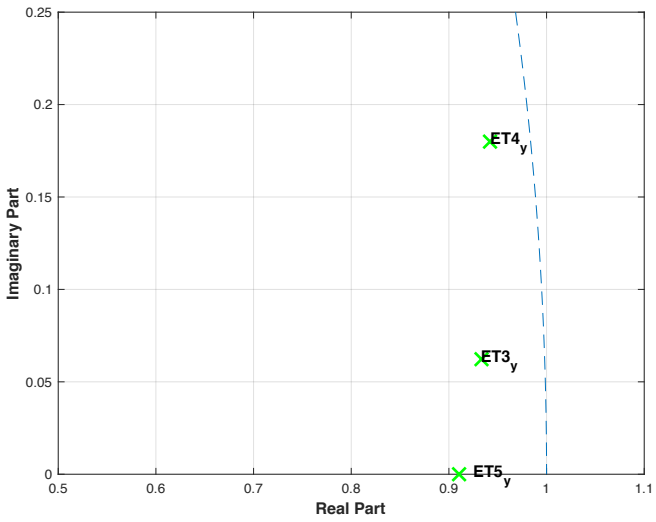

Figure 4.2.12: Combined Y-axis data pole-zero plot for ET patients (green) - conjugate counterparts are mirror image.

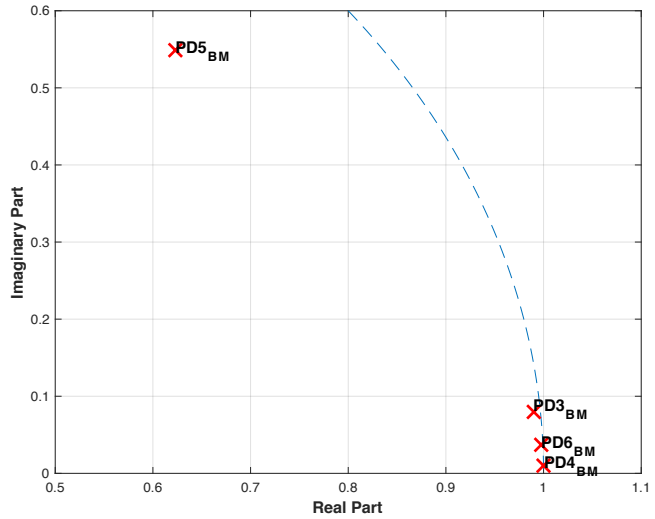

Figure 4.2.13: Combined Y-axis data pole-zero plot for PD patients before medication (red) - conjugate counterparts are mirror image.

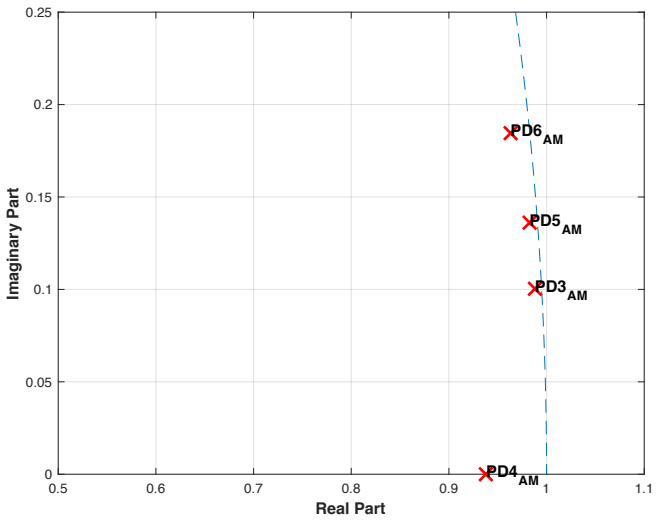

Figure 4.2.14: Combined Y-axis data pole-zero plot for PD patients after medication (red) - conjugate counterparts are mirror image.

The pole-zero plot for control subjects (Y-axis) in figure 4.2.11, the pole-zero plots for ET patients (Y-axis) in figure 4.2.12, the pole-zero plots for PD patients before medication (Y-axis) in figure 4.2.13 and the pole-zero plots for PD patients after

medication in figure 4.2.14 show that show that using a 2nd order transfer function can be used to describe some of the subject's Y-axis data for the triangle pattern as different diseases and controls could be distinguished. However, higher order poles are required to effectively describe the test subject's Y-axis data.

A comparison between each of the movement disorders were plotted similarly to the X-axis pole-zero plots above. The pole-zero plot between control subjects and ET patients, control subjects and PD patients (before medication), control subjects and PD patients (after medication), and PD patients before and after medication are shown in figures 4.2.15, 4.2.16, 4.2.17 and 4.2.18 respectively.

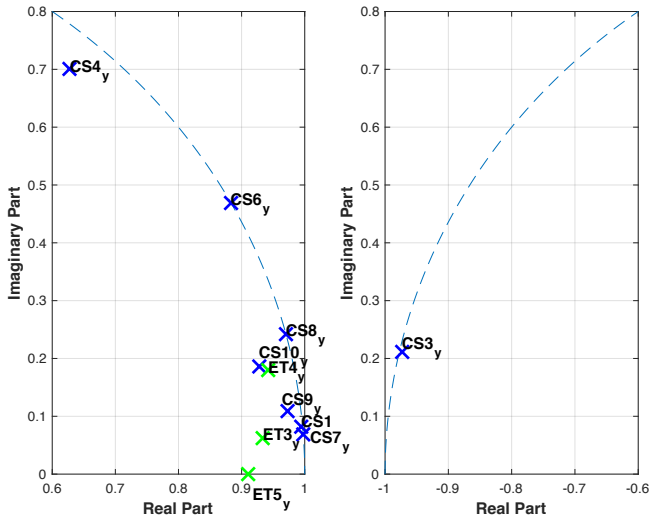

Figure 4.2.15: Pole-zero plot between control subjects (blue) and ET patients (green) using Y-axis data - conjugate counterparts are mirror image.

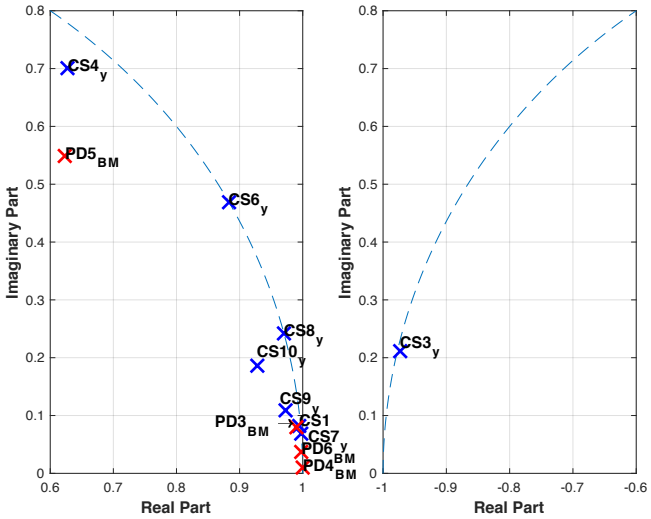

Figure 4.2.16: Pole-zero plot between control subjects (blue) and PD patients before medication (red) using Y-axis data - conjugate counterparts are mirror image.

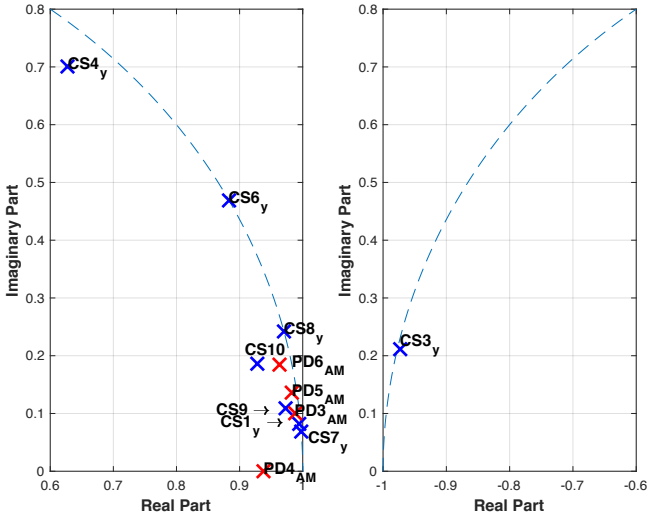

Figure 4.2.17: Pole-zero plot between control subjects (blue) and PD patients after medication (red) using Y-axis data - conjugate counterparts are mirror image.

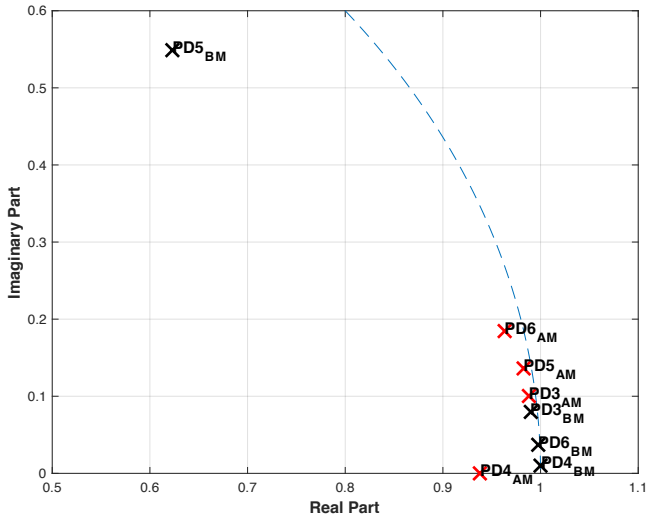

Figure 4.2.18: Pole-zero plot between PD patients before medication (black) and PD patients after medication (red) using Y-axis data - conjugate counterparts are mirror image.

The pole-zero plots between the control subjects and ET patients in figure 4.2.15, the pole-zero plot between the control subjects and PD patients before medication in figure 4.2.16 and the pole-zero plot between the control subjects and PD patients after medication in figure 4.2.17 shows some trends, however, more data are required to verify the results.

The pole-zero plot of PD patients before medication and after medication in figure 4.2.18 may show some clustering within the pole-zero plot. The PD patient's poles (before medication) and PD patient's poles (after medication) are each clumped into their respective areas, but the separation is not distinct and more PD patient's data, before and after medication, from the triangle pattern are needed to verify this trend.

A conclusion was made that more repeated triangle pattern's Y-axis data from PD patients (before and after medication) are required to verify the trends seen above.

4.3 Black Box Model: Circle Pattern

The control subjects, ET and PD patients had to complete the circle pattern test after completing the repeated triangle pattern. Similarly, to the above tests, a circle pattern was shown on the computer screen and the subjects had to trace the pattern using their dominant fingers, using the Leap Motion.

The X and Y trajectories for the circle pattern were squared and combined to get R^2 (radial distance) unlike the step-function and the repeated triangle pattern test where the X and Y trajectories were separated and analysed individually. There were two reasons for using the radial distance *viz.*:

(1) This dissertation was aimed at creating a methodology that was data driven. Analysing the X and Y trajectories separately for the step-pattern and triangle pattern did not yield a conclusive result. Therefore, the radial distance analysis, even though it eliminates common ground, was performed on the circular signals to understand if this methodology could yield a conclusive result.
(2) It is more natural to use polar coordinates for circular motions than analysing the X and Y trajectories separately.

The pole-zero plots and trajectories using R^2 of each the control subjects, ET and PD patients are given in Appendix E. An example of an "acceptable" R^2 data plot for the circle pattern is shown below in figure 4.3.1.

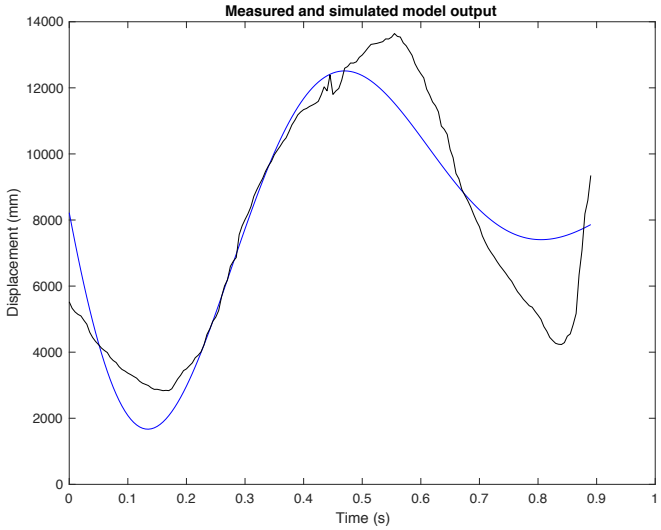

Figure 4.3.1: An example of a R^2 measured data plotted against simulated output data from the circle pattern with 63% best fit.

The R^2 pole-zero plots from the control subjects, ET and PD (after medication) patients are then combined into their respective groups and plotted using pole-zero plots in figure 4.3.2, 4.3.3 and 4.3.4 respectively. PD patients (before medications) pole-zero plots are not shown as none of the transfer function met the 50% best fit threshold criteria.

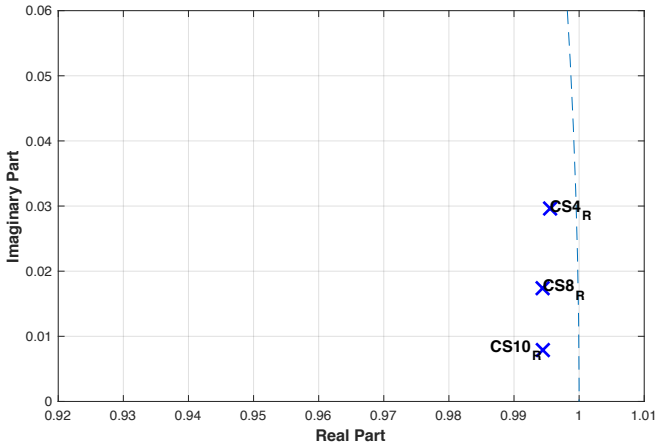

Figure 4.3.2: Combined R^2 data pole-zero plot for control subjects (blue) - conjugate counterparts are mirror image.

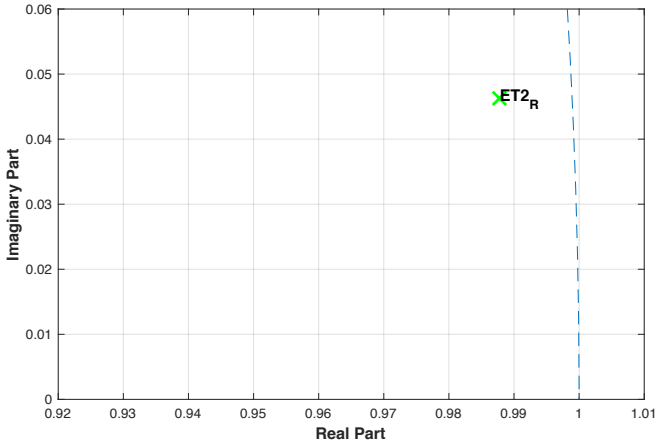

Figure 4.3.3: Combined R^2 data pole-zero plot for ET patients (green) - conjugate counterparts are mirror image.

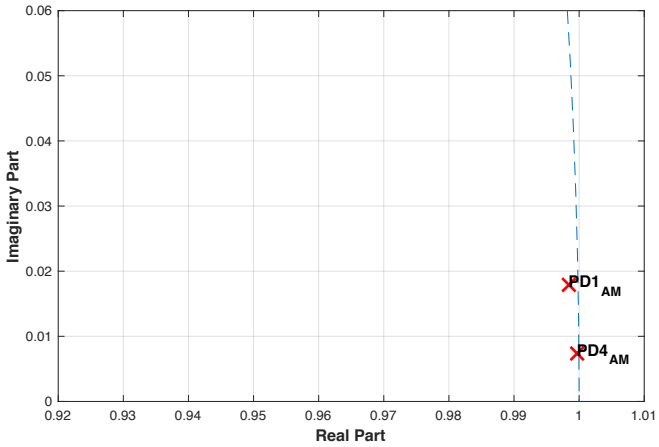

Figure 4.3.4: Combined R^2 data pole-zero plot for PD patients after medication (red) - conjugate counterparts are mirror image.

The pole-zero plot for control subjects in figure 4.3.2, the pole-zero plot for ET patients in figure 4.3.3 and the pole-zero plots for PD patients after medication in figure 4.3.4 shows that using a 2nd order transfer function to describe the test subject's R^2 data is not ideal. A higher order poles are required to effectively describe the test subject's R^2 data. A comparison between the different test subjects are not done because there are insufficient data points that can be compared. Another analysis method was required. It was decided to analyse the R^2 data using Fourier analysis to see whether there would be any difference between the various neurological movement disorders in the frequency domain. This is discussed in the next chapter.

4.4 Fourier Analysis

All the control subjects' FFT plots are given in Appendix F. An example of a representative control subject's FFT plot (shown in figure 4.4.1) was chosen for further comparisons between the patients.

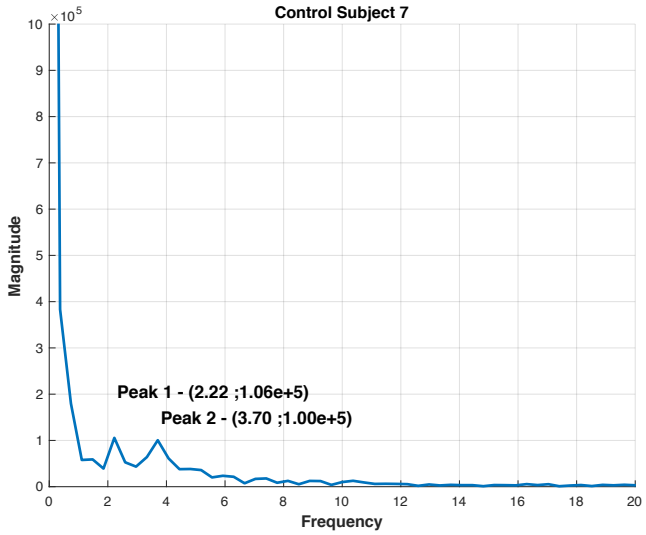

Figure 4.4.1: An example of a FFT plot of a 'good' control subject.

After plotting the control subject's R^2 data using FFT, MATLAB's 'findpeaks' function was used to find the peaks with magnitudes greater than 1 x10^5. This magnitude value was chosen as a reference value based on the typical control subject's FFT plot (figure 4.4.1) so that a comparison between different neurological movement disorders can be done. As seen in figure 4.4.1, the FFT plots shows the first two peak's magnitude at specific frequencies. Then the MATLAB's 'findpeaks' function was used to find the first two peaks at their respective frequencies. This is not subjected to the 1 x10^5 threshold. These were the features that were extracted from the control subject's plots and they are tabulated in Table 4.4.1 below for all the control subjects.

Table 4.4.1: Control subject's features from the FFT of R^2 data.

	No. Peaks above $1x10^5$	1st Peak (Hz)	1st Peak (mag) $x10^5$	2nd Peak (Hz)	2nd Peak (mag) $x10^5$
CS1	0	1.53	0.96	3.57	0.73
CS2	1	1.04	2.97	3.12	0.91
CS3	3	0.76	6.19	1.33	2.73
CS4	0	4.93	0.64	6.90	0.24
CS5	2	2.48	1.13	3.54	1.13
CS6	5	0.67	7.58	1.51	4.10
CS7	2	2.22	1.06	3.70	1.00
CS8	1	2.43	3.00	4.26	0.71
CS9	0	3.81	0.60	5.45	0.40
CS10	0	4.08	0.42	5.44	0.22
Average	**1.4**	**2.40**	**2.46**	**3.88**	**1.22**

The same approach was taken for ET patient's R^2 data. An example of an ET patient's FFT plot is shown in figure 4.4.2.

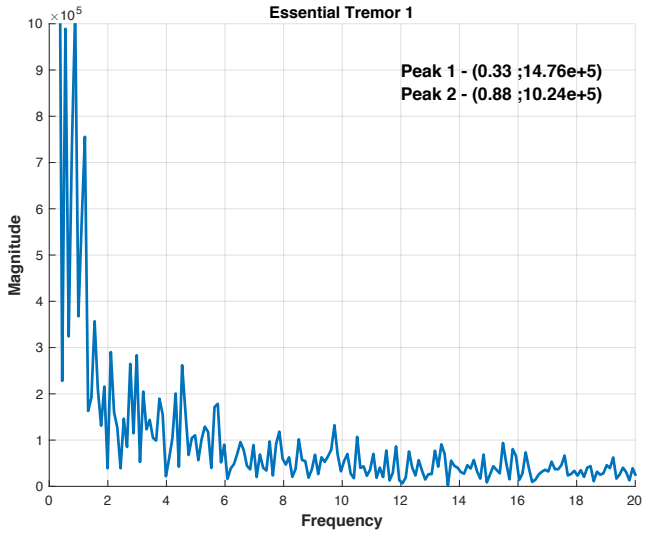

Figure 4.4.2: An example of a FFT plot of ET patient 1.

The features that were extracted from all the ET patients are tabulated in Table 4.4.2 below.

Table 4.4.2: ET patient's features from the FFT of R^2 data.

	No. Peaks above $1x10^5$	1st Peak (Hz)	1st Peak (mag) $x10^5$	2nd Peak (Hz)	2nd Peak (mag) $x10^5$
ET1	22	0.33	14.76	0.88	10.24
ET2	0	5.59	0.25	8.94	0.20
ET3	11	0.62	15.02	1.71	6.60
ET4	2	0.69	8.93	2.43	1.66
ET5	8	1.48	7.04	2.81	4.87
Average	**8.6**	**1.74**	**9.20**	**3.35**	**4.71**

The same approach was taken for PD patient's R^2 data (before and after medication). An example of a PD patient's FFT plot (before and after medication) is shown below in figure 4.4.3.

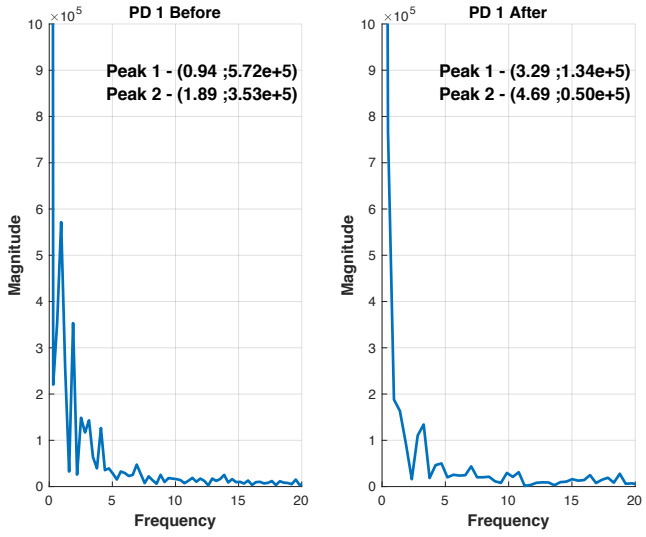

Figure 4.4.3: An example of a FFT plot of PD patient 1 (before and after medication) using R^2 data.

The features were extracted and tabulated in Table 4.4.3 and 4.4.4 below.

Table 4.4.3: PD patient's features (before medication) from the FFT of R^2 data.

	No. Peaks above $1x10^5$	1st Peak (Hz)	1st Peak (mag) $x10^5$	2nd Peak (Hz)	2nd Peak (mag) $x10^5$
$PD1_B$	5	0.94	5.72	1.89	3.53
$PD3_B$	4	0.74	11.18	1.48	3.39
$PD4_B$	2	1.88	4.36	2.50	2.44
$PD5_B$	7	1.39	4.74	3.25	3.71
$PD6_B$	1	1.73	4.38	2.52	3.46
Average	**3.8**	**1.34**	**6.08**	**2.33**	**3.31**

Table 4.4.4: PD patient's features (after medication) from the FFT of R^2 data.

	No. Peaks above $1x10^5$	1st Peak (Hz)	1st Peak (mag) $x10^5$	2nd Peak (Hz)	2nd Peak (mag) $x10^5$
$PD1_A$	1	3.29	1.34	4.69	0.50
$PD3_A$	2	3.66	1.36	4.88	1.24
$PD4_A$	2	1.19	3.24	2.14	1.73
$PD5_A$	0	3.14	0.79	6.81	0.34
$PD6_A$	1	2.39	2.47	5.73	0.83
Average	**1.2**	**2.73**	**1.84**	**4.85**	**0.93**

The average features from Tables 4.4.1, 4.4.2, 4.4.3 and 4.4.4 are then combined to get a graphical representation of the data and this is shown in figure 4.4.4 below.

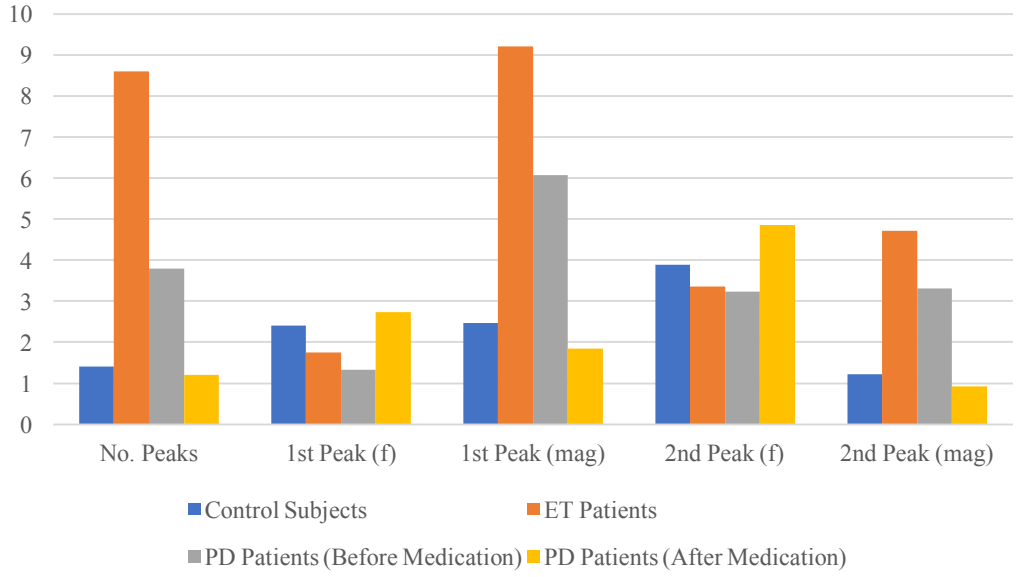

Figure 4.4.4: Average feature values shown graphically from tables 4.4.1, 4.4.2, 4.4.3 and 4.4.4.

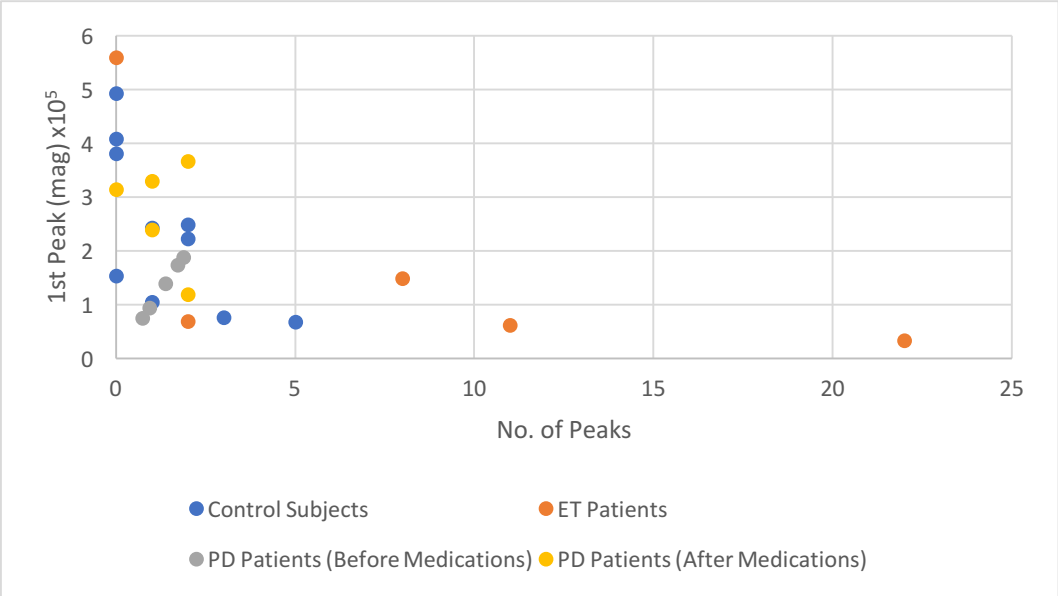

Figure 4.4.5: Scatter plot of the number of peaks versus the first peak magnitude of all subjects.

Figure 4.4.4 shows the average features values (e.g., number of peaks, location of the first and second peak and their corresponding magnitudes) that were extracted from the R^2 FFT plots. A scatter plot of the number of peaks versus the first peak magnitude of all the subjects is given in figure 4.4.5 to see if there was a trend.

A trend can be seen for the average number of peaks for the control subjects, ET patients and PD patients (before and after medication) in figure 4.4.4. The average number of peaks above a certain threshold ($1x10^5$) for the control subjects and PD patients (after medications) are within close ranges e.g., 1.4 and 1.2 respectively. This suggests that the PD medications lowers the number of peaks to that of the control subjects level. The PD patient's (before medication) average peaks has a value of 3.8 and this value drops to an average value of 1.2 after the patients have taken their medications, which shows that the medications had an effect. The ET patients have the highest average number of peaks (e.g., 8.6) and this was due to ET patients generally having more hand tremors than the other neurological movement disorders. This resulted in more higher frequency components in the data.

A trend can be seen for the average frequency at which the first peak occurs for the control subjects, ET patients and PD patients (before and after medication) in figure 4.4.4. It is seen that the PD patient's (before medication) plot generally showed the first peak above a magnitude threshold of $1x10^5$ at lower frequencies. The average frequency at which the first peak showed up was around 1.34 Hz followed by the ET patients at around 1.74 Hz. Similarly, the control subject's and PD patient's (after medications) average frequency values at which they showed their first peak above a magnitude threshold of $1x10^5$ was around 2.40 and 2.73 respectively.

There is a trend to be observed for the average first peak's magnitude for the control subjects, ET patients and PD patients (before and after medication) in figure 4.4.4. The

average first peak's magnitude above a threshold (1 $x10^5$) for the control subjects and PD patients (after medications) are within close ranges e.g., 2.46 $x10^5$ and 1.84 $x10^5$ respectively. The ET patients have the highest number of average first peak's magnitude of 9.20$x10^5$ followed by the PD patients (after medications) average first peak's magnitude of 6.08$x10^5$.

A trend can also be seen for the average frequency at which the second peak occurs for the control subjects, ET patients and PD patients (before and after medication) in figure 4.4.4. The PD patients (before medication) generally showed first peak above a magnitude threshold of 1$x10^5$ at lower frequencies. The average frequency at which the second peak showed up for PD patients (before medication) is around 2.33 Hz followed by the ET patients at around 3.35 Hz. Similarly, the control subject's and PD patient's (after medications) average frequency values at which they showed their second peak above a magnitude threshold of 1$x10^5$ was around 3.88 and 4.85 respectively.

A similar trend of the average first peak's magnitude can be seen for the average second peak's magnitude for the control subjects, ET patients and PD patients (before and after medication). The average second peak's magnitude above a threshold (1 $x10^5$) for the control subjects and PD patients (after medications) are within close ranges e.g., 1.22 $x10^5$ and 0.93 $x10^5$ respectively. The ET patients have the highest number of average second peak's magnitude of 4.71 $x10^5$ followed by the PD patients (after medications) average second peak's magnitude of 3.31$x10^5$.

The average frequency at which the first peak occurs has the same trend as the average frequency at which the second peak occurs. Similarly, the average first peak's magnitude has the same trend as the average second peak's location. This together with the number of average peaks can be used as a classifier in differentiating different neurological movement disorders.

4.5 Concluding Discussions and Future Recommendations

The signals (X and Y trajectories of the subject's hand movement data) captured from the Leap Motion from control subjects and the three movement disorder subjects, were modelled using control theories. The first control theory model for the captured signals was a unity feedback system. This control theory model was discarded, as the human hand and arm plant parameters were from data of subjects who did not have any neurological movement disorders e.g., the plant model was created from subjects with 'normal' functioning hand and arm movements. This would have biased the results in favour of control subjects. Therefore, a new approach was taken where the subjects was modelled as a black box model.

The black box model theory allowed all the subject's movement characteristic to be captured within a transfer function. The transfer function was then plotted using a pole-zero plot to be compared with each other. The modelling was carried out for the X and Y signals for each of the three subsections: step-function, triangular and circular patterns. It was established that estimating the subject's hand movement characteristic using a 2nd order transfer function, produced a best fit line and a good approximation to the subject's measured data if the lines were relatively straight and the data met the initial fit criterion (e.g., step-function and triangle pattern's Y and X signals respectively). This was demonstrated by plotting the estimated model with the actual trajectory and measuring the fit using MATLAB's NRMSE function. It was however determined, that if there was a lot of curves and 'kinks' in the signal, the estimating of the subject's hand movement characteristics using a 2nd order transfer function was not accurate enough and a higher order pole transfer function may be required (e.g., R^2 signal from the circle pattern). A threshold of 50% NRMSE was chosen and only trajectories that exceeded this threshold were included in the pole-zero analysis.

The pole-zero analysis of the Y signal (step-function pattern) showed a trend that distinguishes between control subjects and PD patients (after medication), and between PD patients (before medications) and PD patients (after medications). Similarly, the pole-zero analysis in the X signal (triangle pattern) showed that there are trends between: control subjects and PD patients (before medication), control subjects and PD patients (after medication), and PD patients (before medication) and PD patients (after medication).

Although it may seem that the X axis motion for a triangle and not for a step are in the same direction, they may not in fact be similar and hence the differences in the models. The control systems involved in a pure horizontal movement separated in the "step" discontinuity, may be very different than those responsible for a triangular trajectory involving both horizontal and vertical motion. More research is required to identify the causes for these differences.

For many fits that did not meet the threshold, a 2nd order model was omitted as not being accurate enough. This finding was observed in all the four categories studied: PD, HD, ET and control subjects. The amount of data rejection was different between different patterns and between the X and Y axis signals of the patterns: In the case of the X signals of the step-function pattern, nearly 23% of the total measured data was omitted, whereas for the Y signals of the step-function pattern, only 7% of the total measured data was omitted. The X signals of the step-function pattern did not show distinct features between the categories, whereas the Y signals features from the step-function pattern were able to distinguish between the categories. In the case of the triangle pattern, no data were omitted from the X signal and these signals provided distinct features between the categories. However, for the Y signal of the triangle pattern, nearly 18% of the measured data was omitted and no distinct features between the categories were identified. These results show that the initial fit of the measured and simulated data is a valid selection tool

and is an important step in the analysis methodology. The following conclusion can thus be made:

(1) The simulated and measured data must meet an initial fit criterion e.g. 50%.
(2) If more than 10% of the total measured data do not fit the simulated signal's fit criterion, the whole dataset is not considered. The analysis must be performed with a higher order model.
(3) The analysis must be done on each axis separately, as each axis may produce different results.

These observations, however, needs to be verified by obtaining more data and performing the same analysis.

The pole-zero analysis for the circle pattern was not done because the threshold rejected too many subjects' transfer functions and therefore yielded insufficient points on the pole-zero plots. Therefore, a Fourier analysis was done for the circle pattern's R^2 data.

The Fourier analysis for the circle trajectory signal showed the most promising result. The first trend that was seen was the visual differences between each of the different neurological movement disorder graphs (e.g., the control subject's FFT graph was much smoother than the ET patient's and PD patient's (before medication) graphs). In addition, the ET patient's FFT graph had higher frequency components than the others leading to a visually more 'jagged' or 'spiky' graph. This was then analysed using MATLAB's 'findpeak' function to find the total number or peaks above a magnitude threshold of $1x10^5$, 1st and 2nd peak's magnitude and location for each of the different neurological movement disorders. This led to more trends being discovered (e.g., the average frequency at which the first peak occurs has the same trend as the average frequency at which the second peak occurs). Similarly, the average first peak's magnitude has the

same trend as the average second peak's location). This, however, needs to be verified with more subjects.

Future work recommendation: the analysis should be enhanced by using higher order models. This may or may not verify the trends seen when a second order models were used. This, however, should be done when more data is collected from each of the different movement disorder classes. This should provide a better characterization of both the different movement disorders and the effect of medication.

The Z axis was not used due to time constraints and should be performed in future work. Using the Z axis signals for each of the three subsections (step-function, triangular and circular patterns) may add robustness to the analysis of the 1D and 2D case, which did not produce a reliable biomarker.

The user interface of the experimental system should also be re-designed. A friendlier interface could potentially alleviate patients' anxiety and enable to collect more severe cases of patients, which the current system was not able to do. In addition, the current interface, which shows a static pattern on the screen which the subjects must trace, could be more efficient and provide better data, if a dynamic point that follows a specific pattern is used. This will eliminate the anticipated movements from the data and possibly provide a 'genuine' movement characteristics. This will also make the tracing more intuitive.

5 CONCLUSION

This study presented the development of a potentially new biomarker to categorise the different neurological movement disorders (ET and PD). A gaming device called the Leap Motion device was used to record the position, in terms of X, Y and Z trajectories, of the subject's finger as they trace simple shapes in the air. A computational analysis involving pole-zero plots and FFT was performed on the data which provided a graphical and numerical information. Thus, the following conclusions were made:

(1) For the step-function pattern, no trends were seen in the X signal's (transfer functions) pole-zero plots when a 2nd order transfer function was estimated. A higher order transfer function may be required. However, trends of dissimilarities were observed between the control subjects and PD patients after medication, and between PD patients before medication and PD patients after medication from the Y signal's (transfer functions) pole-zero plots using a 2nd order transfer function.

(2) For the triangle pattern, trends were seen between the control subjects and PD patients before medication, between the control subjects and PD patients after medication, and between PD patients before medication and PD patients after medication for the X signal's (transfer functions) pole-zero plots using a 2nd order transfer function. No trends were seen from the Y signal's plots. A higher order transfer function may be required in this case, as well as, more data to verify the X-axis data trends.

(3) For the circle pattern, no trends were seen in the R^2 signal's (transfer functions) pole-zero plots using an estimated 2nd order transfer function. However, using FFT, visual and numerical trends were seen. More subjects are required to verify the trends.

This preliminary study only showed the feasibility of the Leap Motion gaming apparatus to be used as a diagnostic tool. More data from the various movement disorder patients, as well as further signal processing and analysis are required to verify the conclusions drawn here and to further study its applicability for medical application.

REFERENCES

[1] D. Heisters, “Parkinson's: symptoms, treatments and research,” *British Journal of Nursing,* vol. 20, no. 9, pp. 548-554, 2011.

[2] L. I. Golbe, M. H. Mark and J. I. Sage, Parkinson's Disease Handbook, New Jersey: The American Parkinson Disease Association, Inc., 2010.

[3] R. W. Angel, W. Alston and J. R. Higgins, “CONTROL OF MOVEMENT IN PARKINSON'S DISEASE,” *Brain: A journal of Neurology,* vol. 93, pp. 1-14, 1970.

[4] J. Jankovic, “Parkinson’s disease: clinical features and diagnosis,” *Journal of Neurology, Neurosurgery & Psychiatry,* vol. 79, no. 4, pp. 368-376, 2007.

[5] D. J. Brooks, “Parkinson's disease: Diagnosis,” *Parkinsonism & Related Disorders,* vol. 18, no. 1, pp. 31-33, 2012.

[6] National Institute of Health, “Parkinson's Disease: Challenges, Progress, and Promise,” in *Parkinson's Disease*, New York, National Institute of Health, 2010, pp. 1-23.

[7] M. D. S. T. F. o. R. S. f. P. Disease, “The Unified Parkinson's Disease Rating Scale (UPDRS): status and recommendations,” *Movement Disorder,* vol. 18, no. 7, pp. 738-50, 2003.

[8] R. Bhidayasiri and D. Tarsy, “Parkinson’s Disease: Hoehn and Yahr Scale,” in *Movement Disorders: A Video Atlas*, New York, Humana Press, 2012, pp. 4-5.

[9] C. A. Davie, “A review of Parkinson's disease,” *British Medical Bulletin,* vol. 86, no. 1, pp. 109-127, 2008.

[10] The Parkinson Study Group, “Levodopa and the Progression of Parkinson's Disease,” *The New England Journal of Medicine,* vol. 351, pp. 2498-2508, 2004.

[11] R. Cools, L. Altamirano and M. D'Esposito, “Reversal learning in Parkinson's disease depends on medication status and outcome valence,” *Neuropsychologia,* vol. 44, no. 10, pp. 1663-1673, 2006.

[12] M. S. Okun and K. D. Foote, “Parkinson’s disease DBS: what, when, who and why? The time has come to tailor DBS targets,” *Expert Review of Neurotherapeutics,* vol. 10, no. 12, pp. 1847-1857, 2010.

[13] Gulcher, JR, Jonsson, P, Kong, A, Kristjansson, K, Frigge, ML, Karason, A, Einarsdottir, IE, Stefansson, H, Einarsdattir, AS, Sigurthoardattir, S, Baldursson, S, Hrafnkelsdóttir, SM, Björnsdóttir, S, Jakobsson, F, Benedickz, J and Stefánsson K, “Mapping of a familial essential tremor gene, FET1, to chromosome 3q13,” *Europe PMC,* pp. 84-87, 1997.

[14] J.-S. Lou and J. Jankovic, “Essential tremor,” *Neurology,* vol. 41, no. 2, p. 234, 1991.

[15] R. J. Elble, “Diagnostic criteria for essential tremor and differential diagnosis,” *Europe PMC,* vol. 54, no. 11, pp. 2-6, 2000.

[16] R. J. Elble, “Physiologic and essential tremor,” *Neurology,* vol. 36, no. 2, p. 225, 1986.

[17] M. Critchley, “Observations on Essential (Heredofamilial) Tremor,” *Brain,* vol. 72, no. 2, pp. 113-139, 1949.

[18] W. C. Koller and B. Vetere-Overfield, “Acute and chronic effects of propranolol and primidone in essential tremor,” *Neurology,* vol. 39, no. 12, p. 1587, 1989.

[19] G. Huntington, “On Chorea,” *Medical and Surgical Reporter of Philadelphia,* vol. 26, pp. 317-321, 1872.

[20] S. C. Warby, R. K. Graham and M. R. Hayden, “GeneReviews,” NCBI, 11 December 2014. [Online]. Available: http://www.ncbi.nlm.nih.gov/books/NBK1305/. [Accessed 28 January 2016].

[21] R. H. Myers, “Huntington's Disease Genetics,” *NeuroRX,* vol. 1, no. 2, pp. 255-262, 2004.

[22] . F. O. Walker, “Huntington's disease,” *The Lancet,* vol. 369, no. 9557, p. 2180228, 2007.

[23] K. Duff, J. Paulsen, J. Mills, L. J. Beglinger, D. J. Moser, M. M. Smith, D. Langbehn, J. Stout, S. Queller and D. L. Harrington, “Investigators and Coordinators of the Huntington Study Group. Mild cognitive impairment in prediagnosed Huntington disease,” *Neurology,* vol. 75, no. 6, pp. 500-7, 2010.

[24] A. Ho and M. Hocaoglu, “Impact of Huntington Disease across the entire disease spectrum: The phases and stages of disease from the patient perspective,” *Clinical Genetics,* vol. 80, no. 3, pp. 235-239, 2011.

[25] M. Nance, J. S. Paulsen, A. Rosenblatt and V. Wheelock, A Physician's Guide to the Management of Huntington's Disease, Huntington's Disease Society of America, 2011.

[26] R. A. Roos, "Huntington's disease: a clinical review," *Orphanet Journal of Rare Diseases,* pp. 5-40, 2010.

[27] J. T. Simmons, B. Pastakia, T. N. Chase and C. W. Shults, "Magnetic Resonance Imaging in Huntington Disease," *American Journal of Neuroradiology,* vol. 7, no. 1, pp. 25-28, 1986.

[28] United States Huntington's Disease Genetic Testing Group, Genetic Testing for Huntington's Disease, Huntington's Disease Society of America & Athena diagnostics, 2001.

[29] Huntington Study Group, "Unified Huntington's Disease Rating Scale: Reliability and Consistency," *Movement Disorders,* vol. 11, no. 2, pp. 136-142, 1996.

[30] K. Strimbu and J. A. Tavel, "What are Biomarkers?," *Current opinion in HIV and AIDS,* vol. 5, no. 6, pp. 463-466, 2010.

[31] W. Poewe and J. Jankovic, "Principles of management in movement disorders," in *Movement Disorders in Neurologic and Systemic Disease*, New York, Cambridge University Press, 2014, pp. 31-37.

[32] J. C. Morgan, S. H. Mehta and K. D. Sethi, "Biomarkers in Parkinson's Disease," *Current Neurology and Neuroscience Reports,* vol. 10, pp. 423-430, 2010.

[33] S. Lesage and A. Brice, “Parkinson's disease: from monogenic forms to genetic susceptibility factors,” *Hum Mol Genet,* vol. 18, no. 1, pp. R48-R59, 2009.

[34] H. Deng, W. Le and J. Jankovic, “Genetics of essential tremor,” *Brain,* vol. 18, pp. 1456-1464, 2007.

[35] S. N. J. J. E. R. L. H. S. A. e. a. Shatunov A, “Genomewide scans in North American families reveal genetic linkage of essential tremor to a region on chromosome 6p23,” *Brain,* vol. 129, pp. 2318-31, 2006.

[36] M. Bogdanov, W. R. Matson and L. Wang, “Metabolic profiling to develop blood biomarkers for Parkinson's disease,” *Brain,* vol. 131, pp. 389-396, 2008.

[37] M.-H. Disatnik, A. U. Joshi, N. L. L. Saw, M. Shamloo, B. R. Leavitt, X. Qi and D. Mochly-Rosen, “Potential biomarkers to follow the progression and treatment response of Huntington’s disease,” *Journal of Experimental Medicine,* 2016.

[38] D. E. Vaillancourt, M. B. Spraker, . J. Prodoehl, I. Abraham, D. M. Corcos, X. J. Zhou, C. L. Comella and D. M. Little, “High-resolution diffusion tensor imaging in the substantia nigra of de novo Parkinson disease,” *Neurology,* vol. 72, no. 16, pp. 1378-1384, 2009.

[39] APDM, “APDM Wearable Technologies,” 29 June 2016. [Online]. Available: http://www.apdm.com/. [Accessed 15 November 2016].

[40] NeuroScript, “MovAlyzeR - Movement Analysis System,” BORG Limited, 16 July 2016. [Online]. Available: http://www.neuroscript.net/. [Accessed 20 November 2016].

[41] I. Leap Motion, “Leap Motion,” Leap Motion, Inc, January 2016. [Online]. Available: https://www.leapmotion.com/. [Accessed 1 February 2016].

[42] R. V. Dukkipati, Analysis and Design of Control Systems Using MATLAB, New Delhi: NEW AGE INTERNATIONAL (P) LIMITED, PUBLISHERS, 2006.

[43] N. Wiener, Cybernetics: Or Control and Communication in the Animal and the Machine, 2, Ed., New York: MIT Press and Wiley, 1961.

[44] E. Eriksson, “Simulation of Biological Tissue using Mass-Spring-Damper Models,” Örebro University, Örebro.

[45] J. Lou , M. Zhang and J. Chen, “Identification of Stiffness, Damping and Biological Force of SMD Model for Human Walking. In,” in *Dynamics of Civil Structures, Volume 2. Conference Proceedings of the Society for Experimental Mechanics Series*, 2015.

[46] J. E. Speich, L. Shao and M. Goldfarb, “Modeling the human hand as it interacts with a telemanipulation system,” *Mechatronics,* vol. 15, pp. 1127-1142, 2005.

[47] MathWorks, “MATLAB,” 2017. [Online]. Available: https://www.mathworks.com/help/ident/ref/compare.html. [Accessed 15 02 2017].

[48] G. E. Alexander, “Biology of Parkinson's disease: pathogenesis and pathophysiology of a multisystem neurodegenerative disorder,” *Dialogues in Clinical Neuroscience,* vol. 6, no. 3, pp. 259-280, 2004.

[49] J. L. Lanciego, N. Luquin and J. A. Obeso, “Functional Neuroanatomy of the Basal Ganglia,” *Cold Spring Harbor Perspectives in Medicine,* pp. 1-20, 2012.

[50] BruceBlaus.com staff, Artist, *Basal Ganglia.* [Art]. Blausen Gallery, 2014.

[51] J. M. Rabey and F. Hefti, “Neuromelanin synthesis in rat and human substantia nigra,” *Journal of Neural Transmission - Parkinson's Disease and Dementia,* vol. 2, no. 1, pp. 1-14, 1990.

[52] J. M. Fearnley and A. J. Lees, “AGEING AND PARKINSON'S DISEASE: SUBSTANTIA NIGRA REGIONAL SELECTIVITY,” *Brain: A journal of Neurology,* vol. 114, no. 5, pp. 2283-2301, 1991.

[53] R. Cano-de-la-Cuerda, M. Pérez-de-Heredia, J. C. Miangolarra-Page, E. Muñoz-Hellín and C. Fernández-de-las-Peñas, “Is There Muscular Weakness in Parkinson's Disease?,” *American Journal of Physical Medicine & Rehabilitation,* vol. 89, no. 1, pp. 70-76, Jan 2010.

APPENDIX A – ETHIC CLEARANCE DOCUMENTS

A1 Protocol

1. As part of the routine visit, the neurologist will score/rate the patient's symptoms at the time of testing using the standard clinical scoring systems for Huntington's and Parkinson's disease respectively. The scoring will form the basis of comparison of the numerical data produced by the study using the Unified Parkinson's Disease Rating Scale (UPDRS) & Unified Huntington's Disease Rating Scale (UHDRS).
2. The measurement procedure will consist of the following stages:
    a. Use a mobile tablet and a 3D Leap Motion camera to take measurements of the position and speed of movement of a patient's finger as they trace simple shapes both on the tablet.
    b. Five-minute rest
    c. Simple 3D shapes will be shown to the participants on a computer screen and the participants will be asked to trace the shapes in the air in front of a 3D camera. It emphasised that care will be taken to ensure that the patient's facial features will not appear in the images to preserve anonymity. In any case the video footage will only be available to the researchers.
    d. To prevent fatigue, the total session per subject will not exceed fifteen minutes, and should the subject require longer breaks between the two measurements, then the five-minute rest period will be extended as is necessary.
3. For Parkinson's patients, if the patient is willing and it is convenient for them, they will be requested to come back once to repeat the process on another day

ideally at a different time of day when they are in a different stage of their treatment cycle.

4. The recorded data will be anonymised and stored in a database for processing.
5. The data will be analysed and the required graphical and numerical output will be compared with the rating scales used by the neurologist.
6. All the measurements will be repeated on normal (no known neurological pathology) adult subjects who will include the researchers themselves (5 people) and an additional 5 - 20 subjects of various ages who will not be subordinate to the researchers.

A2 Human Research Ethics Committee (Medical) Clearance Certificate

R14/49 Ms Sarah Rachel Ward

HUMAN RESEARCH ETHICS COMMITTEE (MEDICAL)

CLEARANCE CERTIFICATE NO. M160235

NAME: (Principal Investigator)	Ms Sarah Rachel Ward
DEPARTMENT:	School of Electrical and Information Engineering Wits Donald Gordon Medical Centre Charlotte Maxeke Johannesburg Academic Hospital
PROJECT TITLE:	Measurements of Hand Movement to Characterise Parkinson's and Huntington's Disease
DATE CONSIDERED:	26/02/2016
DECISION:	Approved unconditionally
CONDITIONS:	Additional Study Site
SUPERVISOR:	Prof David Rubin and Dr D Anderson
APPROVED BY:	Professor P. Cleaton-Jones, Chairperson, HREC (Medical)
DATE OF APPROVAL:	24/06/2016

This clearance certificate is valid for 5 years from date of approval. Extension may be applied for.

DECLARATION OF INVESTIGATORS

To be completed in duplicate and **ONE COPY** returned to the Research Office Secretary in Room 10004,10th floor, Senate House/2nd floor, Phillip Tobias Building, Parktown, University of the Witwatersrand. I/We fully understand the the conditions under which I am/we are authorised to carry out the above-mentioned research and I/we undertake to ensure compliance with these conditions. Should any departure be contemplated,from the research protocol as approved, I/we undertake to resubmit to the Committee. **I agree to submit a yearly progress report**. The date for annual re-certification will be one year after the date of convened meeting where the study was initially reviewed. in this case, the study was initially review in February and will therefore be due in the month of February each year.

Principal Investigator Signature Date

PLEASE QUOTE THE PROTOCOL NUMBER IN ALL ENQUIRIES

Figure A2.1: Human Research Ethics Committee (Medical) Certificate.

A3 HREC Medical Information Sheet

INFORMATION DOCUMENT

Measurement of hand movement to characterize Parkinson's and Huntington's disease

To whom it may concern

We, Sarah Ward and Kimoon Kim, are doing research on movement disorders. With this research we are hoping to be able to identify signs that indicate the presence of either Parkinson's disease or Huntington's disease. We are also hoping to be able to determine the severity of the movement related symptoms. We are hoping that this will allow easier diagnosis and treatment of patients with movement disorders in the future.

We are inviting you to take part in a research study if you are willing to.

What is involved in the study: Dr. D. Anderson will in the course of his routine clinical examination note specific features on a document known as a rating scale (e.g. Unified Parkinson's Disease Rating Scale (UPDRS) & Unified Huntington's Disease Rating Scale (UHDRS)). Then this study makes use of a mobile tablet and a 3D imaging device called Leap Motion™. The entire process is non-invasive. We will then ask you to trace a few simple shapes on the tablet and then in front of the 3D imaging device called Leap Motion™. There will be a 5-minute break between using the tablet and using the 3D imaging device called Leap Motion™. The measurements and break will take approximately fifteen minutes.

Between 10 and 25 patients with either Huntington's disease or Parkinson's disease have been chosen to participate in this study. In addition, 10 to 25 participants without any movement disorder have been chosen to participate.

Risks: There are no risks involved in participating in the study.

Benefits: There are no benefits to participating in the study aside from helping us with our research.

The participant will be given pertinent information on the study while involved in the project and after the results are available.

Participation is voluntary, that refusal to participate will involve no penalty or loss of benefits to which the participant is otherwise entitled, and that the subject may discontinue participation at any time without penalty loss of benefits to which the participant is otherwise entitled.

Confidentiality: Efforts will be made to keep personal information confidential. We will identify you by a research number and your demographic information, age, race, gender,

Figure A3.1: Page 1 of 3 of information document shown to study subjects.

movement disorder type and severity will be kept on the research record, however it will not be possible to identify you from this data. Personal information may be disclosed if required by law.
Organizations that may inspect and/or copy your research records for quality assurance and data analysis include groups such as the Research Ethics Committee and the Medicines Control Council (where appropriate).
If results are published, you will not be identified. Only overall statistics will be reported.

Contact Details: For further information please feel free to contact either of us and we will attempt to answer any questions you have.

Sarah Ward: 456263@students.wits.ac.za

Kimoon Kim: kimoon-kim@outlook.com

Should you have any complaints or problems with the research and how it is being conducted, please contact:

Zanele Ndlovi (Wits REC Administrator)
Tel: 011 717 1252/2700 email: zanele.ndlovu@wits.ac.za

Langutani Masingi (Wits REC Administrator)
Tel: 011 717 1234 email: langutani.masingi@wits.ac.za

Prof. Cleaton Jones (HREC Chair)
Tel: 011 717 2301

Prof Feldman (HREC Chair)
Tel: 011 488 3840

Prof Woodiwiss (HREC Chair)
Tel: 011 717 2153

Figure A3.2: Page 2 of 3 of information document shown to study subjects.

CONSENT

I, _____ (full name) have read the information document entitled **"Measurements of hand movements to characterize Parkinson's and Huntington's disease"** and fully understand what is requested of me. I declare that my decision to participate in this study is completely voluntary and has not been forced upon me my any superior or other party.
Should I wish to withdraw from this study at any time I may do so without needing any explanation and reason.

Sign: _____ Date: _____

Figure A3.3: Page 3 of 3 of information document shown to study subjects.

APPENDIX B – SOFTWARE SETUP

The Leap Motion software can either run as a service on a Window's operating system or as a daemon on a UNIX environment (Linux and Macintosh) [41]. The Leap Motion software development kit (SDK), also known as V2, connects to the Leap Motion Controller over a USB bus. There are two application programming interfaces (APIs) that could be used to get the tracking data from the device, by either applying the native interface and/or the WebSocket interface [41]. The native interface API is a library, which can be used to create a Leap-enabled application, while the WebSocket interface and JavaScript client library can be used to create a Leap-enabled web or mobile applications [41]. The system architecture for the native application interface, which will be used, is shown in figure B1.

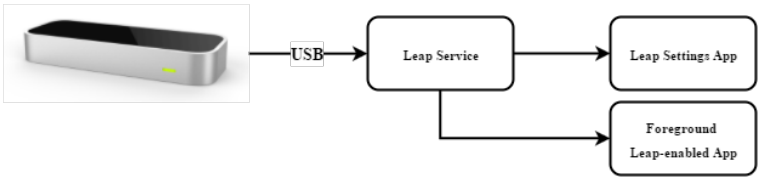

Figure B1: Leap Motion system architecture [41].

A new software application was developed using the Microsoft Visual Studio 2013 integrated development environment (IDE). The IDE was linked with the Leap Motion native library for the software application to get tracking data from the Leap Motion service which in turn received tracking data information from the Leap Motion Controller over the USB bus. The software application was developed using the C++ programming language with OpenCV and Leap Motion native libraries.

The first task was to get the Leap Motion Controller to respond to events and inputs in the application. This was done by adding the listener instance and a generic controller code in the main function as seen below in figure B2.

```
int main() {
	Quickstart listener;
	Leap::Controller controller;
	controller.addListener(listener);
	return 0;
}
```

Figure B2: Sample code to respond to events and inputs [41].

The generic controller instance provides an interface between the SDK and the Leap Motion. A function which tells the controller to start sending events to the listener subclass is shown in figure B3 below.

```
class Quickstart : public Leap::Listener {
public:
	virtual void onConnect(const Leap::Controller &);
	virtual void onFrame(const Leap::Controller &);
};
```

Figure B3: Sample code for Quickstart object [41].

The listener subclass contains two call-back methods: OnConnect() and OnFrame(). A call-back method was used opposed to polling for inputs as this would make the application more responsive, as input events would be acted on immediately. The OnConnect() handler made sure the controller driver and SDK were communicating with the device properly. The Quickstart::onFrame() class, shown in figure B4, will trigger the onFrame() handler when the device detects a hand. Once the hand is detected, the controller.frame() function returns a frame instance and this instance contains information about the hand such as fingers (e.g., PointableList) at a specific point in time. The

PointableList objects are used to track the finger's position (X, Y and Z components) and velocity using the tipPosition() and tipVelocity() function respectively.

```
void Quickstart::onFrame(const Leap::Controller &controller) {

	const Leap::Frame frame = controller.frame();

	if (frame.hands().isEmpty())
		return;

	const Leap::Hand firstHand = frame.hands()[0];

	const Leap::PointableList pointables = firstHand.pointables();
	if (pointables.isEmpty()) return;

	const Leap::FingerList fingers = firstHand.fingers();
	if (fingers.isEmpty()) return;

	for (int i = 0; i < fingers.count(); i++) {

		const Leap::Finger finger = fingers[i];

		std::cout << "Detected finger " << i << " at position (" <<
			finger.tipPosition().x << ", " <<
			finger.tipPosition().y << ", " <<
			finger.tipPosition().z << ")" << std::endl;

	}
}
```

Figure B4: Code sample in detecting finger coordinates [41].

With the first task completed, the second task was to draw the right index finger on the computer screen using the Leap Motion controller. OpenCV was used and integrated into the application to create the graphical user interface (GUI). A window with a resolution size of 3200x1800 pixels was created and within that window a grid with a step function was drawn. The tracking of the right index finger was shown as a red circular dot that was 50 pixels in diameter on the screen and it's X, Y and Z components, and velocity component was recorded in a text file. It was found out after finishing the second task that there were three problems associated with using this methodology.

APPENDIX C – X & Y DATA PLOTS FROM STEP-FUNCTION PATTERN

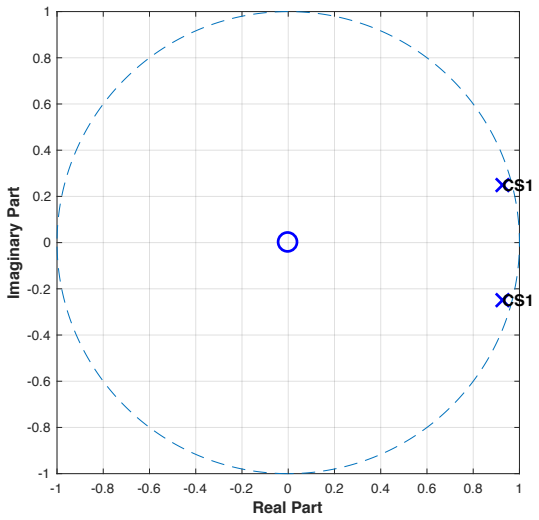

Figure C1: Pole-zero plot of control subject 1 using X-axis data.

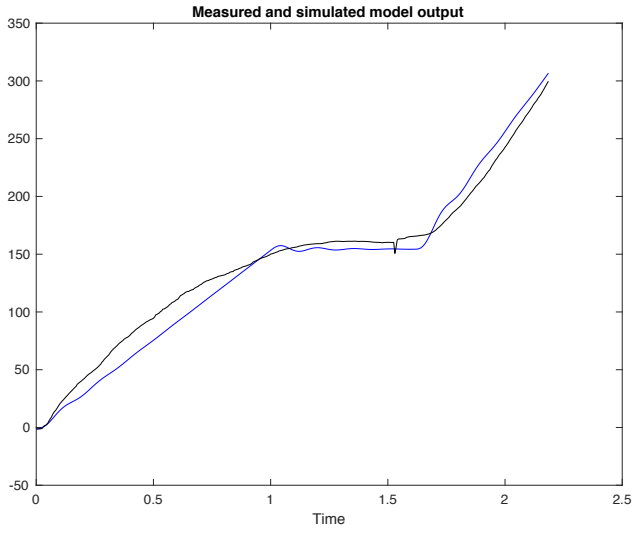

Figure C2: Measured (black) and simulated model (blue) output of control subject 1 with 82.0% best fit.

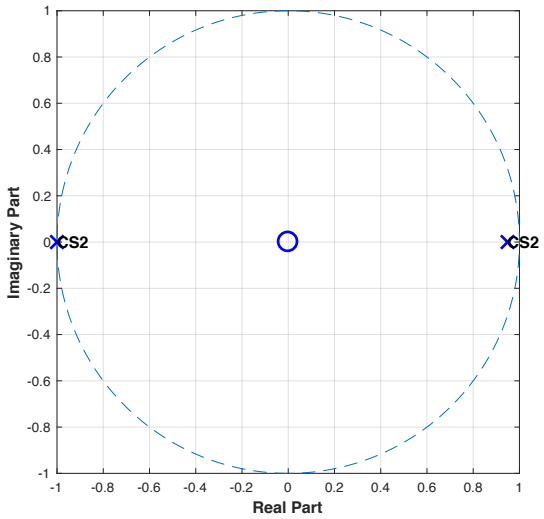

Figure C3: Pole-zero plot of control subject 2 using X-axis data.

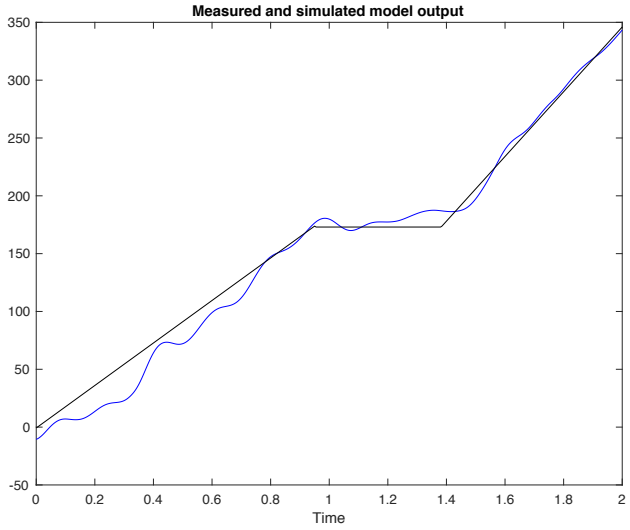

Figure C4: Measured (black) and simulated model (blue) output of control subject 2 with 86.5% best fit.

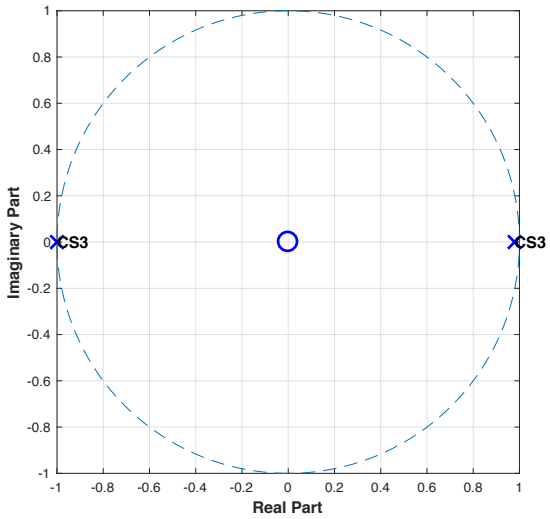

Figure C5: Pole-zero plot of control subject 3 using X-axis data.

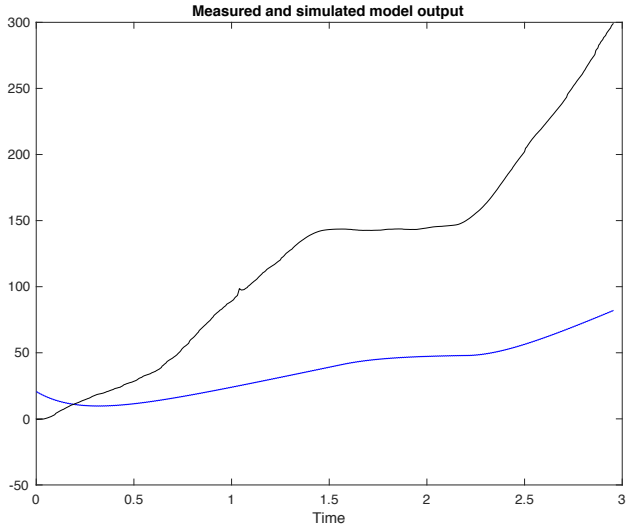

Figure C6: Measured (black) and simulated model (blue) output of control subject 3 with -34.3% best fit - omitted from the analysis.

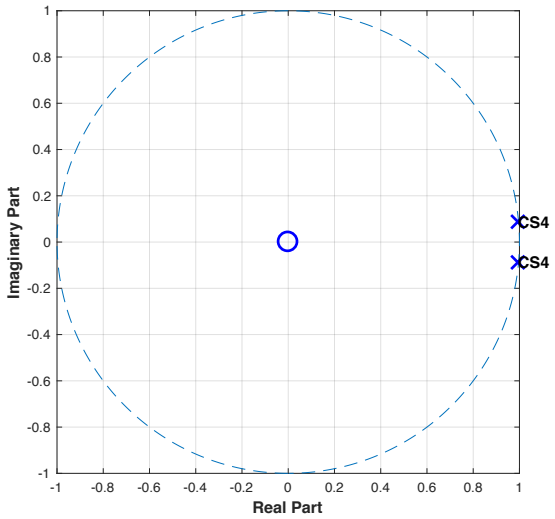

Figure C7: Pole-zero plot of control subject 4 using X-axis data.

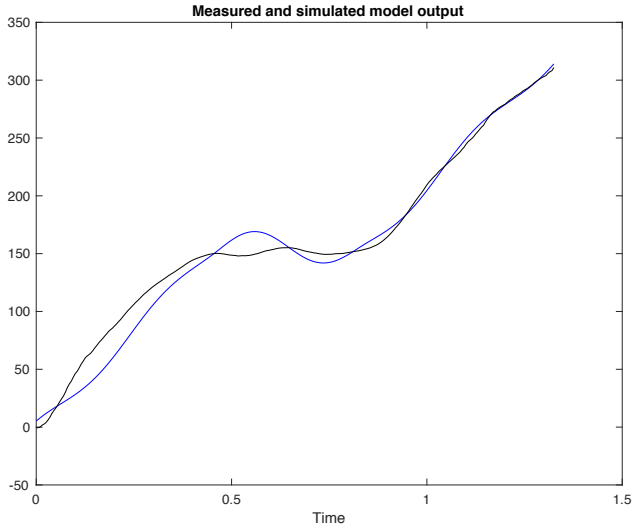

Figure C8: Measured (black) and simulated model (blue) output of control subject 4 with 84.4% best fit.

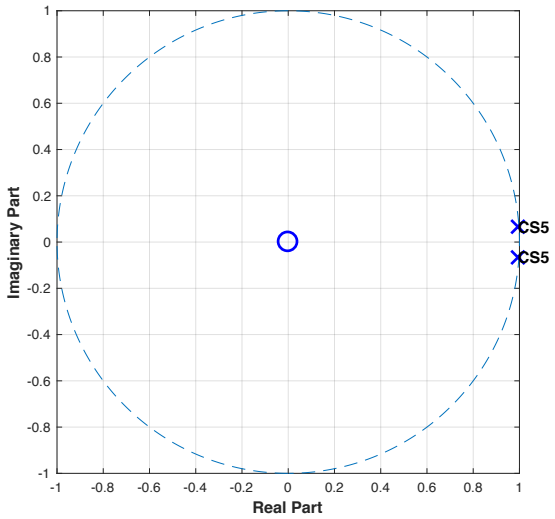

Figure C9: Pole-zero plot of control subject 5 using X-axis data.

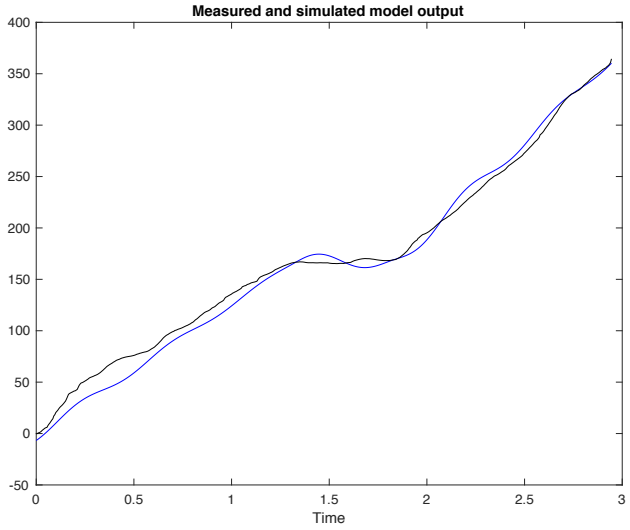

Figure C10: Measured (black) and simulated model (blue) output of control subject 5 with 89.3% best fit.

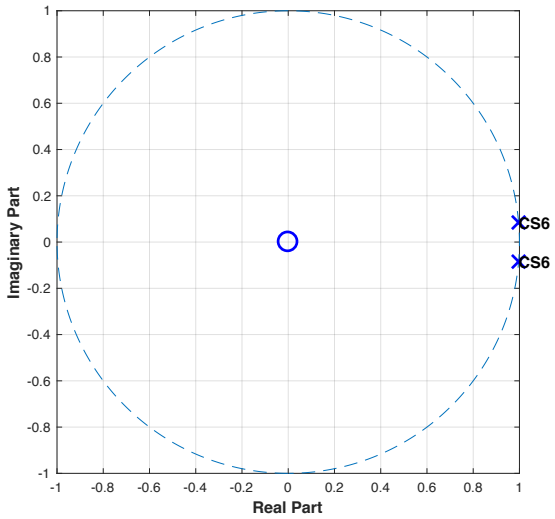

Figure C11: Pole-zero plot of control subject 6 using X-axis data.

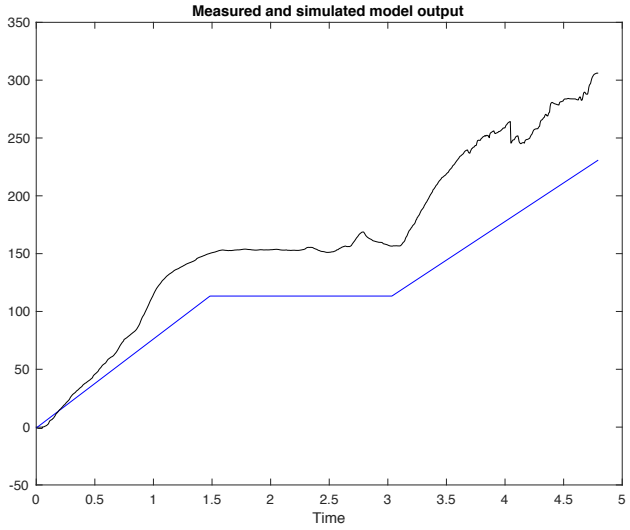

Figure C12: Measured (black) and simulated model (blue) output of control subject 6 with 33.9% best fit - omitted from the analysis.

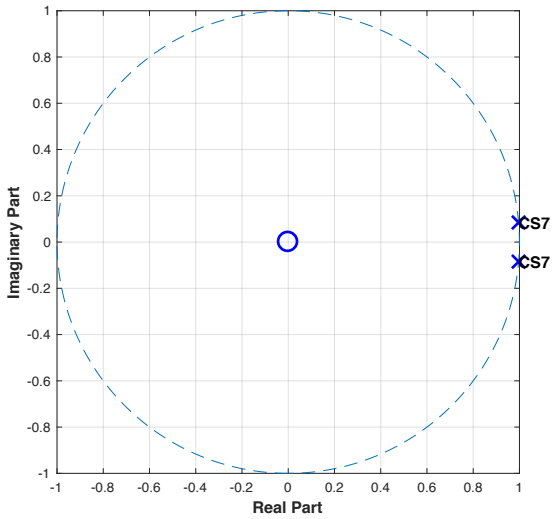

Figure C13: Pole-zero plot of control subject 7 using X-axis data.

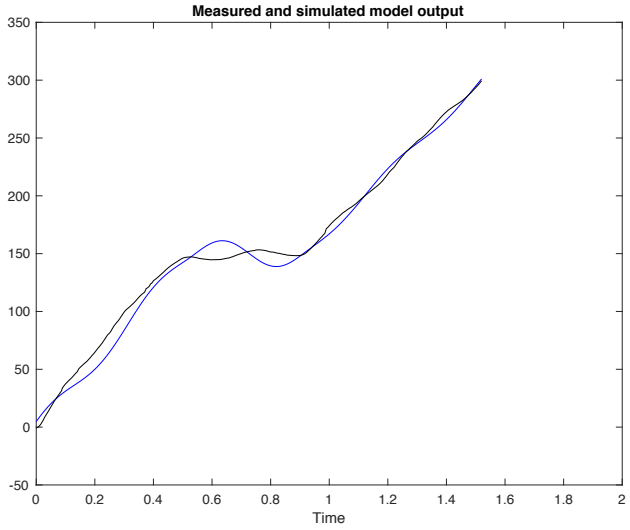

Figure C14: Measured (black) and simulated model (blue) output of control subject 7 with 88.8% best fit.

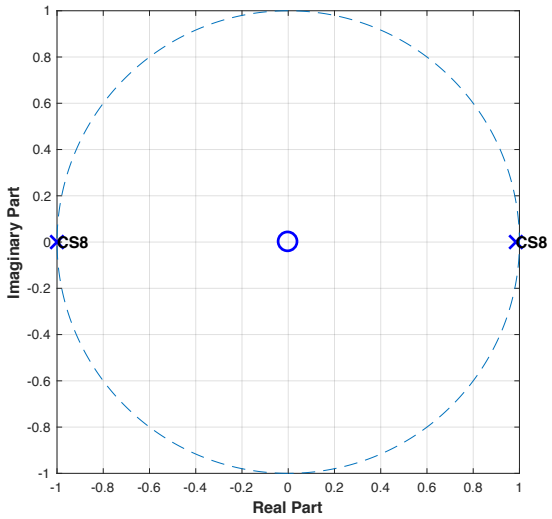

Figure C15: Pole-zero plot of control subject 8 using X-axis data.

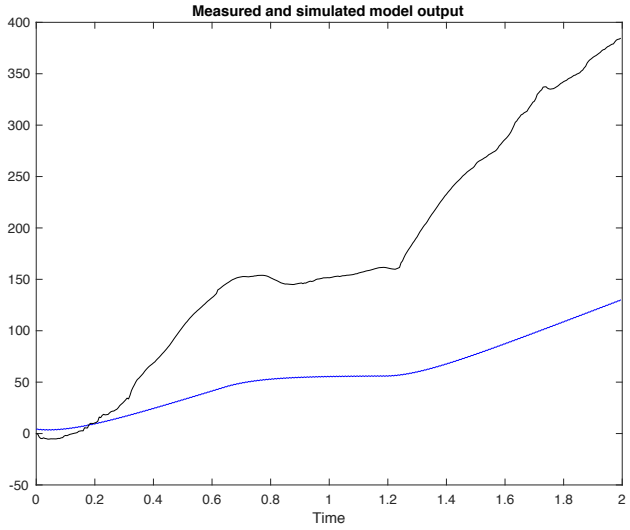

Figure C16: Measured (black) and simulated model (blue) output of control subject 8 with -25.5% best fit - omitted from the analysis.

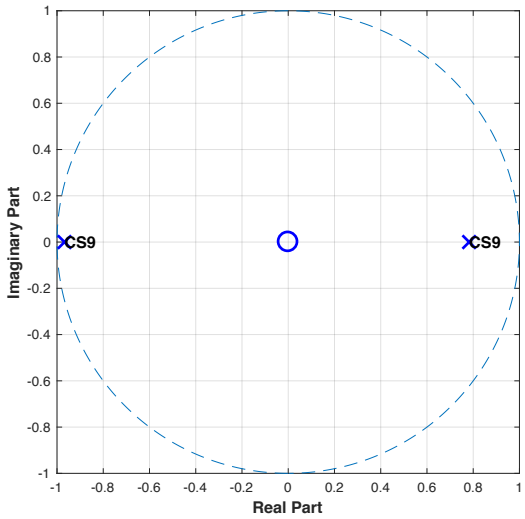

Figure C17: Pole-zero plot of control subject 9 using X-axis data.

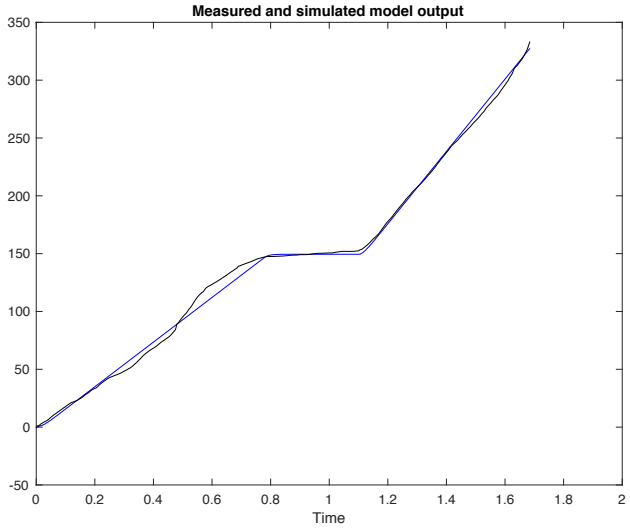

Figure C18: Measured (black) and simulated model (blue) output of control subject 9 with 94.7% best fit.

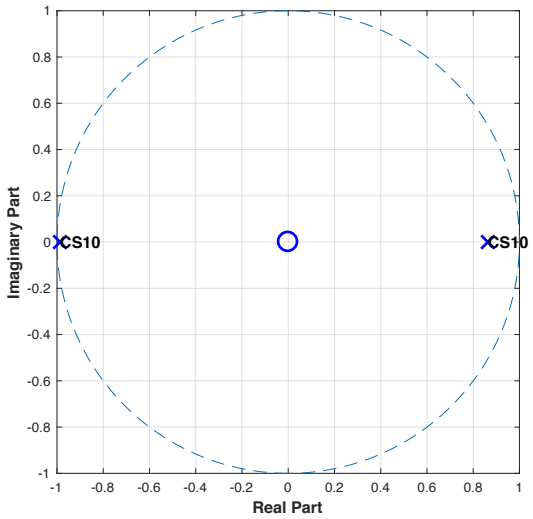

Figure C19: Pole-zero plot of control subject 10 using X-axis data.

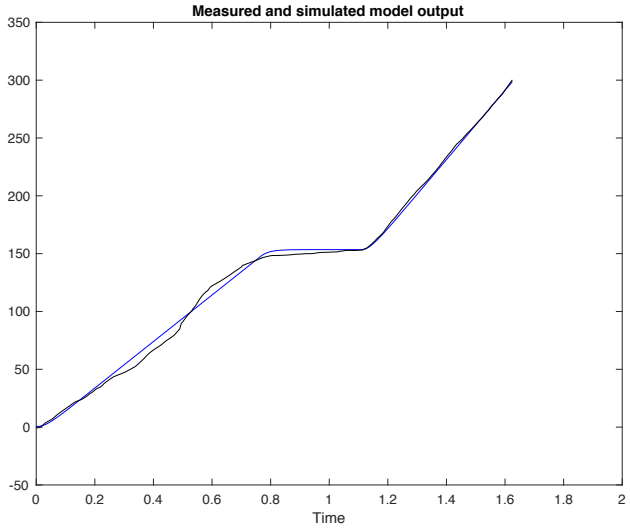

Figure C20: Measured (black) and simulated model (blue) output of control subject 10 with 95.0% best fit.

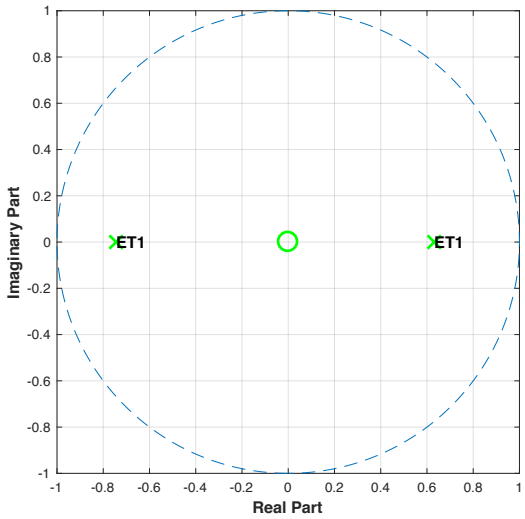

Figure C21: Pole-zero plot of ET patient 1 using X-axis data.

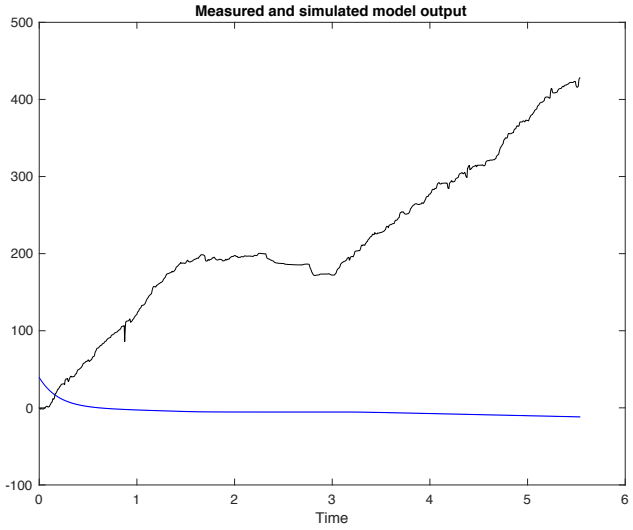

Figure C22: Measured (black) and simulated model (blue) output of ET patient 1 with -134.8% best fit - omitted from the analysis.

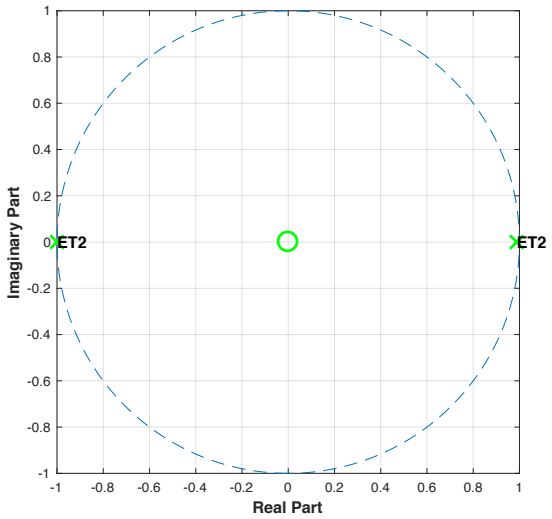

Figure C23: Pole-zero plot of ET patient 2 using X-axis data.

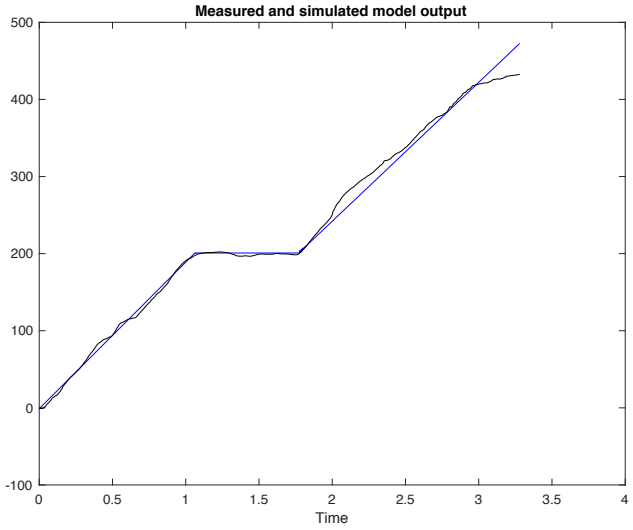

Figure C24: Measured (black) and simulated model (blue) output of control ET patient 2 with 92.1% best fit.

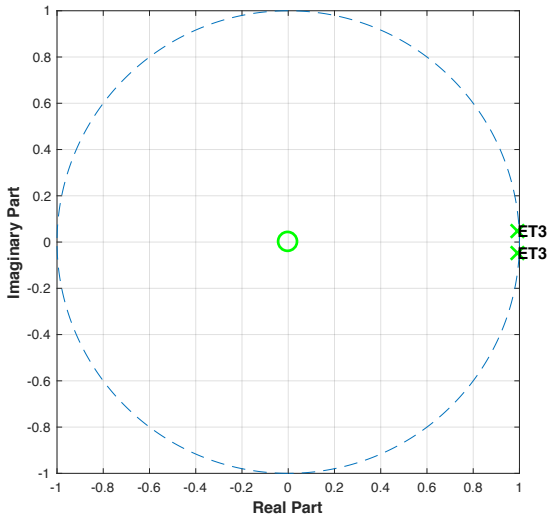

Figure C25: Pole-zero plot of ET patient 3 using X-axis data.

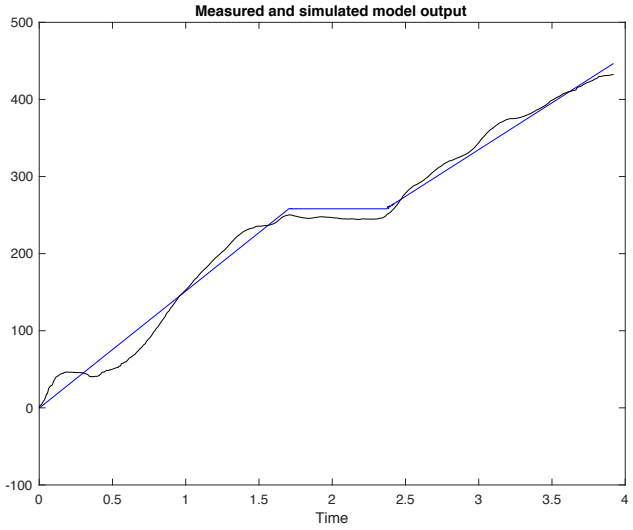

Figure C26: Measured (black) and simulated model (blue) output of ET patient 3 with 89.5% best fit.

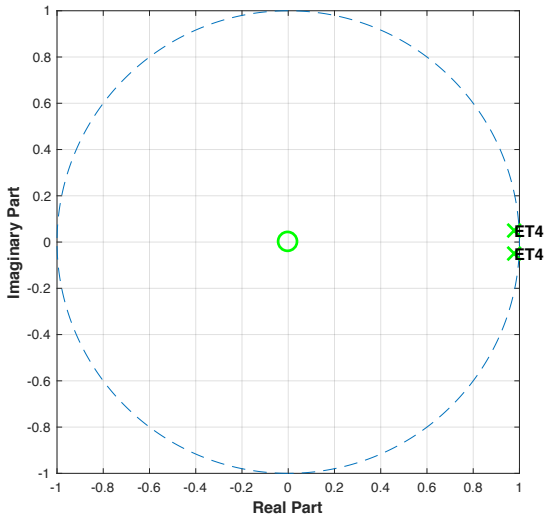

Figure C27: Pole-zero plot of ET patient 4 using X-axis data.

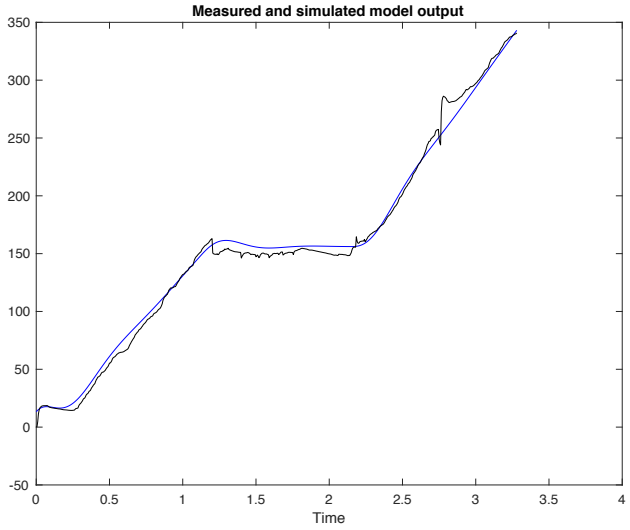

Figure C28: Measured (black) and simulated model (blue) output of ET patient 4 with 92.3% best fit.

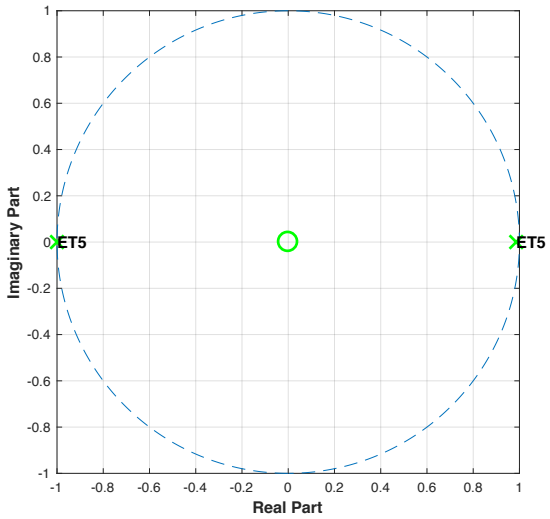

Figure C29: Pole-zero plot of ET patient 5 using X-axis data.

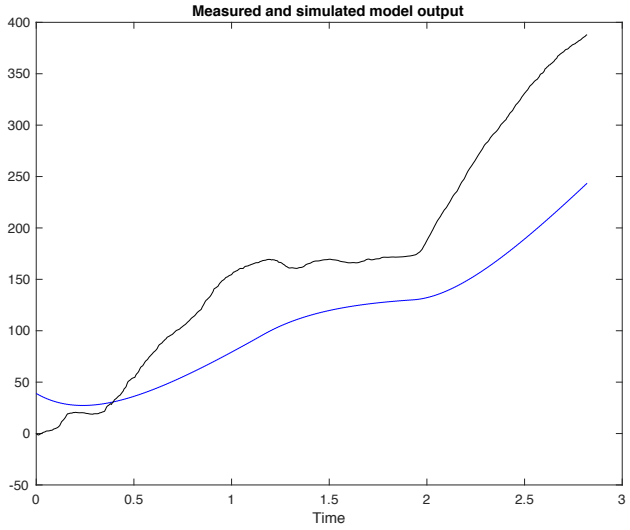

Figure C30: Measured (black) and simulated model (blue) output of ET patient 5 with 24.9% best fit - omitted from the analysis.

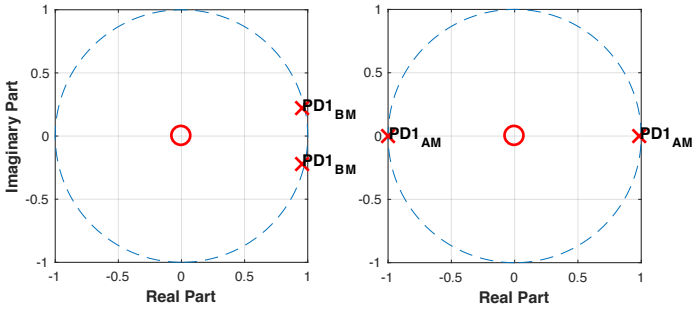

Figure C31: Pole-zero plot for PD patient 1 before and after medication using X-axis data.

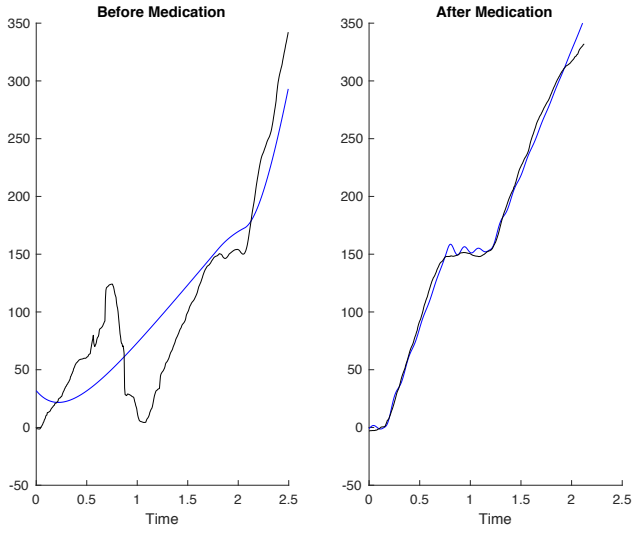

Figure C32: Measured (black) and simulated model (blue) output of PD patient 1 before and after medication with 85.1% and 93.3% best fit respectively.

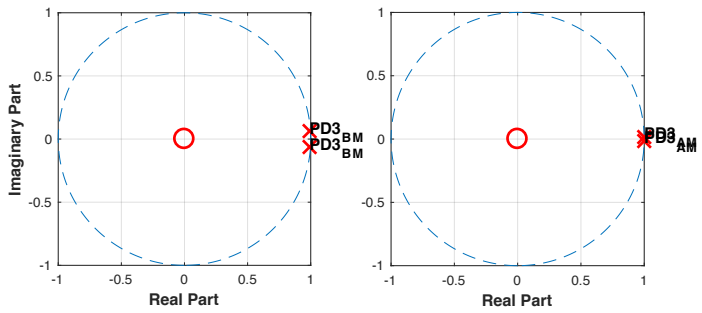

Figure C33: Pole-zero plot for PD patient 3 before and after medication using X-axis data.

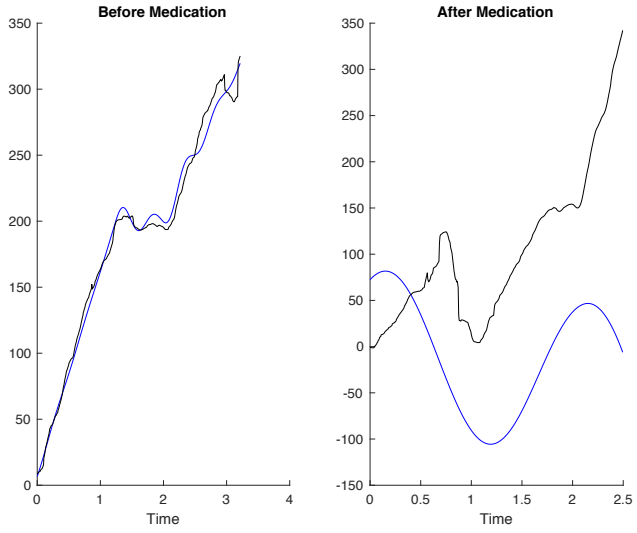

Figure C34: Measured (black) and simulated model (blue) output of PD patient 3 before and after medication with 89.7% and -89.6% (omitted from the analysis) best fit respectively.

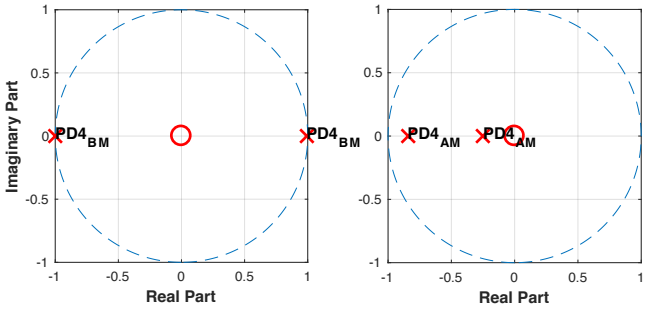

Figure C35: Pole-zero plot for PD patient 4 before and after medication using X-axis data.

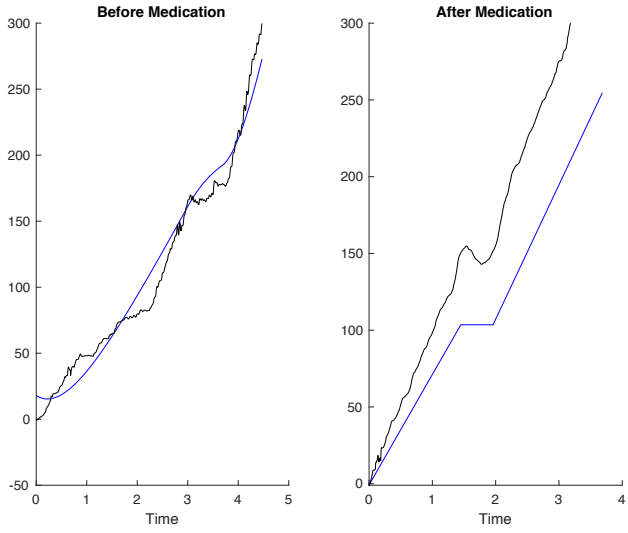

Figure C36: Measured (black) and simulated model (blue) output of PD patient 4 before and after medication with 82.6% and -39.2% (omitted from the analysis) best fit respectively.

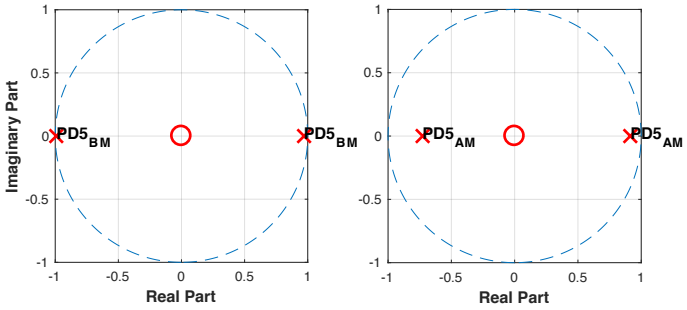

Figure C37: Pole-zero plot for PD patient 5 before and after medication using X-axis data.

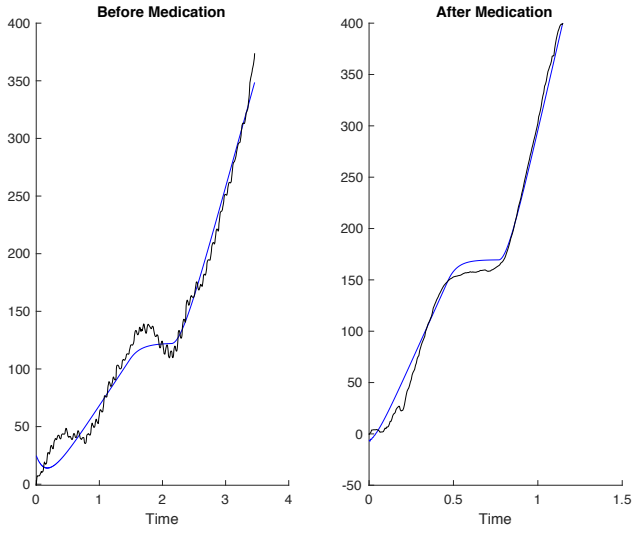

Figure C38: Measured (black) and simulated model (blue) output of PD patient 5 before and after medication with 87.7% and 90.9% best fit respectively.

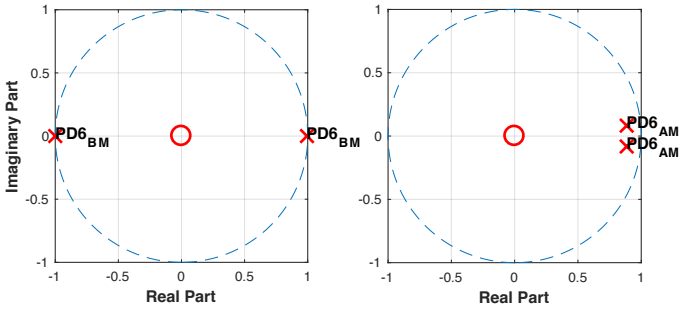

Figure C39: Pole-zero plot for PD patient 6 before and after medication using X-axis data.

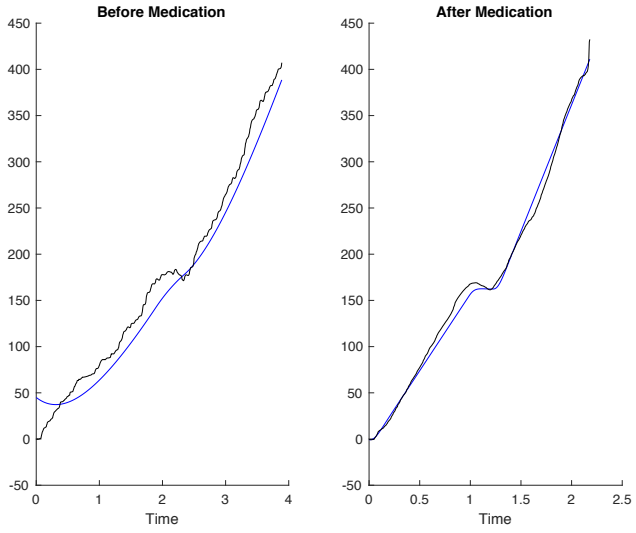

Figure C40: Measured (black) and simulated model (blue) output of PD patient 6 before and after medication with 82.0% and 92.8% best fit respectively.

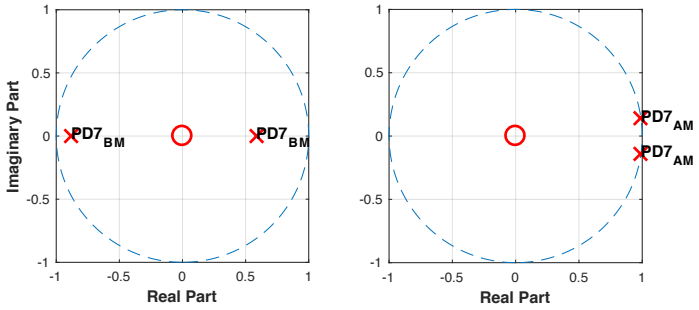

Figure C41: Pole-zero plot for PD patient 7 before and after medication using X-axis data.

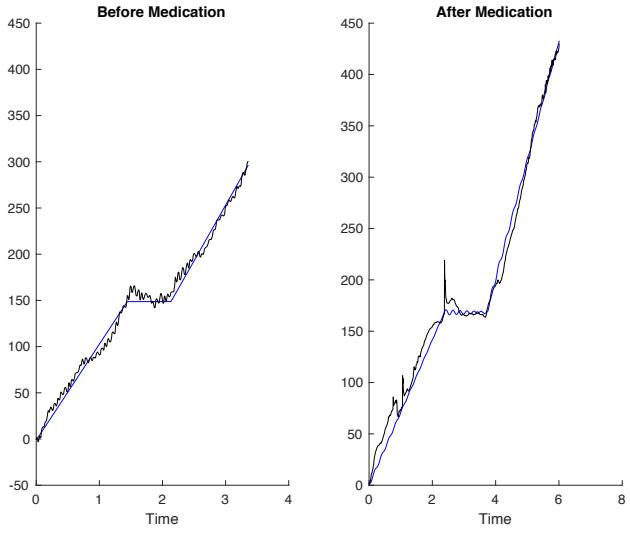

Figure C42: Measured (black) and simulated model (blue) output of PD patient 7 before and after medication with 90.2% and 89.3% best fit respectively.

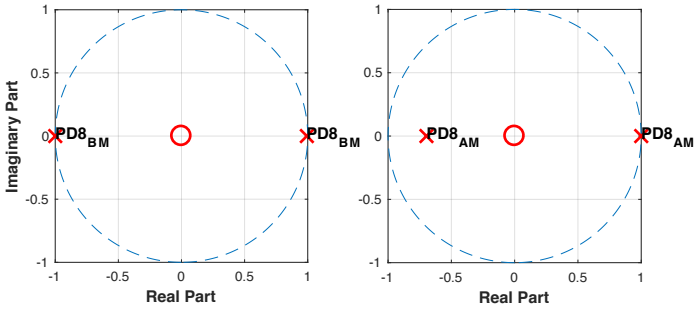

Figure C43: Pole-zero plot for PD patient 8 before and after medication using X-axis data.

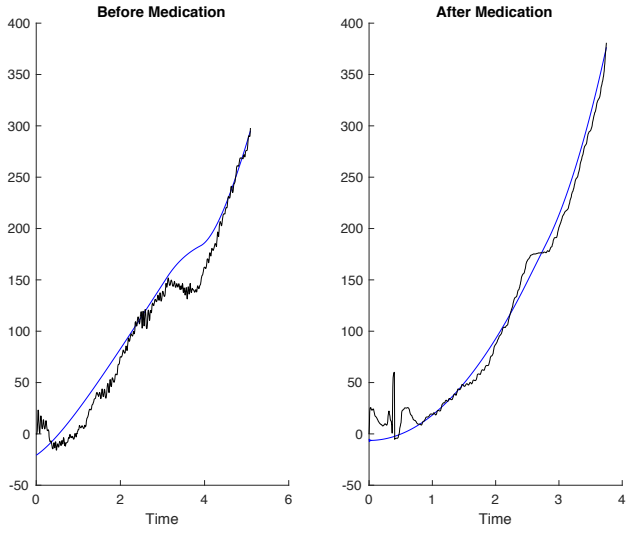

Figure C44: Measured (black) and simulated model (blue) output of PD patient 8 before and after medication with 78.2% and 86.8% best fit respectively.

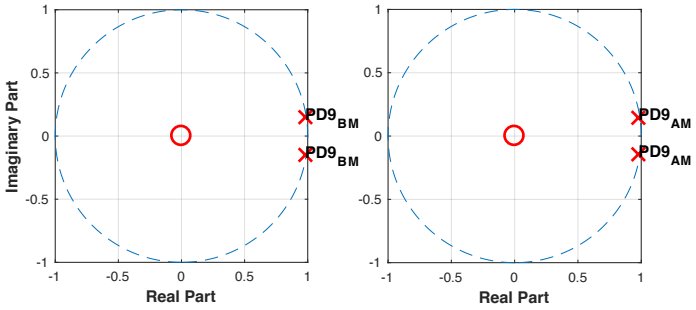

Figure C45: Pole-zero plot for PD patient 9 before and after medication using X-axis data.

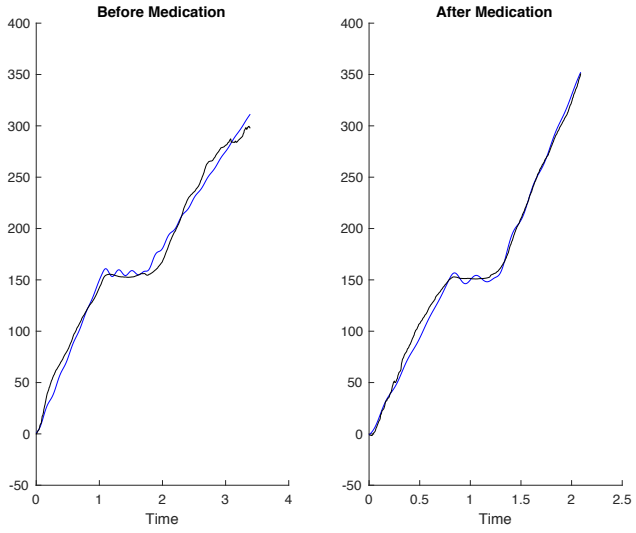

Figure C46: Measured (black) and simulated model (blue) output of PD patient 9 before and after medication with 89.9% and 93.5% best fit respectively.

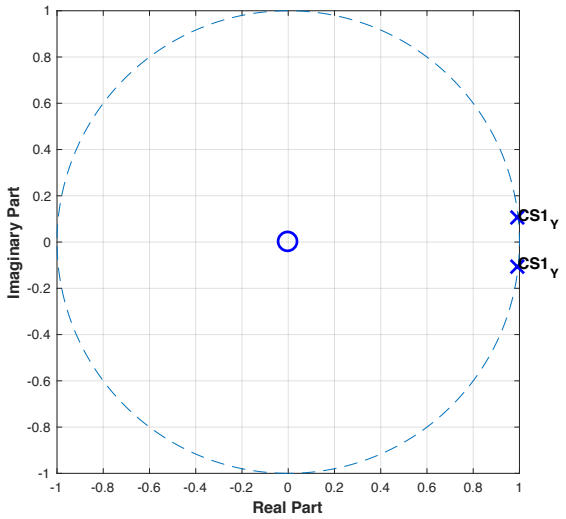

Figure C47: Pole-zero plot of control subject 1 using Y-axis data.

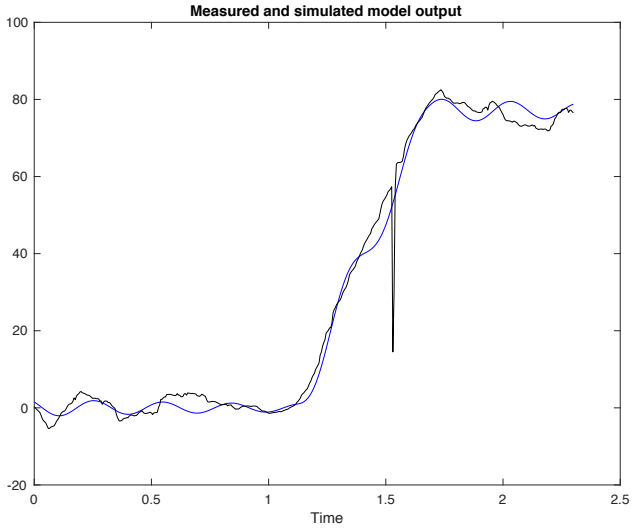

Figure C48: Measured (black) and simulated model (blue) output of control subject 1 with 90.2% best fit.

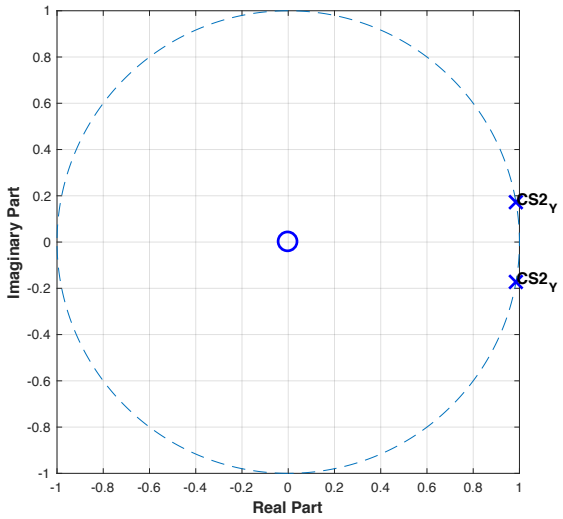

Figure C49: Pole-zero plot of control subject 2 using Y-axis data.

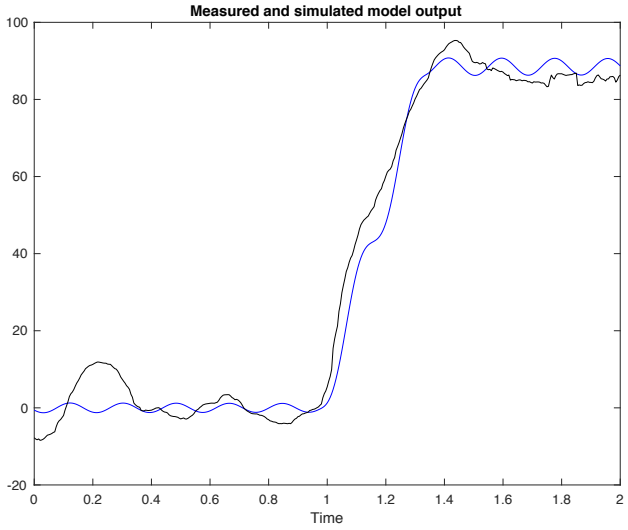

Figure C50: Measured (black) and simulated model (blue) output of control subject 2 with 86.9% best fit.

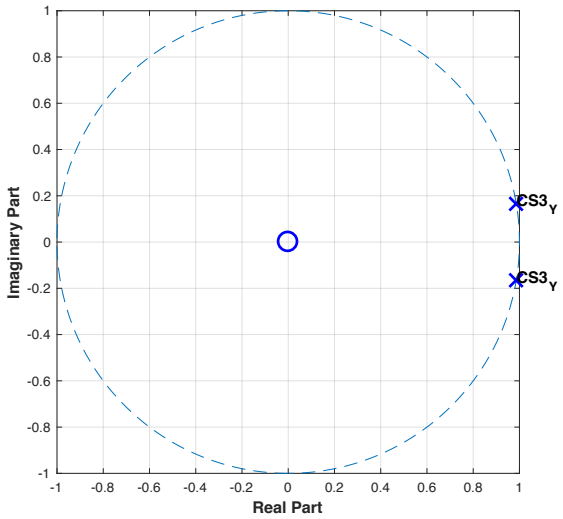

Figure C51: Pole-zero plot of control subject 3 using Y-axis data.

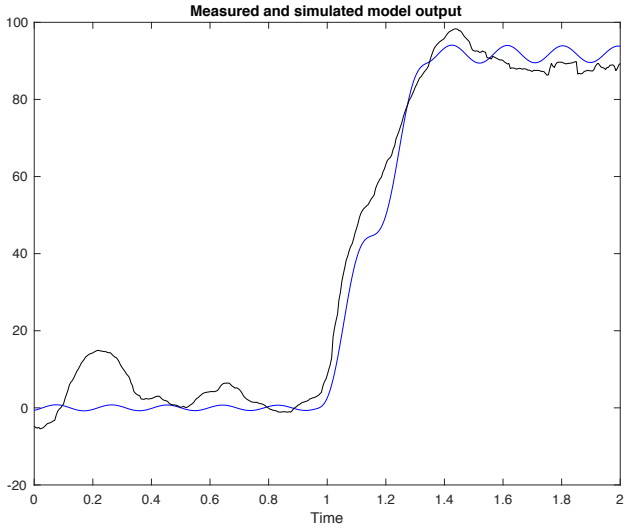

Figure C52: Measured (black) and simulated model (blue) output of control subject 3 with 85.4% best fit.

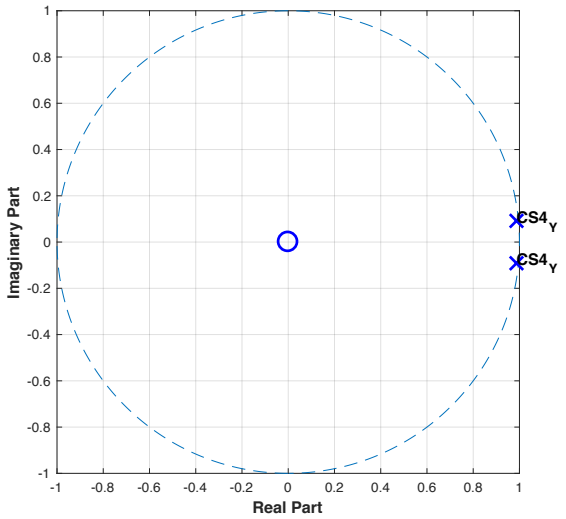

Figure C53: Pole-zero plot of control subject 4 using Y-axis data.

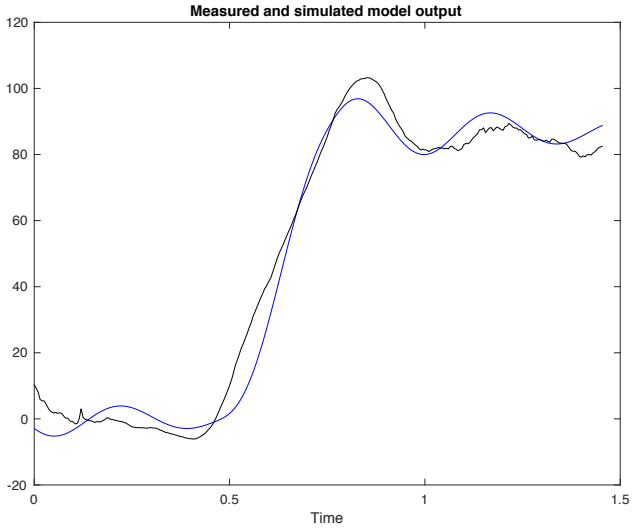

Figure C54: Measured (black) and simulated model (blue) output of control subject 4 with 86.2% best fit.

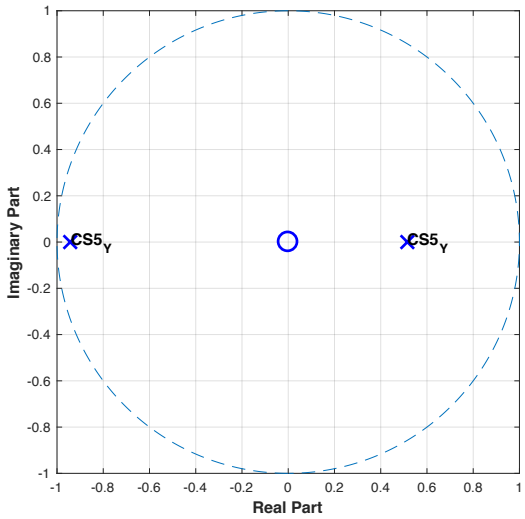

Figure C55: Pole-zero plot of control subject 5 using Y-axis data.

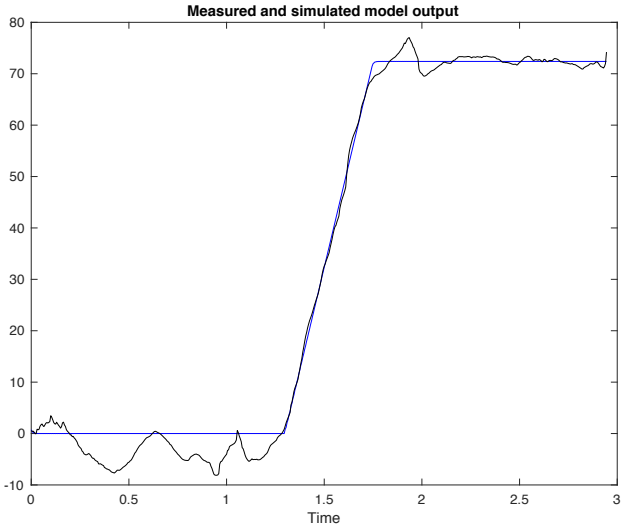

Figure C56: Measured (black) and simulated model (blue) output of control subject 5 with 91.9% best fit.

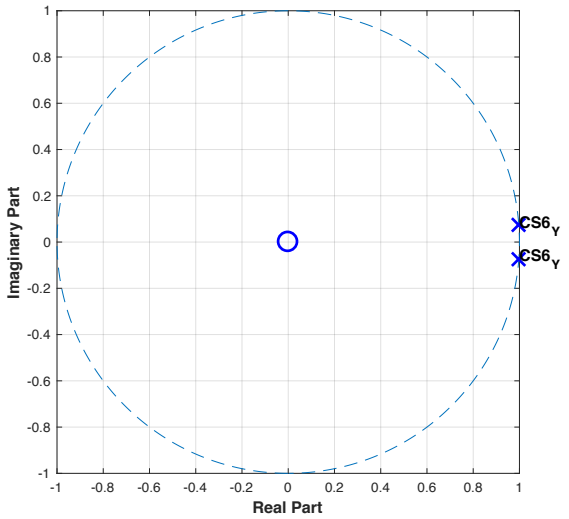

Figure C57: Pole-zero plot of control subject 6 using Y-axis data.

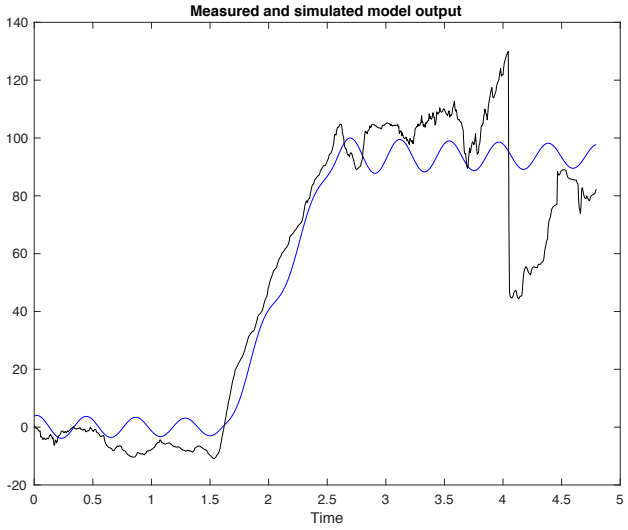

Figure C58: Measured (black) and simulated model (blue) output of control subject 6 with 69.2% best fit.

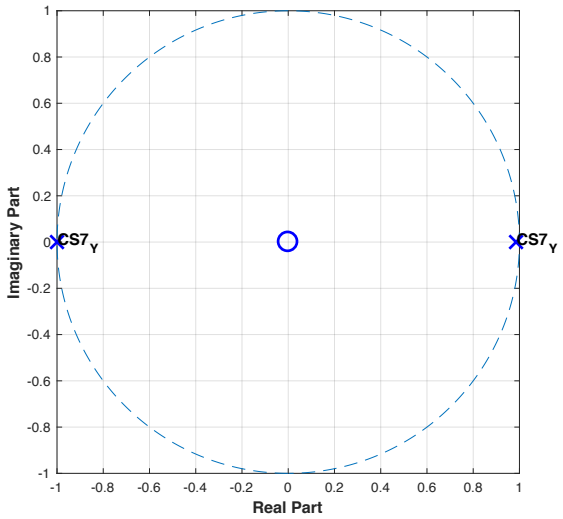

Figure C59: Pole-zero plot of control subject 7 using Y-axis data.

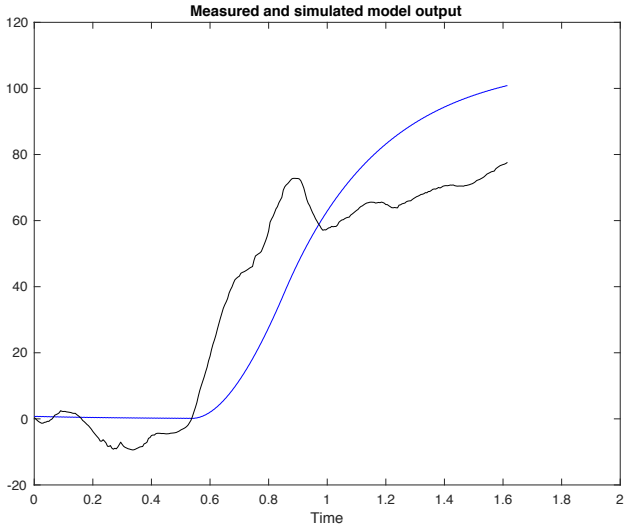

Figure C60: Measured (black) and simulated model (blue) output of control subject 7 with 84.1% best fit.

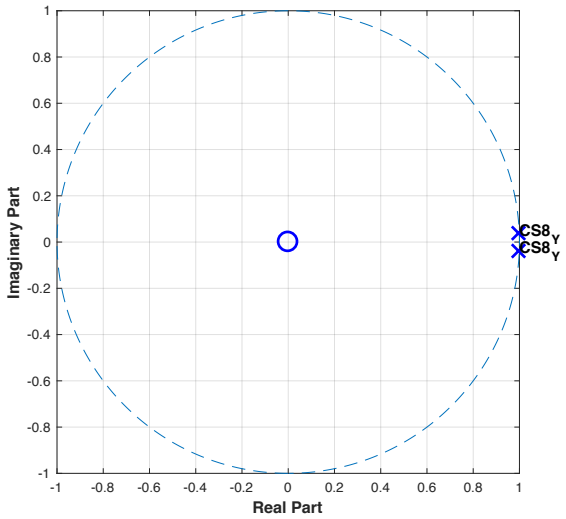

Figure C61: Pole-zero plot of control subject 8 using Y-axis data.

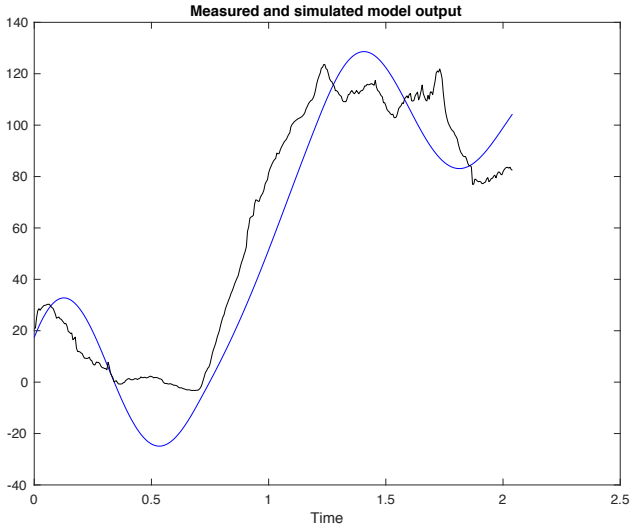

Figure C62: Measured (black) and simulated model (blue) output of control subject 8 with 64.5% best fit.

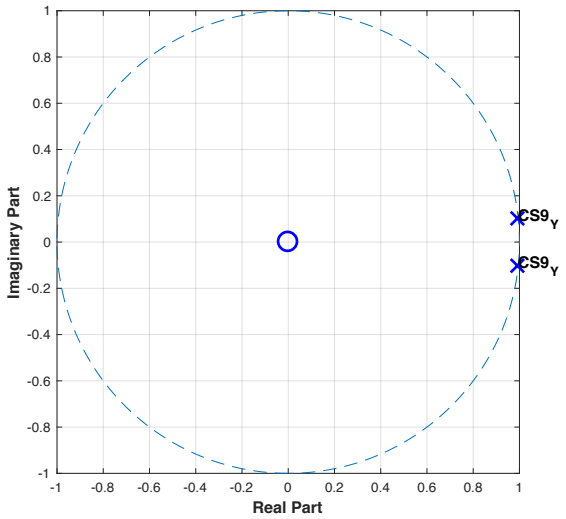

Figure C63: Pole-zero plot of control subject 9 using Y-axis data.

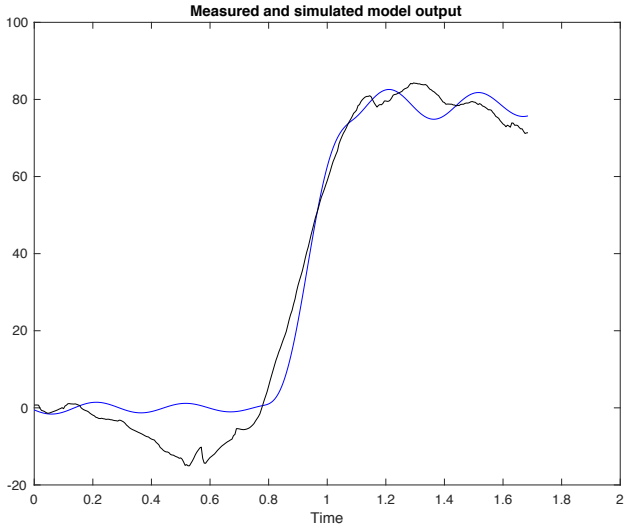

Figure C64: Measured (black) and simulated model (blue) output of control subject 9 with 84.2% best fit.

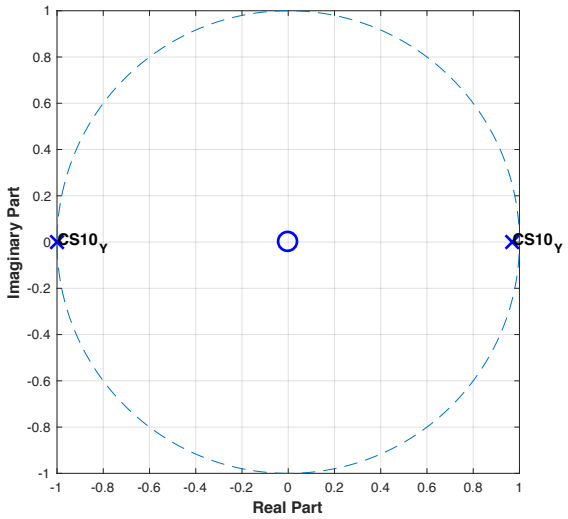

Figure C65: Pole-zero plot of control subject 10 using Y-axis data.

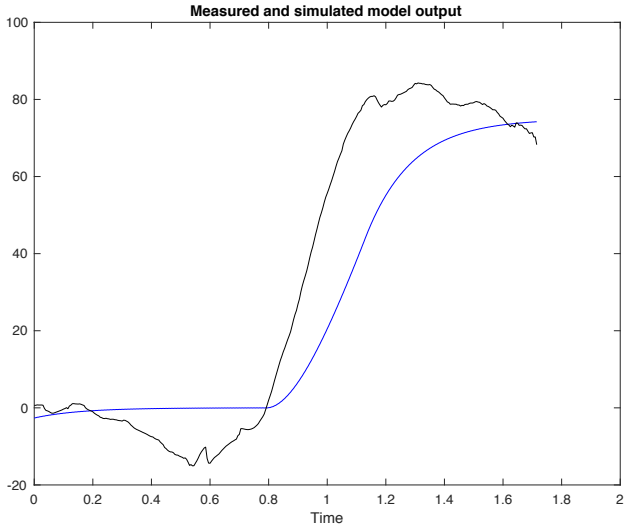

Figure C66: Measured (black) and simulated model (blue) output of control subject 10 with 49.4% best fit.

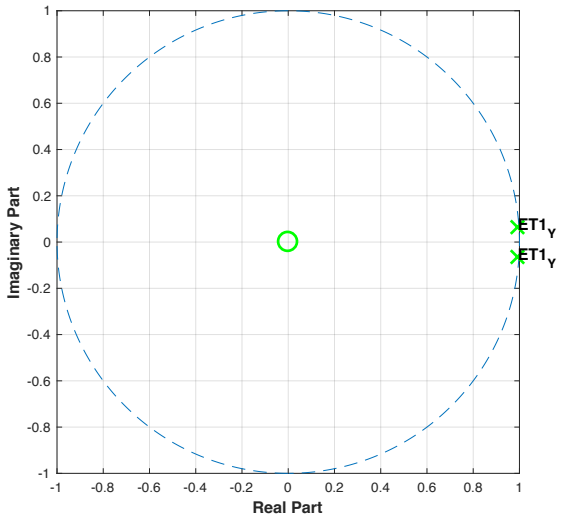

Figure C67: Pole-zero plot of ET patient 1 using Y-axis data.

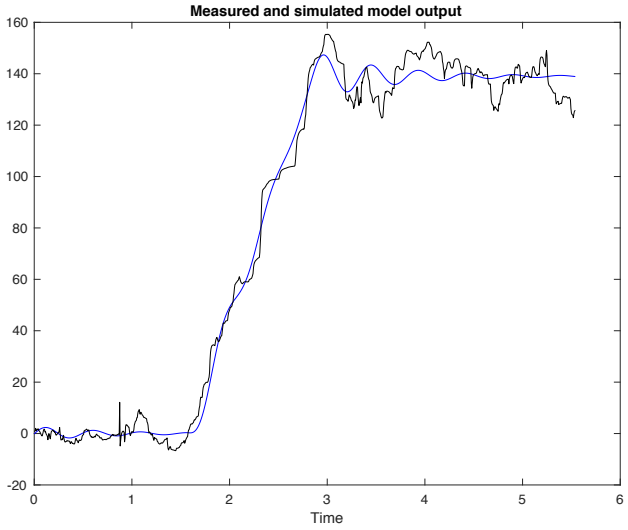

Figure C68: Measured (black) and simulated model (blue) output of ET patient 1 with 90.5% best fit.

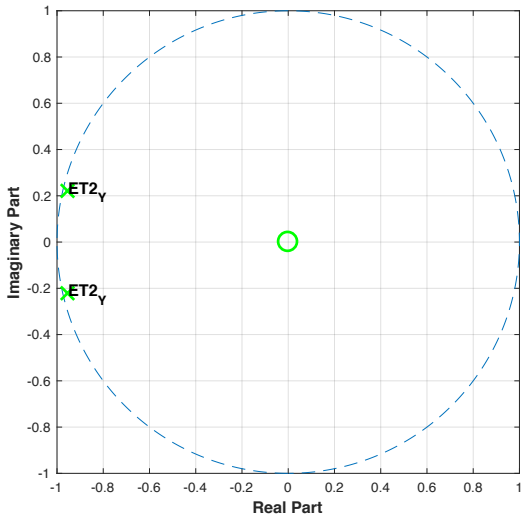

Figure C69: Pole-zero plot of ET patient 2 using Y-axis data.

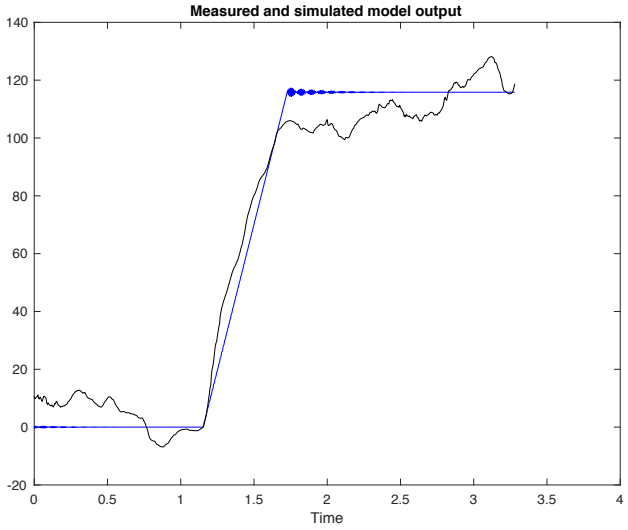

Figure C70: Measured (black) and simulated model (blue) output of ET patient 2 with -3.7% best fit - omitted from the analysis.

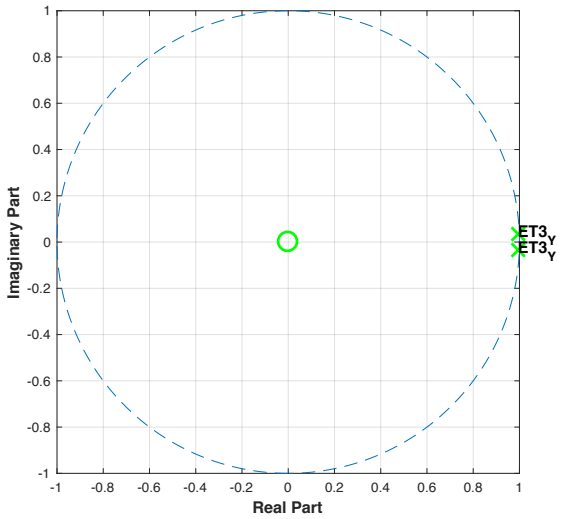

Figure C71: Pole-zero plot of ET patient 3 using Y-axis data.

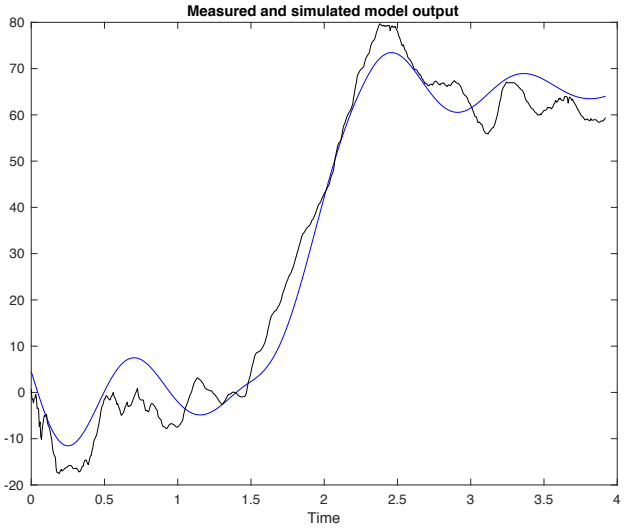

Figure C72: Measured (black) and simulated model (blue) output of ET patient 3 with 83.6% best fit.

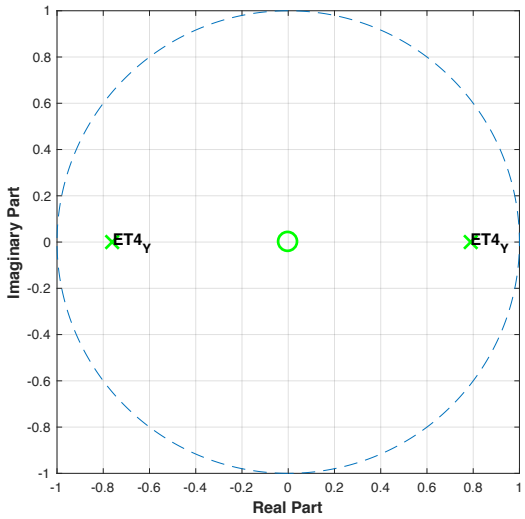

Figure C73: Pole-zero plot of ET patient 4 using Y-axis data.

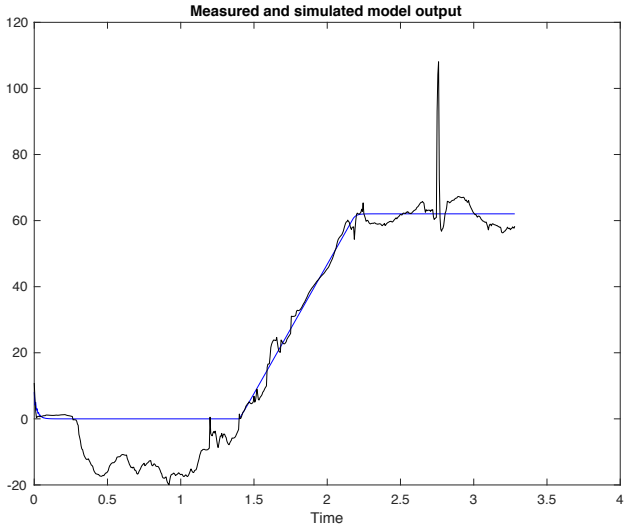

Figure C74: Measured (black) and simulated model (blue) output of ET patient 4 with 74.4% best fit.

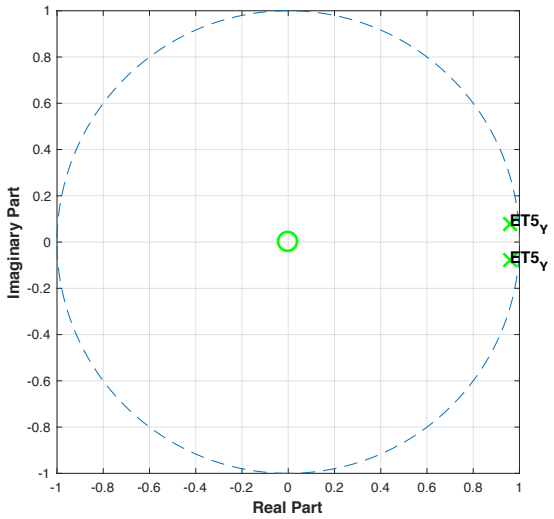

Figure C75: Pole-zero plot of ET patient 5 using Y-axis data.

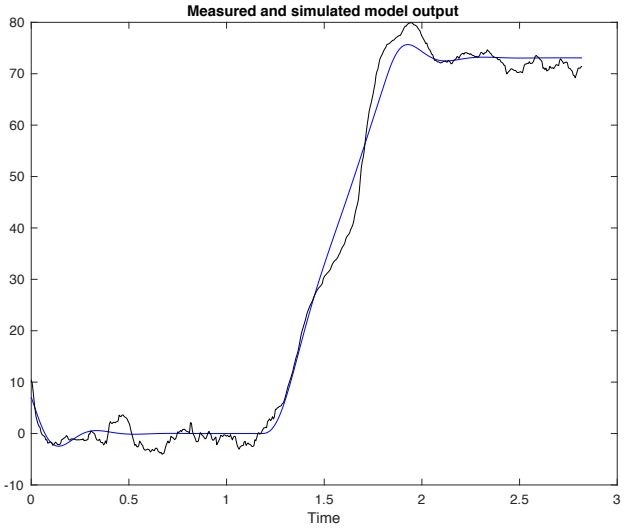

Figure C76: Measured (black) and simulated model (blue) output of ET patient 5 with 92.1% best fit.

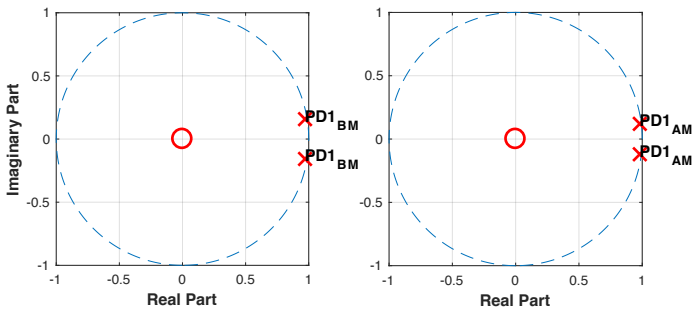

Figure C77: Pole-zero plot for PD patient 1 before and after medication using Y-axis data.

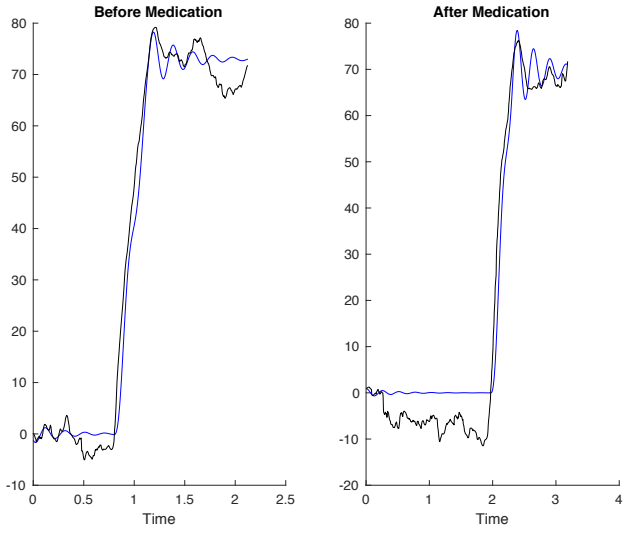

Figure C78: Measured (black) and simulated model (blue) output of PD patient 1 before and after medication with 87.6% and 81.0% best fit respectively.

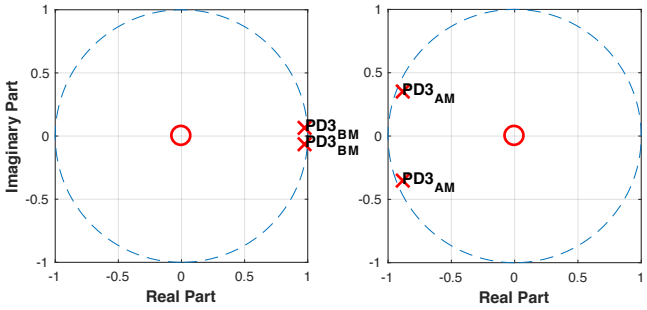

Figure C79: Pole-zero plot for PD patient 3 before and after medication using Y-axis data.

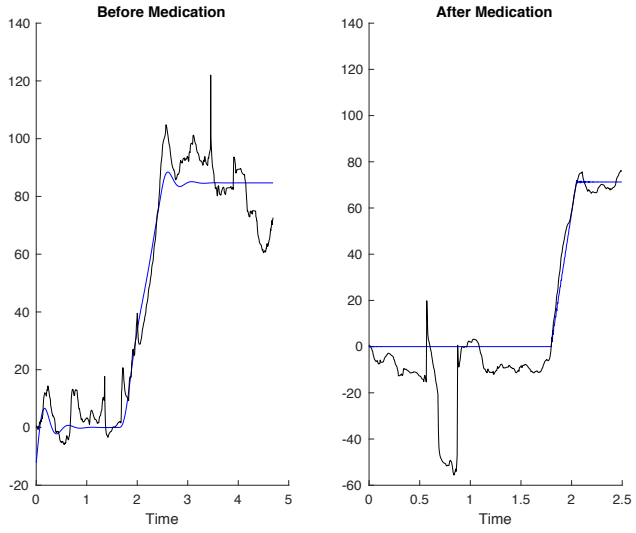

Figure C80: Measured (black) and simulated model (blue) output of PD patient 3 before and after medication with 77.5% and 55.7% best fit respectively.

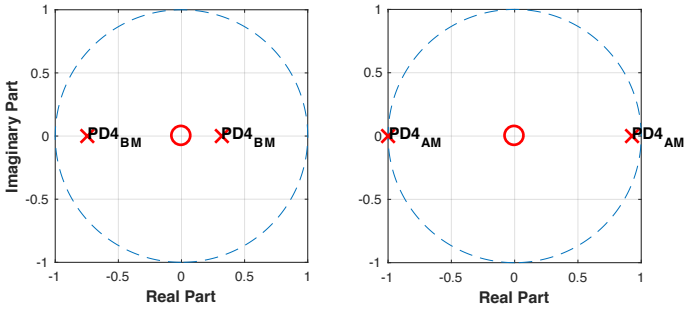

Figure C81: Pole-zero plot for PD patient 4 before and after medication using Y-axis data.

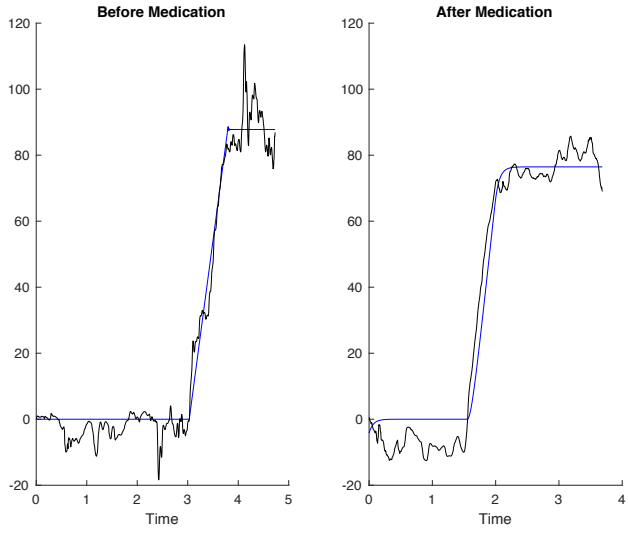

Figure C82: Measured (black) and simulated model (blue) output of PD patient 4 before and after medication with 85.4% and 82.3% best fit respectively.

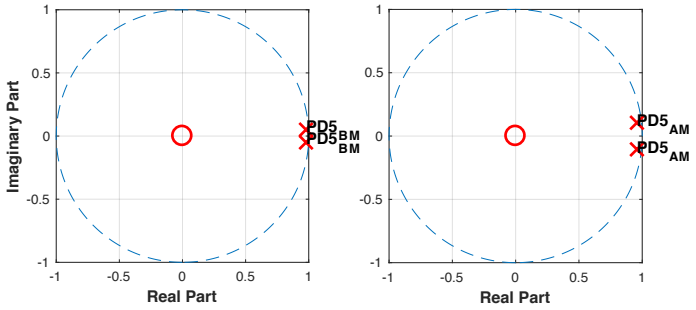

Figure C83: Pole-zero plot for PD patient 5 before and after medication using Y-axis data.

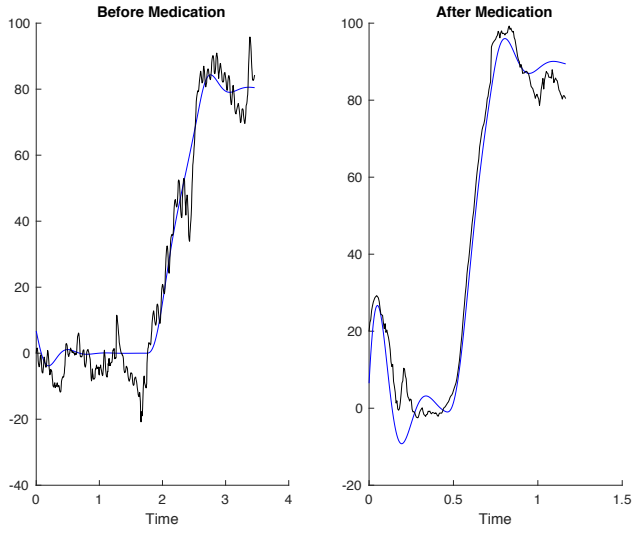

Figure C84: Measured (black) and simulated model (blue) output of PD patient 5 before and after medication with 82.1% and 84.6% best fit respectively.

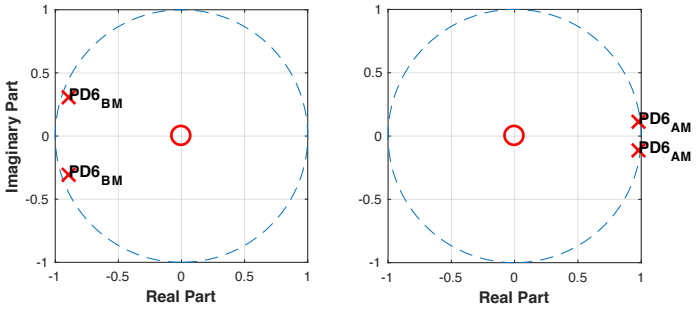

Figure C85: Pole-zero plot for PD patient 6 before and after medication using Y-axis data.

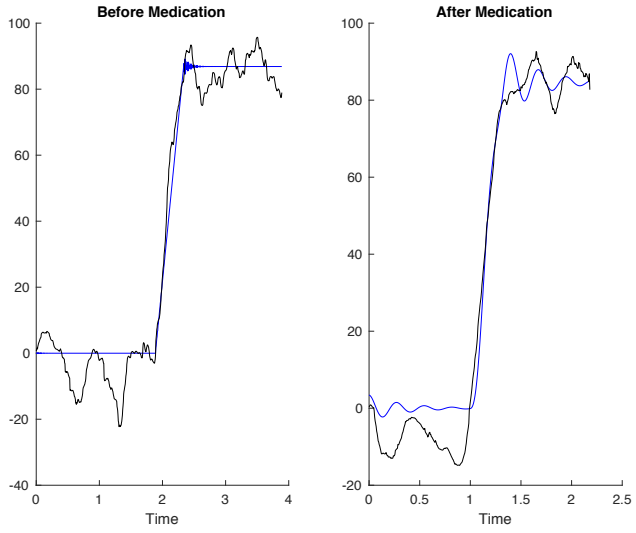

Figure C86: Measured (black) and simulated model (blue) output of PD patient 6 before and after medication with 84.0% and 83.6% best fit respectively.

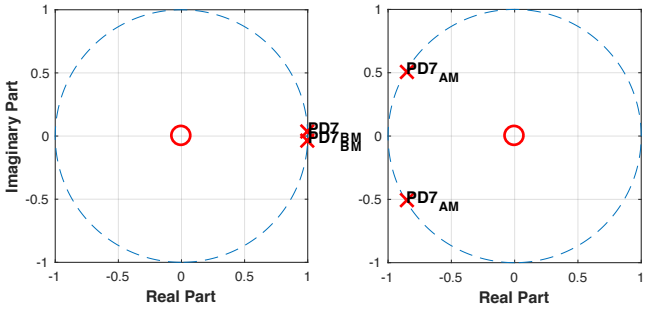

Figure C87: Pole-zero plot for PD patient 7 before and after medication using Y-axis data.

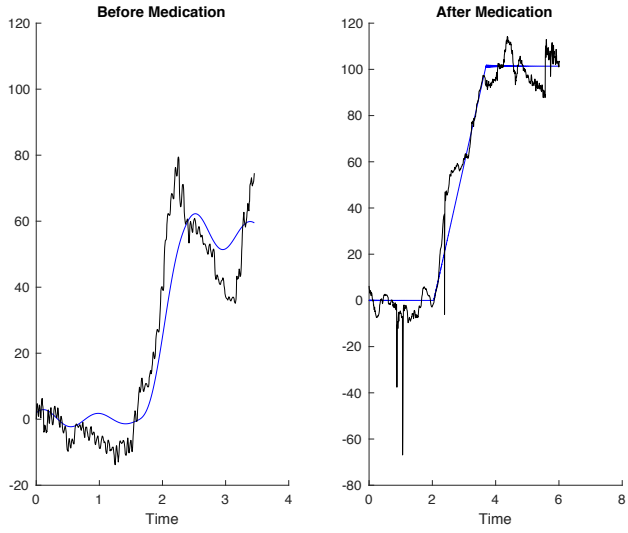

Figure C88: Measured (black) and simulated model (blue) output of PD patient 7 before and after medication with 64.7% and 82.4% best fit respectively.

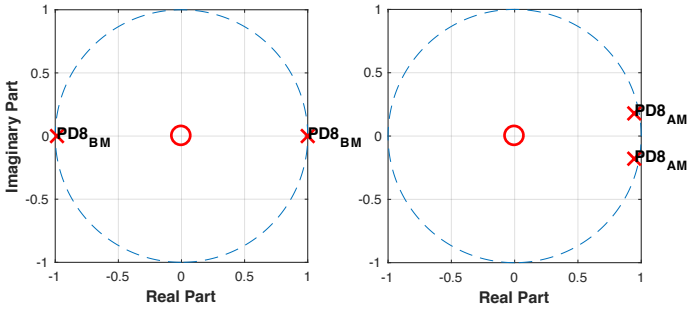

Figure C89: Pole-zero plot for PD patient 8 before and after medication using Y-axis data.

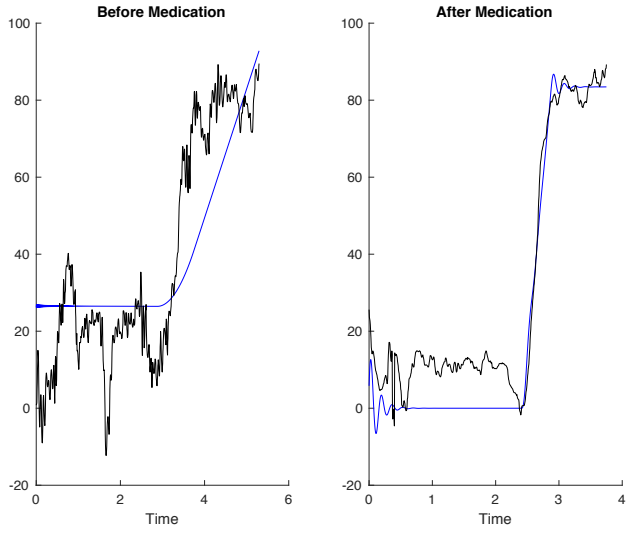

Figure C90: Measured (black) and simulated model (blue) output of PD patient 8 before and after medication with 44.1% (omitted from the analysis) and 72.1% best fit respectively.

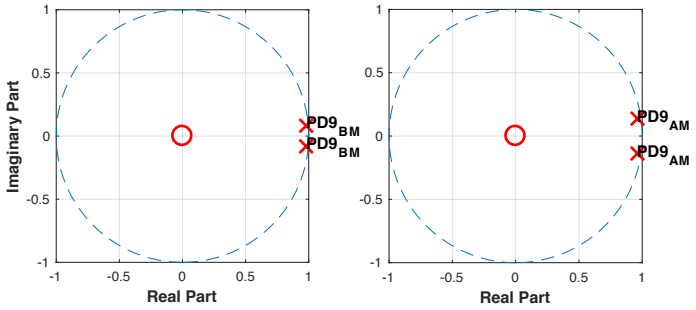

Figure C91: Pole-zero plot for PD patient 9 before and after medication using Y-axis data.

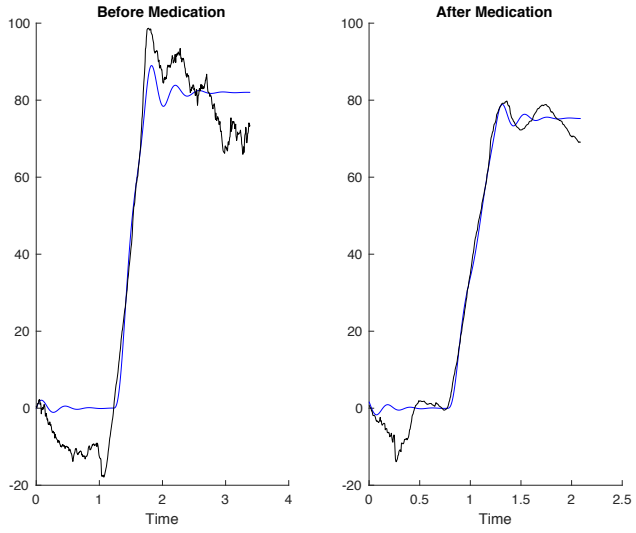

Figure C92: Measured (black) and simulated model (blue) output of PD patient 9 before and after medication with 80.0% and 89.3% best fit respectively.

APPENDIX D - X & Y DATA PLOTS FROM TRIANGLE PATTERN

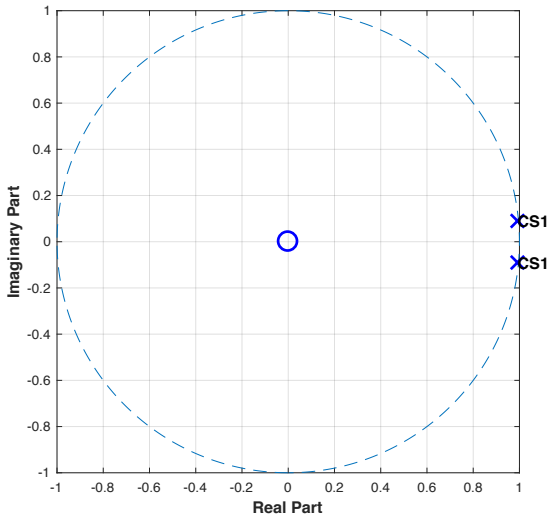

Figure D1: Pole-zero plot of control subject 1 using X-axis data.

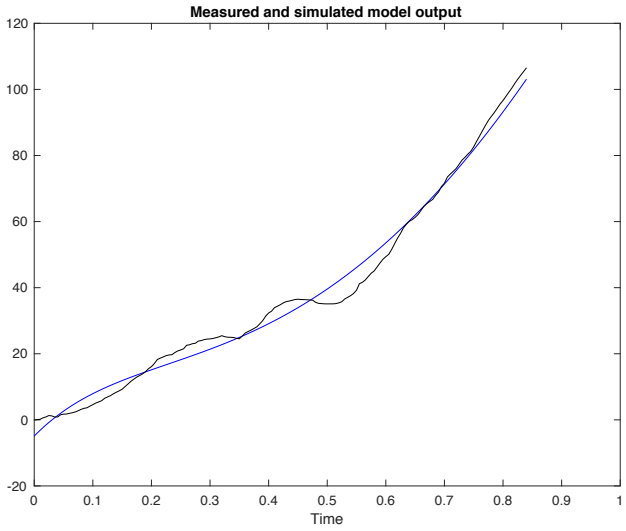

Figure D2: Measured (black) and simulated model (blue) output of control subject 1 with 89.2% best fit.

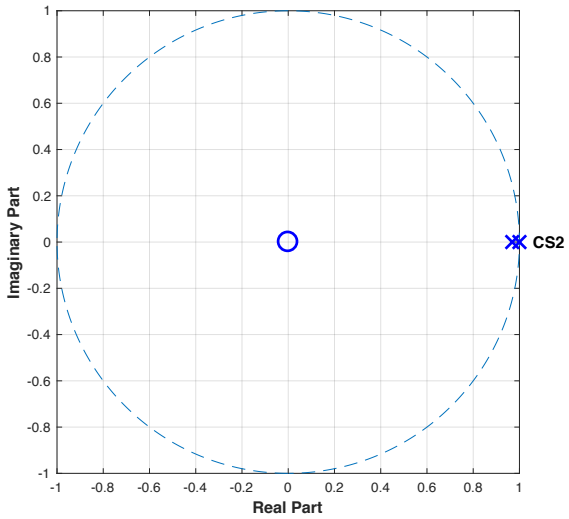

Figure D3: Pole-zero plot of control subject 2 using X-axis data.

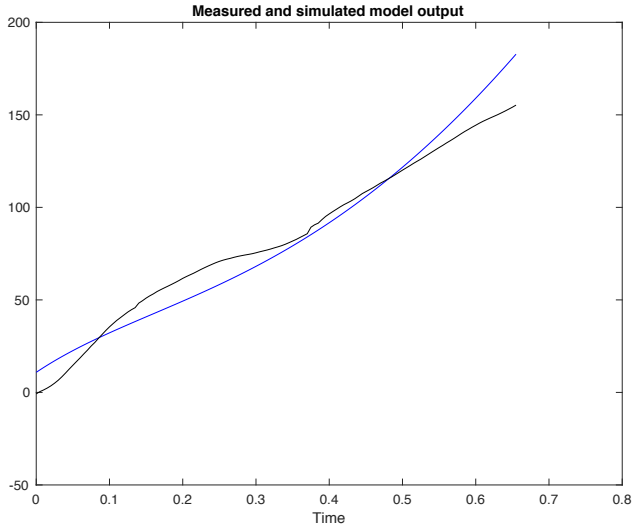

Figure D4: Measured (black) and simulated model (blue) output of control subject 2 with 76.5% best fit.

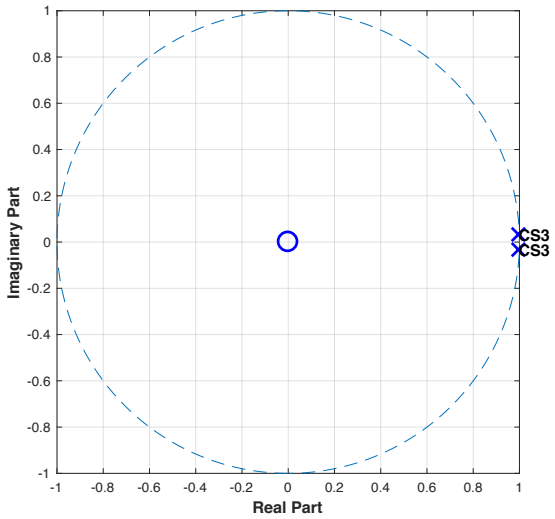

Figure D5: Pole-zero plot of control subject 3 using X-axis data.

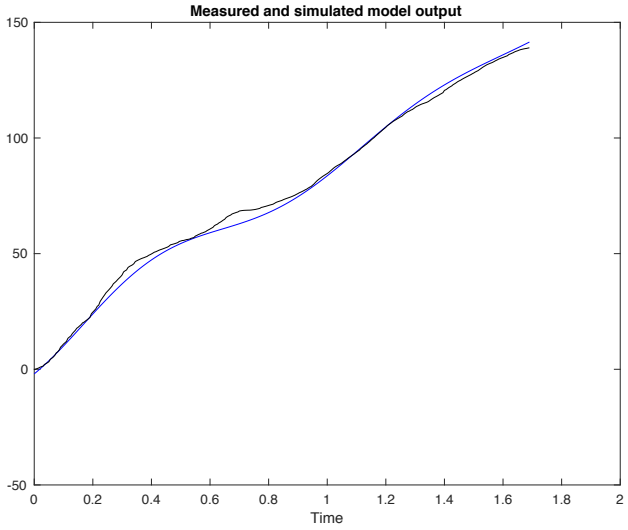

Figure D6: Measured (black) and simulated model (blue) output of control subject 3 with 94.2% best fit.

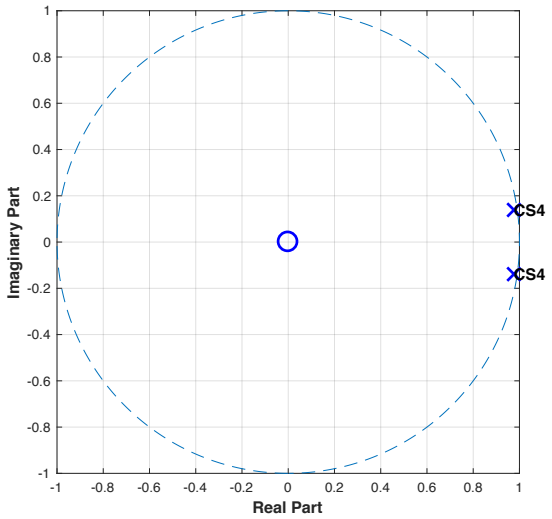

Figure D7: Pole-zero plot of control subject 4 using X-axis data.

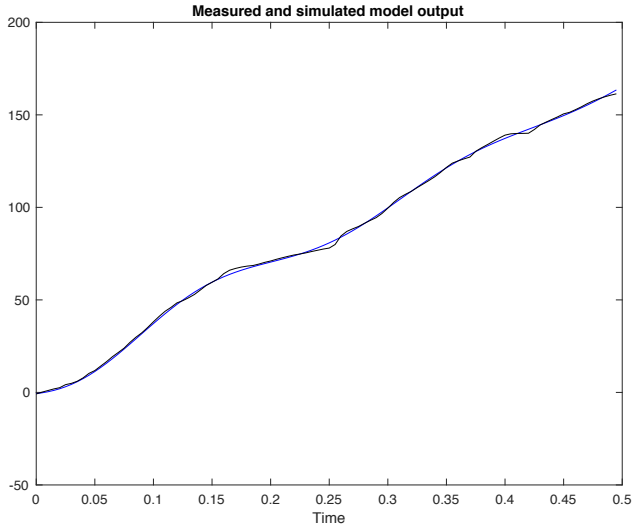

Figure D8: Measured (black) and simulated model (blue) output of control subject 4 with 98.0% best fit.

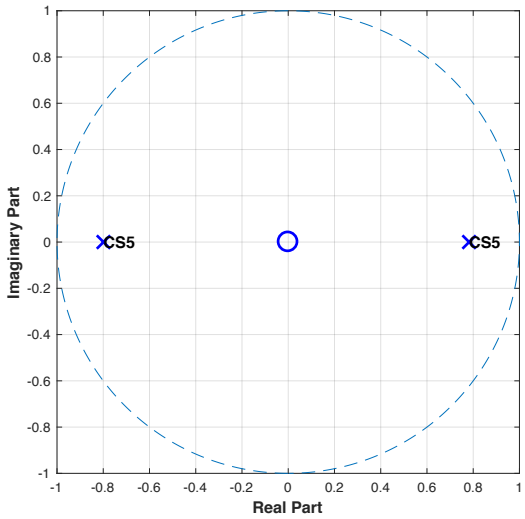

Figure D9: Pole-zero plot of control subject 5 using X-axis data.

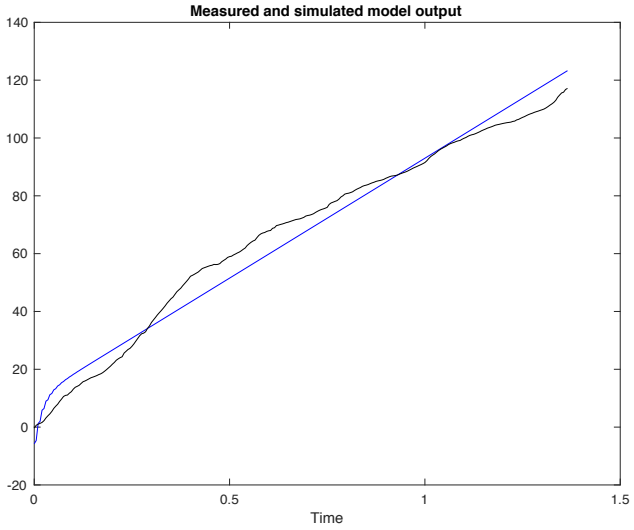

Figure D10: Measured (black) and simulated model (blue) output of control subject 5 with 86.3% best fit.

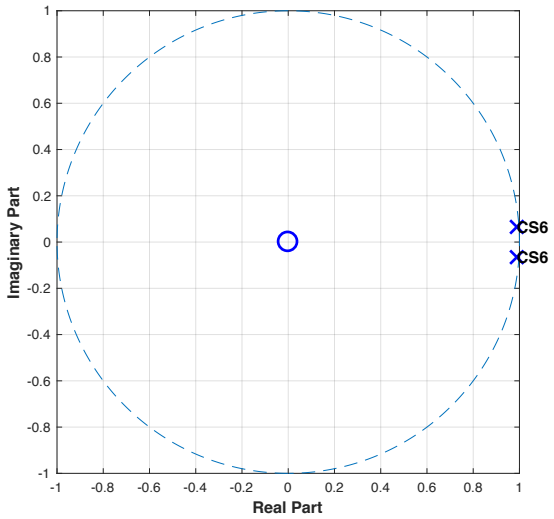

Figure D11: Pole-zero plot of control subject 6 using X-axis data.

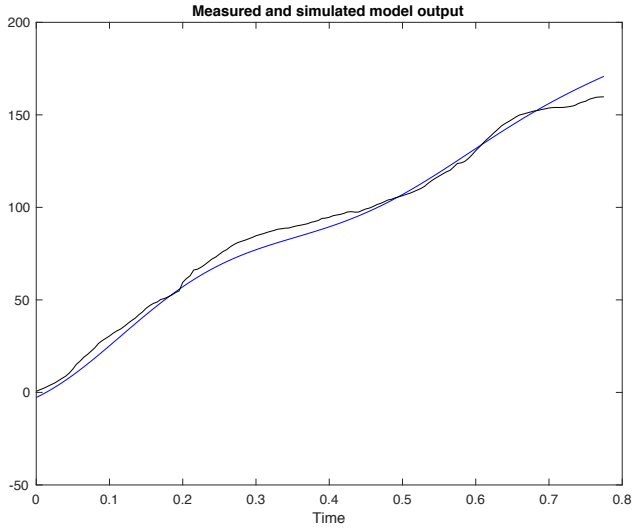

Figure D12: Measured (black) and simulated model (blue) output of control subject 6 with 89.7% best fit.

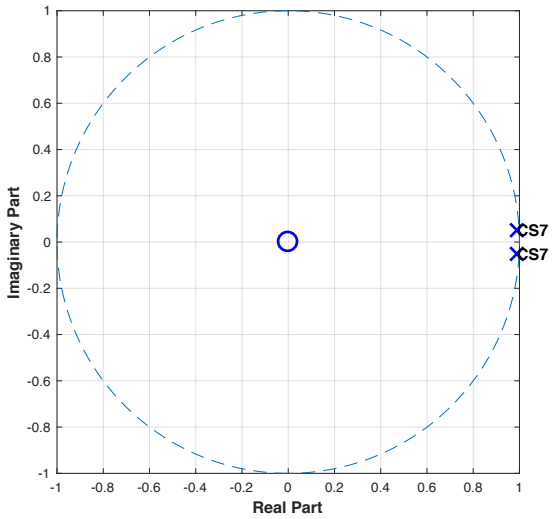

Figure D13: Pole-zero plot of control subject 7 using X-axis data.

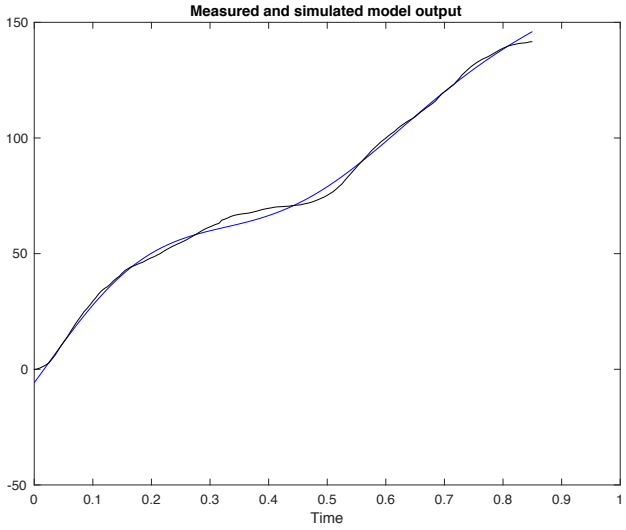

Figure D14: Measured (black) and simulated model (blue) output of control subject 7 with 94.7% best fit.

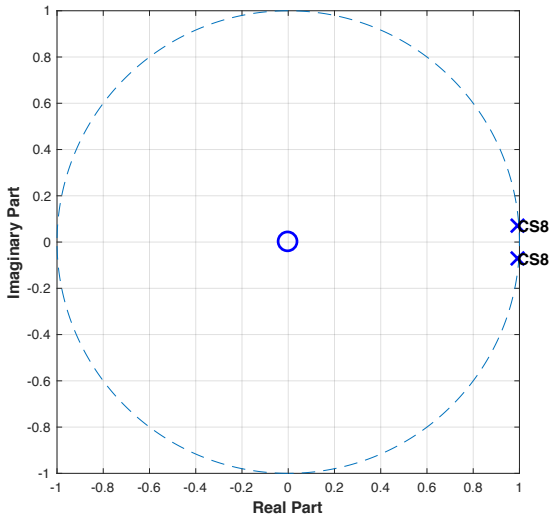

Figure D15: Pole-zero plot of control subject 8 using X-axis data.

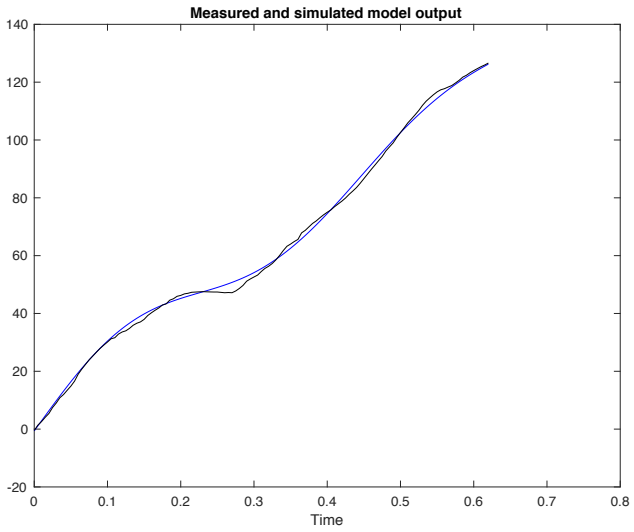

Figure D16: Measured (black) and simulated model (blue) output of control subject 8 with 96.1% best fit.

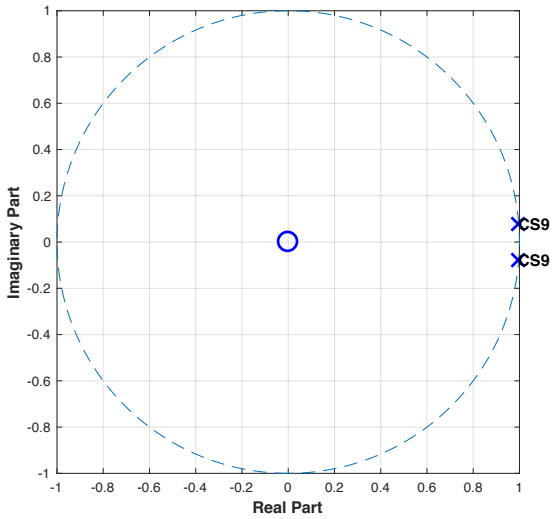

Figure D17: Pole-zero plot of control subject 9 using X-axis data.

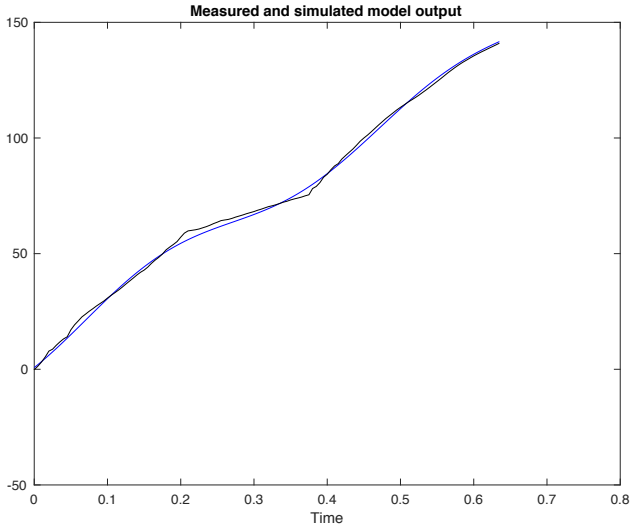

Figure D18: Measured (black) and simulated model (blue) output of control subject 9 with 96% best fit.

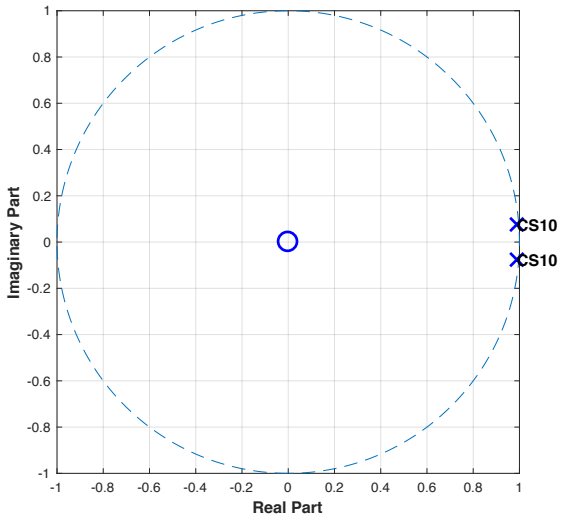

Figure D19: Pole-zero plot of control subject 10 using X-axis data.

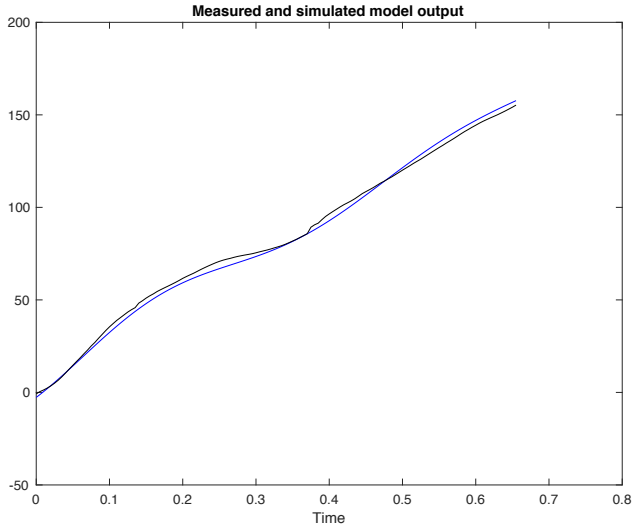

Figure D20: Measured (black) and simulated model (blue) output of control subject 10 with 94.3% best fit.

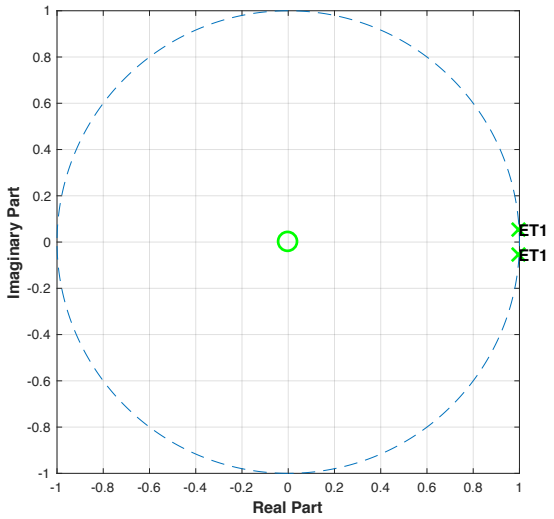

Figure D21: Pole-zero plot of ET patient 1 using X-axis data.

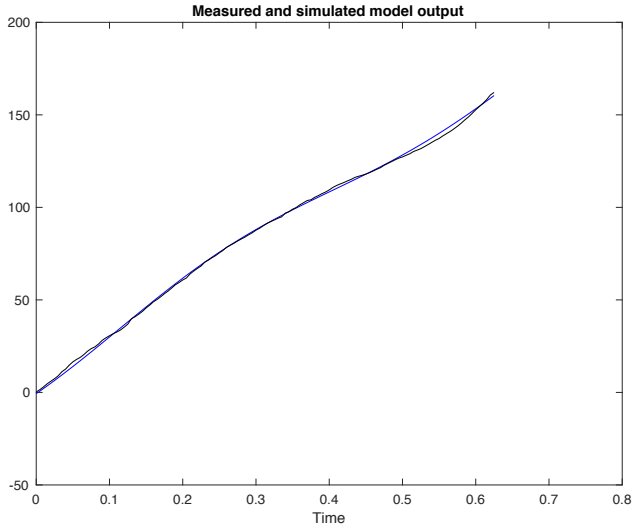

Figure D22: Measured (black) and simulated model (blue) output of ET patient 1 with 97.2% best fit.

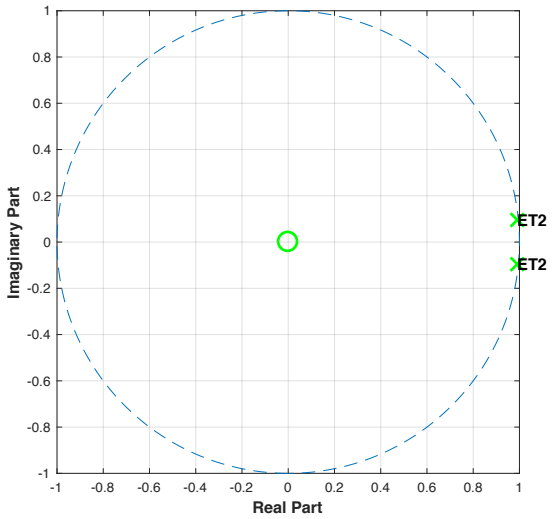

Figure D23: Pole-zero plot of ET patient 2 using X-axis data.

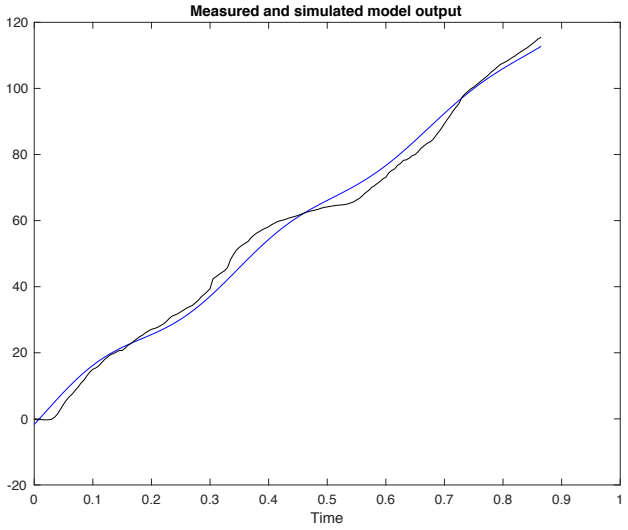

Figure D24: Measured (black) and simulated model (blue) output of control ET patient 2 with 91.1% best fit.

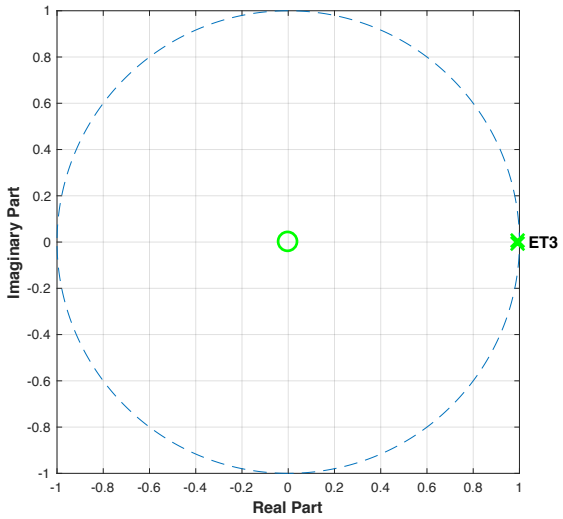

Figure D25: Pole-zero plot of ET patient 3 using X-axis data.

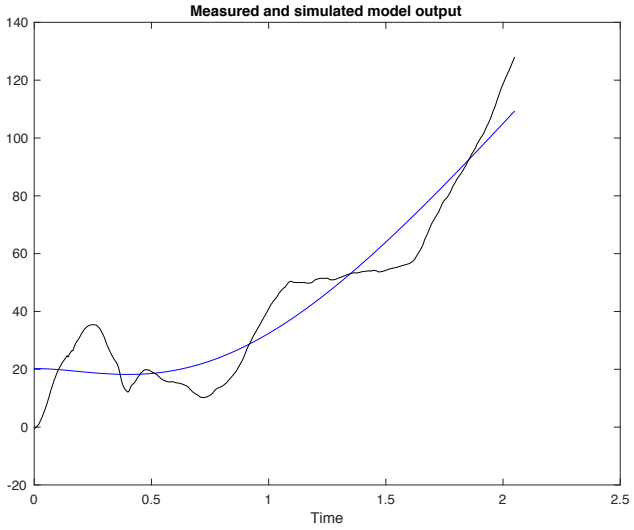

Figure D26: Measured (black) and simulated model (blue) output of ET patient 3 with 69.7% best fit.

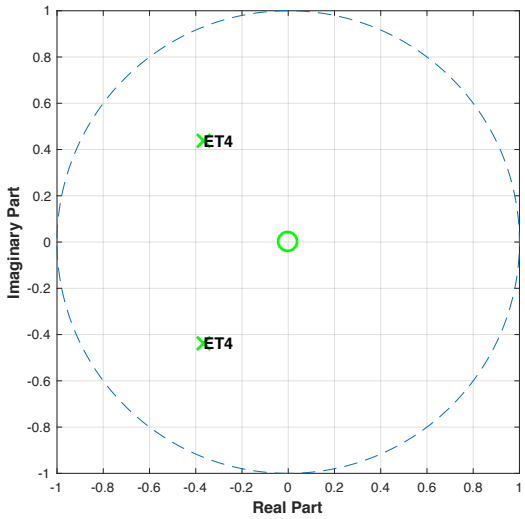

Figure D27: Pole-zero plot of ET patient 4 using X-axis data.

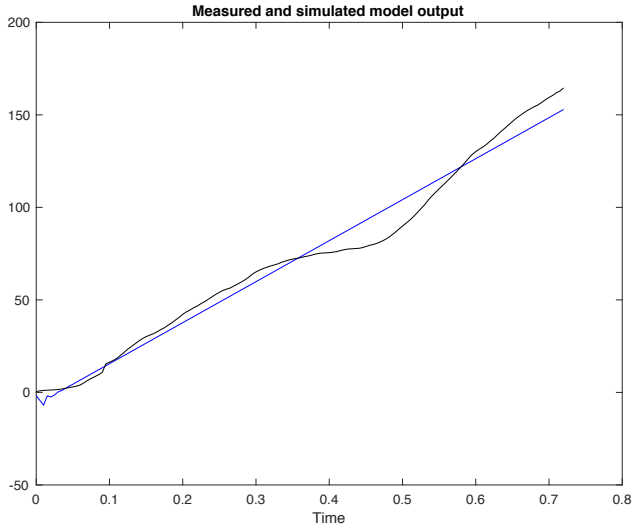

Figure D28: Measured (black) and simulated model (blue) output of ET patient 4 with 84.2% best fit.

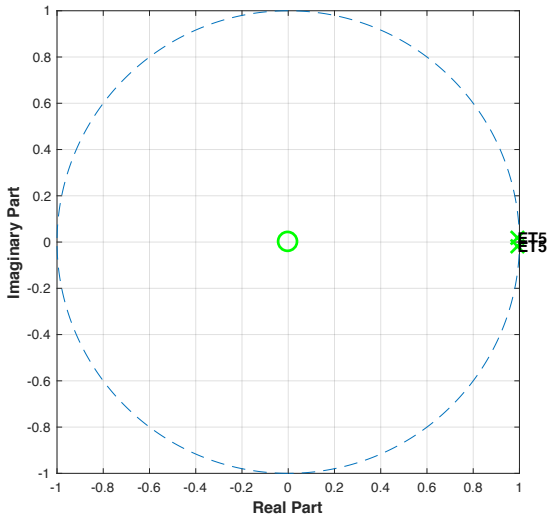

Figure D29: Pole-zero plot of ET patient 5 using X-axis data.

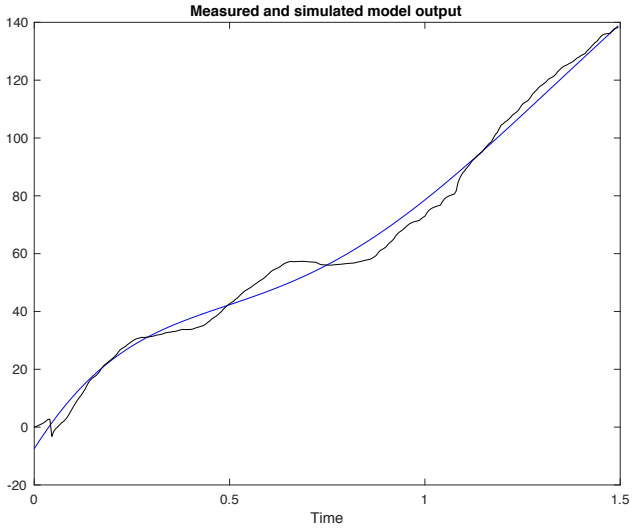

Figure D30: Measured (black) and simulated model (blue) output of ET patient 5 with 90.2% best fit.

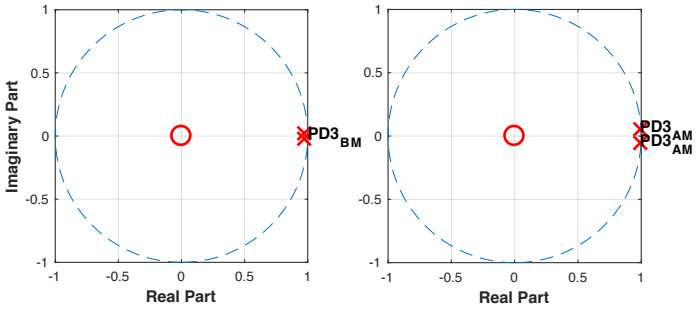

Figure D31: Pole-zero plot for PD patient 3 before and after medication using X-axis data.

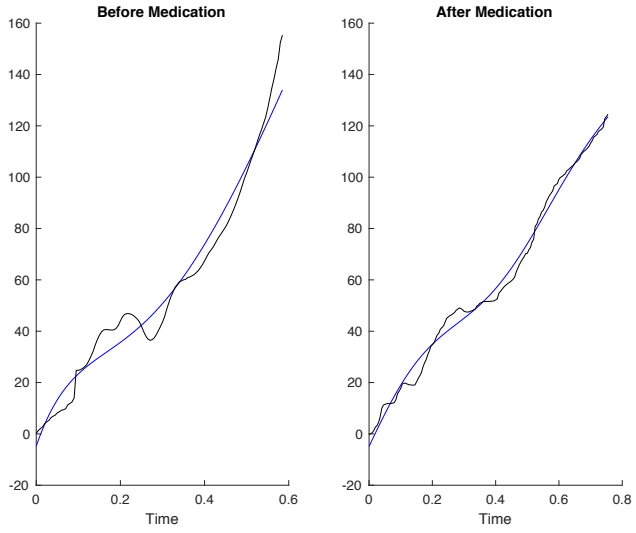

Figure D32: Measured (black) and simulated model (blue) output of PD patient 3 before and after medication with 82.1% and 90.6% best fit respectively.

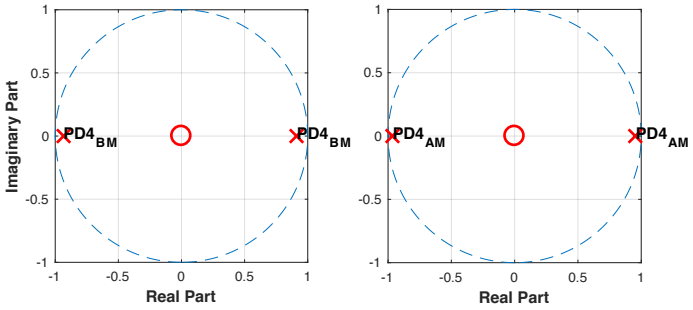

Figure D33: Pole-zero plot for PD patient 4 before and after medication using X-axis data.

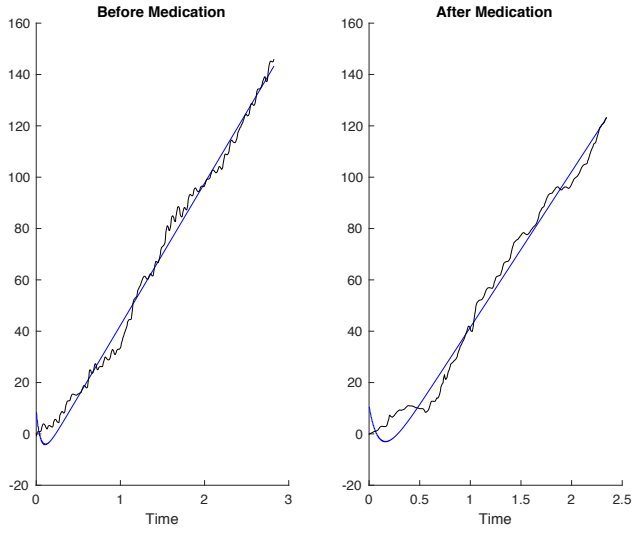

Figure D34: Measured (black) and simulated model (blue) output of PD patient 4 before and after medication with 91.0% and 87.16% best fit respectively.

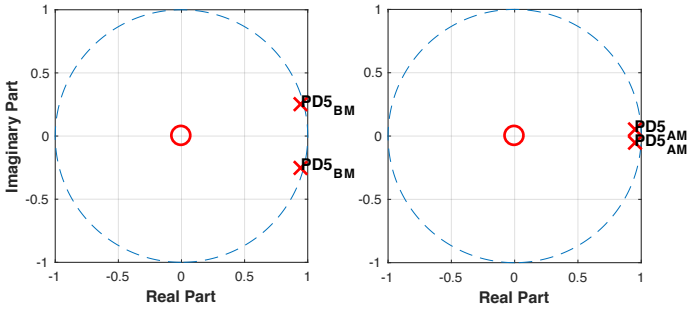

Figure D35: Pole-zero plot for PD patient 5 before and after medication using X-axis data.

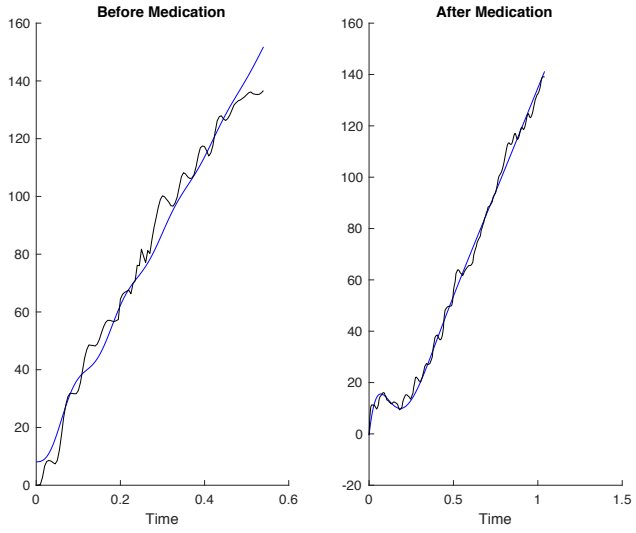

Figure D36: Measured (black) and simulated model (blue) output of PD patient 5 before and after medication with 86.2% and 93.6% best fit respectively.

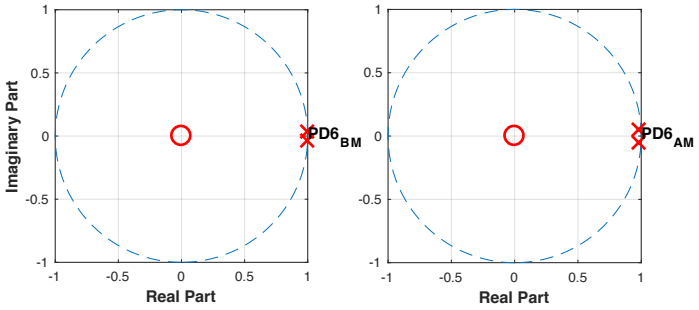

Figure D37: Pole-zero plot for PD patient 6 before and after medication using X-axis data.

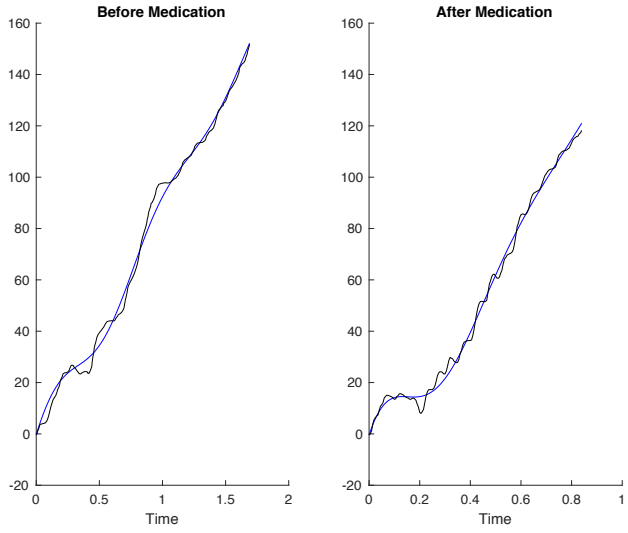

Figure D38: Measured (black) and simulated model (blue) output of PD patient 6 before and after medication with 93.0% and 93.8% best fit respectively.

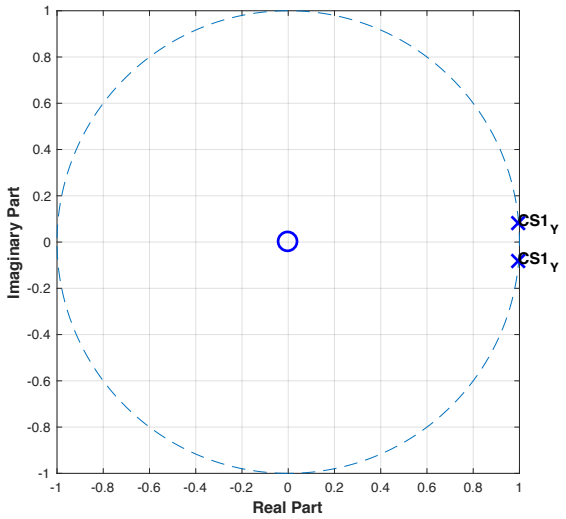

Figure D39: Pole-zero plot of control subject 1 using Y-axis data.

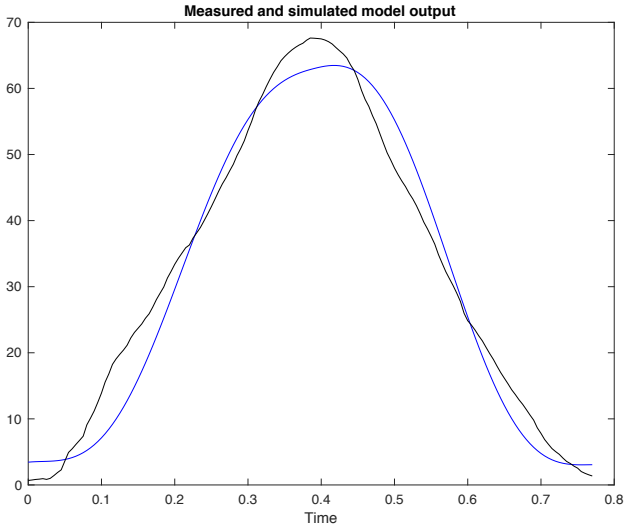

Figure D40: Measured (black) and simulated model (blue) output of control subject 1 with 81.4% best fit.

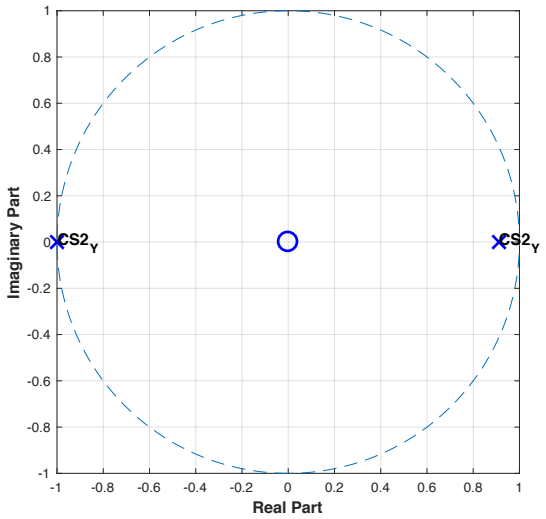

Figure D41: Pole-zero plot of control subject 2 using Y-axis data.

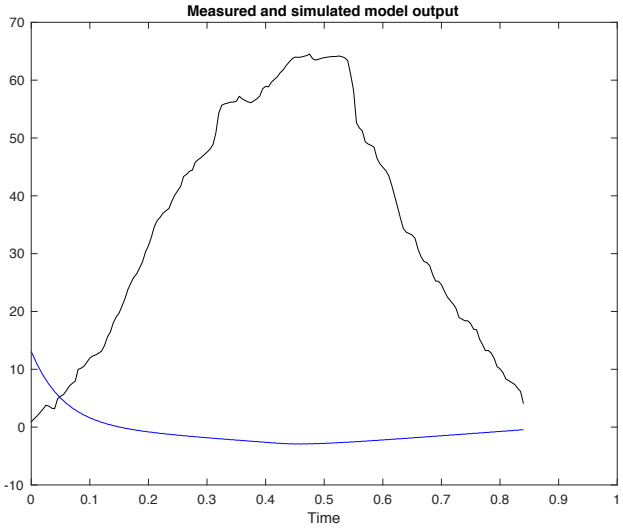

Figure D42: Measured (black) and simulated model (blue) output of control subject 2 with -105.4% best fit - omitted from the analysis.

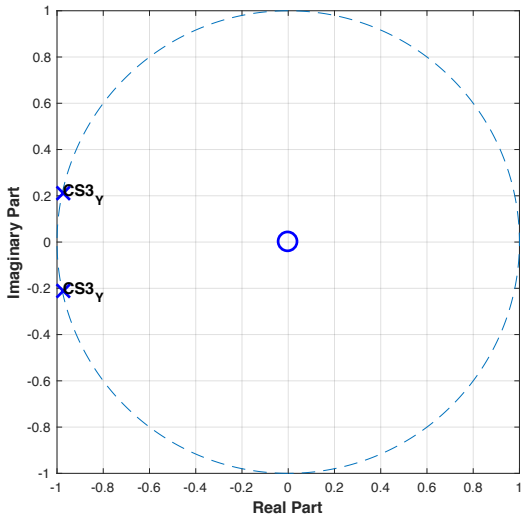

Figure D43: Pole-zero plot of control subject 3 using Y-axis data.

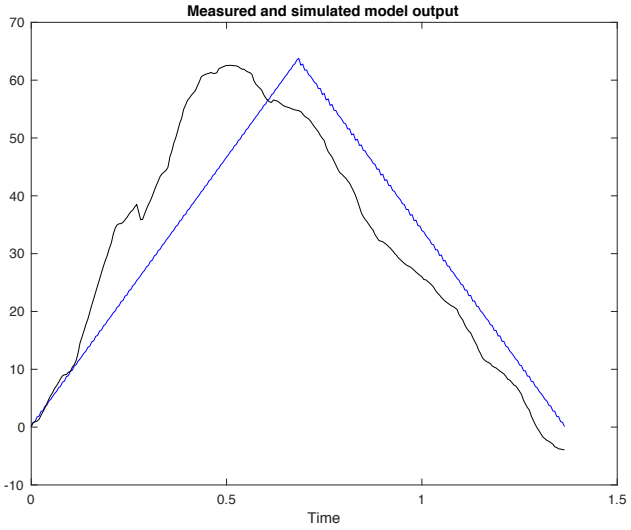

Figure D44: Measured (black) and simulated model (blue) output of control subject 3 with 51.9% best fit.

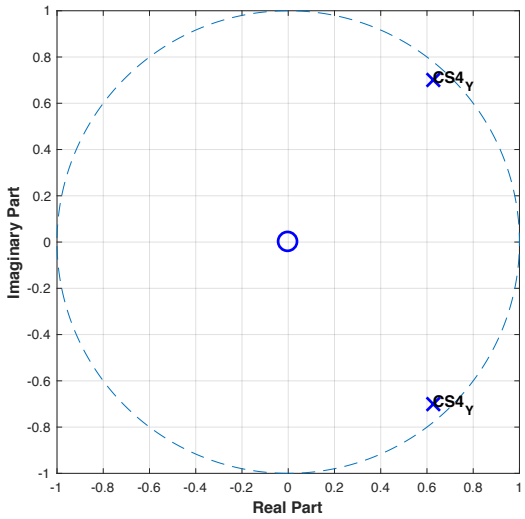

Figure D45: Pole-zero plot of control subject 4 using Y-axis data.

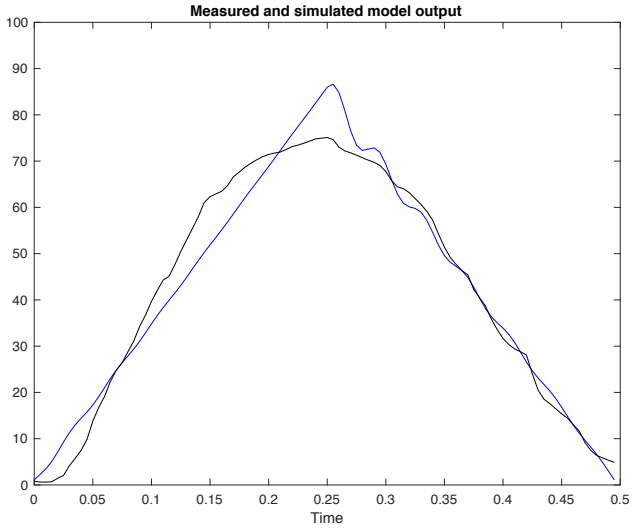

Figure D46: Measured (black) and simulated model (blue) output of control subject 4 with 80.6% best fit.

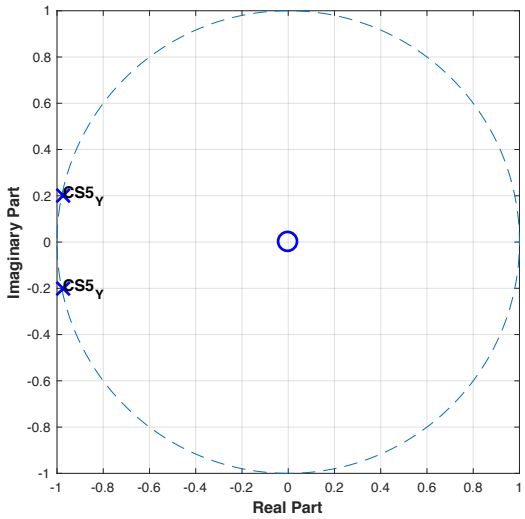

Figure D47: Pole-zero plot of control subject 5 using Y-axis data.

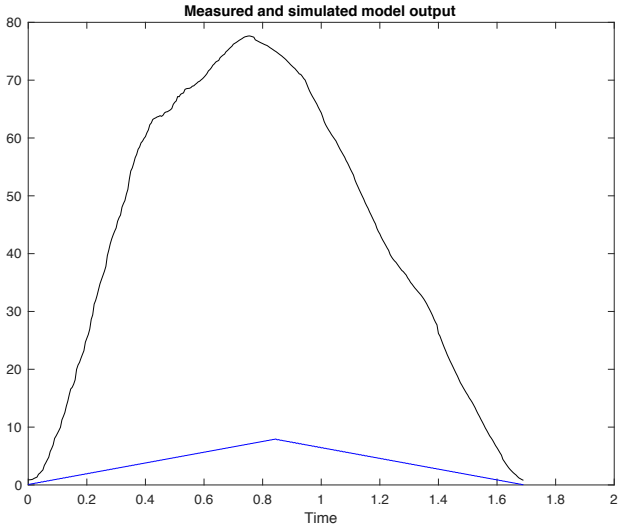

Figure D48: Measured (black) and simulated model (blue) output of control subject 5 with -83.3% best fit - omitted from the analysis.

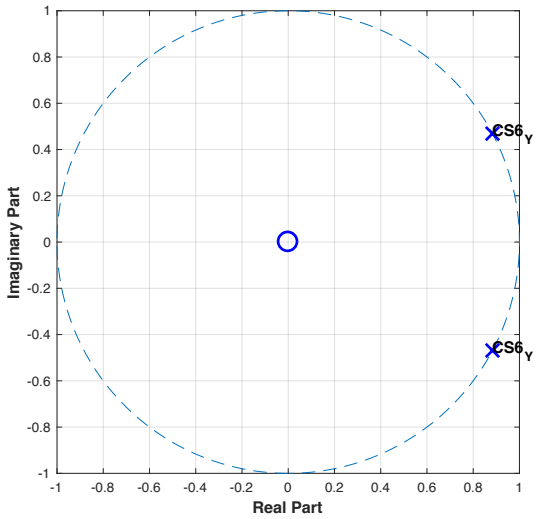

Figure D49: Pole-zero plot of control subject 6 using Y-axis data.

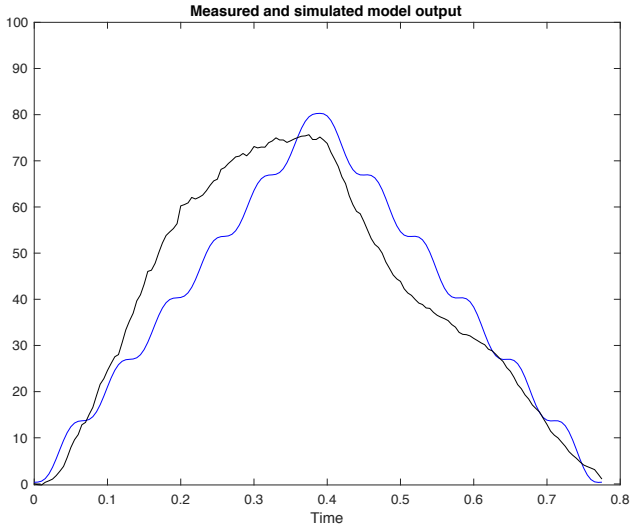

Figure D50: Measured (black) and simulated model (blue) output of control subject 6 with 62.7% best fit.

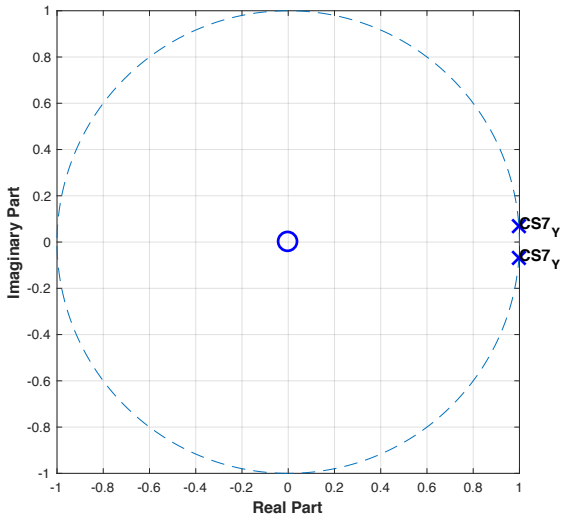

Figure D51: Pole-zero plot of control subject 7 using Y-axis data.

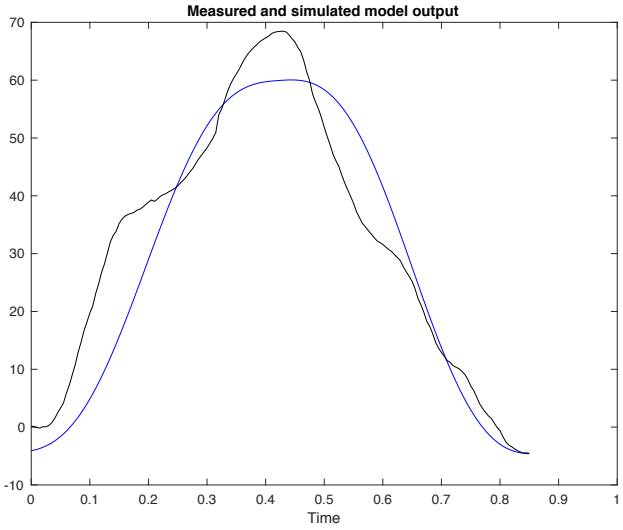

Figure D52: Measured (black) and simulated model (blue) output of control subject 7 with 62.5% best fit.

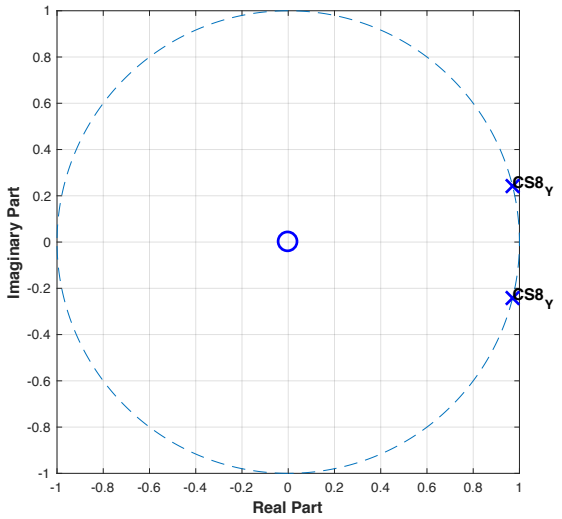

Figure D53: Pole-zero plot of control subject 8 using Y-axis data.

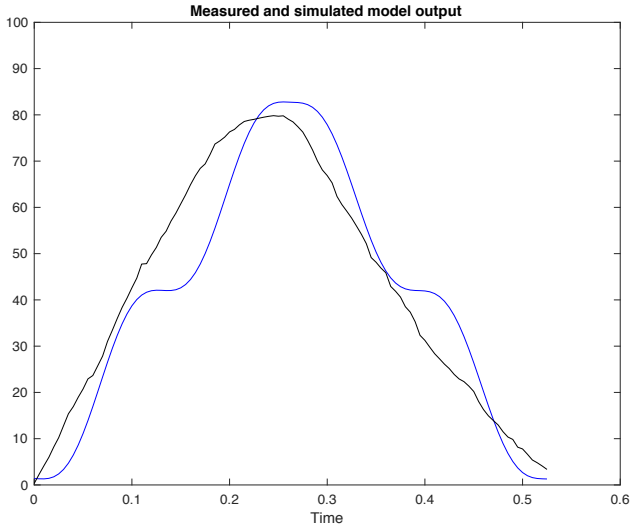

Figure D54: Measured (black) and simulated model (blue) output of control subject 8 with 63.9% best fit.

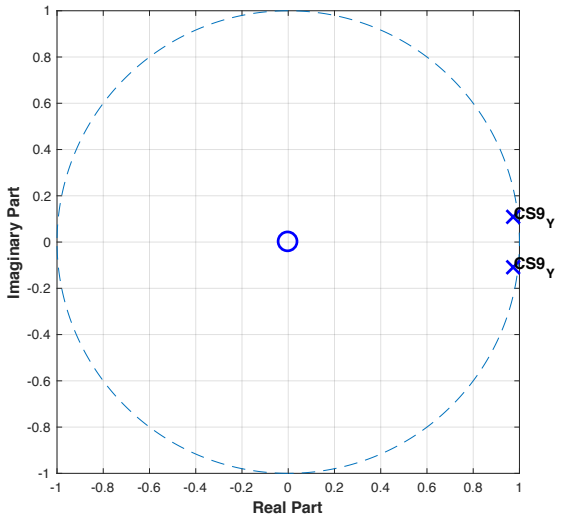

Figure D55: Pole-zero plot of control subject 9 using Y-axis data.

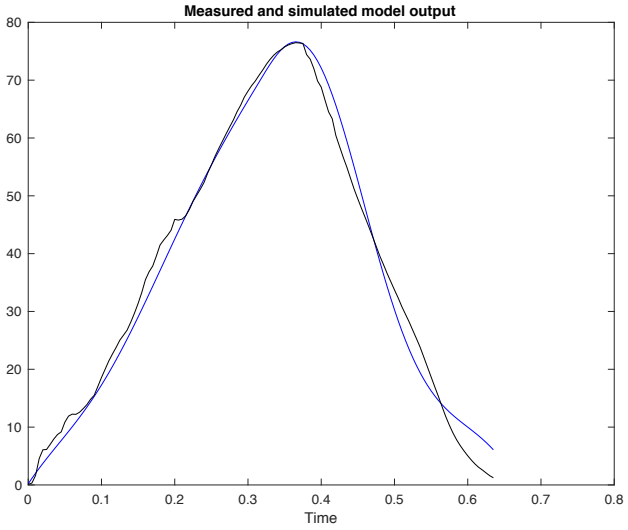

Figure D56: Measured (black) and simulated model (blue) output of control subject 9 with 88.6% best fit.

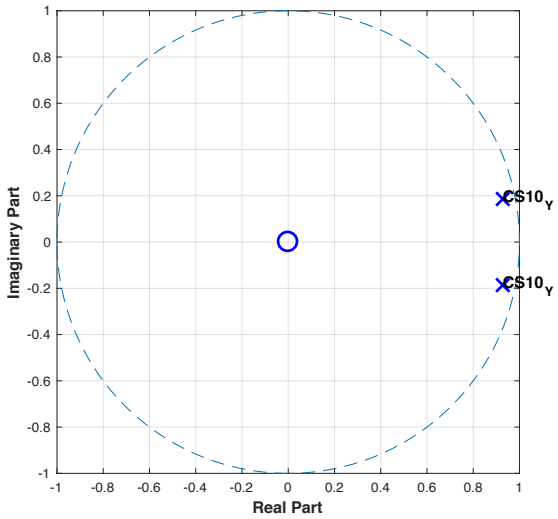

Figure D57: Pole-zero plot of control subject 10 using Y-axis data.

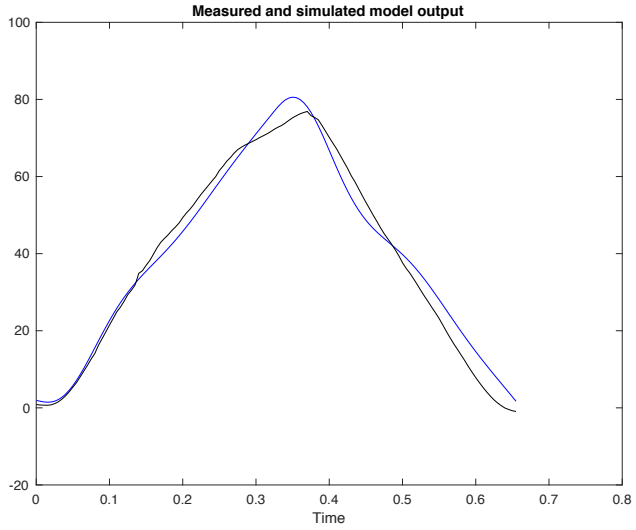

Figure D58: Measured (black) and simulated model (blue) output of control subject 10 with 85.5% best fit.

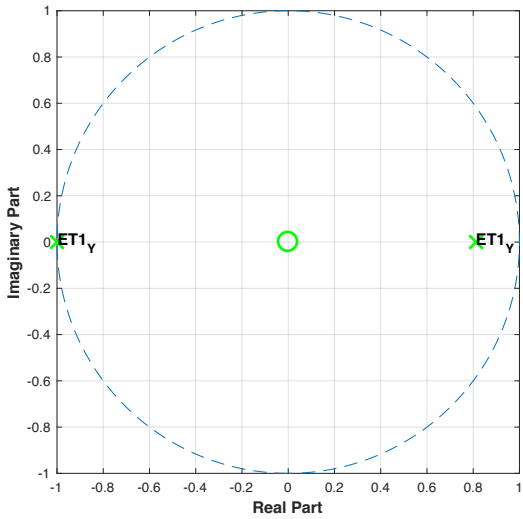

Figure D59: Pole-zero plot of ET patient 1 using Y-axis data.

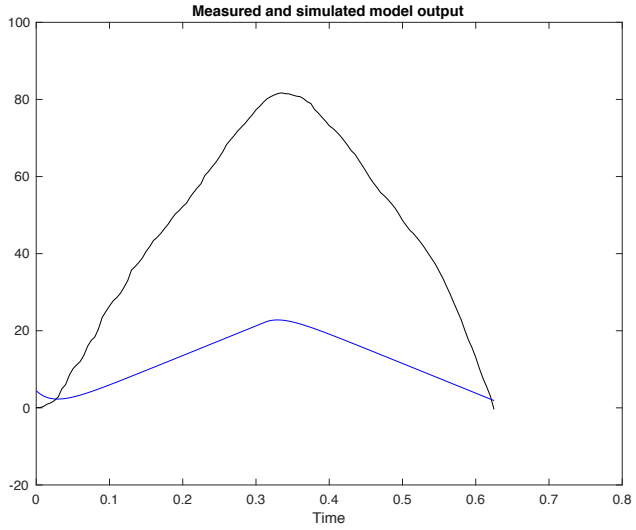

Figure D60: Measured (black) and simulated model (blue) output of ET patient 1 with -54.4% best fit - omitted from the analysis.

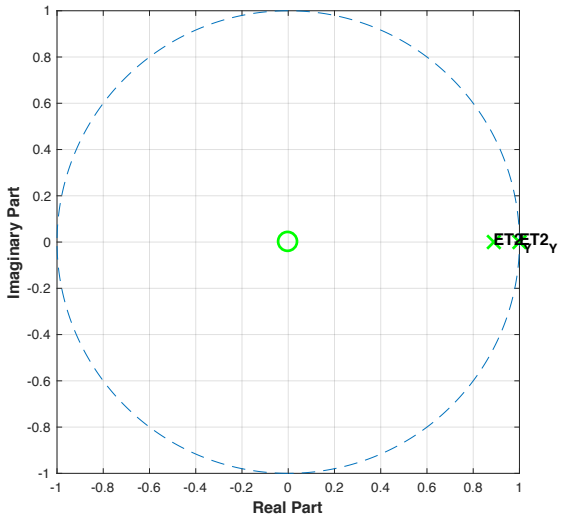

Figure D61: Pole-zero plot of ET patient 2 using Y-axis data.

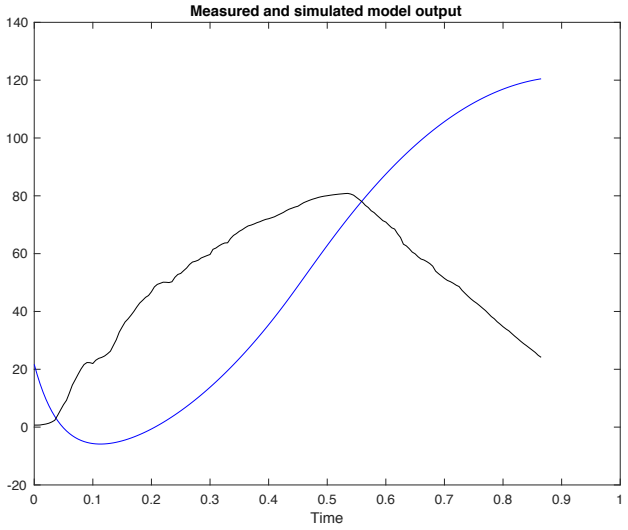

Figure D62: Measured (black) and simulated model (blue) output of ET patient 2 with -110.0% best fit - omitted from the analysis.

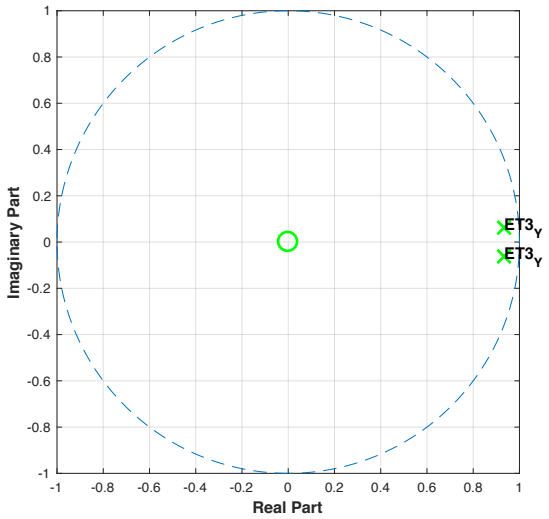

Figure D63: Pole-zero plot of ET patient 3 using Y-axis data.

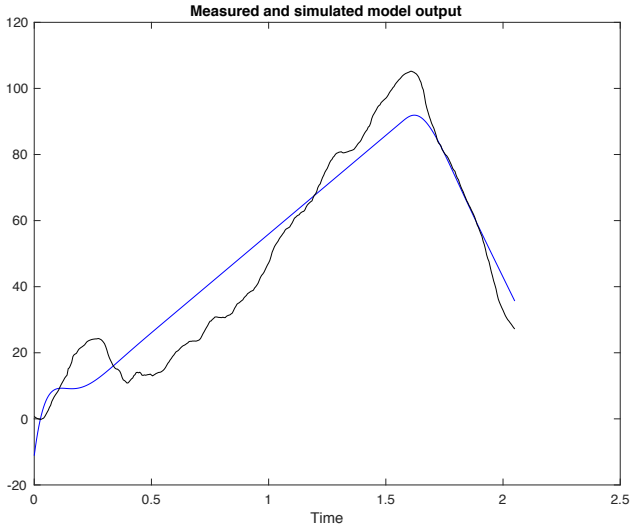

Figure D64: Measured (black) and simulated model (blue) output of ET patient 3 with 70.7% best fit.

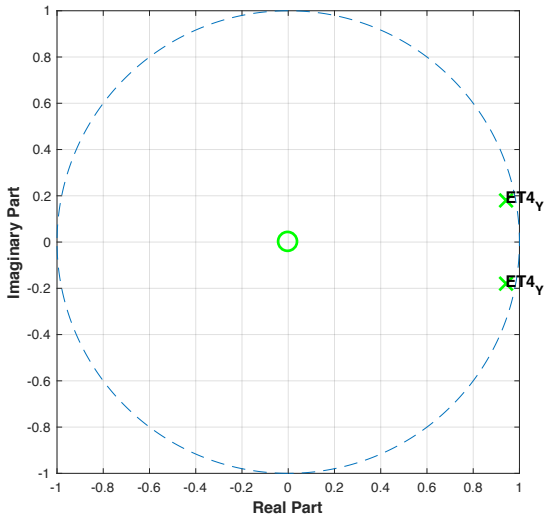

Figure D65: Pole-zero plot of ET patient 4 using Y-axis data.

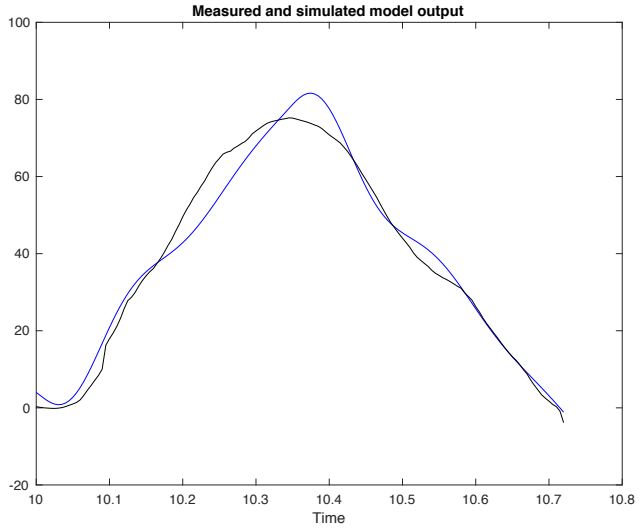

Figure D66: Measured (black) and simulated model (blue) output of ET patient 4 with 83.3% best fit.

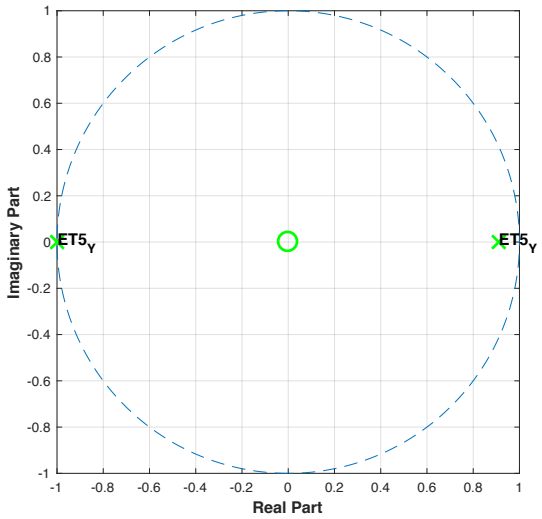

Figure D67: Pole-zero plot of ET patient 5 using Y-axis data.

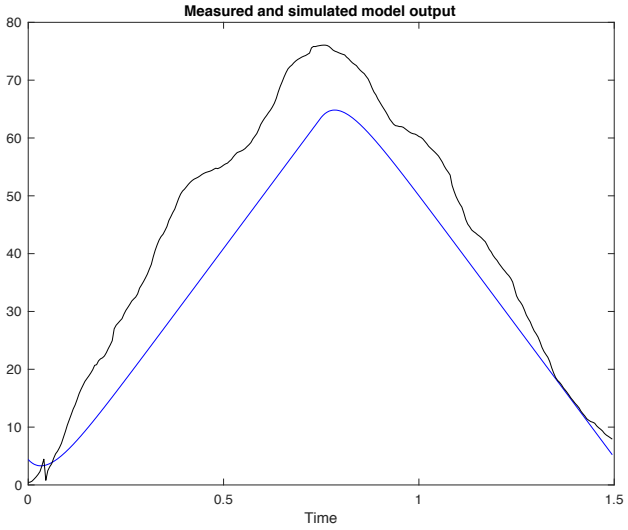

Figure D68: Measured (black) and simulated model (blue) output of ET patient 5 with 53.0% best fit.

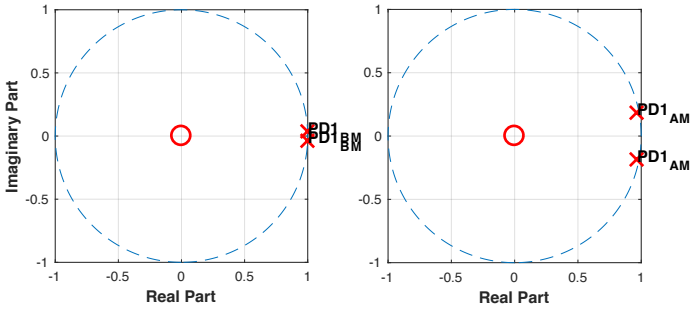

Figure D69: Pole-zero plot for PD patient 1 before and after medication using Y-axis data.

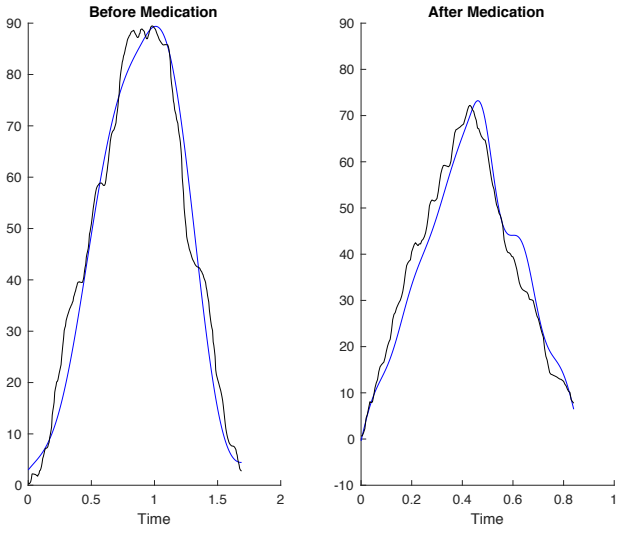

Figure D70: Measured (black) and simulated model (blue) output of PD patient 1 before and after medication with 81.5% and 76.3% best fit respectively.

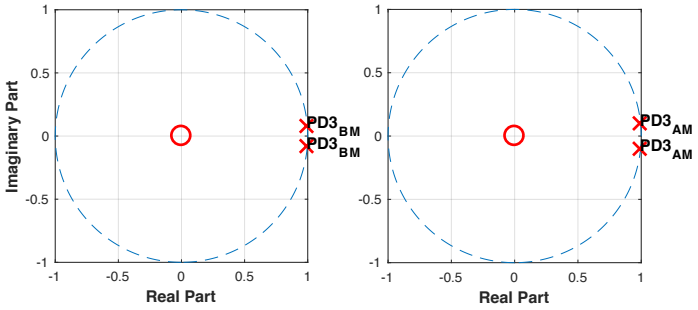

Figure D71: Pole-zero plot for PD patient 3 before and after medication using Y-axis data.

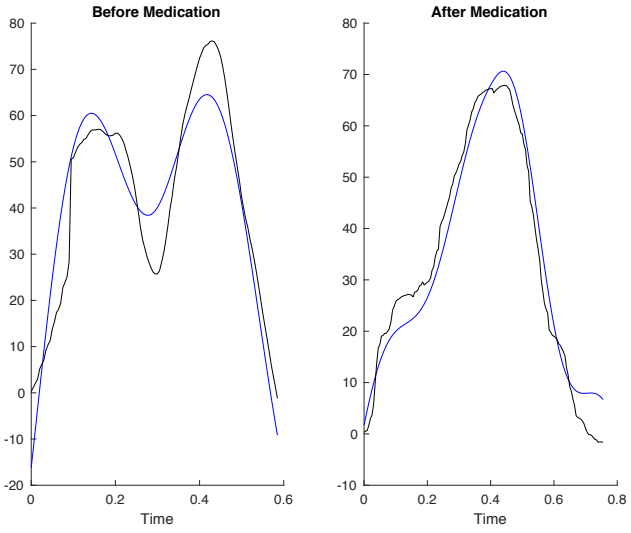

Figure D72: Measured (black) and simulated model (blue) output of PD patient 3 before and after medication with 60.6% and 79.8% best fit respectively.

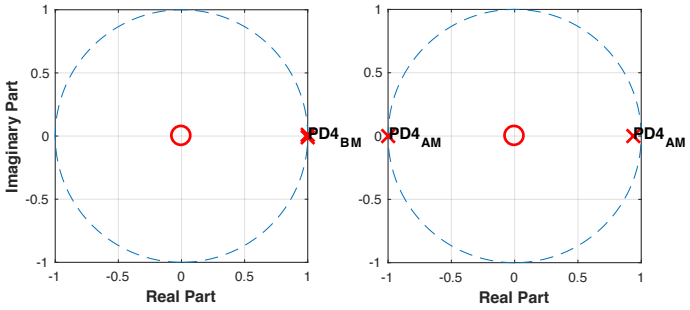

Figure D73: Pole-zero plot for PD patient 4 before and after medication using Y-axis data.

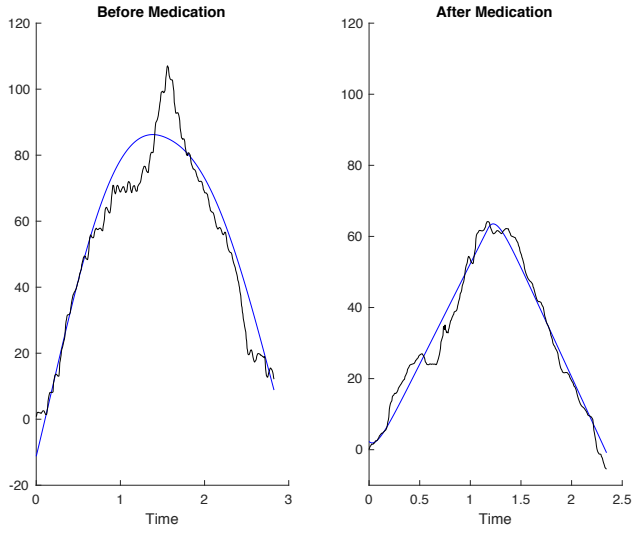

Figure D74: Measured (black) and simulated model (blue) output of PD patient 4 before and after medication with 71.3% and 82.5% best fit respectively.

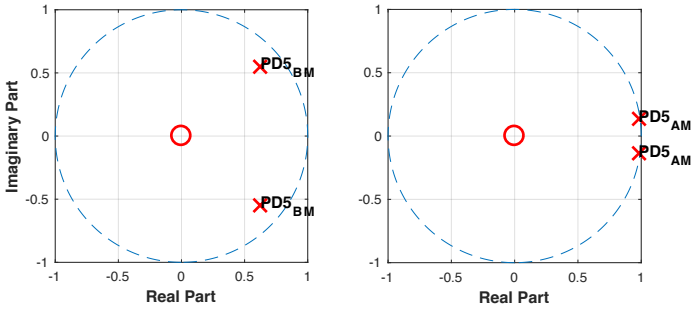

Figure D75: Pole-zero plot for PD patient 5 before and after medication using Y-axis data.

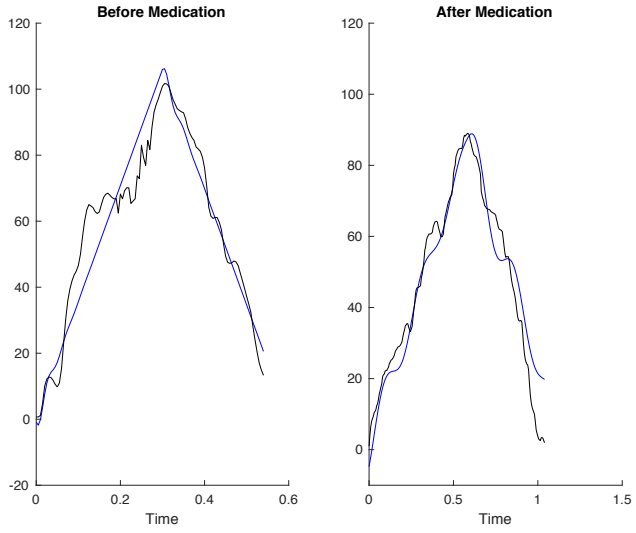

Figure D76: Measured (black) and simulated model (blue) output of PD patient 5 before and after medication with 71.3% and 73.1% best fit respectively.

APPENDIX E – X & Y DATA PLOTS FROM CIRCLE PATTERN

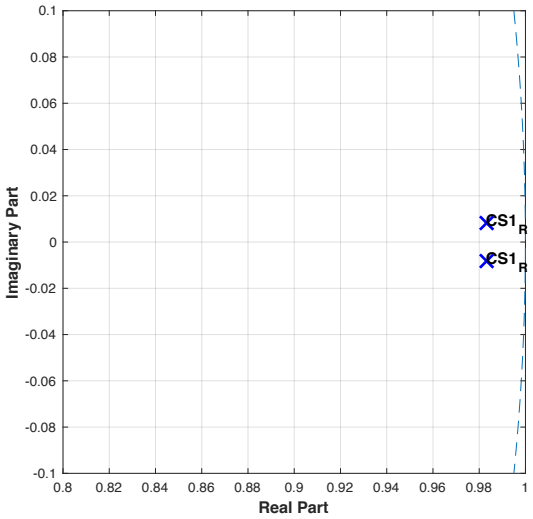

Figure E1: Pole-zero plot for control subject 1 using R^2 data.

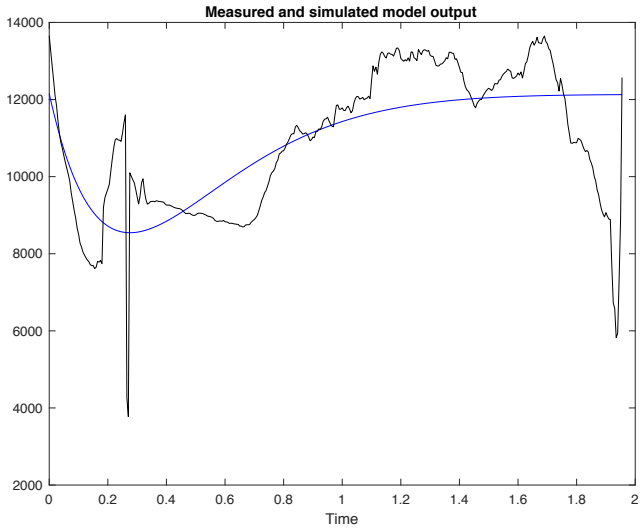

Figure E2: Measured (black) and simulated model (blue) output of control subject 1 with 27.6% best fit - omitted from the analysis.

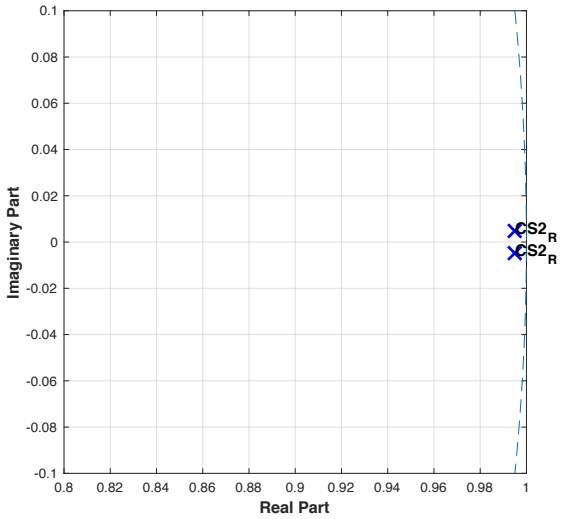

Figure E3: Pole-zero plot for control subject 2 using R^2 data.

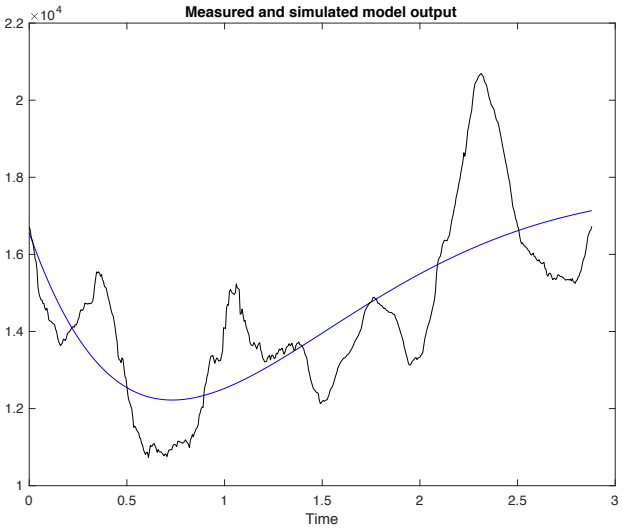

Figure E4: Measured (black) and simulated model (blue) output of control subject 2 with 32.4% best fit - omitted from the analysis.

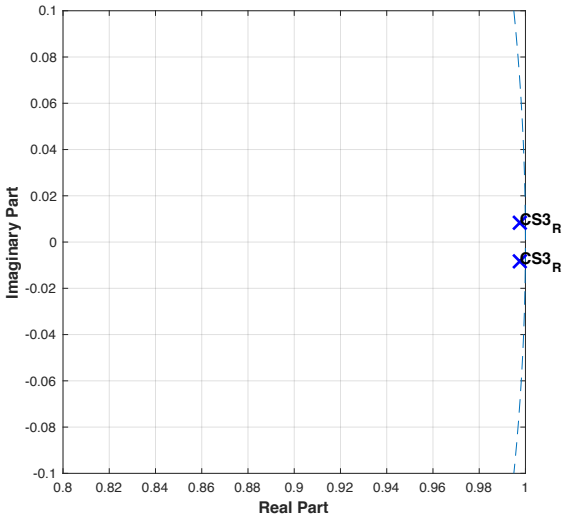

Figure E5: Pole-zero plot for control subject 3 using R^2 data.

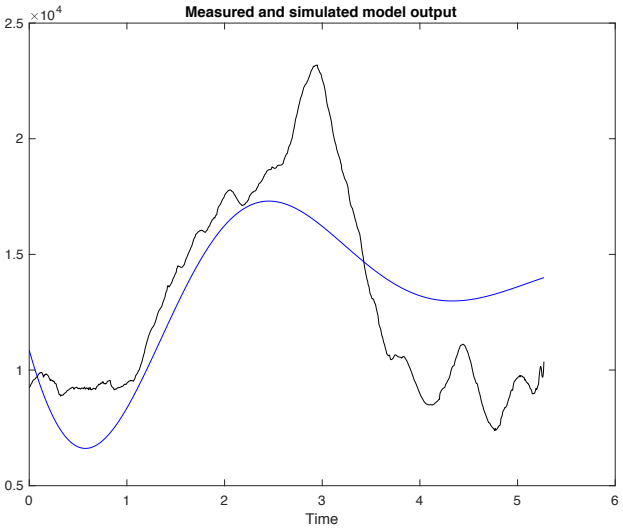

Figure E6: Measured (black) and simulated model (blue) output of control subject 3 with 31.0% best fit - omitted from the analysis.

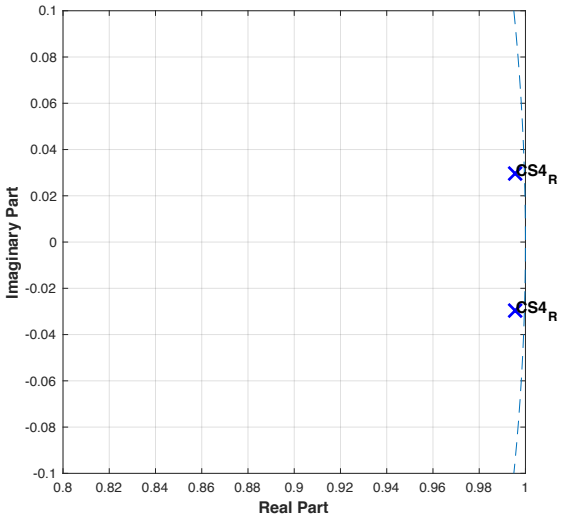

Figure E7: Pole-zero plot for control subject 4 using R^2 data.

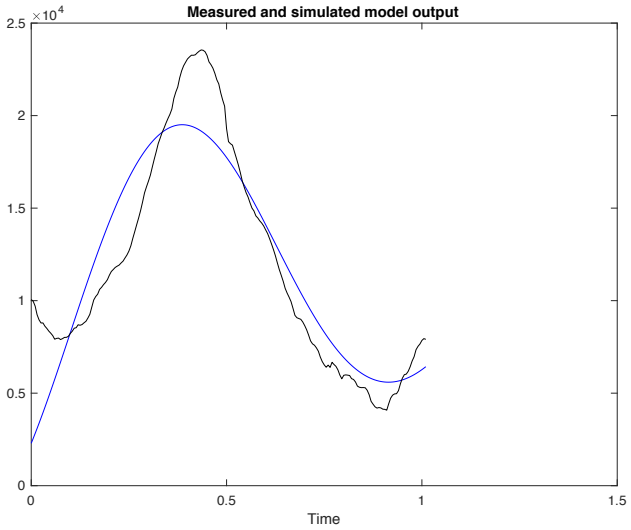

Figure E8: Measured (black) and simulated model (blue) output of control subject 4 with 59.3% best fit.

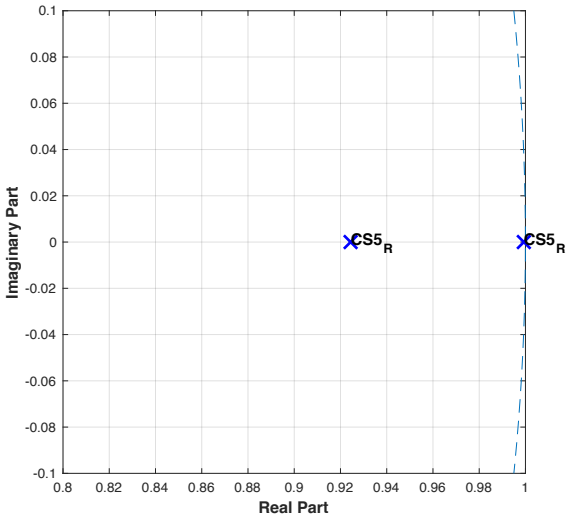

Figure E9: Pole-zero plot for control subject 5 using R^2 data.

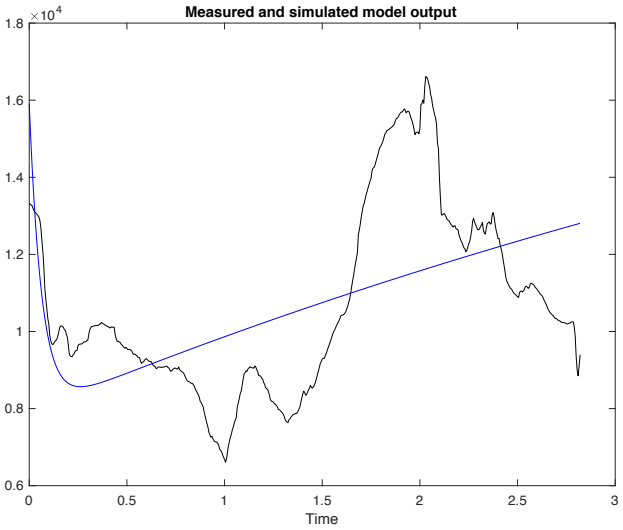

Figure E10: Measured (black) and simulated model (blue) output of control subject 5 with 15.5% best fit - omitted from the analysis.

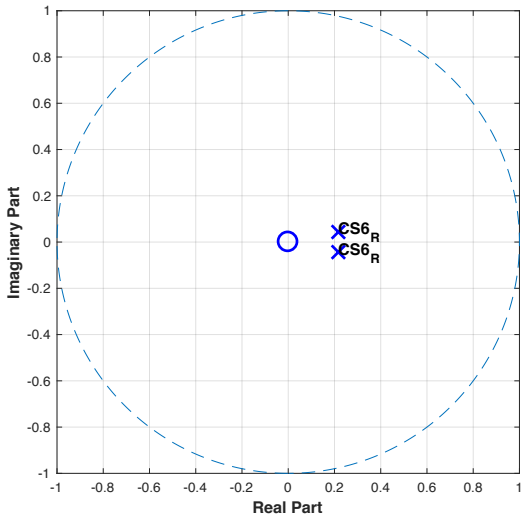

Figure E11: Pole-zero plot for control subject 6 using R^2 data.

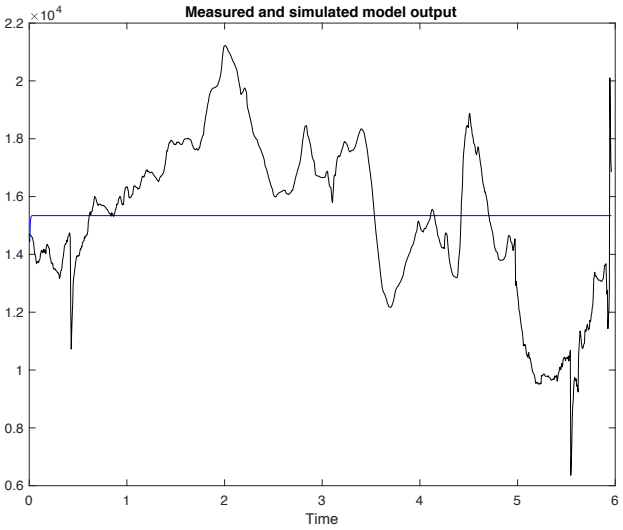

Figure E12: Measured (black) and simulated model (blue) output of control subject 6 with -1.3% best fit - omitted from the analysis.

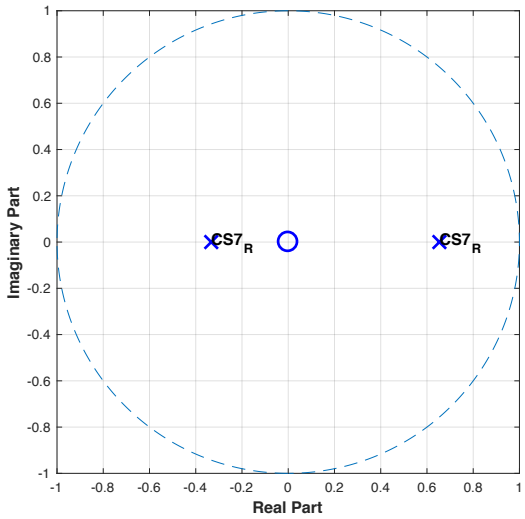

Figure E13: Pole-zero plot for control subject 7 using R^2 data.

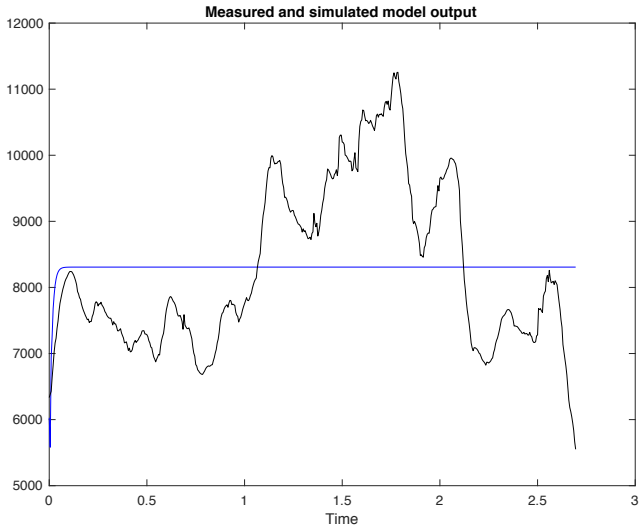

Figure E14: Measured (black) and simulated model (blue) output of control subject 7 with -1.7% best fit - omitted from the analysis.

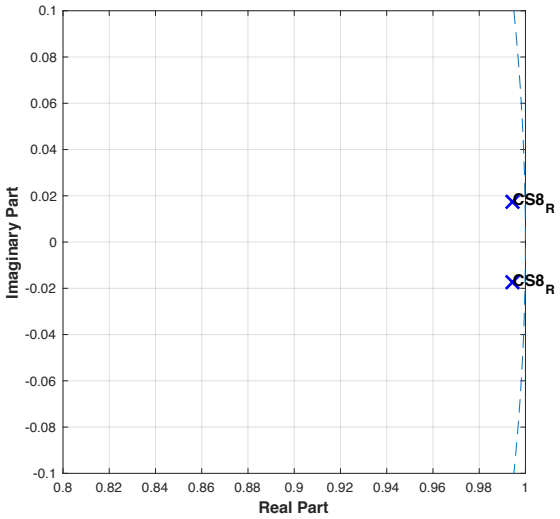

Figure E15: Pole-zero plot for control subject 8 using R^2 data.

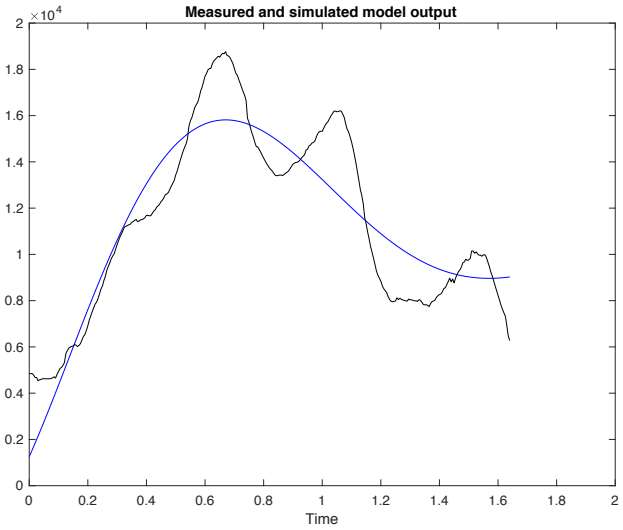

Figure E26: Measured (black) and simulated model (blue) output of control subject 8 with 58.3% best fit.

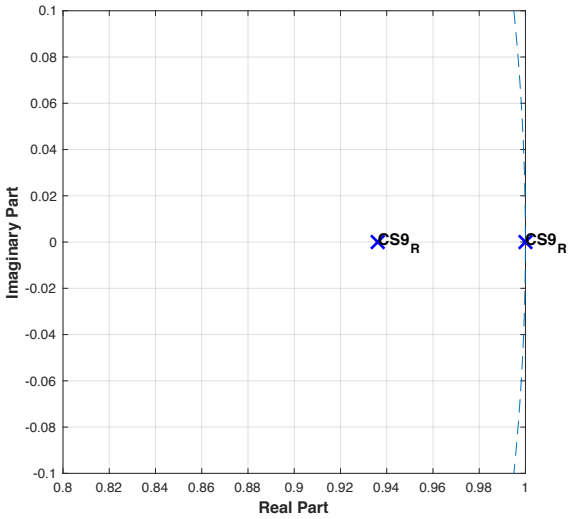

Figure E17: Pole-zero plot for control subject 9 using R^2 data.

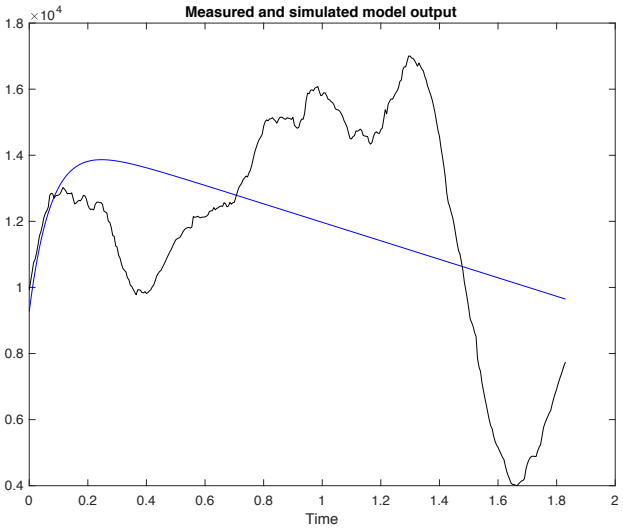

Figure E18: Measured (black) and simulated model (blue) output of control subject 9 with 7.1% best fit - omitted from the analysis.

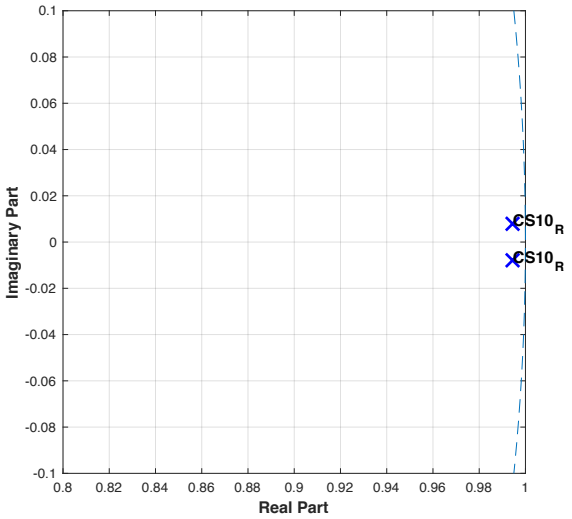

Figure E19: Pole-zero plot for control subject 10 using R^2 data.

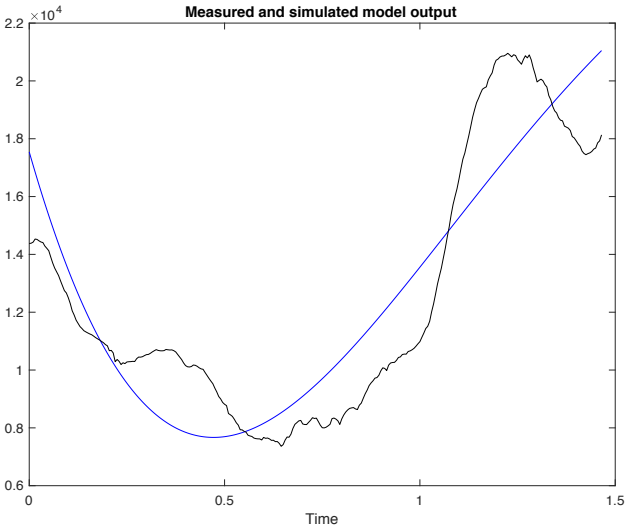

Figure E20: Measured (black) and simulated model (blue) output of control subject 10 with 55.1% best fit.

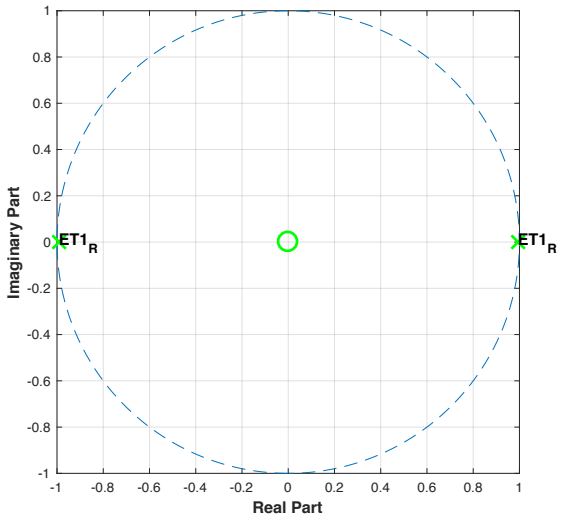

Figure E21: Pole-zero plot of ET patient 1 using R^2 data.

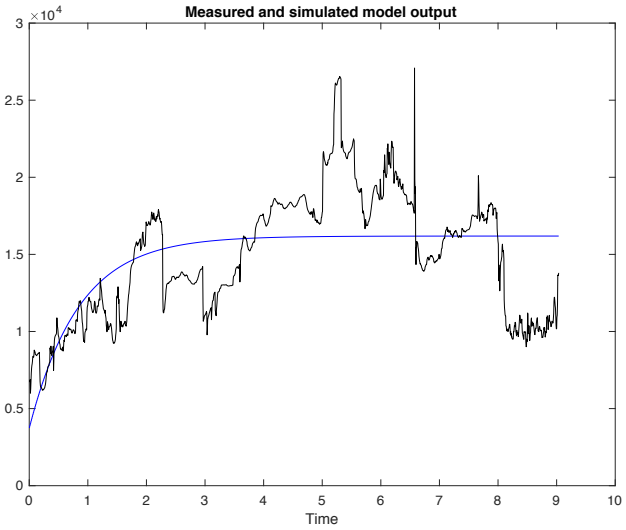

Figure E22: Measured (black) and simulated model (blue) output of ET patient 1 with 16.4% best fit - omitted from the analysis.

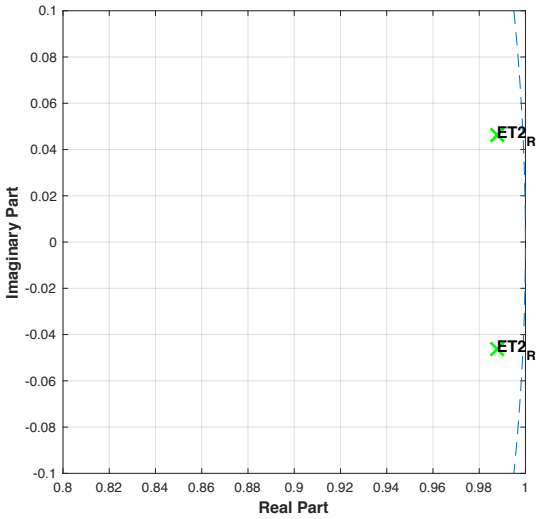

Figure E23: Pole-zero plot of ET patient 2 using R^2 data.

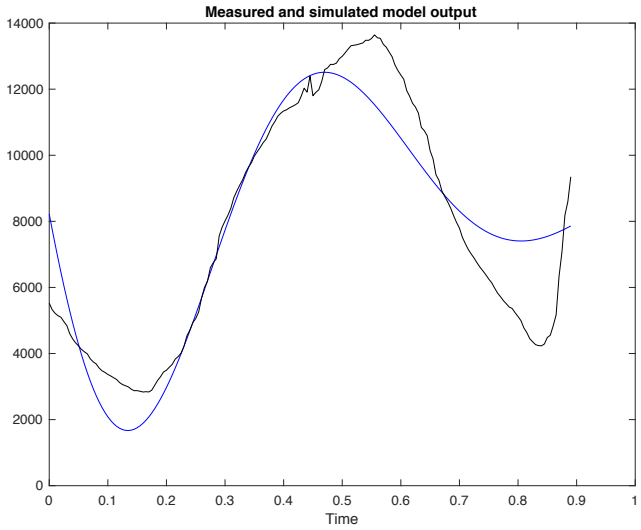

Figure E24: Measured (black) and simulated model (blue) output of ET patient 2 with 63.0% best fit.

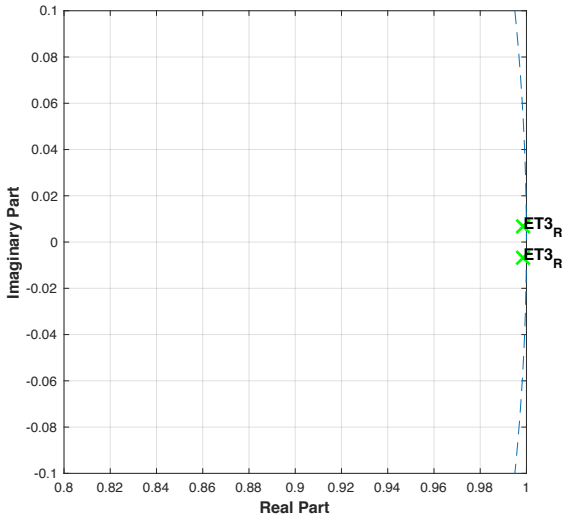

Figure E25: Pole-zero plot of ET patient 3 using R^2 data.

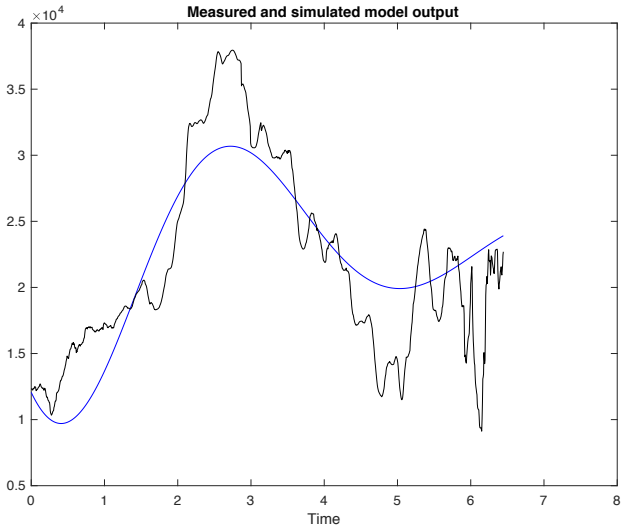

Figure E26: Measured (black) and simulated model (blue) output of ET patient 3 with 44.6% best fit - omitted from the analysis.

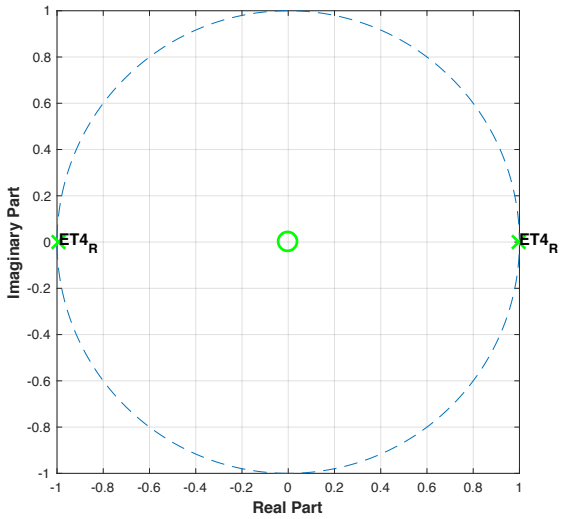

Figure E27: Pole-zero plot of ET patient 4 using R^2 data.

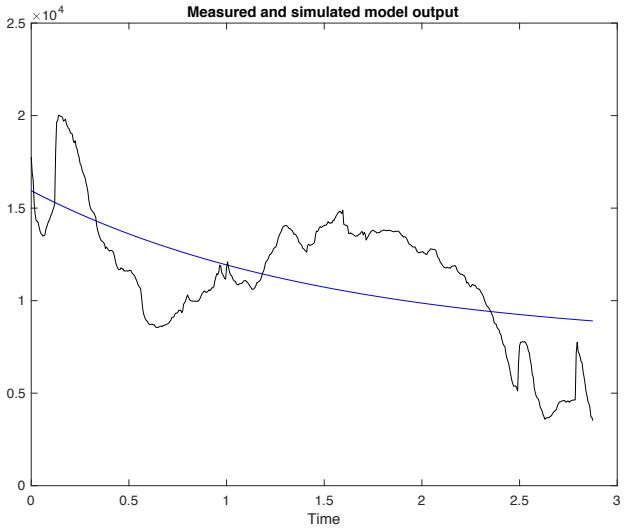

Figure E28: Measured (black) and simulated model (blue) output of ET patient 4 with 17.4% best fit - omitted from the analysis.

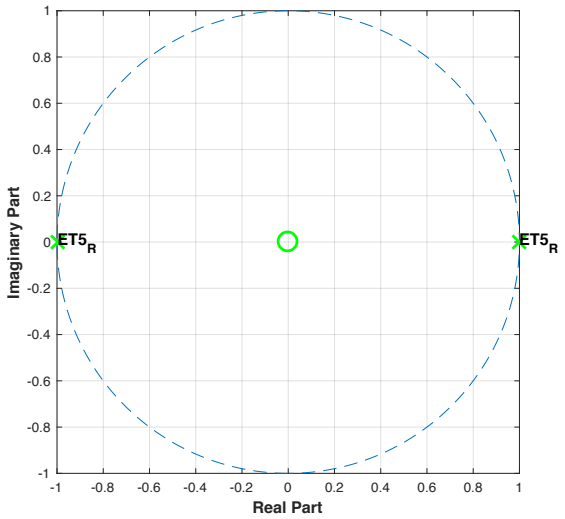

Figure E29: Pole-zero plot of ET patient 5 using R^2 data.

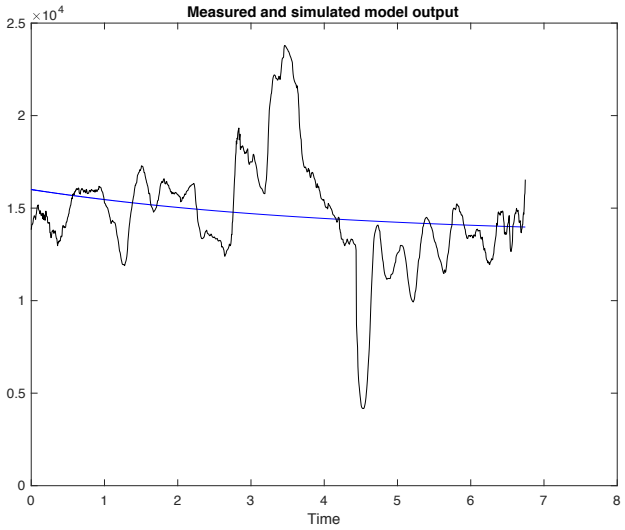

Figure E30: Measured (black) and simulated model (blue) output of ET patient 5 with 2.0% best fit - omitted from the analysis.

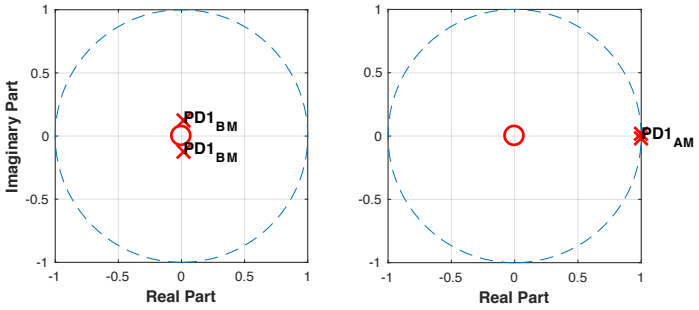

Figure E31: Pole-zero plot for PD patient 1 before and after medication using R^2 data.

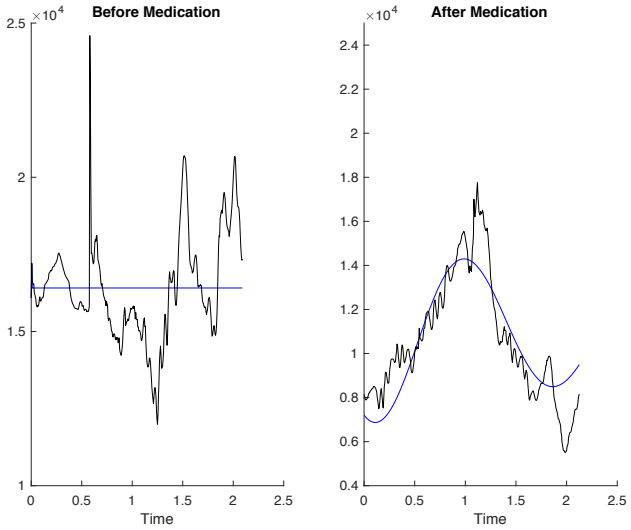

Figure E32: Measured (black) and simulated model (blue) output of PD patient 1 before and after medication with -9.9% (omitted from the analysis) and 50.8% best fit respectively.

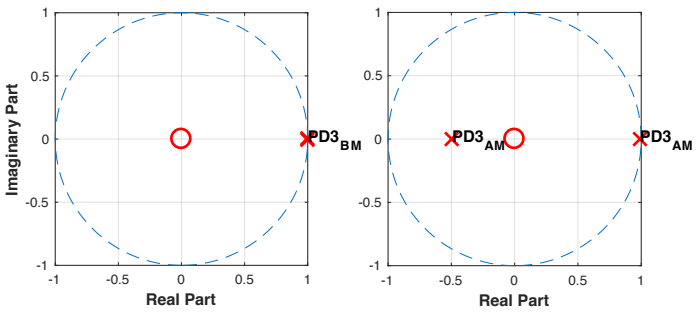

Figure E33: Pole-zero plot for PD patient 3 before and after medication using R^2 data.

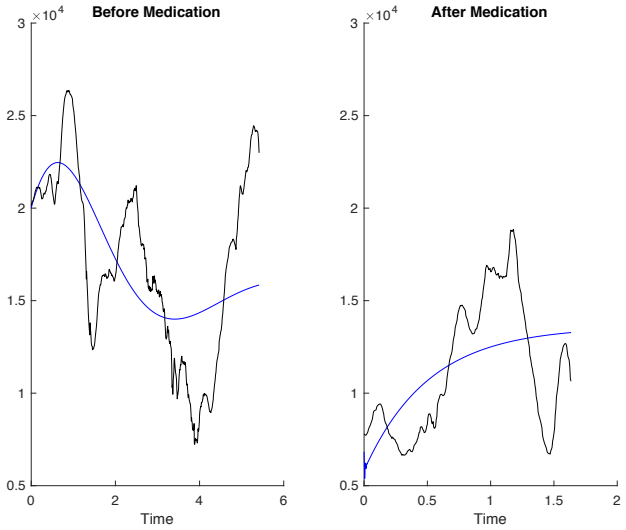

Figure E34: Measured (black) and simulated model (blue) output of PD patient 3 before and after medication with 21.3% and 16.7% best fit respectively - omitted from the analysis.

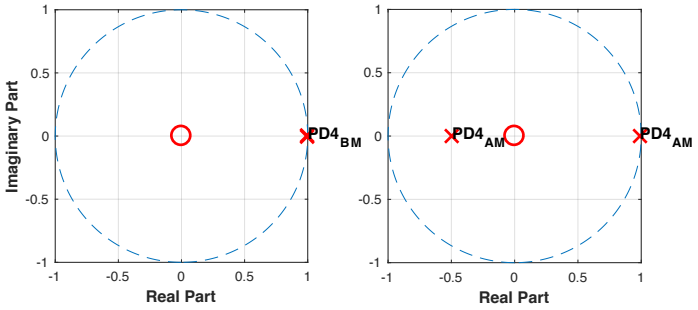

Figure E35: Pole-zero plot for PD patient 4 before and after medication using R^2 data.

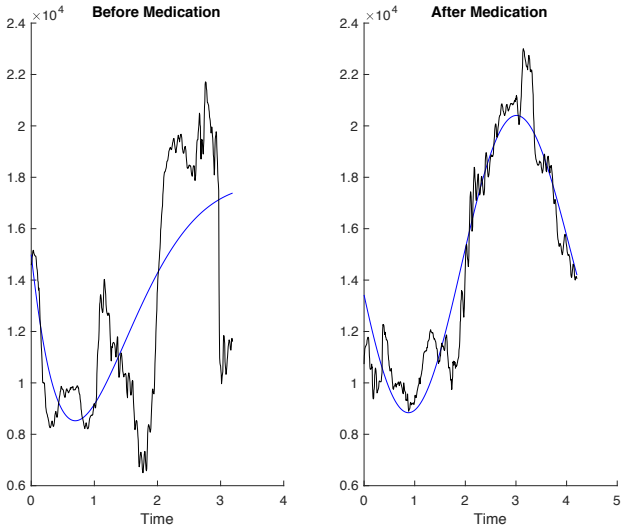

Figure E36: Measured (black) and simulated model (blue) output of PD patient 4 before and after medication with 28.2% (omitted from the analysis) and 71.49% best fit respectively.

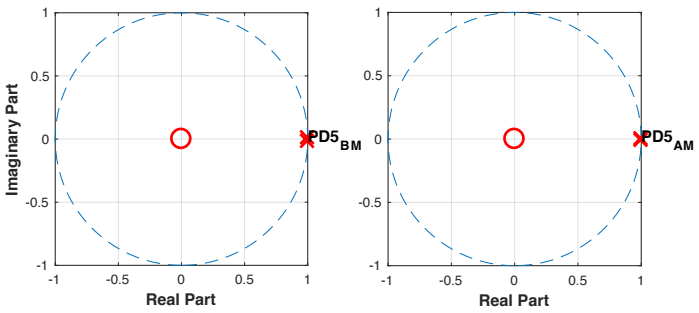

Figure E37: Pole-zero plot for PD patient 5 before and after medication using R^2 data.

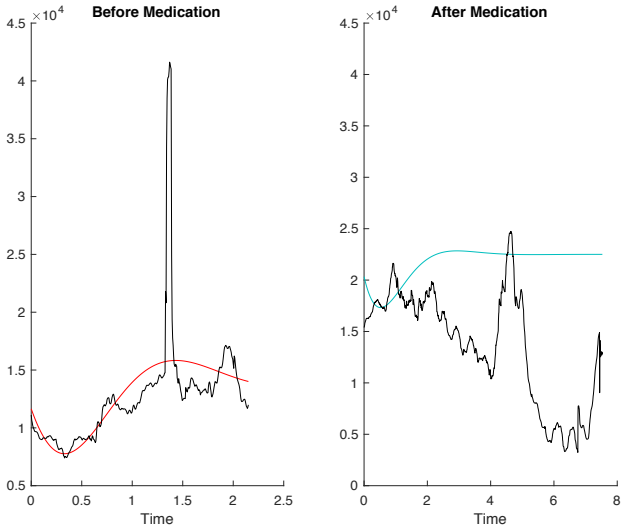

Figure E38: Measured (black) and simulated model (blue) output of PD patient 5 before and after medication with 18.87% and -90.1% best fit respectively - omitted from the analysis.

APPENDIX F – FFT ANALYSIS OF R^2 DATA FROM CIRCLE PATTERN

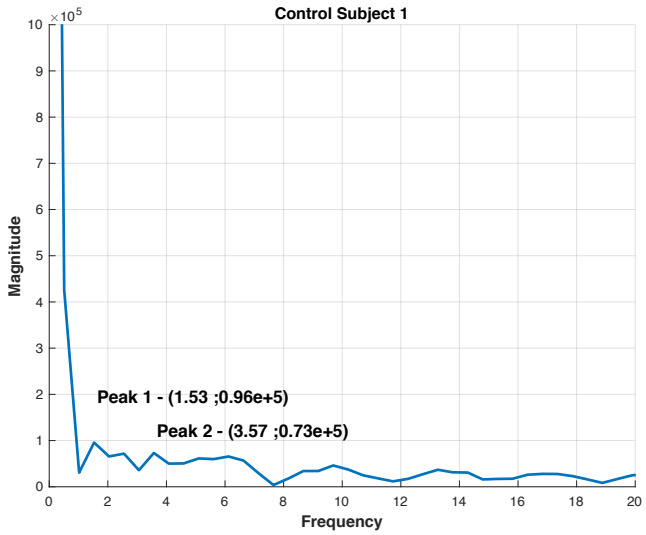

Figure F1: A FFT plot of control subject 1 using R^2 data.

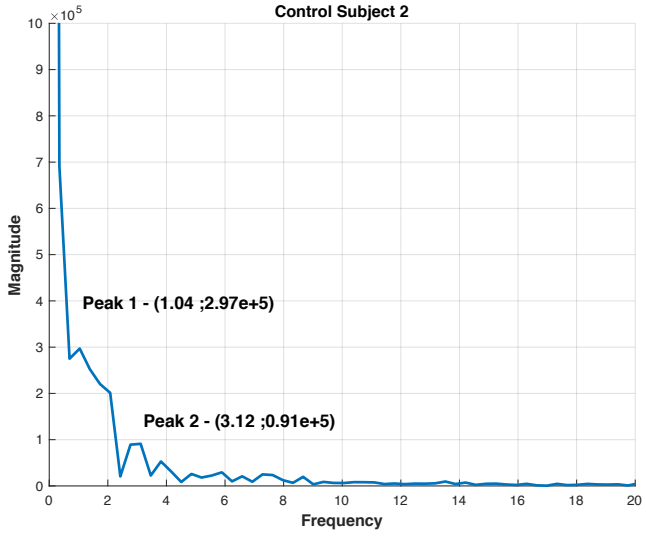

Figure F2: A FFT plot of control subject 2 using R^2 data.

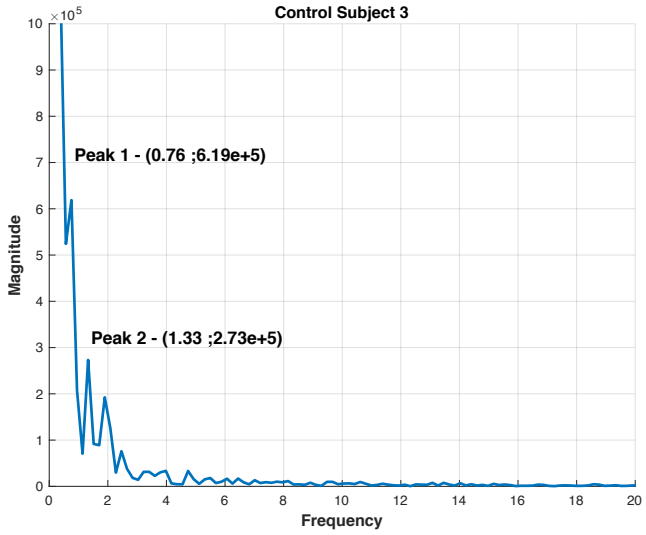

Figure F3: A FFT plot of control subject 3 using R^2 data.

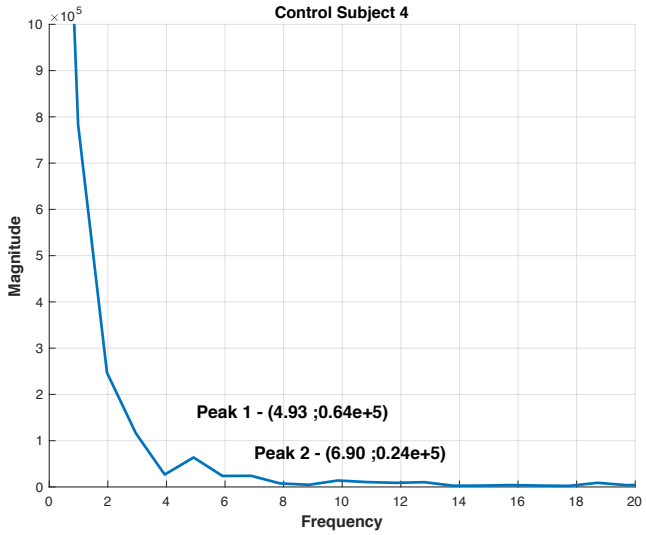

Figure F4: A FFT plot of control subject 4 using R^2 data.

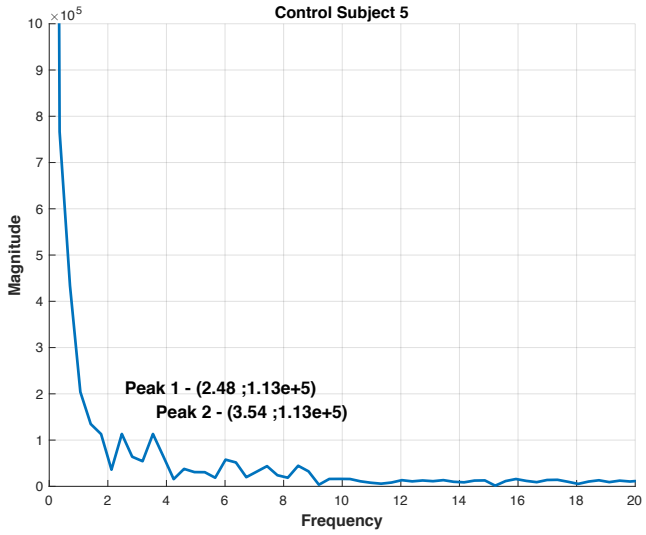

Figure F5: A FFT plot of control subject 5 using R^2 data.

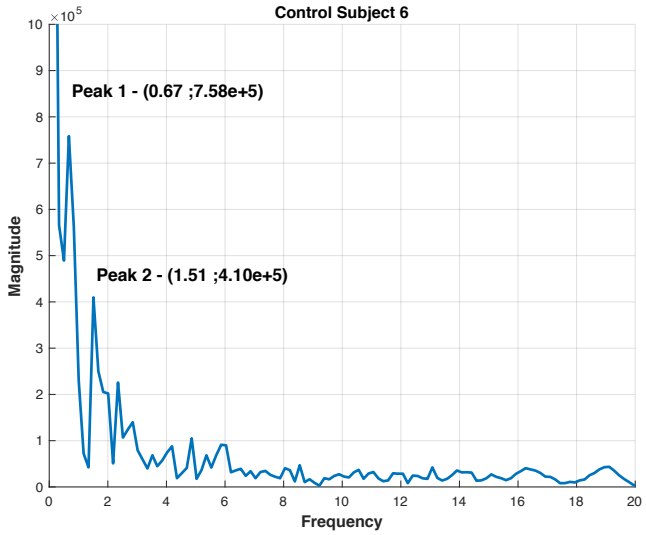

Figure F6: A FFT plot of control subject 6 using R^2 data.

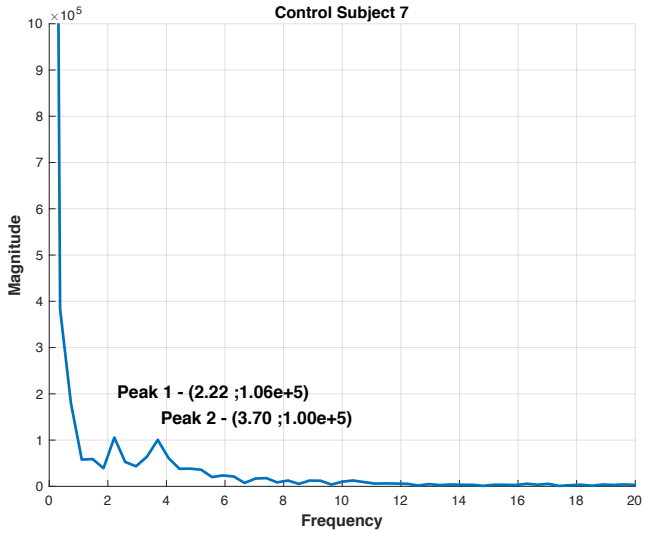

Figure F7: A FFT plot of control subject 7 using R^2 data.

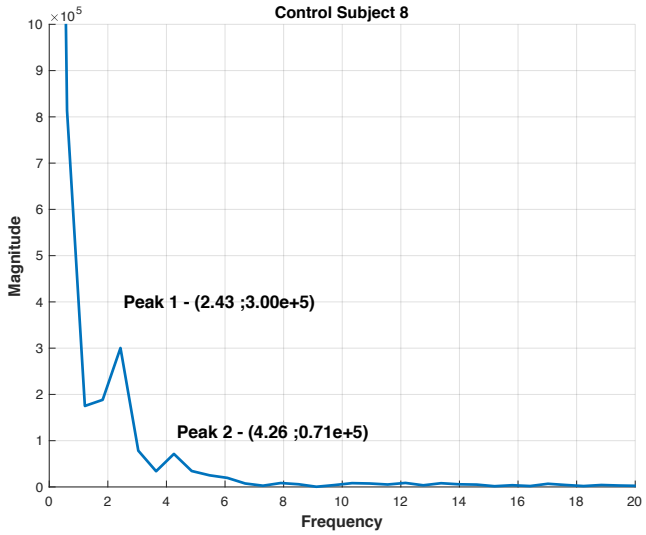

Figure F8: A FFT plot of control subject 8 using R^2 data.

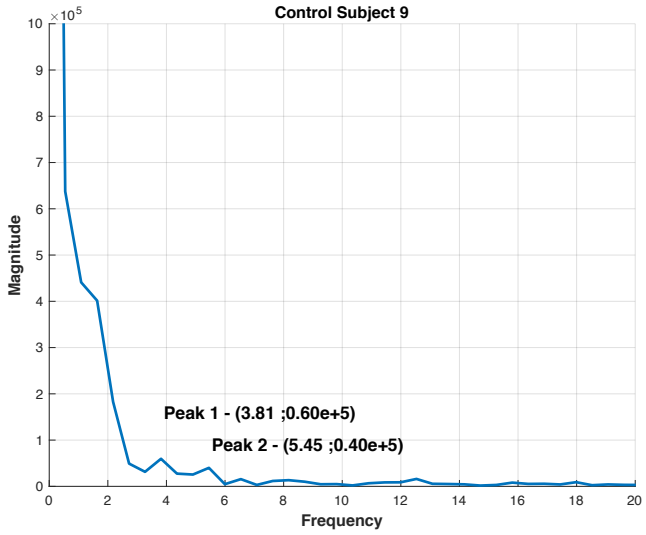

Figure F9: A FFT plot of control subject 9 using R^2 data.

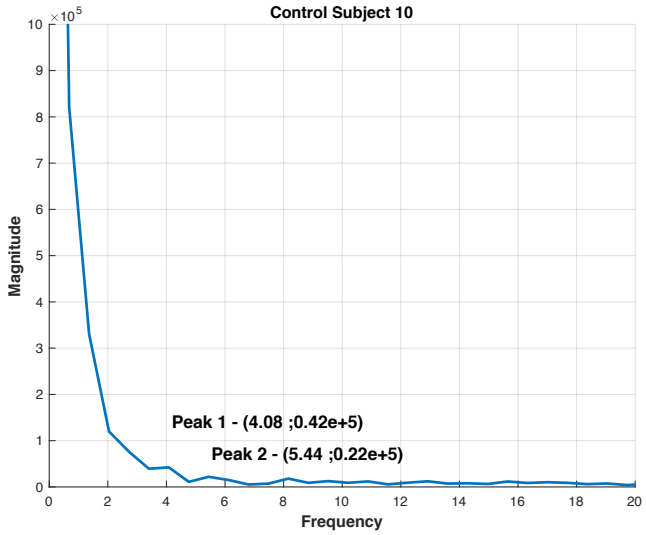

Figure F10: A FFT plot of control subject 10 using R^2 data.

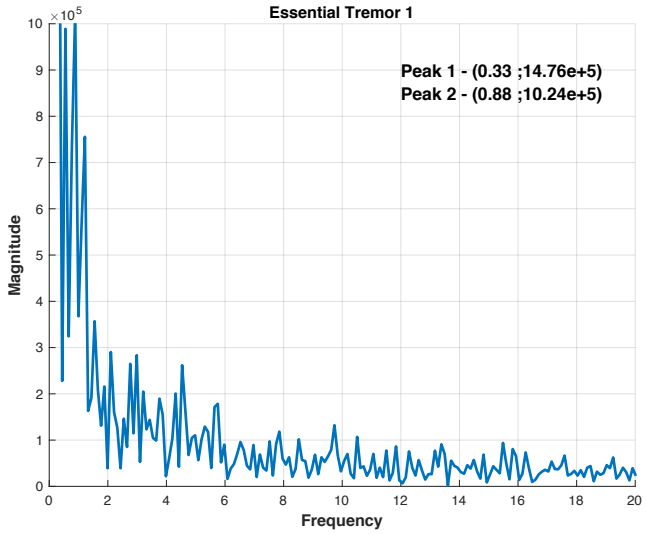

Figure F11: A FFT plot of ET patient 1 using R^2 data.

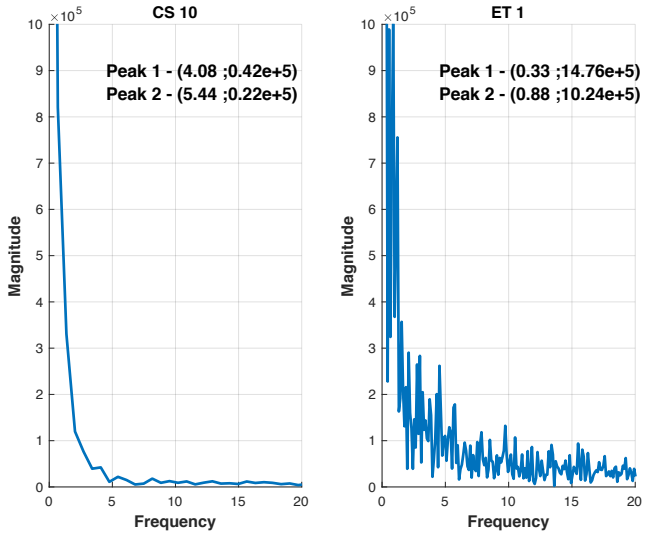

Figure F12: A comparison FFT plots between ET patient 1 and control subject 10 using R^2 data.

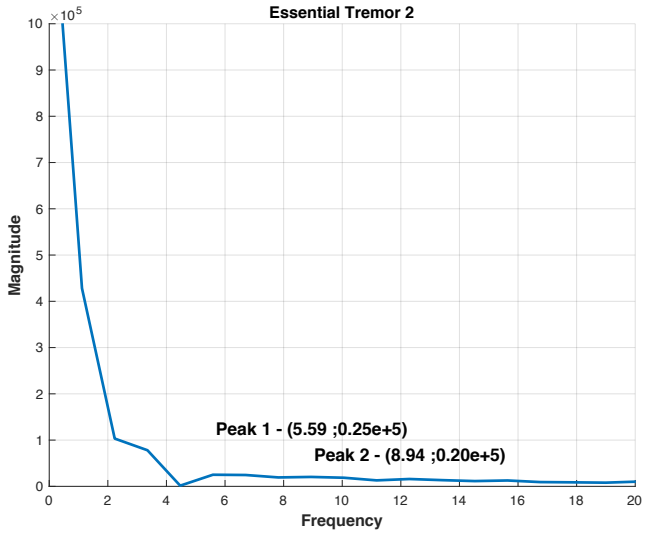

Figure F13: A FFT plot of ET patient 1 using R^2 data.

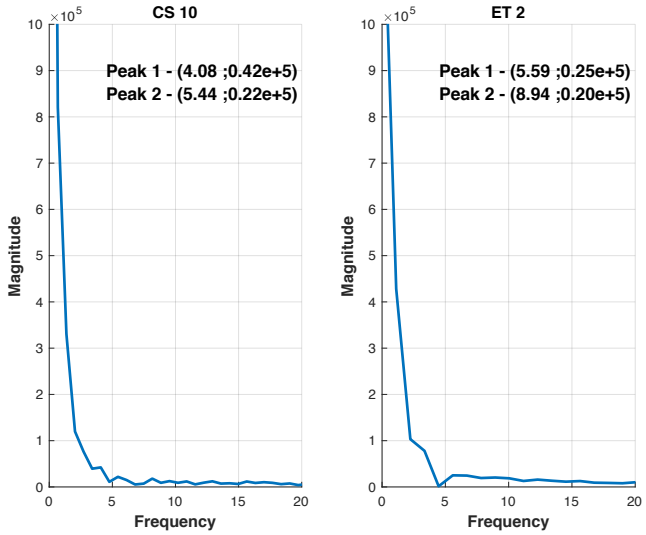

Figure F14: A comparison FFT plots between ET patient 2 and control subject 10 using R^2 data.

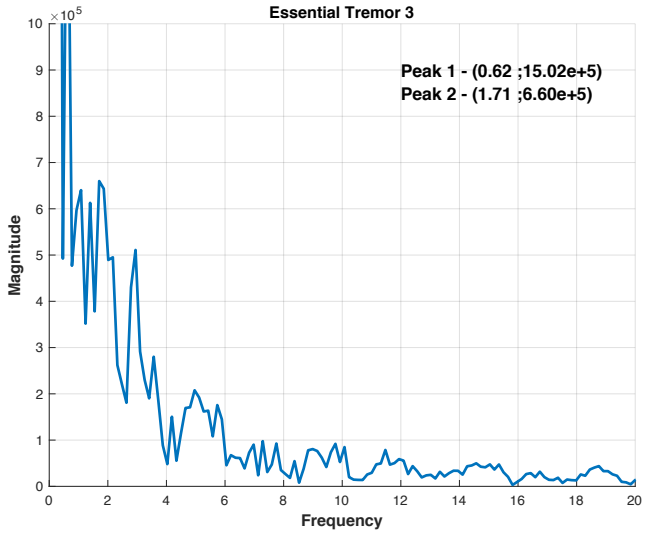

Figure F15: A FFT plot of ET patient 1 using R^2 data.

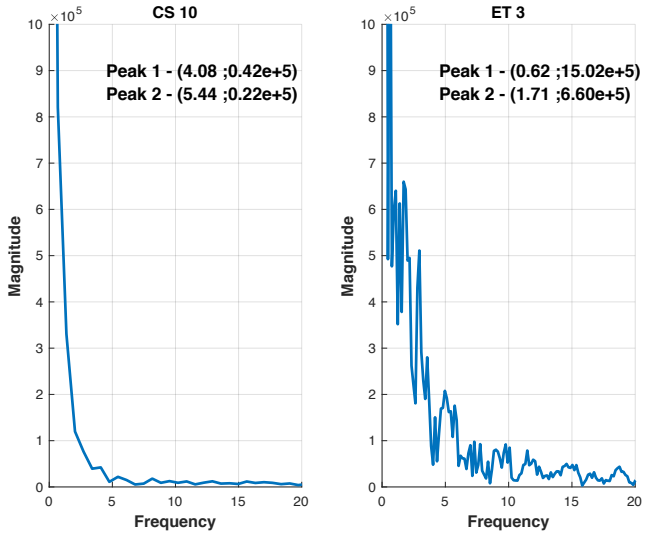

Figure F16: A comparison FFT plots between ET patient 3 and control subject 10 using R^2 data.

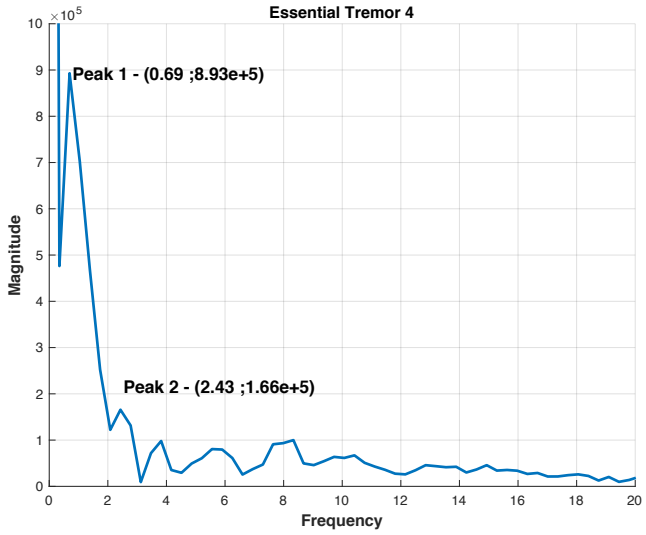

Figure F17: A FFT plot of ET patient 1 using R^2 data.

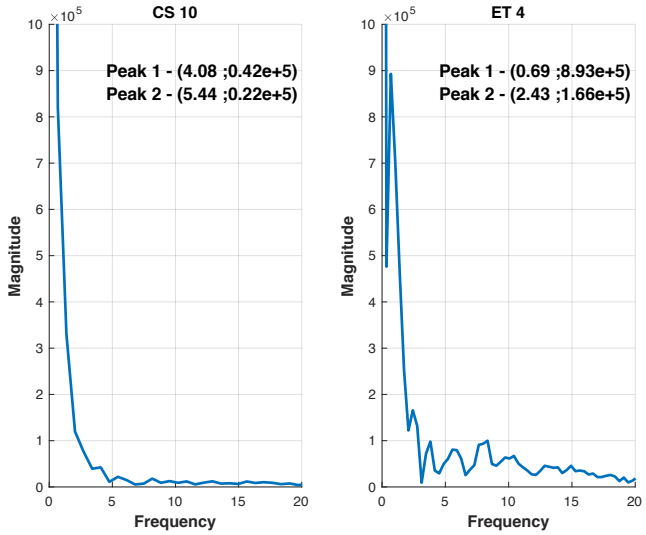

Figure F18: A comparison FFT plots between ET patient 4 and control subject 10 using R^2 data.

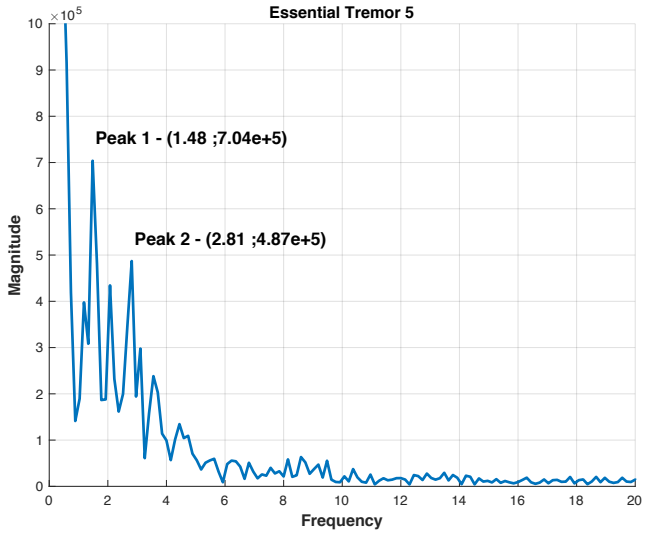

Figure F19: A FFT plot of ET patient 1 using R^2 data.

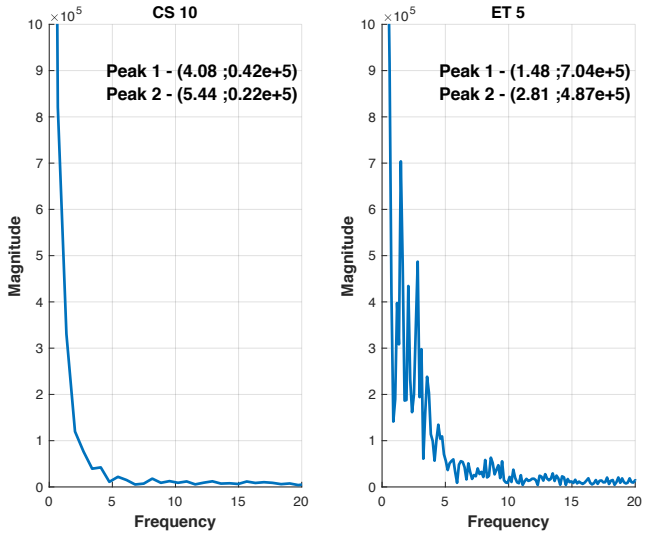

Figure F20: A comparison FFT plots between ET patient 5 and control subject 10 using R^2 data.

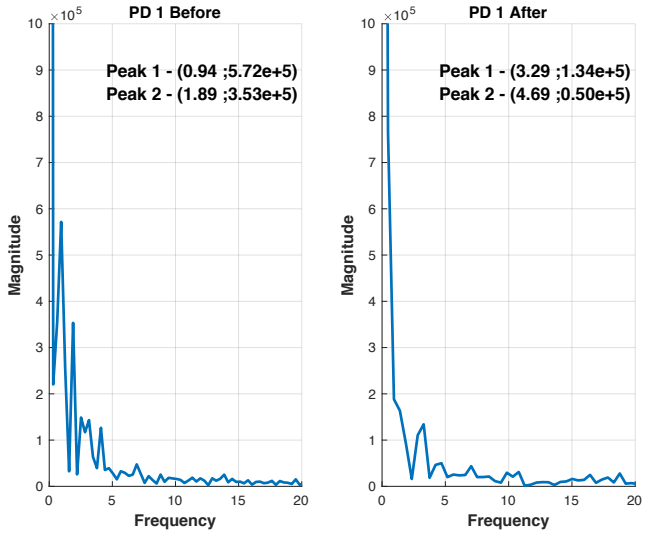

Figure F21: A FFT plot of PD patient 1 (before and after medication) using R^2 data.

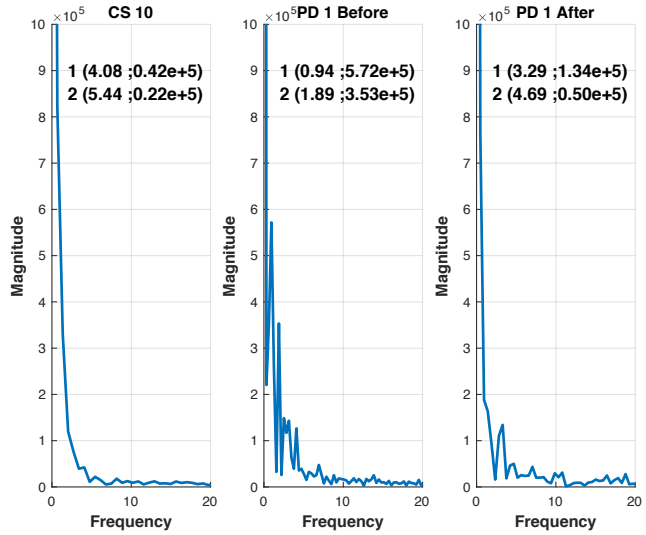

Figure F22: A comparison FFT plots between PD patient 1 (before and after medication) and control subject 10 using R^2 data.

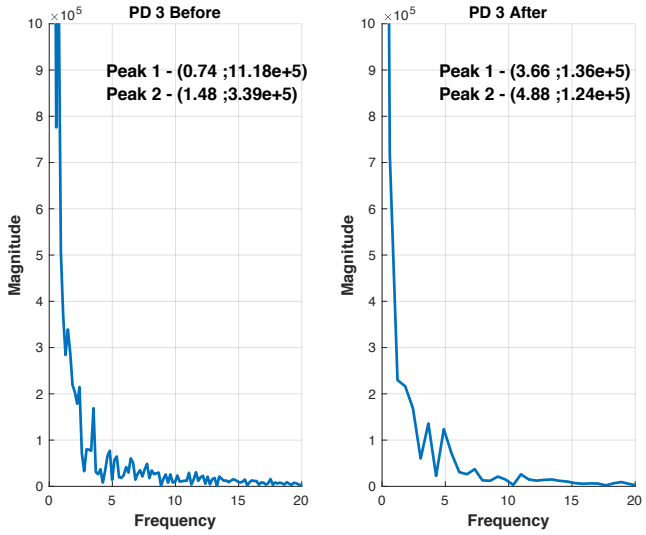

Figure F23: A FFT plot of PD patient 3 (before and after medication) using R^2 data.

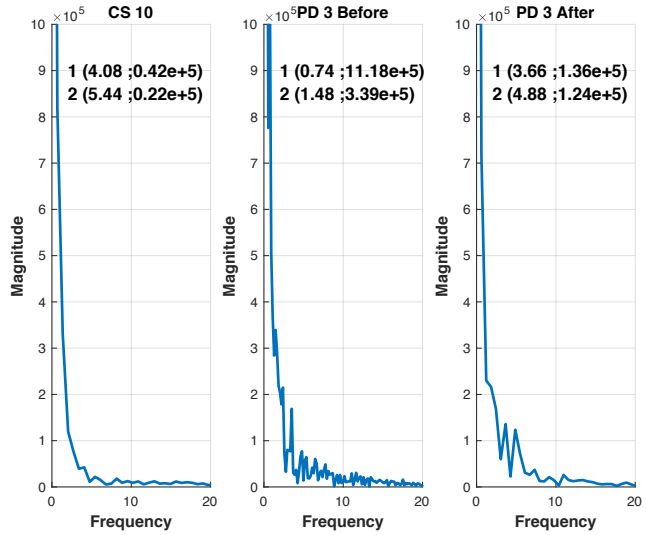

Figure F24: A comparison FFT plots between PD patient 3 (before and after medication) and control subject 10 using R^2 data.

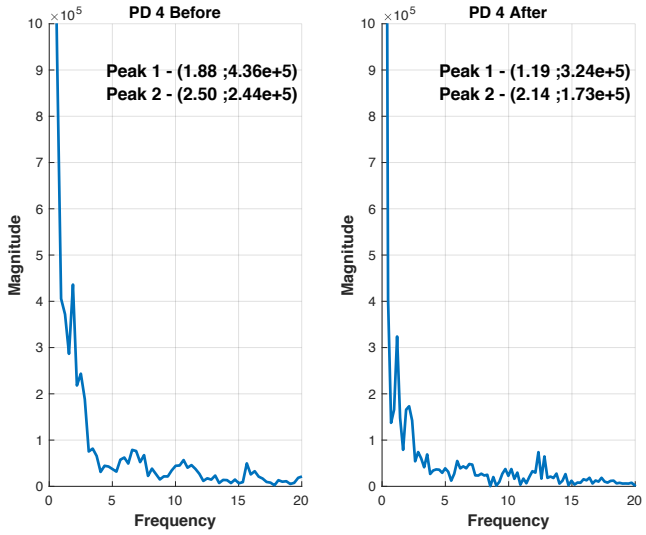

Figure F25: A FFT plot of PD patient 4 (before and after medication) using R^2 data.

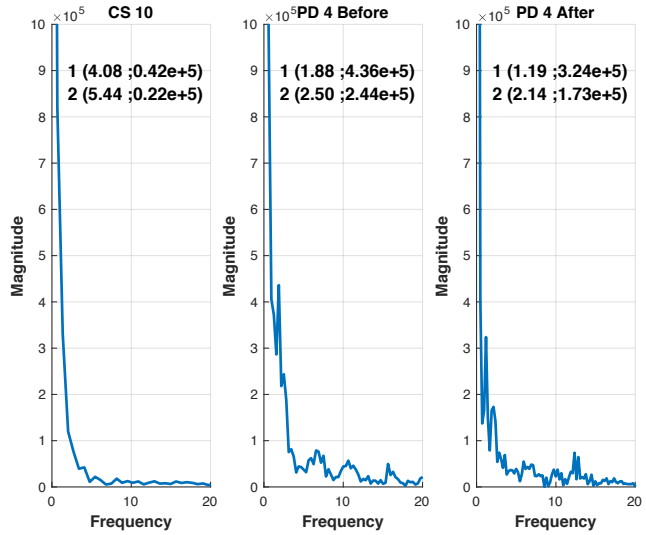

Figure F26: A comparison FFT plots between PD patient 4 (before and after medication) and control subject 10 using R^2 data.

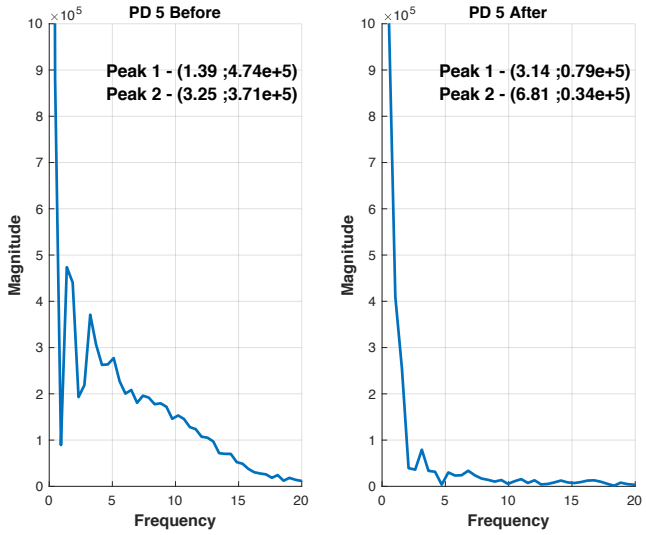

Figure F27: A FFT plot of PD patient 5 (before and after medication) using R^2 data.

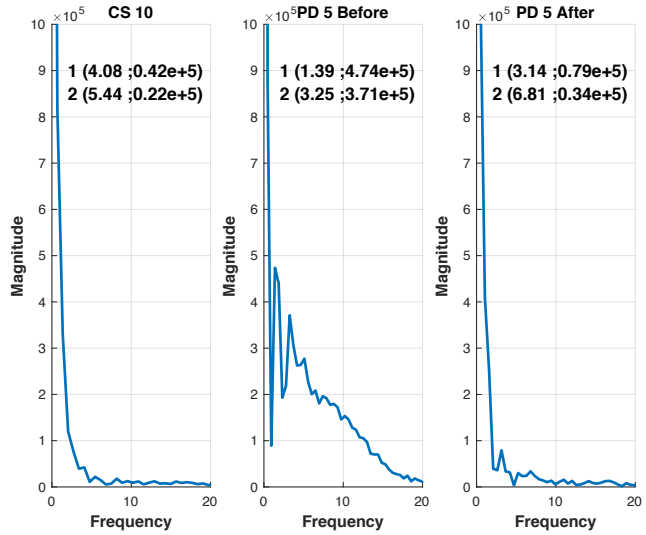

Figure F28: A comparison FFT plots between PD patient 5 (before and after medication) and control subject 10 using R^2 data.

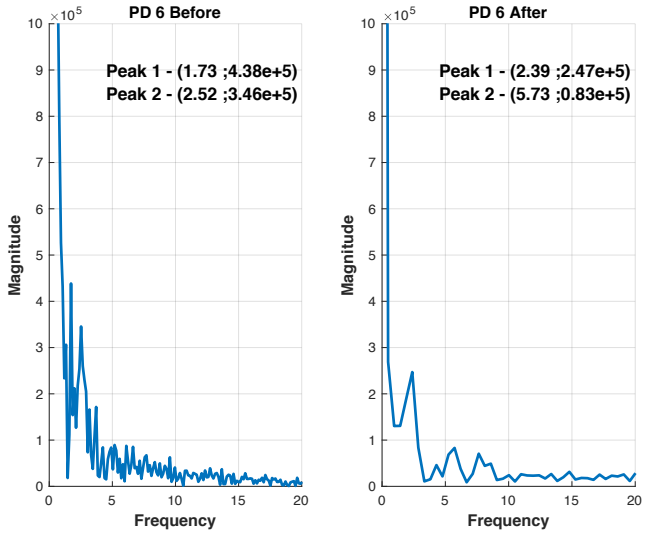

Figure F29: A FFT plot of PD patient 6 (before and after medication) using R^2 data.

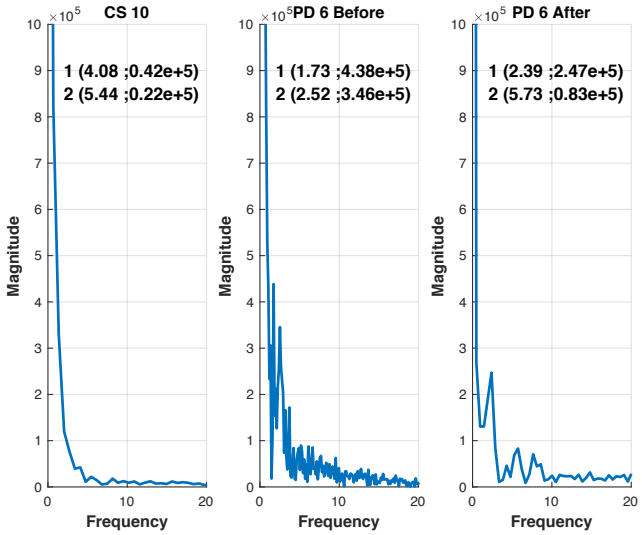

Figure F30: A comparison FFT plots between PD patient 6 (before and after medication) and control subject 10 using R^2 data.